Multifunctional Oligopeptides as an Artificial Toolkit for Molecular Recognition Events

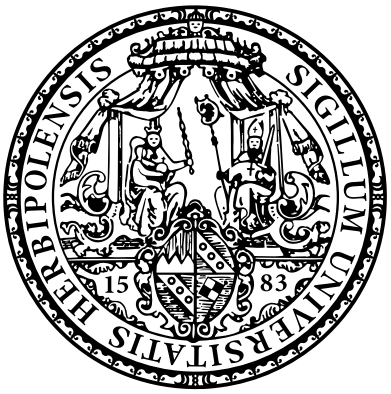

Dissertation
zur Erlangung des naturwissenschaftlichen Doktorgrades
der Julius-Maximilians-Universität Würzburg

vorgelegt von
Diplom-Chemiker
Peter Richard Wich
aus Bamberg

Würzburg 2009

Eingereicht am: .....

bei der Fakultät für Chemie und Pharmazie

1. Gutachter: .....

2. Gutachter: .....

der Dissertation

1. Prüfer: .....

2. Prüfer: .....

3. Prüfer: .....

des öffentlichen Promotionskolloquiums

Tag des öffentlichen Promotionskolloquiums: .....

Doktorurkunde ausgehändigt am: .....

List of Publications

Peer-Reviewed Publications

1. C. Schmuck, P. Wich, *Angew. Chem. Int. Ed.* **2006**, *45*, 4277–4281.

   "Sequence-Dependent Stereoselectivity in the Binding of Tetrapeptides in Water by a Flexible Artificial Receptor"

2. C. Schmuck, P. Wich, *New J. Chem.* **2006**, *30*, 1377–1385.

   "Combinatorial receptor finding – small and focused vs. large and random libraries"

3. G. Bringmann, H. Scharl, K. Maksimenka, K. Radacki, H. Braunschweig, P. Wich, C. Schmuck, *Eur. J. Org. Chem.* **2006**, 4349–4361.

   "Atropodiastereoselective Cleavage of Configurationally Unstable Biaryl Lactones with Amino Acid Esters"

4. C. Schmuck, P. Wich, B. Küstner, W. Kiefer and S. Schlücker, *Angew. Chem. Int. Ed.* **2007**, 46, 4786–4789.

   "Direct and Label-Free Detection of Solid-Phase-Bound Compounds by Using Surface-Enhanced Raman Scattering Microspectroscopy"

5. C. Schmuck, P. Wich, *Topics Curr. Chem.* **2007**, *277*, 3–30.

   "The Development of Artificial Receptors for Small Peptides Using Combinatorial Approaches"

6. B. Küstner, C. Schmuck, P. Wich, C. Jehn, S. K. Srivastava, S. Schlücker, *Phys. Chem. Chem. Phys.* **2007**, *32*, 4598–4603.

   "UV resonance Raman spectroscopic monitoring of supramolecular complex formation: peptide recognition in aqueous solution"

7. C. Schmuck, V. Bickert, M. Merschky, L. Geiger, D. Rupprecht, J. Dudaczek, P. Wich, T. Rehm, U. Machon, *Eur. J. Org. Chem.* **2008**, *2*, 324–329.

   "A Facile and Efficient Multi-Gram Synthesis of N-Protected 5-(Guanidinocarbonyl)-1H-pyrrole-2-carboxylic Acids"

8. S. K. Srivastava, S. Niebling, B. Küstner, P. R. Wich, C. Schmuck, S. Schlücker, *Phys. Chem. Chem. Phys.* **2008**, *10*, 6770–6775.

   "Characterization of guanidiniocarbonyl pyrroles in water by pH-dependent UV Raman spectroscopy and component analysis"

Oral Presentations

1. P. Wich, SFB 630-Colloquium, Würzburg, Germany, 17. Jul **2005**.

   "Combinatorial libraries as a tool to identify peptide binders: New insights into substrate- and sequence-selectivity"

2. P. Wich, Intensive Course Medicinal Chemistry 2006, HoChiMinh-City, Vietnam, 02. Nov **2006**.

   "Small and focused combinatorial libraries as a perfect tool to identify peptide binders"

3. P. Wich, Second Joint Ph.D. Students Meeting SFB 544/630, New Trends in Infectious Disease Research, Heidelberg, Germany, 23.–25. Nov **2006**.

   "Molecular recognition by one-armed artificial receptors in water – New insights from combinatorial methods as an ideal tool to identify peptide binders"

4. P. R. Wich, 11th JCF Frühjahrssymposium (JCF Spring Symposium), Essen, Germany, 11.–14. Mar **2009**.

   "Artificial Oligopeptides as a Versatile Toolkit for Molecular Recognition Events – New Insights into Multivalency Effects, Protein Recognition and Enzyme Inhibition"

Poster Presentations

1.–3. P. Wich, M. Heil, C. Schmuck,
Medicinal Chemistry Summer School Shanghai, China, 25.–28. Sep **2005**;
Novel Agents against Infectious Diseases, Würzburg, Germany, 12.–15. Feb **2006**;
1st European Chemistry Congress, Budapest, Hungary, 27.–31. Aug **2006**.

"Peptide binding by one-armed artificial receptors in water – Molecular recognition towards new lead structures"

4. B. Küstner, C. Schmuck, P. Wich, M. Heil, W. Kiefer, S. Schlücker, Novel Agents against Infectious Diseases, Würzburg, Germany, 12.–15. Feb **2006**.

   "Femtomolar Detection of Peptide Receptors with Molecular Specificity: A microspectroscopic Approach Based on Surface Enhanced Raman Scattering (SERS)"

5.–7. P. Wich, B. Küstner, S. Schlücker, C. Schmuck,
ACS 234th National Meeting Exposition, Boston, USA, 19.–23. Aug **2007**;
Wissenschaftsforum Chemie, Ulm, Germany, 16.–19. Sep **2007**;
Chem-SyStM 2007, Würzburg, Germany 04. Dec **2007**.

"Multivalent Peptide Receptors for the Selective Recognition of Biological Relevant Structures in Water - Insights into Combinatorial Libraries, Screening Methods and Biological Applications"

ACKNOWLEDGMENTS

Mit dem Abschluss dieser Arbeit geht eine tolle Zeit zu Ende. Ich durfte die Welt bereisen, habe viel gelernt und neue Freunde gefunden. Einige davon haben nicht nur zu einer schönen Zeit während der Doktorarbeit, sondern auch maßgeblich zum Gelingen dieser Arbeit beigetragen. Deshalb möchte ich folgenden Personen hiermit noch mal ein großes ***Dankeschön*** aussprechen:

An erster Stelle möchte ich meinem Doktorvater **Prof. Dr. Carsten Schmuck** für die Möglichkeit danken interessante und vielseitige Themen bearbeiten zu dürfen. Besonders möchte ich mich für die stetige Unterstützung bei all meinen Projekten danken. Er hatte stets die passenden Tipps parat und immer ein offenes Ohr für alle Probleme. Vielen Dank auch für die andauernde Unterstützung und das entgegengebrachte Vertrauen, was meine Projekte, Ideen und Zukunftsvorstellungen angeht. Dies hat wesentlich dazu beigetragen meine Faszination für die Naturwissenschaften, insbesondere die Chemie zu bestärken.

Des Weiteren möchte ich allen Kooperationspartnern für den produktiven Erfahrungs- und Forschungsaustausch danken, namentlich aber besonders...

... **Prof. Dr. Tanja Schirmeister** und **Cornelia Heindl** (Institut für Pharmazie und Lebensmittelchemie, Universität Würzburg) für die Möglichkeit die Enzym-Assays durchführen zu können und immer für Fragen und Anregungen zur Verfügung zu stehen.

... **Prof. Dr. Sebastian Schlücker**, **Bernd Küstner**, **Stephan Niebling** und **Dr. Sunil Kumar Srivastava** (Fachbereich Physik, Universität Osnabrück) für die ergiebige Zusammenarbeit auf dem Gebiet der Raman Spektroskopie. Vielen Dank für die vielen Messungen und Analysen der von mir synthetisierten Proben.

... **Prof. Jerry Yang** und **Petra Inbar** (Department of Chemistry and Biochemistry, UC San Diego, USA) für das Kooperationsangebot und die Unterstützung meiner Forschungsarbeit während meiner zwei Forschungsaufenthalte in ihrem Labor.

... **Prof. Bradley Smith** und **Alexander White** (Department of Chemistry and Biochemistry, University of Notre Dame, USA) für die Kooperation und das Angebot mit meinen Substanzen Bakterien zum Leuchten zu bringen.

... **Prof. Dr. Gerhard Bringmann** sowie folgenden Mitarbeitern des SFB 630:
Dr. Tobias Ölschläger, **PD Dr. med. August Stich**, **Elena Katzowitsch**, **Jennifer Rath** und **Martina Schultheis** vom Teilprojekt Z1 für die Durchführung der mikrobiologischen Tests und **Dr. Heike Bruhn** für die Unterstützung bei organisatorischen Fragen.

... **Dipl. Ing. Wilhelm Sicking** (Institut für Organische Chemie, Universität Duisburg-Essen) für die Berechnungen der Tryptase-Komplexstrukturen.

... allen Mitarbeitern in der Analytikabteilungen des Instituts für Organische Chemie der Universität Würzburg: in der NMR-Abteilung **Elfriede Ruckdeschel** und **Dr. Matthias Grüne** und in der Abteilung für Massenspektrometrie **Dr. Michael Büchner** und **Fritz Dadrich**. Danke für die technische und fachliche Unterstützung zur Aufklärung meiner Molekülstrukturen.

... allen weiteren Mitarbeitern des Instituts für Organische Chemie die im Hintergrund das Uhrwerk am Laufen halten. Ein besonderer Dank geht besonders an **Markus Braun** für die vielen kleinen und großen Dinge ohne die der Laboralltag nicht oder nur schwer funktioniert hätte.

Weiterhin möchte ich allen Freunden und Kollegen für die gemeinsame Zeit (nicht nur im Labor) danken, insbesondere:

... **Moritz Milde** für die Zusammenarbeit im Zuge seines F-Praktikums sowie **Jens Schmidt** und **Maximilian Köhler** für die gemeinsame Forschungsarbeit und die Hilfe während ihrer Ausbildung.

... **Karsten Schneider**, für die Initiierung des Fördervereins und die vielen kleinen Dinge und Hilfestellungen im Hintergrund des Arbeitskreises.

... **Ben Bulheller**, für das Korrekturlesen einiger Teile dieser Arbeit und vor allem für die vielen Tipps rund um LaTeX, ohne die ich wahrscheinlich doppelt so lange zum Zusammenschreiben benötigt hätte.

... meinen Laborkollegen **Michael Merschky**, **Tassilo Fenske**, **Dr. Martin Heil** und **Dr. Michael Schwegmann** für die angenehme Atmosphäre im Laboralltag und die vielen heiteren Momente. Ein extra großes Dankeschön geht an meinen "Lieblingslaborkollegen" **Christian Urban** für das Korrekturlesen einiger Teile dieser Arbeit.

... allen Kollegen und Mitarbeitern die im Laufe der Jahre kamen, wieder gingen oder noch im Arbeitskreis Schmuck sind. Danke für die tolle Zusammenarbeit, die lustigen Feierstunden, die coolen Wakeboardtrips, die auflockernden Kickerrunden und entspannenden Kaffeepausen zwischendurch. Freue mich schon euch wieder mal zu treffen!

... ein ganz großer Dank geht vor allem an **Dr. Uwe Machon** und seine stetige Bereitschaft zu Helfen, sei es bei den vielen Fragen, die ich im Zusammenhang mit den Enzymassays hatte, oder im normalen Laboralltag. Vielen Dank auch für das zügige und gewissenhafte Korrekturlesen meiner Dissertation. Danke für so viel!

Abschließend und für mich eigentlich am wichtigsten, möchte ich meiner **ganzen Familie** danken, meinem Bruder **Thomas** und vor allem meinen lieben **Eltern Inge und Ferdl**. Danke für die Unterstützung, sowohl natürlich finanzieller Art, aber noch viel wichtiger moralischer Art. Das Vertrauen in mich und meine Pläne hat mir sehr geholfen diese Arbeit zu vollenden und an dem Punkt anzukommen an dem ich heute stehe. Vielen lieben Dank auch an meine **Freundin Daniela**, die mir immer zur Seite stand, mir den Rücken beim Zusammenschreiben frei hielt, sich als Biologin beim Korrekturlesen bravourös durch die Untiefen der Chemie schlug und mich in allen meinen Lebenslagen und Vorhaben unterstützt.

Whenever you find yourself on the side of the majority, it is time to pause and reflect.

Mark Twain

Mystery creates wonder and wonder is the basis of man's desire to understand.

Neil Armstrong

Für meine Eltern

–

Danke für Alles!

CONTENTS

Chapter 1

Introduction

1.1 Molecular Recognition

In many biological systems the molecular recognition between host and guest plays an important role. Many vital processes as for example immune defense, control of cell growth, signal transduction or metabolic regulation are controlled by the selective interaction between hormones or exogenous agents and their specific receptor systems. Frequently, these bioactive substances are proteins, small peptides or peptide fragments. For instance the self aggregation of peptides is responsible for a variety of neurodegenerative diseases like *Parkinson's* or *Alzheimer's*.[1]

The understanding of these binding events and molecular interactions is of crucial importance for the selective influence on biological processes and represents an interesting challenge. However, the study of natural peptides and proteins is often very difficult due to their complexity and is therefore very demanding. A perfect way to examine and understand these effects are small bioorganic model systems. These are small molecules with specific binding motifs or structures that can undergo selective, non-covalent interactions with biologically relevant substrates. The investigation of these tailor-made host-guest systems will not only help to understand the necessary fundamental interactions but will also help to influence and tune the biological effect of related natural relevant peptides. Any new insight gained this way can then be used to improve the understanding of the underlying biological processes and help to develop for example new therapeutics, medical diagnostics, molecular sensors and enzyme-like catalysts.

Whereas the early work in the area of peptide recognition mostly was limited to organic solvents,[2,3] some progress has been made in the last few years for peptide binding in more polar solvents. Some examples of oligopeptide binding in aqueous solvents based on metal-ligand[4] or hydrophobic interactions,[5–7] as well as even purely electrostatic interactions (H-bonds and ion pairs)[8,9] have been reported. However, this is still a very challenging area of research and the aim to achieve the same efficiency and potency like biological systems could not be accomplished so far, especially in water. One of the most promising attempts to synthesize strong artificial systems is to utilize the principle of multivalency.

1.2 The Power of Multivalency

Nowadays, multivalency gets an increased interest as a powerful tool for the development of artificial receptors with high affinity and specificity for biological targets. In nature this concept plays a central role in many biomolecular recognition processes, e.g. the adhesion of viruses, bacteria or antibodies to the cell surface[10,11] or the interaction between proteins.[12] Multivalent ligands also act as powerful inhibitors, for example oligosaccharide inhibitors which are able to capture pentameric Shiga-like toxins based on the simultaneous occupation of multiple binding sites.[13]

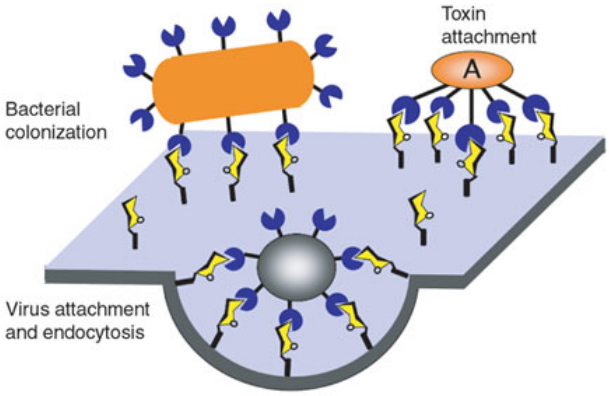

Figure 1.1: *The attachment of microbes and microbial toxins to host cells is mediated via multiple simultaneous interactions of cell-surface glycan ligands.*[304]

Both nature and the synthetic chemist have discovered ways to strengthen additive interactions between binding centers. The common basic concept behind multivalency is the simultaneous interaction between multiple complementary functionalities on two (or more) entities. This host-guest system leads to the formation of an complex with a binding affinity higher than the sum of the corresponding monovalent interactions.[14–16]

In supramolecular chemistry the principle of multivalency has been adapted as an important strategy for the development of synthetic ligands with high affinity and specificity for biological and synthetical targets. One example are dendrimers which are well-defined, hyper-branched polymers with a high density of functional groups and are therefore attractive scaffolds for multivalent display of natural and synthetic ligands. The increase in affinity with dendrimers can be useful in numerous biological related applications, including targeted transport and the release of active agents.[17]

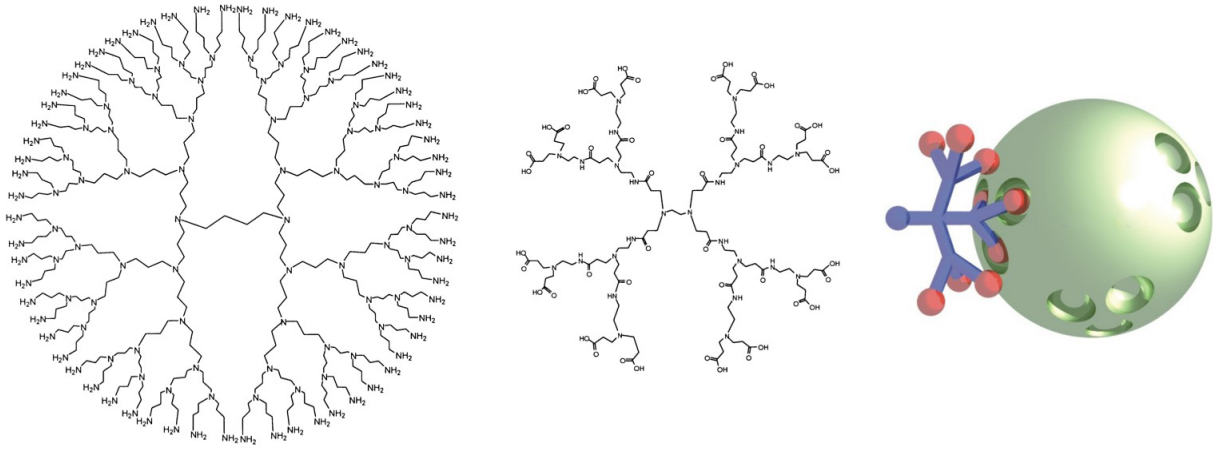

Figure 1.2: *Dendrimers are an example for hyper-branched molecules which use multiple interactions for an efficient interaction e.g. with biomolecules (green).*[17]

Not only in big macromolecules, but already in small systems this concept of multivalency can be adapted as a biomimetic approach to increase the relatively weak binding efficiency of artificial systems in water via multiple simultaneous non-covalent interactions. This results in much higher thermodynamic and kinetic stability leading to highly efficient molecular associations.

The aim of this thesis is a better understanding of the non-covalent interaction of small peptide systems with various biological relevant structures. The project starts with an in-depth investigation of small and strong peptide complexes. Reduced to only few intermolecular interactions the basic principles were studied with the help of different analytical tools such as Raman and NMR spectroscopy. The gained knowledge was then applied for the efficient and selective recognition of several more complex and biological relevant peptides systems. The final project expands the scope of recognition to proteins and describes the search for potent peptide based enzyme inhibitors.

CHAPTER 2

PROJECTS AND OBJECTIVES

2.1 Insights into the Non-Covalent Interactions of Small Peptide Sequences

For the understanding of intermolecular interactions between peptides it is advantageous to study their complexation behavior with the help of small model systems. Therefore, following the definition of synthetic receptors by Nobel laureate *Jean-Marie Lehn*,[18] the term "peptide receptor" is here used to describe a chemical host which binds to a given peptide guest and may not be mixed up with the biochemical definition of biological receptors, which are proteins to which signaling molecules like neurotransmitter, hormones, drugs or toxins may attach. Hence, this notation "peptide receptor", or more general "receptor" is used throughout this thesis for oligopeptide structures and their non-covalent interaction with other peptides, membranes or proteins.

In earlier studies it has been shown that small tetrapeptides can interact with high binding affinity with peptide receptors developed by *Schmuck et al.* In the center of the investigations was the tris-cationic receptor Gua-Lys-Lys-Phe (Gua = guanidiniocarbonyl pyrrole) that efficiently binds various tetrapeptide sequences even in solvents with high polarity like water.[9] This high affinity is based on the combination of several well directed non-covalent interactions between the peptide backbones and a strong complexation of the free C-terminal carboxylate.

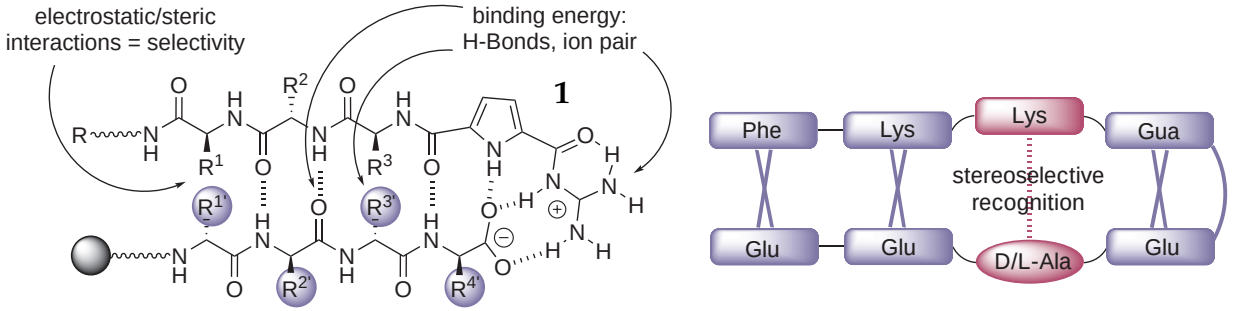

Figure 2.1: *Schematic representation of the interaction between a triscationic guanidiniocarbonyl pyrrole peptide receptor* ***1*** *(R^1 = Phe, R^2 = R^3 = Lys) and a combinatorial tetrapeptide library (left); The receptor can stereoselectively recognize specific tetrapeptides due to strong electrostatic interactions resulting in a rigid complex (right).*

Interestingly, the peptide receptor showed not only a significant substrate selectivity but also a remarkable sequence dependent stereoselectivity in the binding of polar tetrapeptides. The best binding substrate found in the screening of a combinatorial library of 320 members was N-Ac-D-Glu-D-Glu-D-Glu-D-Glu-OH with a binding constant of 26500 M^{-1}, which is remarkably high, keeping in mind that both receptor and substrate are small and fully flexible molecules. This emphasizes that multiple charge interactions can be very efficient, even in water.

However, the screening of the triscationic receptor **1** against the immobilized library of substrates revealed only information about the types of amino acids as well as the proposed best position in the tetrapeptide sequence for a good complexation. Exact structural information of the detailed interactions in the complex could not be determined. The question which amino acids interact with each other still remained open, as well as if the guanidinio group of the receptor indeed binds to the free C-terminal carboxylate of the substrate.

To gain more information about the structure of this and other small peptide complexes, several spectroscopic methods were in the focus of interest. With the help of one- and two dimensional NMR experiments, it should be possible to obtain information about the spatial arrangement of the amino acid side chains and the interactions of the peptidic backbones in the complex structure. To elucidate the influence of the carboxylate binding site and its binding mode, the use of UV resonance Raman spectroscopy was chosen as selective and very sensitive (in the submillimolar range) method.

Especially the unique features associated with Raman spectroscopy should then be adopted to develop a new screening method for combinatorial libraries. The binding studies with members from a combinatorial library of peptide receptors mentioned above are usually performed with fluorophore-labeled substrates for probing their binding affinities. This approach, however, is not capable of probing any structural information. Analytical methods like NMR or IR may allow some information about the immobilized compound; however, they need a large amount of material and have trouble to distinguish this from the excess of polymer support. So far, the most common way to identify the actual library member on a specific bead is to pick the individual bead and analyze the peptide with mass spectrometric methods. However, this method requires a cleavage of the compound from the bead prior to analysis and can therefore not be performed directly in a screening assay. An alternative fast and direct analysis method would be a big step forward in the research on solid phase bound compounds, which are nowadays widely used in chemistry, not only for the chemical synthesis itself—as for DNA, peptides and carbohydrates—but also for further studies and direct applications of such bead-bound compounds in supramolecular or medicinal chemistry.

Therefore, it was one part of my project to synthesize analytical pure samples of peptide receptor **1** in solution as well as immobilized ones on a solid support for such studies. In cooperation with the Institute of Physical Chemistry of the University of Würzburg these samples should then be analyzed for specific changes in their Raman-active bands upon complexation.

2.2 Multifunctional Oligopeptides as Toolkit for Molecular Recognition Events

Small peptides are known to be involved in many biological recognition processes. It is also well known that some peptides with basic amino acid residues (especially arginine rich peptides) have good membrane translocation properties and are taken up rapidly by cells. The already mentioned guanidiniocarbonyl pyrroles (CBS) represent an interesting alternative to the natural amino acid arginine. Due to the fact that the guanidiniocarbonyl pyrroles bind carboxylates much stronger than guanidine, it could have an enormous effect on the chemical and biological properties of peptides and proteins in direct comparison with arginine.[19] In addition the high affinity towards free carboxylates

of these "aromatic" arginine analogs may also be interesting in terms of antimicrobial activity. Known anti-microbial peptides (AMPs) cover a wide range of size, sequence and structure, but interestingly they are all sharing amphipathicity and positive charge.[20,21] However, their mode of action is not yet clearly understood. Current models emphasize the need to coat a significant fraction of the membrane surface to produce a lethal effect. Others propose a membrane destabilization by the cationic antimicrobial peptides leading to a membrane disruption and the death of the cell.

All these examples attracted interest to test small artificial peptide receptors containing the guanidiniocarbonyl pyrroles (CBS) for their activity towards several biological targets. To accomplish this task, divers modifications of the artificial peptides had to be synthesized, i.e. a more hydrophilic form with a triethylene glycol chain (**3**), or a fluorescence active form (**4**) (see Figure 2.2).*

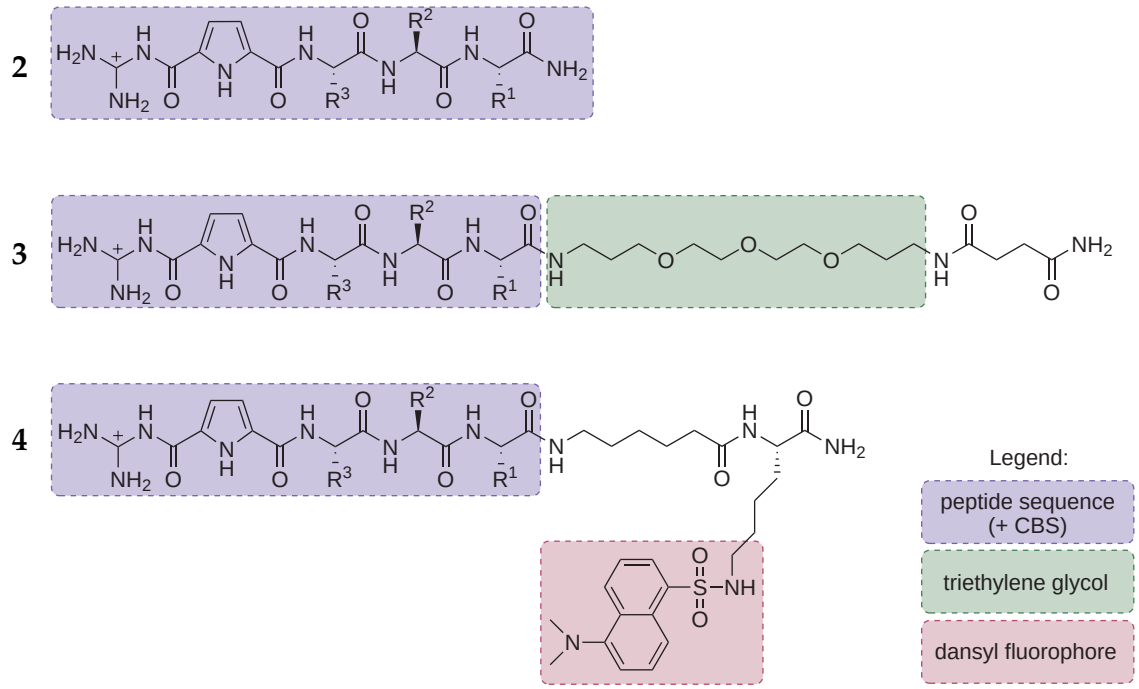

Figure 2.2: *Several variations (**2–4**) of the initial peptide receptor (**1**) were planed to be synthesized in order to investigate their biological activity.**

One point of interest was to study their interaction with the *Alzheimer's* related β-amyloid (Aβ) fibrils. In cooperation with the group of *Prof. Jerry Yang*, UC San Diego (USA), it was the aim to investigate the possible binding of the peptide receptors to the free C-terminal sequence VVIA of Aβ and therefore inhibit its interaction with other neuro-active proteins as possible new therapeutic strategy. In cooperation with the

* To simplify matters, amino acid residues are numbered according to their synthesis steps. This notation scheme is used systematically throughout the thesis.

group of *Prof. Bradley Smith*, University of Notre Dame (USA), their potential for membrane crossing should be investigated, and in cooperation with the Institute for Molecular Infection Biology of the University of Würzburg their antimicrobial potential and the ability of bacterial biofilm inhibition should be tested.

However, regarding an *in vivo* application the affinities and activities might have to be increased by some order of magnitude. In this context it was the aim to extend the structural assembly of the receptors via attaching several identical binding units to a common template. This idea can be used to increase the relatively weak binding efficiency in water via multiple simultaneous non-covalent interactions resulting in much higher thermodynamic and kinetic stability. For that reason, several multivalent structures based on branched trisamine and lysine scaffolds had to be synthesized and subjected to microbiological tests as well (see Figure 2.3).

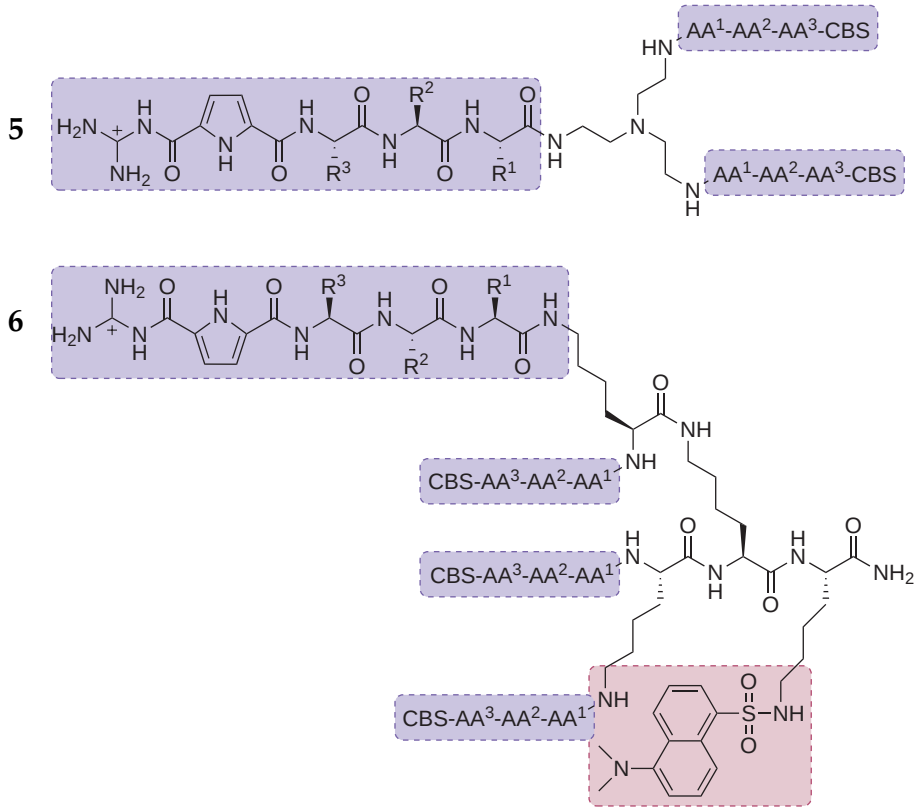

Figure 2.3: *Multivalent peptide structures based on tri- and tetravalent scaffolds with possible enhanced activity over biological targets.*

This thorough evaluation of the biological activity of mono- and multivalent peptides will expand the understanding of their mode of molecular recognition necessary for any potential application as drug candidates or diagnostic sensors.

2.3 The Search for Multivalent Peptides as Potent Enzyme Inhibitors

This multivalent approach should also be applied for the directed and selective interaction with more complex biological systems. Hence, the attractive features of the tetravalent peptide structures were in the main focus for the recognition of protein surfaces and the screening as potent enzyme inhibitors. In this context the serine protease β-tryptase, which plays an important role in the pathogenesis of asthma and other allergic and inflammatory disorders was of special interest.[22,23] The structure of tryptase is very unique and exhibits a frame-like tetramer structure with four active sites directed towards a central pore. A blocking of the entrance to this center opening would prevent the access of possible substrates to the binding pockets and therefore inhibit the enzyme activity.

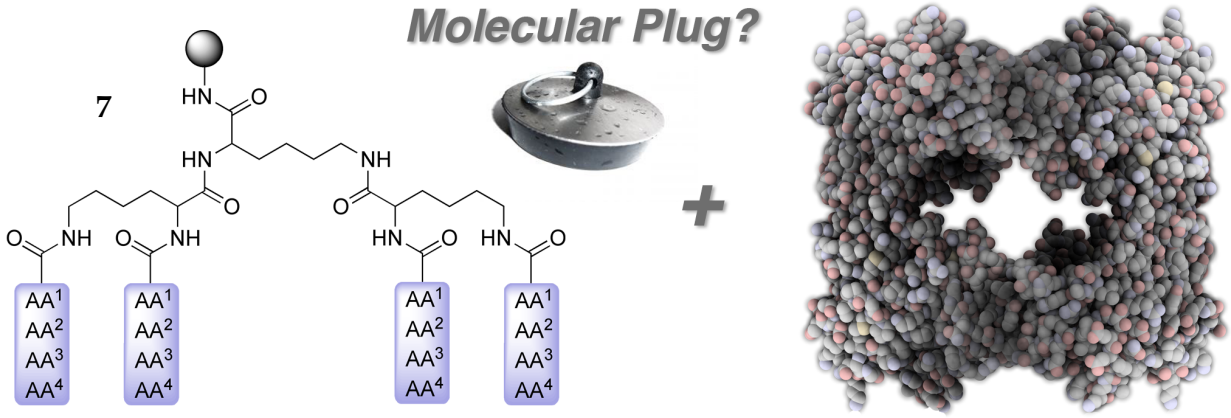

Figure 2.4: *Multivalent peptides (7) might block the active sites of β-tryptase (right) and therefore inhibit the enzyme activity.*

Basic force field calculations revealed that a tetravalent lysine scaffold with four amino acids in each side chain (**7**) would be large enough to stretch over the opening and "seal" the entrance. It is very important for this attempt, that the amino acid residues of tryptase at the entrance of the pore and the surrounding area of the active sites are in average of acidic nature, i.e. bearing carboxylates from aspartic and glutamic acid. According to that, basic amino acids like lysine and arginine should be important for an effective and tight interaction of the tetravalent inhibitor with the protein surface. Hence, part of the investigations was the search for the best amino acid combination necessary for an effective inhibitor. Therefore, a combinatorial library of 216 different inhibitors had to be synthesized and screened with a special on-bead enzyme assay developed in the *Schmuck* group.

CHAPTER 3

BACKGROUND INFORMATION AND BASIC CONCEPTS

3.1 Analytical Methods for the Determination of Non-Covalent Interactions Between Peptides

From the viewpoint of chemists there is still a huge lack of knowledge on the molecular level about the details of the non-covalent interaction between peptides. However, more exact information is essential to improve the structural features of the molecular systems and to influence the binding events to a greater degree, especially in water. There are several analytical techniques to quantify non-covalent interactions and elucidate the three-dimensional structure of supramolecular complexes. Generally the choice is dictated by analytical fundamentals such as sensitivity, speed, specificity, analyte and solvent compatibilities, accessibility and the type of information desired.

By far, the most widely applied analytical technique in systems involving complex formation between partners based on electrostatic interactions or H-bonding is nuclear magnetic resonance spectroscopy. NMR can observe the formation of a complex in solution through the observation of changes in the chemical shifts. Similar observations can be made with vibrational spectroscopy methods such as UV, fluorescence and Raman spectroscopy where upon complexation vibrational shifts and changes in the band intensities can be observed. Other popular instrumental techniques for study-

ing non-covalent binding interactions include different mass spectrometry based methods. Modern soft ionization methods, such as electrospray ionization (ESI) and matrix-assisted laser-desorption/ionization (MALDI), have significantly improved the ionization of molecules and complexes in a nondestructive way.[24,25] However, one of the main problems—especially for biological systems—is the limitation to gas phase studies. In particular proteins, peptides and other large biomolecules are known to behave quite differently in the gas phase relative to the solution phase.[26,27] Another powerful technique that is often used for the determination of binding equilibria data is isothermal titration calorimetry (ITC). In general, calorimetry is used as an approach to gain insight into the thermodynamics of an association reaction. The technique is fast and accurate and provides directly the parameters ΔH and ΔS.[28,29] Recent publications report a new technique to measure the supramolecular interactions of molecules with the help of atomic force microscope (AFM) measurements. It was possible to observe single host-guest binding events and measure the individual rupture forces of strong complexes with cyclodextrins or calixarenes.[30,31] The most accurate visual representation of the interacting species can be achieved through X-ray crystallography, where a diffraction pattern can be used to localize specific atoms in a solid crystal. This is one of the most frequently applied techniques for large supramolecular structures. However, one of the biggest drawbacks is the need for a stable complex in the solid phase.[32,33] Especially small peptides are often too flexible and can be hardly crystallized. Finally, quantum chemical calculations can also offer a rich source of supplementary information about non-covalent interactions using semiempirical, *ab initio*, and density functional models.[34] These calculations help not only to obtain useful visual information, but provide also insight into complexation behaviors and are an useful addition to instrumental-based methods. However, the obtained data sometimes need additional interpretation and a compromise between the cost of highly accurate simulations (time) and the level of desired information (interaction geometries, binding energies, etc.) has to be made.

The present thesis will focus—as part of research cooperations—on NMR and Raman spectroscopy methods to investigate the non-covalent interaction between peptides. Therefore, the following sections will briefly describe the theoretical basics of these techniques.

3.1.1 NMR Structure Determination

NMR experiments can be used to follow binding events by observing resonance signals of a host or guest molecule. With this method it is often possible to obtain information about the three-dimensional structure of peptides and proteins.[35–37] For example, NMR can monitor the formation of a protein-ligand complex in solution through observation of changes in chemical shifts of the protein (host) or the ligand (guest). The biggest advantage of NMR—compared for example with X-ray crystallography—is, that it can provide information about molecules in solution and under controlled environments characterized by specific pH, temperature, presence of buffer, etc. This allows to actually address the sample under physiological conditions.

In addition to binding information taken from chemical-shift data, also techniques for monitoring changes in relaxation times, diffusion constants and NOEs, are useful for gathering precise knowledge of solution-phase binding events. In high resolution NMR, two major parameters, the chemical shifts and the scalar coupling constants are needed to characterize a molecule. In addition, the nuclear Overhauser effect provides very important information regarding the spatial proximity of non-bond nuclei.[38] The sum of data, however, is responsible for an increased complexity in the spectrum, due to severe overlap of spectral features. This led to the development of 2-dimensional NMR techniques. Generally, 2D experiments are a set of 1D spectra, recorded and collected by systematically varied time intervals. The data acquired over the detection period is then Fourier-transformed and plotted in form of a 2-dimensional contour spectrum, where the peak intensity is proportional to the number of contours encircling the peak position (Figure 3.1). Peaks which occur on the 45° diagonal of the 2D spectrum correspond to the normal peaks of the 1D spectrum and have no additional information. Off-diagonal peaks or cross peaks represent interactions either through bond or space and are very important for the interpretation of the structure. The four most important homonuclear 2D NMR experiments are chemical shift correlation spectroscopy (COSY),[39,40] total correlation spectroscopy (TOCSY),[41] nuclear Overhauser effect spectroscopy (NOESY),[42,43] and rotating frame Overhauser enhancement spectroscopy (ROESY).[44,45]

COSY and TOCSY experiments allow the identification of J-coupled protons through bond correlation. In the case of COSY experiments direct neighboring protons are detected, whereas TOCSY in principle permits the correlation of all protons within a given coupling network. TOCSY experiments show—in addition to COSY signals—also cross peaks between spins which are coupled indirectly via a larger number of intervening

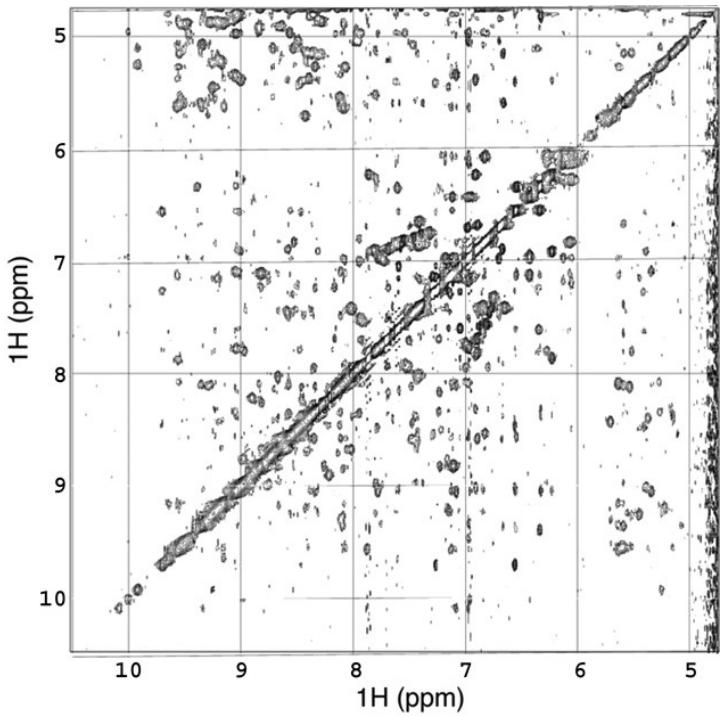

Figure 3.1: *Sample 2D NOESY spectrum of the 25-kDa core domain of the tumor suppressor protein p53.*[305]

J-coupled spins. NOESY and ROESY experiments are based on a different principle, the nuclear Overhauser effect, that makes it possible to achieve information about the through-space connectivity. This is especially important for the three-dimensional structure determination of proteins or the investigation of intermolecular interactions between peptides. Most of such NOE correlations are short range, i.e. they correspond to pairs of protons that are in close proximity of each other. However, a substantial number of long-range NOEs can also be present, providing some information about further spatial proximity. Depending on the intensity of the NOE peaks, the detectable distances between intra- and inter-residue protons can be classified into three regions: short (2.5 Å), medium (2.5–3.5 Å) and long (3.5–5 Å). NOESY experiments work well for molecules of very low and very high molecular weight. They do not work well for molecules with molecular weights of approximately 1000–2000 $g \cdot mol^{-1}$ at typical field strengths, where the NOE's are very close to zero, which results in a lack of correlations peaks. However, ROESY experiments (rotating frame NOE) are preferred for medium-sized molecules since the ROE (the equivalent to the NOE) is always positive, which allows to observe cross peaks that may not be visible in NOESY spectra. Therefore, ROESY experiments represent a useful additional NOE experiment in order to get information about molecules in this intermediate range of molecular mass.

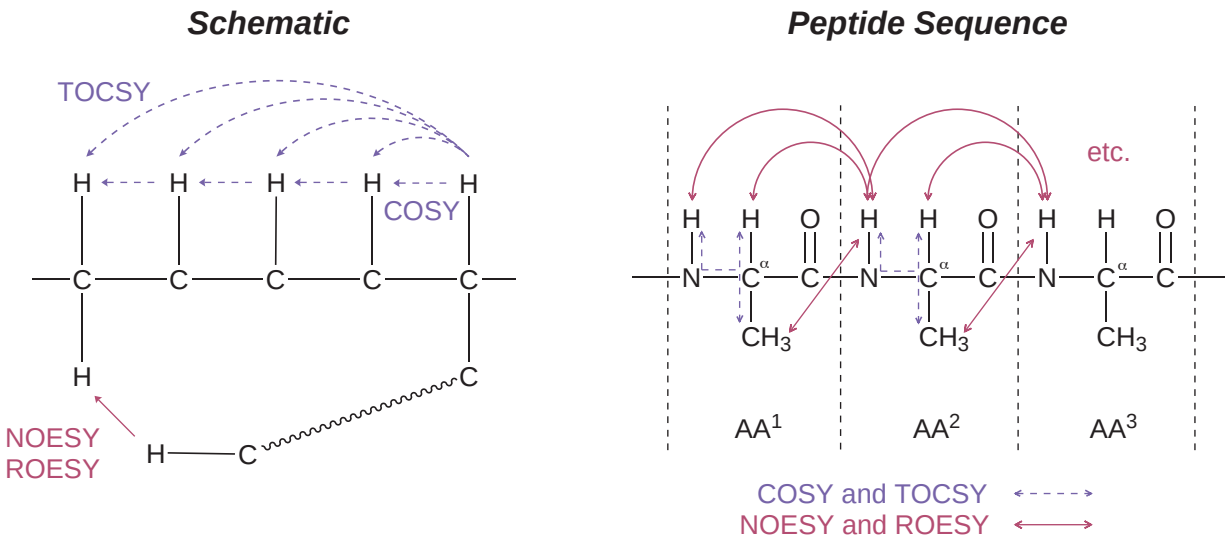

Figure 3.2: *COSY and TOCSY experiments can help to elucidate the individual amino acid sequence within a peptide, whereas NOESY and ROESY mainly help to determine the three-dimensional information, e.g. β-sheet-like structures or intermolecular interactions.*

The combination of COSY and TOCSY already allows the determination of the sequential connectivity between two amino acid residues, leading to the elucidation of the peptide sequence. The additional analysis of NOESY and ROESY experiments may then reveal characteristic patterns of short distance interactions, corresponding to various structural motifs, such as α-helixes or β-sheets. Especially interesting is the fingerprint region of the 2D spectra where the $C_\alpha H$–NH correlations can be found.

In summary, the broad choice of NMR experiments permits an in-depth analysis of the three-dimensional structures of peptides and small proteins in solution. Within the last two decades important methodological developments were observed for the determination of complex structures. Just recently even a new high-resolution in-cell NMR technique was introduced, which enables observations of conformations and functions of proteins in living cells.[46] These developments point out how potential and powerful NMR spectroscopy can be. However, one drawback of NMR spectroscopy for the determination of peptide structures and supramolecular investigations is the requirement of a significant sample amount and a compatibility with deuterated solvents, which may limit the applicability of the technique to some systems. Hence, the following section will focus on an alternative method for the structure determination.

3.1.2 Raman Spectroscopy

In addition to NMR, the formation of supramolecular complexes between a host and a guest can be monitored by a variety of spectroscopic techniques, such as electronic absorption or fluorescence spectroscopy.[47–49] With these methods, however, it is difficult to obtain information about the structure of the complex or the non-covalent interactions responsible for substrate binding. In contrast, Raman spectroscopic techniques are capable of probing both structure and dynamics of molecular systems.[50,51] Applications cover, for example, proteins and hydrogen-bonded mixtures.[52,53]

Raman spectroscopy takes advantage of Raman scattering, discovered by C. V. Raman in 1928.[54] Raman scattering, also referred to as inelastic light scattering, is caused by the interaction between the optical oscillations of light with the vibrational motion of molecules. In many aspects it is similar to IR spectroscopy, but has its individual features. When incident photons interact with molecules, they can either be absorbed or scattered. The majority of the light is reflected back at the same wavelength in an elastic type of scattering (Rayleigh scattering). However, a smaller portion of the light is scattered at either a lower or higher energy than the incident light (Stokes and anti-Stokes scattering, respectively). With Stokes and anti-Stokes scattering, the electrons are excited into a virtual state. This virtual state, however, is not a true quantum state; rather this virtual state can be regarded as a momentary distortion in the electron distribution. Hence, Raman spectroscopy is the measurement of the intensity and frequency of this inelastically scattered light. Raman scattering can occur due to changes in vibrational, rotational, or electronic energy of a molecule.

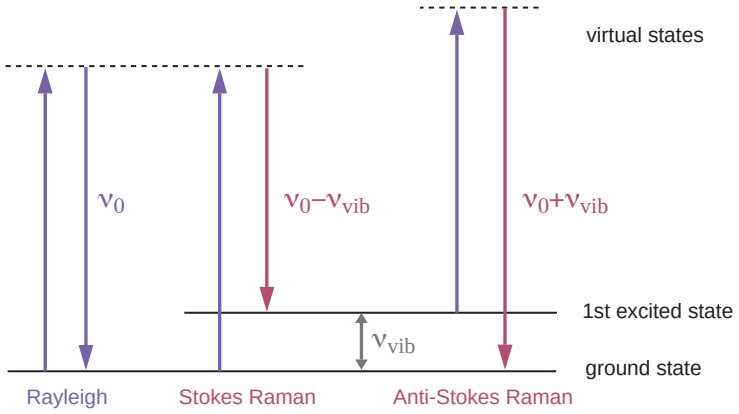

Figure 3.3: *The Stokes-Raman effect results from a transition from the ground energy level to a higher one, whereas the anti-Stokes effect has the opposite transition. The anti-Stokes intensity is less than the Stokes intensity because the anti-Stokes scattering occurs from an excited state, which is, according to the Boltzmann distribution, less populated than the ground state.*

Although Raman scattering was discovered in 1928, it has become a convenient and available technique only in the last two decades. The detection of the Raman signals—compared to other optical signals—is a difficult task. In general, the scattering is a relatively weak process and the number of photons Raman scattered is quite small. However, there are several processes which can be used to enhance the sensitivity of Raman measurements.

One possibility is the resonance Raman effect, that can be observed when the used laser wavelength is close to the absorption wavelength of the molecule required for an electronic excitation.[55,56] Often Resonance Raman scattering is observed when the laser excitation coincides with an electronic absorption of a chromophore. Upon electronically resonant excitation, normal modes of the corresponding chromophore are selectively enhanced resulting in strongly increased intensities (up to 10^6 times stronger than normal Raman scattering).[57] For example, this occurs in biological chromophores such as porphyrins for a laser excitation in the visible spectral region.[51,58] Hence, one advantage of this method is the selective amplification of the chromophore bands, without spectral interference from the surrounding environment. For example the same analyte can produce different Raman spectra depending on the excitation wavelength, especially if different segments of the molecule have different absorption bands. This leads in some cases to a tremendous simplification of the obtained spectra due to the fact that the part of the molecule without chromophore has almost no spectral contributions. The second advantage of this method is, that it permits the analysis of molecules even at very low concentrations where "normal" Raman spectroscopy can not operate. However there are also disadvantages, such as "fluorescence noise" which can interfere with the Raman signals, and the destruction of the compounds due to photo reactions and the development of heat.

Another relatively new technique for the enhancement of the Raman signals is the surface enhanced Raman spectroscopy (SERS). It combines the advantages of Raman spectroscopy with surface selectivity and ultra-sensitive detection employing noble metal nano-structures.[59–62] First surface-enhanced Raman scattering (SERS) observation was made by *Fleischmann et al.* on the pyridine molecules adsorbed from aqueous solution onto a roughened silver electrode in 1974.[63] It produced a Raman spectrum that is at times a millionfold more intense than expected. Since then the effect has been demonstrated with many molecules and with a number of different metals. All experiments showed that in particular noble metal nanoparticles tremendously enhance Raman signals up to a factor of 10^{14} but only of those molecules which are close to their surface

as the SERS effect falls off with r^{-10}. Different models were proposed to explain the enhancement mechanisms of SERS. The first is based on an electromagnetic enhancement mechanism produced by an exceptionally large electromagnetic field at the surface of the metal. The second explanation, known as the chemical enhancement, is based on an assumption of a charge transfer interaction between the metal and the adsorbed molecules.

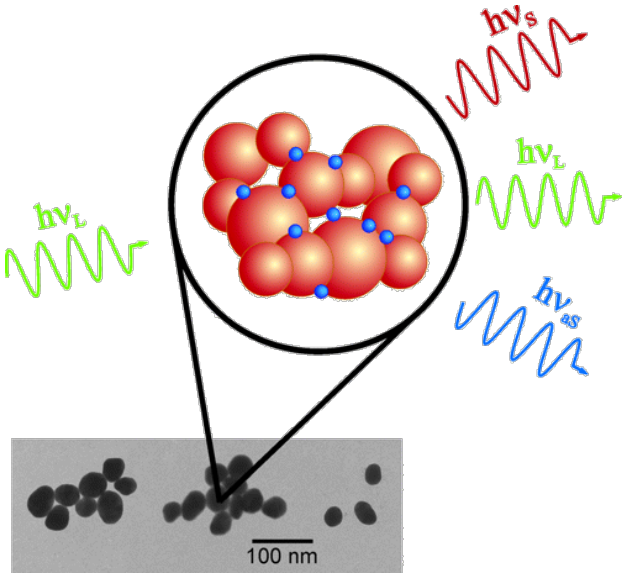

Figure 3.4: *Schematic of a surface enhanced Raman scattering experiment. Molecules (blue dots) are attached to metal nanoparticles (orange balls). Upon laser excitation elastic ($h\nu_L$) and inelastic scattering ($h\nu_S$, $h\nu_{aS}$) can be observed with tremendously increased signal intensity.*[306]

The applications of SERS have been successfully extended to many fields including the study of biological samples such as DNA, peptides and proteins.[60,64] Although the theoretical understanding of the mechanism of surface enhancement is not definite and still evolving, the experimental data accumulated in the last years has demonstrated SERS to be a sufficiently sensitive spectroscopic method for surface science, analytical applications and biophysics, thus it is a valuable microanalytical tool.

In summary, Raman spectroscopy is—in comparison with NMR spectroscopy, which is only very powerful in solution—more versatile and thus a perfect tool for structure determination. Especially signal enhancing approaches like SERS even allow experiments in alternative environments, such as organic materials, human tissue or polymeric surfaces. Due to the selective detection of vibrational modes it is possible to probe both structure and dynamics of molecular systems, thus making Raman spectroscopy ideally suited for the analysis of supramolecular structures.

3.2 The Advantages of Multivalency

The principle of multivalency is a general concept that is widely spread and utilized in nature and is fundamental for the regulation of many critical biological systems.[10] One of the reasons multiple binding interactions have evolved in nature is to increase the overall strength of interactions between a ligand, usually a low molecular weight species and its receptor, typically a high molecular weight entity, such as enzymes or nucleic acids. Multivalent interactions dominate many important biological processes, e.g. the binding of cells to other cells or bacteria,[65,66] the extremely stable antibody-antigen interaction,[67] but also the interaction of transcriptions factors with multiple sites on the DNA,[68] or the process of carbohydrate-binding at proteins.[69–71]

A typical example represents the first step of an influenza infection, when the virus attaches to the surface of a bronchial epithelial cell.[72] The multivalent attachment occurs by the interaction between multiple trimers of hemagglutinin, a lectin that is densely packed on the surface of the virus and multiple moieties of N-acetylneuraminic acid, the terminal sugar on many glycoproteins on the surface of the target cell (Figure 3.5).

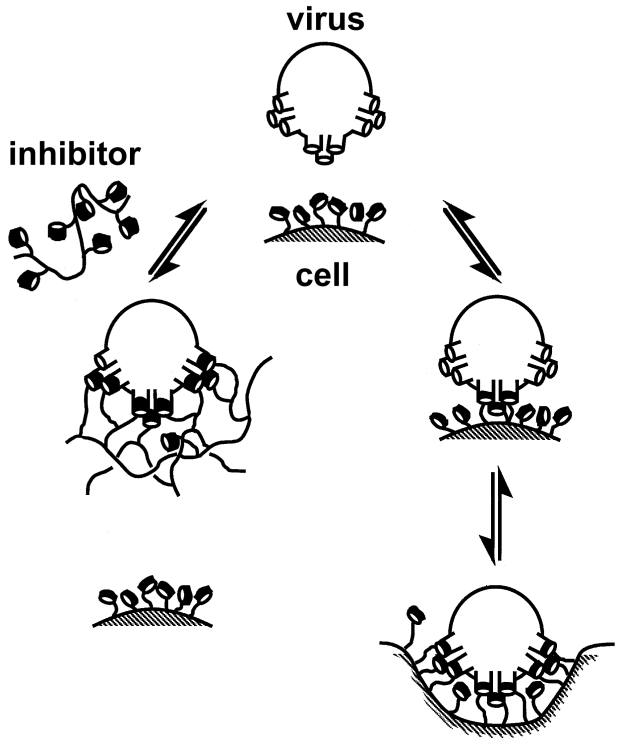

Figure 3.5: *Example of a multivalent interactions in biological systems: The influenza virus attaches to cells by an interaction of trimeric hemagglutinin with several entities of sialic acid on the cell surface. Multivalent inhibitors can prevent the docking to the cell surface.*[307]

One way to inhibit this interaction is the use of polyacrylamide presenting multiple sialic acid groups. This polymeric inhibitor functions through several mechanisms such as high-affinity, entropically enhanced binding, and steric blocking.[72]

In recent years the principle of multivalency attracted much attention in supramolecular chemistry. The aim is to mimic nature and apply this approach to improve the binding between molecular species through non-covalent interactions.[15,16,73] Scientists start to take advantage of this concept as a powerful method to replace some of the previous strategies to enhance the binding efficiency and selectivity of designed ligands. Chemists usually tried to optimize the complementary matching—in terms of size and nature of binding forces—between interacting species. In contrary, multivalency takes advantage of the relative ease of multiplying the number of already existing interactions.

On the basis of research in the literature it seems that the term *multivalency* as used in biological and organic context observes substantial similarities with the expression, long known in inorganic chemistry as *chelate effect*.[73] In general, multivalency can be described as multiple simultaneous non-covalent interactions resulting—compared to the sum of monovalent interactions—in much higher thermodynamic and kinetic stability. In most synthetic supramolecular systems complementary interacting functionalities are referred to as *host* and *guest*, whereas often for the description of biologically related systems the equivalent nomenclature *receptor* and *ligand* is preferred. The interaction between a host and a guest, based on entities bearing complementary functionality, leads to the formation of a complex. The valency of an entity is defined as the number of possible separate interactions of the same kind that it can form, whereas the valency of the complex can be described by the number of shared interactions between the two interacting species. This leads to the definition of multivalent systems which involve at least *two* non-covalent host-guest interactions (Figure 3.6)

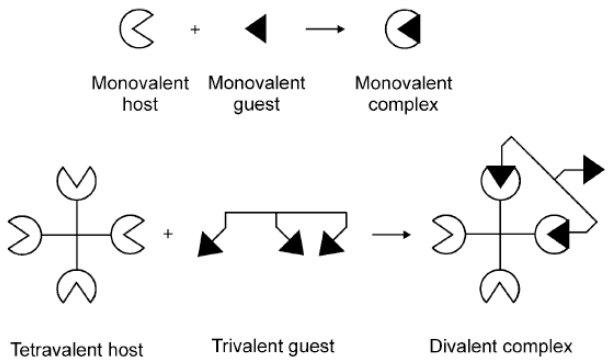

Figure 3.6: *Terminology and examples of mono- and multivalent interactions.*[308]

In most cases, a multivalent compound consists of a main core or scaffold, bearing several covalent linkers or spacers to the peripheral binding units. Hence, the activity of the multivalent agent critically depends on the scaffold, as it controls the spatial orientation of the functional groups. Many different types of multivalent ligands have been introduced within recent years,[74] starting with small molecules bearing low valency, such as benzene derivatives,[75] monosaccharides,[76] transition metal complexes,[77] azamacrocycles, cyclodextrins[78] or calixarenes.[79] This class is often of low molecular mass (<1000 Da) and typically only displays a few recognition elements (<5). Examples of higher valency include dendrimers,[80] polymers,[81] peptoids, proteins, micelles,[82] liposomes and self-assembled monolayers on nanoparticles or plane surfaces.[83]

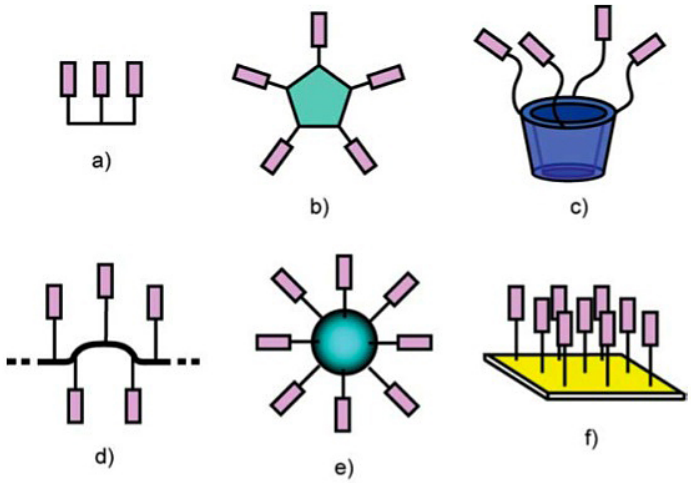

Figure 3.7: *Different possibilities for the design of multivalent scaffolds. The structures include one- to three-dimensional formations with a variety of valencies.*[309]

However, multivalency is not to be confused with cooperativity, which refers to the principle of mutual intensification or weakening of binding sites.[15,73,84] Cooperativity describes the effect of how the binding of one guest molecule influences the affinity of a host system toward further binding interactions. Hence, the stepwise binding effects of monovalent guest molecules are in the focus and not the overall binding affinity. Cooperative effects can be classified into three groups: a) positive (synergistic), when the subsequent binding affinity of another molecule is higher than that for the previous one; b) negative (interfering), when the binding is lower, and c) noncooperative (additive), when the binding is identical. The concept of cooperativity also plays an important role in self-assembly processes.[84]

One of the most prominent examples for cooperativity is the binding of oxygen by the tetrameric hemoglobin.[85–88] This tetrameric protein is capable of binding four individual oxygen molecules, one in each heme-group. If one subunit protein in hemoglobin becomes oxygenated, a structural change in the whole complex is induced, causing the other subunits to gain an increased affinity for oxygen. Hence, the sequential occupation of all four binding sites can be described in a positively cooperative manner. This is also a typical example of allosteric regulation, which describes in general the regulation of an enzyme or protein by the binding of an effector molecule to a site of the protein other than the active site.

Other examples include positively cooperative systems, in which the occupation of one binding center—often with metal ions—increases the affinity at a second center through conformative coupling within the host molecule. Some of these supramolecular allosteric systems can be regarded as simple ON or OFF switches.[89] For example *Schneider et al.* presented a simple model, in which the occupation of a polar site by a metal ion leads to the closing of a hydrophobic pocket. This causes the formation of a hydrophobic binding site, in which a lipophilic guest molecule can be complexed, even in water (Figure 3.8).[90]

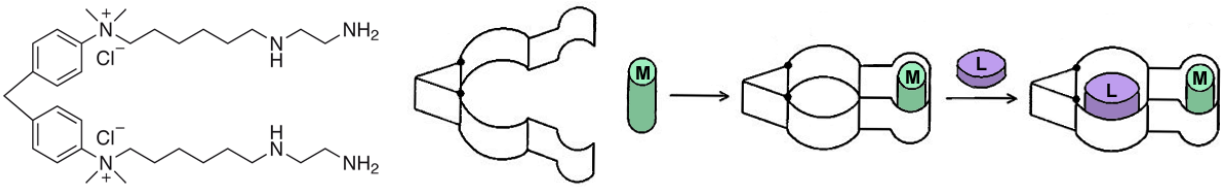

8

Figure 3.8: *Binding of metal ions (M) at the ethylendiamine unit of* ***8*** *leads to a closed cavity and thus to an allosterically controlled and positively cooperative binding of lipophilic substrates (L).*[310]

In conclusion, cooperativity describes the synergistic (or interfering) effects of stepwise binding events. In contrast, multivalency discusses the increased binding affinity through multiple interactions of matching binding centers. This is a result of small and individual contributions that lead to much higher thermodynamic and kinetic stability, than the sum of the monovalent interactions. It is important to mention that both effects do not exclude each other. In many cases, cooperative systems are also multivalent systems. However, in comparison only few multivalent systems show also cooperative effects.

In order to describe the thermodynamic aspects of multivalent binding, an approach based on the additivity of the Gibbs free energies (G°) can be used. The standard free energy for multivalent binding ΔG°_{multi} can be defined as:

$$\Delta G^\circ_{multi} = n\Delta G^\circ_{mono} + \Delta G^\circ_{interaction} \tag{3.1}$$

where $n\Delta G^\circ_{mono}$ is the standard free binding energy of the corresponding monovalent interaction, n is the valency of the complex and $\Delta G^\circ_{interaction}$ is the balance between favorable and unfavorable effects of tethering. Hence, one observation of the multivalent effect is a higher binding energy than expected by the sum of individual affinities.

The affinity constant K_{multi} is defined as the binding strength of the multivalent complex and takes all possible interactions between two multivalent entities into consideration. It is related to the free energy of the association (ΔG°_{multi}) by the Gibbs equation:

$$\Delta G^\circ_{multi} = -RTln(K_{multi}) = \Delta H - T\Delta S \tag{3.2}$$

To describe the thermodynamics of multivalent interactions more precisely, *Whitesides et al.* introduced the parameters α and β, where α is the cooperativity factor and β is an enhancement factor.[10] In estimating the cooperativity in multivalent associations, the free energy of multivalent binding (ΔG°_{multi}) can be related to n monovalent interactions, each represented by ΔG°_{mono}. The ratio between both parameters is an indication of the cooperativity and leads to the following definition of α:

$$\alpha = \frac{\Delta G^\circ_{multi}}{n\ \Delta G^\circ_{mono}} \tag{3.3}$$

Depending on the magnitude of α, multivalent interactions can be—as previously mentioned— positively cooperative ($\alpha > 1$), negatively cooperative ($\alpha < 1$) or only additive ($\alpha = 1$). However, determination of α values requires knowledge about the number of guests which are actually bound, which is in many instances not known. In addition, the term cooperativity is rarely used in multivalent systems, partly because only few of them have been shown to demonstrate positive cooperativity. Hence in practical terms, the contribution of the multivalent phenomenology is often expressed with the enhancement factor β:

$$\beta = \frac{K_{multi}}{K_{mono}} \tag{3.4}$$

This parameter reflects the strength of a multivalent association compared to a monovalent interaction and is often used in the literature to compare the efficiency of guests with different structure or valency. Molecules with a high β factor are more efficient then these with a lower one.

One example that impressively illustrates the advantages of multivalency and demonstrates the difference between α and β is a trivalent host-guest system developed and thoroughly investigated by *Whitesides et al.*[91] They systematically studied the interaction between mono- and trivalent derivatives of vancomycin and mono- and trivalent peptides sequences of D-Ala-D-Ala (DADA), to provide insights into the underlying principles of multivalency (Figure 3.9). Vancomycin is an antibiotic that targets bacterial cell walls by binding tightly to the peptide sequence D-Ala-D-Ala.

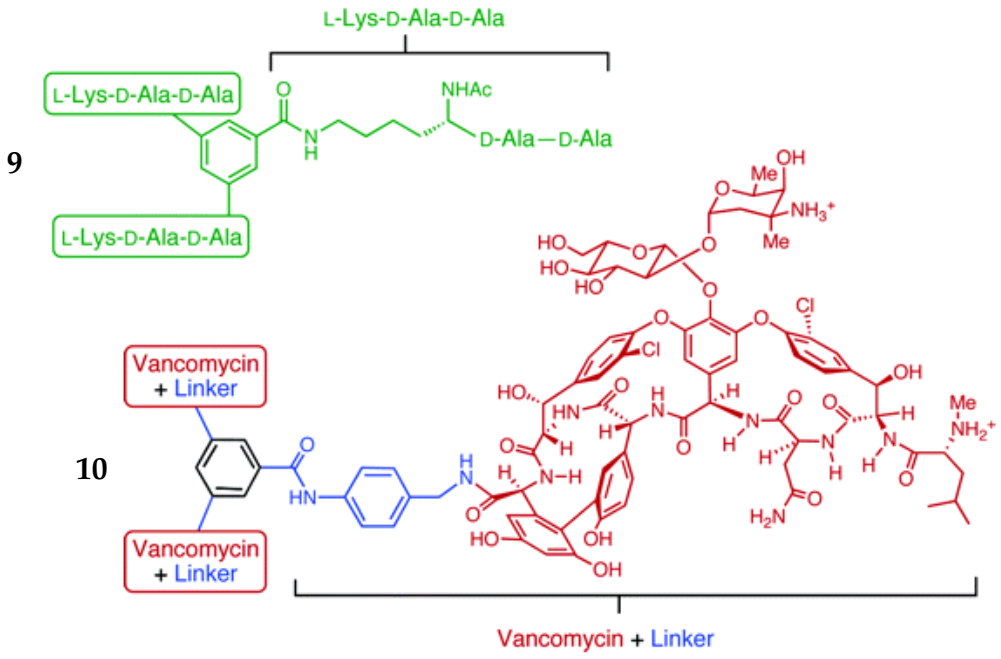

Figure 3.9: *Trivalent vancomycin host (**10**) and trivalent guest* D-*Ala*-D-*Ala (**9**) Each Vancomycin subunit is able to form five hydrogen bonds to* DADA.[311]

The monovalent vancomycin associates with the monovalent model peptide DADA with an association constant (K_a) of 6.3×10^5 M^{-1} in phosphate buffer at pH 7.0, while the trivalent system composed of trivalent vancomycin and trivalent DADA binds ex-

tremely tight in a 1:1 complex (see Figure 3.10) with a K_a of 2.5 $\times$ 10^{16} M^{-1}. The experiments revealed that the cooperativity constant α was 0.95, thus slightly negative cooperative but exceptionally tight. However, looking at the enhancement of binding affinity (factor β) the trivalent complex was binding 4 $\times$ 10^{10} times stronger than the corresponding monovalent complex. The binding strength is even 25 times higher than the biotin-streptavidin complex, which is considered to be the strongest non-covalent interaction known in nature (cf. Figure 3.11 on page 26).[92,93]

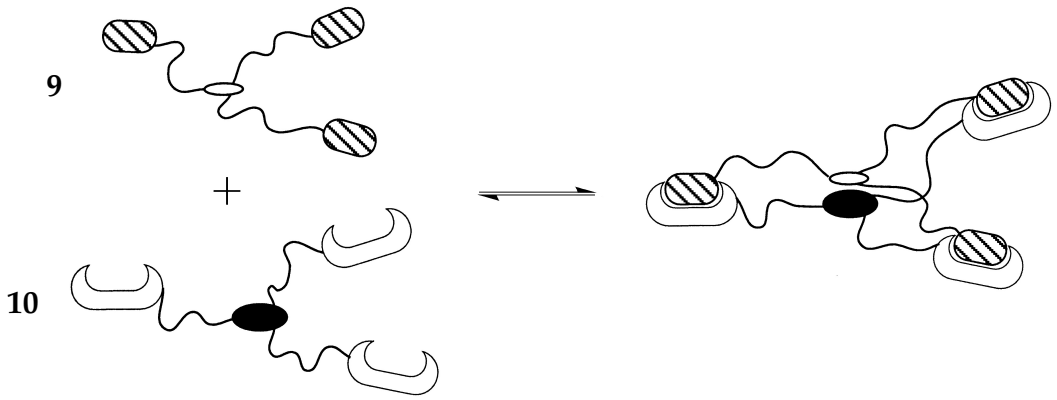

Figure 3.10: *Schematic illustration of the trivalent interaction studied by Whitesides et al. resulting in very high binding affinity.*[312]

In summary, the latter example clearly demonstrates the advantages and the practical value of multivalent systems for the design of high-affinity systems. The principle of the multivalency, the simultaneous involvement of multiple and complementary binding sites, can lead to highly efficient molecular associations, e.g. interesting for the development of effective biomimetic drugs or supramolecular nano-materials.

3.3 Molecular Recognition in Biological and Artificial Systems

The key principle of molecular recognition is based on non-covalent interactions, such as hydrogen bonds, coulomb-, and π-stacking forces as well as charge-transfer interactions. Especially proteins and enzymes utilize these interactions and form powerful complexes with substrates and ligands. One of the strongest and best known complex of a protein and a relatively simple organic molecule is the biotin binding to streptavidin (see Figure 3.11).[92,93] The dissociation constant for this complex with the small biotin molecule is with 10^{-15} M remarkable high.

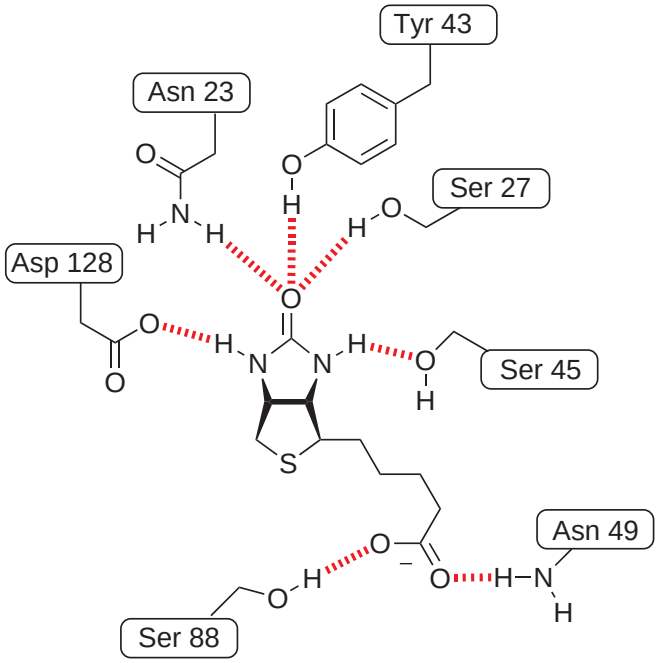

Figure 3.11: *The protein streptavidin (schematic representation of seven amino acids of the specific binding pocket) forms a strong complex with biotin (in the center), due to a series of specific hydrogen bonds, polar interactions and a overall perfect steric fit to the protein.*

The research on synthetic complexes by far is not as advanced as the natural model and concentrates on smaller and more controllable systems, such as calixarenes,[79] cyclodextrins,[94] and aromatic capsules.[95] Most synthetic receptors[96] focus on the recognition of simple metallic ions, single amino acids and nucleotides as well as sugars, but also on more complex structures such as biopolymers[97] and oligopeptides.[98]

The following chapter will present some interesting examples how chemists examine the interaction between small molecules and artificial as well as biological relevant structures. The huge diversity of discoveries due to the success of this research field in recent years does not allow a complete survey. Hence, the subsequent review sections will provide a short overview and will focus on the latest and most important results of molecular recognition events which are related to this thesis.

3.3.1 The Interaction of Small Molecules with Amyloid Fibrils

Amyloid fibrils have been implicated in numerous human diseases. One of the most prominent is the *Alzheimer's* disease (AD), a neurodegenerative disorder characterized by progressively worsening dementia. It is widely accepted that amyloid-β peptide (Aβ) aggregates play a central role in the progression of AD.[99,100] These specific Aβ assemblies contain 4-kDa peptides of different length, which are formed during the enzymatic cleavage of the amyloid precursor protein (APP).[101] The cleavage peptides are varying between 39 and 43 amino acids and have a free C-terminal end. Aβ (1–40) is with approximately 90 % the most prevalent species, but Aβ (1–42) is more toxic.[102,103]

Amyloid fibrils show a three-dimensional structure that is dominated by a β-sheet structure, in which the strands run perpendicularly to the fibril axis. Examination of the morphology by electron microscopy and atomic force microscopy has revealed that the fibrils are long, straight and unbranched. The fibril itself consists of parallel β-sheets that are formed by the peptide residues (Figure 3.12 on page 28).[104,105] However, not all structural details of the amyloid fibrils are completely known.

One potential therapeutic approach is to prevent the assembly of the β-sheets thus hindering the emerging of the amyloid fibrils. Short peptides and small molecules can influence the structure and aggregation of Aβ, and these are effective neuroprotective agents. So-called β-sheet breakers are small peptides, partially homologous to the Aβ peptide, which can intervene in the interactions between the β-sheets.[106] These peptides have been shown not only to inhibit the formation of amyloid fibrils but also to reduce them.

Another approach for a possible treatment is based on the inhibition of binding interactions between amyloid binding proteins and the fibrils. There are strong indications

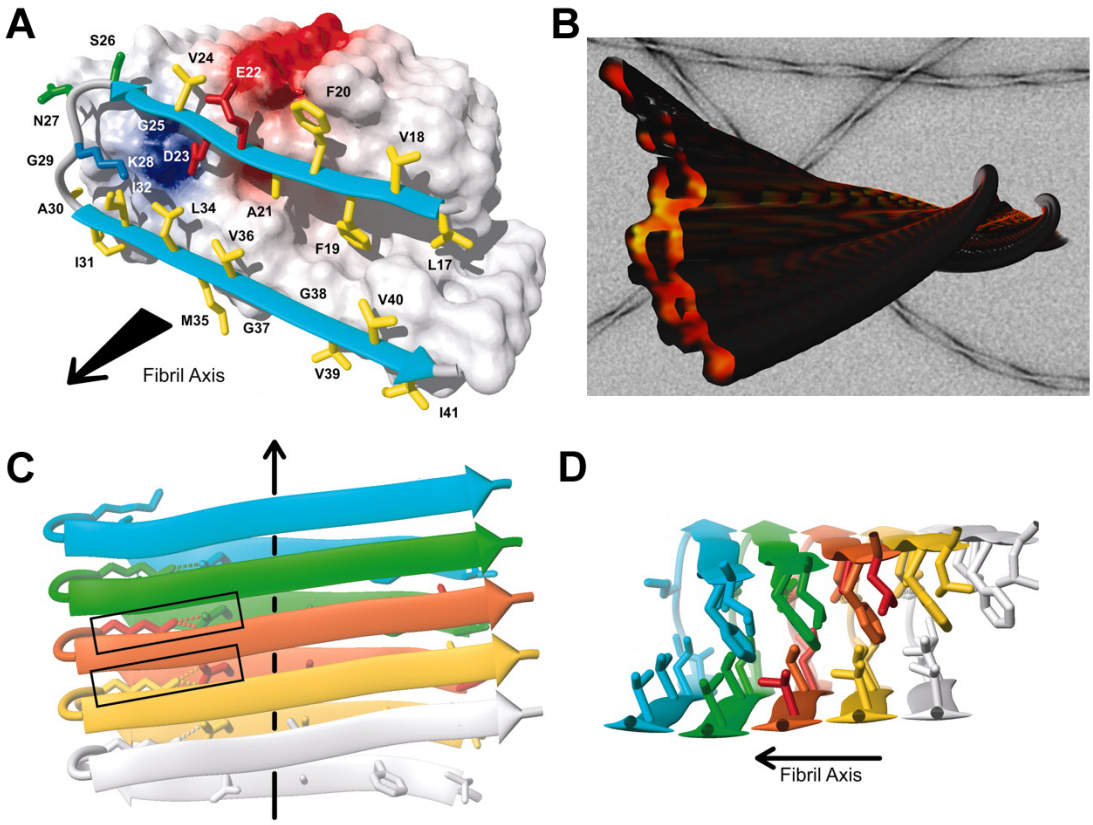

Figure 3.12: *Possible schematic representations of Aβ (1–42) fibrils. Ribbon diagrams of the core structure of residues 17–42 illustrating the intermolecular nature of the parallel β-sheets interactions.*[313]

that one possible cause for the development of AD are not only plagues but also potential contributions of Aβ-induced neurotoxicity. Especially worth mentioning is the interaction of Aβ peptides, oligomers, and fibrils with cellular proteins such as catalase[107] or ABAD.[108] Hence, *Yang et al.* developed a concept for generating protein-resistive coatings on the surface of Aβ fibrils. Therefore, several small molecules that bind tightly to the surface of the fibrils were investigated in an ELISA based assay (Figure 3.13 on page 29).[109] One of the molecules, which is known to specifically bind all kinds of amyloid structures with high affinity, was thioflavine T (ThT). It is normally used in diagnostics to detect amyloid in histological tissue samples.[110,111] With this new screening assay it was possible to show that ThT can inhibit 65±10 % of Aβ-fibril interactions with Aβ-binding IgGs by binding and coating the surface of these fibrils. In addition, the interactions of ethylene glycol-functionalized derivatives of ThT[112] and completely structural different molecules were successful tested with this assay.[113]

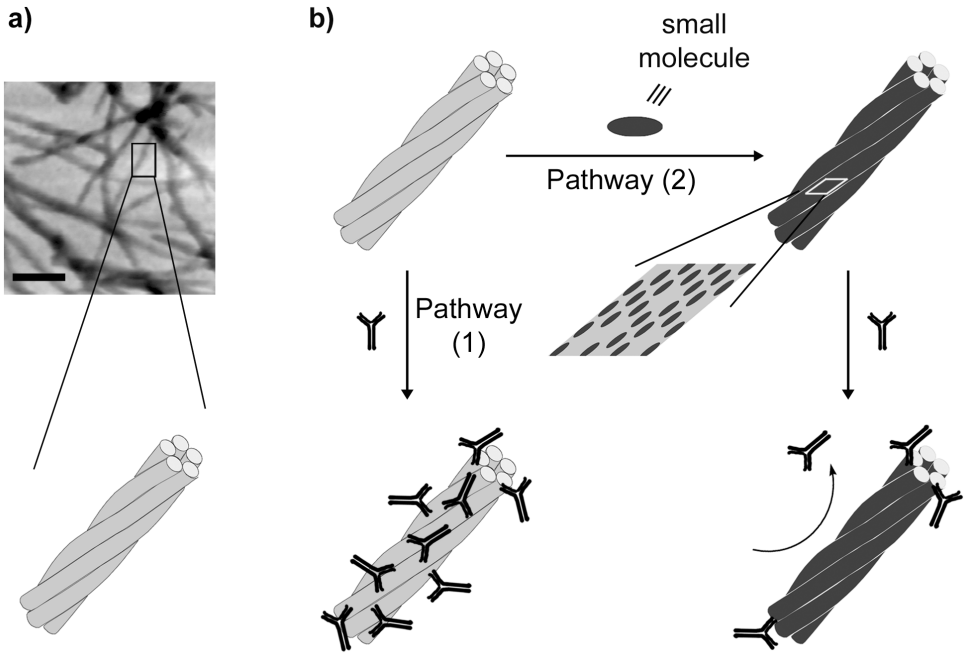

Figure 3.13: *Illustration of the inhibition of IgG-amyloid interactions by coating surfaces of Alzheimer's-related Aβ fibrils with small molecules.*[314]

In summary, the significant advantages of this assay are the ability to screen structurally diverse molecules without requiring them to have specific spectroscopic or radiolabeled properties, the ability to estimate the percentage of the surface of the fibrils covered by the small molecules, and the ability to detect the association of small molecules that potentially bind to different sites along the fibril axis.

The literature also mentions several multivalent approaches for the blocking of Aβ-oligomer aggregation and as useful imaging agents for the disease.[114] It has been reported that Aβ-fibrils have several binding sites,[115] thus multivalent molecules which bind simultaneously to different binding sites are expected to have higher potency. Therefore , multivalent and multifunctional Aβ ligands offer an alternative route by enhancing binding affinity of drug candidates and imaging agents.

Chafekar et al. adopted this approach and studied a dendrimeric scaffold with four side chains containing the pentapeptide KLVFF, which is known to inhibit the formation of amyloid fibrils (Figure 3.14 on page 30).[116] Based on ThT analysis, it was shown that the tetravalent molecule **12** inhibited Aβ aggregation from oligomeric Aβ(1–42) in a concentration-dependent manner. Compared to the monomeric form (**11**), the branched version (**12**) was highly effective in the inhibition of fibril aggregation.[117]

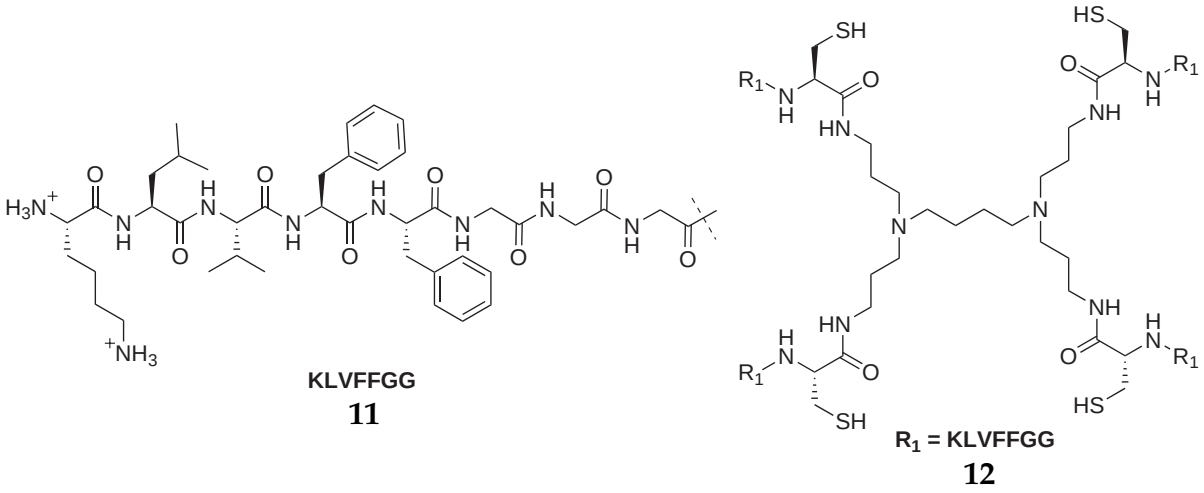

Figure 3.14: *Multivalent structure containing the pentapeptide KLVFF (with GG as spacer) that binds to the amyloid fibrils and inhibits the aggregation.*

But already small and tailor-made peptides can show high specificity to inhibit the amyloid fibril formation. *Schmuck et al.* developed artificial receptors for the molecular recognition of the anionic tetrapeptide L-Val-L-Val-L-Ile-L-Ala-OH (**14**), a model for the C-terminus of the amyloid-peptide Aβ (1–42). The receptors consist of linear tripeptides with additional cationic guanidiniocarbonyl pyrrole groups (CBS = Carboxylate Binding Site), which is one the most efficient binding motifs so far known for the complexation of carboxylates in polar solvents.[118–122] By using a combinatorial receptor library (**13**) and a UV binding assay, efficient receptors for the binding of VVIA under various conditions were identified.

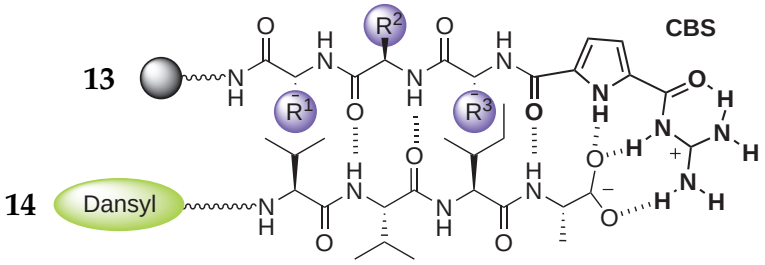

Figure 3.15: *The screening of a combinatorial tripeptide-based library of cationic guanidiniocarbonyl pyrrole receptors (**13**) revealed strong binders for the model substrate* L*-Val-*L*-Val-*L*-Ile-*L*-Ala-OH, a tetrapeptide representing the C-terminus of Aβ.*

The best receptors showed binding constants up to $K = 5 \times 10^3$ M^{-1} in water for this model peptide.[5,123] Additional *in vitro*-studies revealed that these specifically designed artificial receptors are also capable to inhibit the fibril formation of Aβ (1–42).[124]

3.3.2 Oligopeptides with Translocational and Antimicrobial Activity

There are many bioactive molecules with physicochemical properties which can not cross biological membranes, such as proteins, oligonucleotides, liposomes, many drug classes and non-covalent supramolecular structures. It is generally known that the cell membrane allows by passive diffusion only the entrance of hydrophobic molecules. Hence, many drug candidates with promising in vitro activities fail to be developed into useful pharmaceutical agents due to their poor bioavailability.

In recent years, a new strategy has been developed to use membrane-permeable peptide carrier vectors to deliver various kinds of molecules into cells.[125–130] They all have peptide sequences in common which are derived from HIV-1 Tat[131] and *Drosophila Antennapedia* homeodomain proteins.[132] HIV-1 trans-activator of transcription (Tat) is a protein consisting of 86 amino acids and is essential for the HIV-1 replication. It was found, that this protein was rapidly taken up by cultured cells. Detailed investigations revealed, that an arginine-rich segment in the protein at position 49–57 (RKKRRQRRR) is the important component for translocation.[131] This is in particular remarkable because even the artificial Tat nonamer, which bears eight positive charges, is highly water soluble yet paradoxically passes readily through the nonpolar membranes of cells and also enters tissues. Similar properties were found for short basic domains in the *Drosophila Antennapedia* proteins.

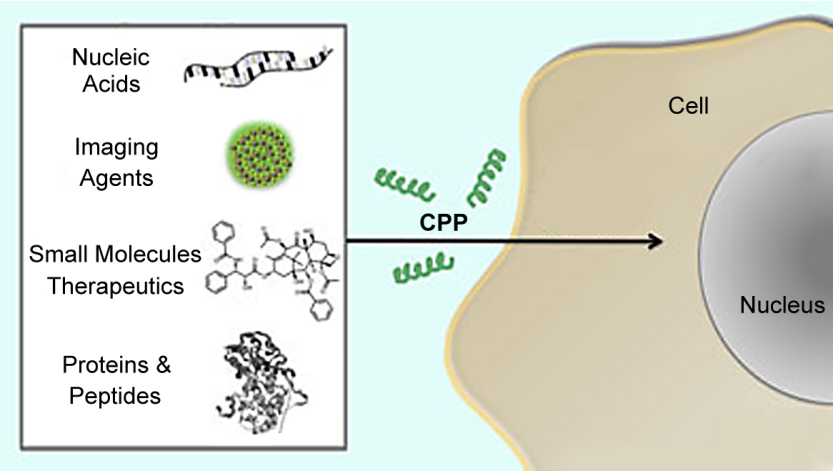

Figure 3.16: *The cell-penetrating peptides (CPP) are membrane-crossing molecules with the potency to transport various kinds of compounds over the cell membrane.*[315]

Starting with these discoveries, a new class of cell-penetrating peptides (CPP) has emerged with high potential to deliver various molecules into cells. All of these natural and synthetic CPP analogs showed an amphipathic structure containing basic and hydrophobic amino acids. Apparently, a high density of positively charged side chains appears to be the most important feature for enhanced cellular uptake efficiency. Especially the guanidino function in arginine residues played an important role in the translocation. It was also reported that oligomers of β-amino acids[133] and peptoids[134] bearing guanidino moieties were able to translocate through cell membranes (Figure 3.17).

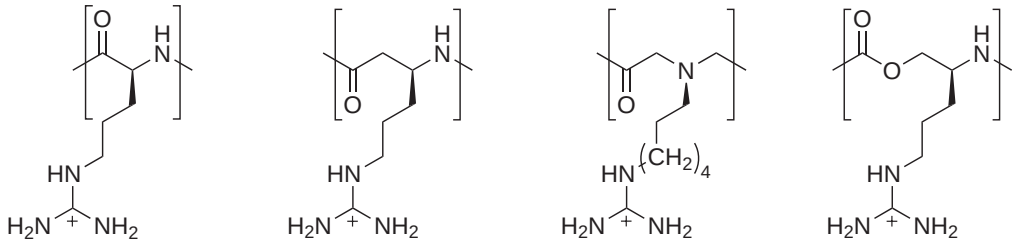

15 **16** **17** **18**

Figure 3.17: *Different structures of carrier units bearing guanidino functions.*

It was also shown that branched peptides rich in arginines, such as $(R_2)_4$ and $(R_1)_8$ also had the ability to internalize into cells (Figure 3.18).[130] Fluorescence microscopic observation showed that the $(R_2)_4$ peptide with a total number of eight arginine residues entered the cells as efficiently as the linear R_8 peptide. However, an increased amount of additional guanidino functions seemed to have no additional enhancement effect.

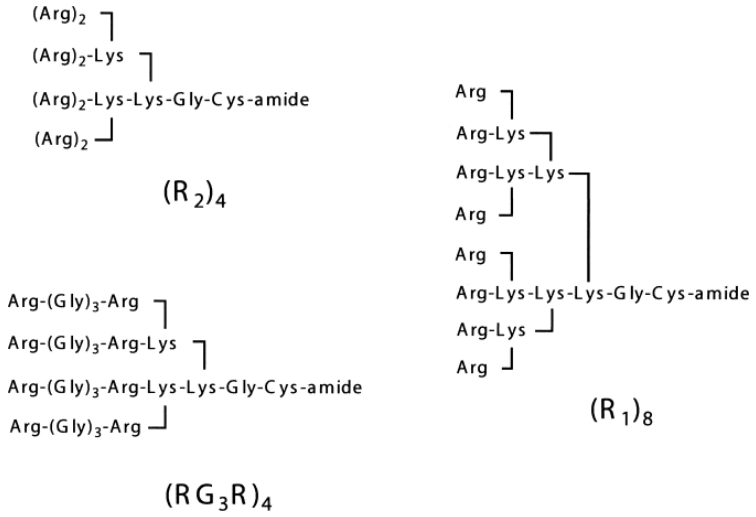

Figure 3.18: *Branched arginine-rich peptides can also translocate into cells.*

These dendritic molecules are very efficient as molecular transporters. *Sugiura et al.* showed that the $(R_2)_4$ peptide, chemically conjugated with the fluorescein-labeled carbonic anhydrase (CA), can easily enter cells and translocate the 29 kDa protein.[130]

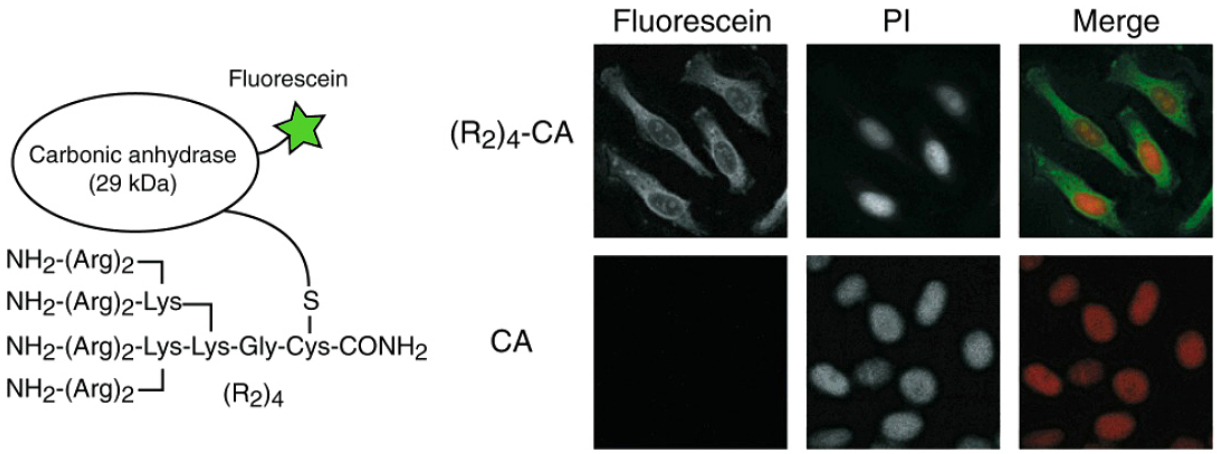

Figure 3.19: *Schematic representation of a branched arginine peptide conjugated to a small and fluorescence labelled protein (CA). Confocal microscopic analysis demonstrated a predominant cytoplasmic localization (green). The nucleus is stained in red for comparison.*[316]

However, it is still not clear why such basic and hydrophilic peptides can enter the cells so efficiently. The complete details of the internalization mechanism are still not known. Today, two distinct processes are under discussion: endocytosis and the direct translocation through the lipid bilayer.[125,135,136]

The previous examples showed, that peptides with guanidinio groups are perfect transporters and possess an unique interaction potential with molecular membranes. Especially the combination of CPPs with imaging labels is an interesting effort to optimize aspects of *in vivo* fluorescence imaging. Several fluorescence active biomarkers, such as fluorescein, rhodamine or dansyl are known and were successfully applied (Figure 3.20).[137]

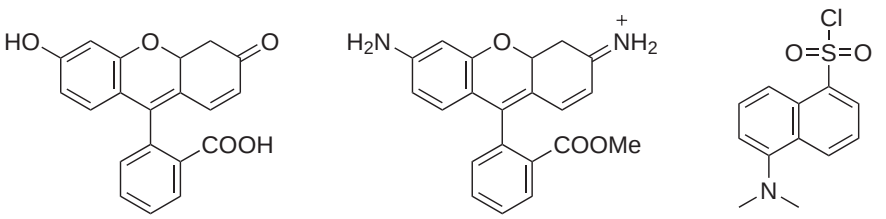

fluorescein **19** | rhodamine **20** | dansyl chloride **21**

Figure 3.20: *Selection of fluorophores commonly used as molecular probes.*

Fluorescent probes can also be used for the optical imaging of bacterial infections, which has many health and environmental applications. *Smith et al.* investigated the combination of near-infrared dyes with zinc-based affinity groups for the selective recognition of bacterial versus mammalian membranes.[138–141] This selectivity is very important, for example for the development of antimicrobial drug candidates. They discovered that zinc(II)coordination complexes with dipicolylamine ligands (**22**) exhibit a remarkable selectivity and affinity for anionic cell membranes, allowing even an *in vivo* bacterial detection (Figure 3.21).

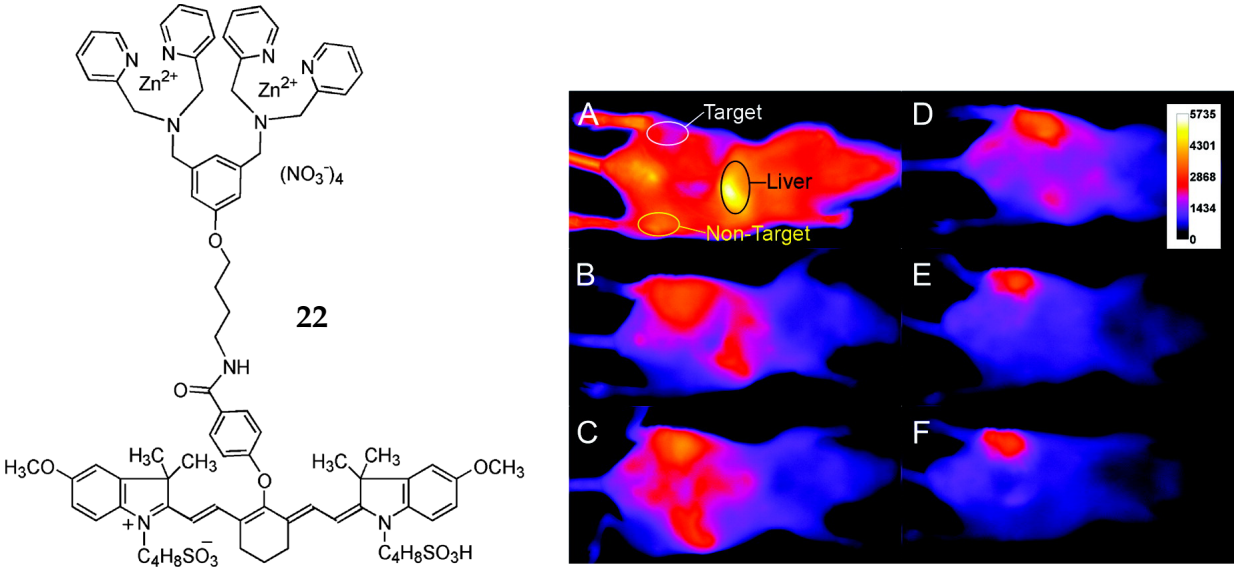

Figure 3.21: *Zn-DPA affinity group for bacteria cell wall targeting attached to a carbocyanine dye as fluorophore (left); Optical images of a mouse with a S. aureus infection in one leg. The images were taken over 21 hours after the intravenous injection of* ***22*** *and illustrate an accumulation in the area of infection (right).*[317]

This selective targeting—in particular the staining of the membranes—is possible, because the cationic molecules are electrostatically attracted by the bacterial cells. Their membranes differ from mammalian cells which contain primarily zwitterionic phospholipids and thus have a near-neutral charge.[142] In contrast, a characteristic feature of nearly all bacterial membranes is the negative surface, resulting from anionic phospholipids and related amphiphiles.[143] For example, the plasma membrane which surrounds the Gram-positive bacterium *Staphylococcus aureus* is composed of approximately 75% anionic phosphatidylglycerol. Extending from this membrane are anionic glycerophosphate polymers called teichoic acids that weave through and anchor the surrounding peptidoglycan cell wall.[144] Gram-negative bacteria such as *Escherichia coli* are

differentiated by the presence of a second outer bilayer membrane. The external leaflet of this outer membrane is composed of lipopolysaccharides whose core structure, known as lipid A, contains two anionic phosphates.[145] Also, whereas in Gram-positive bacteria the peptidoglycan is heavily cross-linked, it is only intermittently cross-linked in Gram-negative bacteria.

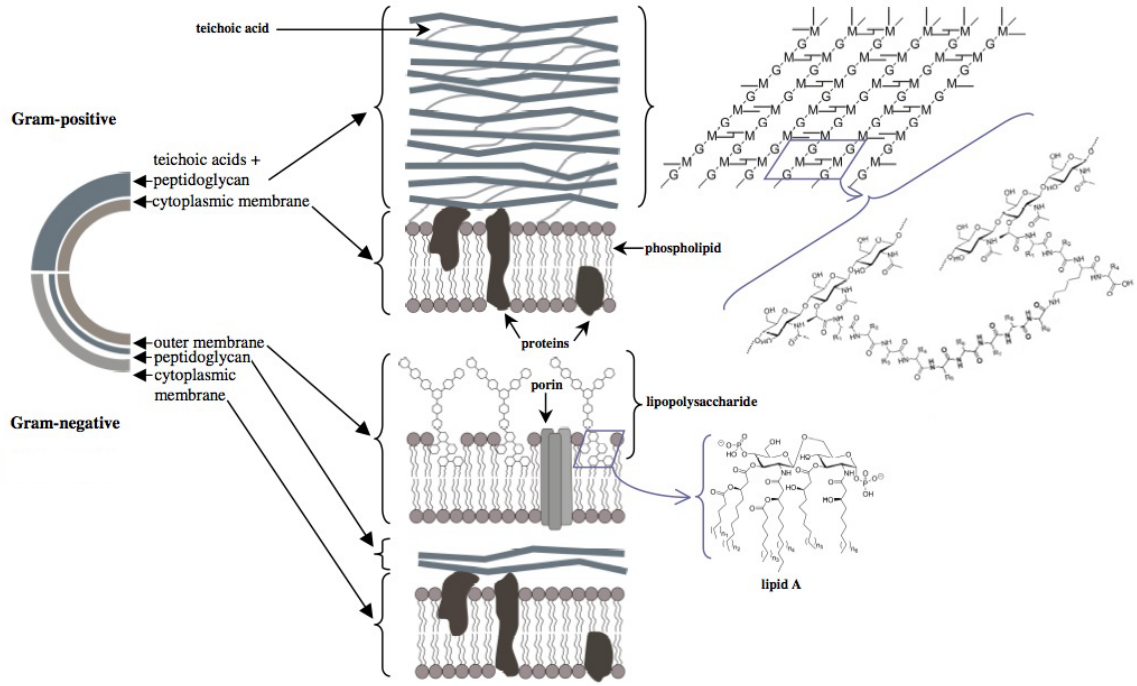

Figure 3.22: *Structural features of the membrane in Gram-positive and Gram-negative bacteria.*

The special properties of the bacterial membranes allow the use of cationic peptides as an antibacterial agent. In fact, many CPPs are structurally similar to antimicrobial peptides (AMPs). As mentioned previously, cationic peptides can translocate through mammalian cell membranes. However the interaction with the negatively charged membranes of bacteria is more complex. The mechanism of action of antimicrobial peptides is not fully established. Nevertheless, it is suggested that they work primarily by compromising the cell wall integrity. Once arrived at the cell surface, the peptides either bind to the lipopolysaccharides or neutralize the charge over an area of membrane, subsequently distorting the membrane structure leading to the permeation of the membrane and the death of the bacteria.[146]

Known AMPs cover a wide range of size, sequence, and structure, but most of them are sharing amphipathicity and positive charge.[21,147] Especially the amino acids tryp-

tophan and arginine are frequent among AMPs and even short Arg/Trp-rich peptides have been found to have antimicrobial activity.[148–151] It seems that the cationic side chains of the amino acids, such as arginine, lysine and histidine interact with negatively charged membranes, whereas the nonpolar and aromatic side chains of amino acids, such as tryptophan and phenylalanine provide the lipophilic anchors that induce the membrane disruption. *Tam et al.* studied properties of dendrimeric peptides which feature tetravalent and octavalent lysine cores, respectively.[152] These multivalent structures were tethered in each of the branched chains with tetrapeptides of the amino acid sequence RLYR, displaying properties desirable for antimicrobials. The tests revealed, that they are broadly active with similar potency against ten test organisms, such as Gram-negative, Gram-positive as well as three fungi strains. The obtained minimal inhibition concentrations (MIC) range between 0.3 and 1.0 μM. Especially notable is that the dendrimeric peptides had, compared with the linear peptides, several desirable attributes, such as enhanced proteolytic stability and decreased hemolytic activity.

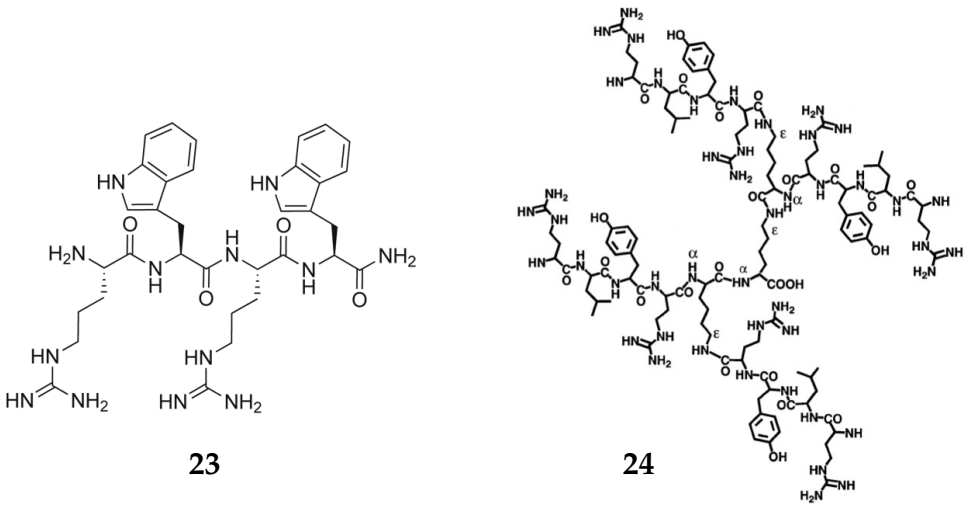

23 **24**

Figure 3.23: *Typical antimicrobial compounds containing amino acids with cationic side chains, as well as nonpolar and aromatic side chains (**23** RWRW[149], **24** $(RLYR)_4$[152]).*

In summary, these examples show that short linear and dendrimeric oligopeptides demonstrate interesting and biological relevant features for effective and versatile membranolytic activities, e.g. translocation and carrier properties in human cells and antimicrobial activity, respectively. The following chapter will return again to the investigation of artificial systems and will focus on the recent advancements of synthetic receptors for the effective molecular recognition of peptides.

3.3.3 Peptide Receptors

As already mentioned in Chapter 2, following the definition of Nobel laureate *Jean-Marie Lehn* the term "receptor" is here used to describe a chemical host which binds to a given guest.[18] Peptide receptors are organic structures that are able to bind peptides selectively by means of various non-covalent intermolecular interactions, leading to the assembly of supramolecular complexes. The studies on these smaller model systems allow deep insights in the underlying principles of recognition, which are still not completely understood. Especially the conformative flexibility of peptides and the sum of weak interactions, such as hydrogen bonding, hydrophobic and polar interactions complicate the examination of such systems. Hence, the study of small model systems not only helps to understand the intermolecular interactions between peptides, but also to improve the understanding of complex structures based on non-covalent interactions, such as proteins. The following chapter will discuss some recently discovered and investigated supramolecular systems for the recognition of peptides. Especially interesting in the context of this thesis are sequence-selective receptors for peptides in water.

Liskamp et al. reported the screening of a large combinatorial receptor library (**25**) derived from a cyclotriveratrylene with three attached peptide arms for the binding of D-Ala-D-Ala and D-Ala-D-Lac (Figure 3.24).[153]

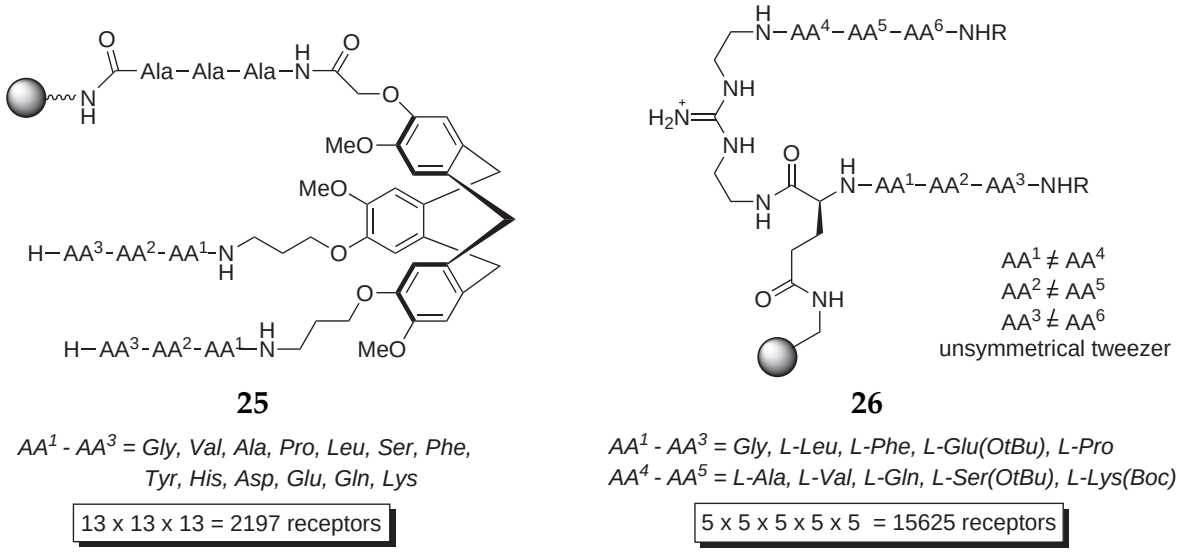

Figure 3.24: *Combinatorial library of tripodal receptors based on a cyclotriveratrylene (CTV) scaffold by Liskamp et al. (**25**) and two-armed tweezer library with a guanidinium head group as a carboxylate binding site by Kilburn et al. (**26**). Both receptor libraries are intended to bind selectively* D-Ala-D-Ala-OH *in aqueous solution.*

Using a color-coded substrate, a 2197-member library of CTV-based synthetic tripodal receptors was screened in water with phosphate buffer (0.1 N, pH = 7.0). Efficient receptors could be identified qualitatively by identification of active beads and subjecting them to Edman degradation. The best receptors were able to bind the dipeptide more efficiently than the related depsipeptide D-Ala-D-Lac. *Kilburn et al.* also applied a combinatorial library of tweezer-receptors (>15 000 members) to find efficient receptors for the binding of the tripeptide N-Ac-L-Lys-D-Ala-D-Ala.[154] A guanidinium scaffold was incorporated as a specific recognition site for carboxylate functionality into the receptor structure to identify receptors for peptides with free carboxylate groups. The receptors were screened in aqueous buffer (pH 8.5, borate) with the dye labelled tripeptide N-Ac-Lys-D-Ala-D-Ala, using a qualitative binding assay by the observation of stained beads, visualized under a microscope. Some good binding receptors were identified and the most promising one was then resynthesized and studied in more detail. Weak binding with low mM affinities was found for two diastereomeric tripeptides with the resin-bound receptor but no binding data in free solution could be obtained.

Wennemers et al. developed the class of diketopiperazine receptors for the selective molecular recognition of peptides both in organic and aqueous solvents. These two-armed receptors consisted of a structure-directing diketopiperazine template and peptidic side chains as recognition modules. For example, the incorporation of aspartic acids in the receptor arms led to the selective binding of arginine-rich tripeptides (**27**).[155] This was revealed in the screening of a combinatorial library (in aqueous tris buffer at pH 7.2) of immobilized tripeptides with almost 30000 members containing 31 different D- and L-amino acids (including lysine and histidine) (Figure 3.25, left).

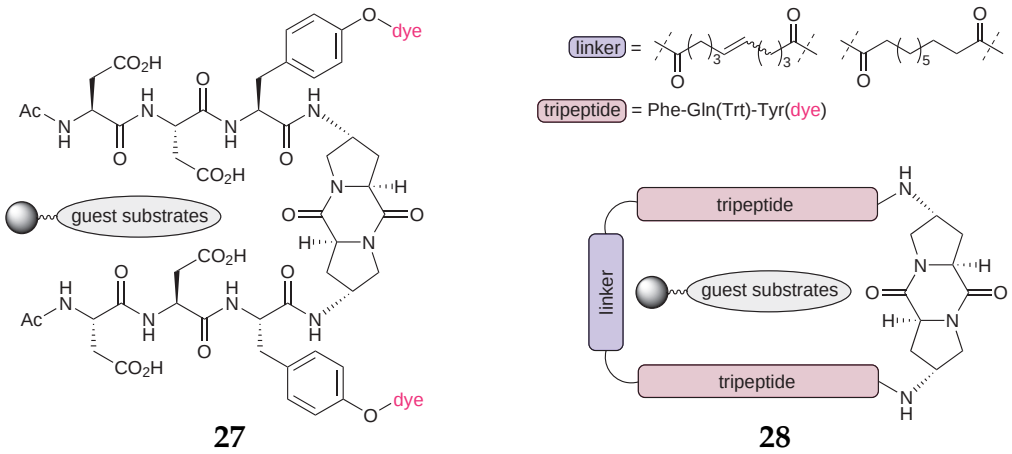

Figure 3.25: *Dye-marked diketopiperazine receptors developed by Wennemers et al. can selectively detect tripeptides.*

The group of *Wennemers* also tested the difference between macrocyclic two-armed diketopiperazine receptors (**28**) and their open-chain analog in a solid-phase binding assay (Figure 3.25, right).[156] The introduction of different linker molecules led to significantly modified binding properties in chloroform. For example, for the immobilized tripeptide D-Val-D-Val-D-His and the "open" receptor a binding affinity of 2500 M^{-1} was observed, whereas the binding constants with the cyclic hosts systems always resulted in values of <100 M^{-1}.

The previously mentioned arginine specific receptors (**27**) were also modified into functional peptide-based nano-structured materials using a method called ionic self-assembly (ISA) (Figure 3.26). The addition of the surfactant dihexadecyldimethyl ammonium bromide (DiC) to the receptors led to the formation of receptor-surfactant complexes with liquid-crystalline properties.[157] The complexes were then again examined for their peptide binding properties in solution using the same combinatorial library as before. Surprisingly, now the receptors featured a distinct selectivity for histidine-rich peptides, in contrast to the previous selectivity for arginine containing peptides. These results illustrate the possibilities of fine-tuning for the molecular recognition properties of supramolecular structures.

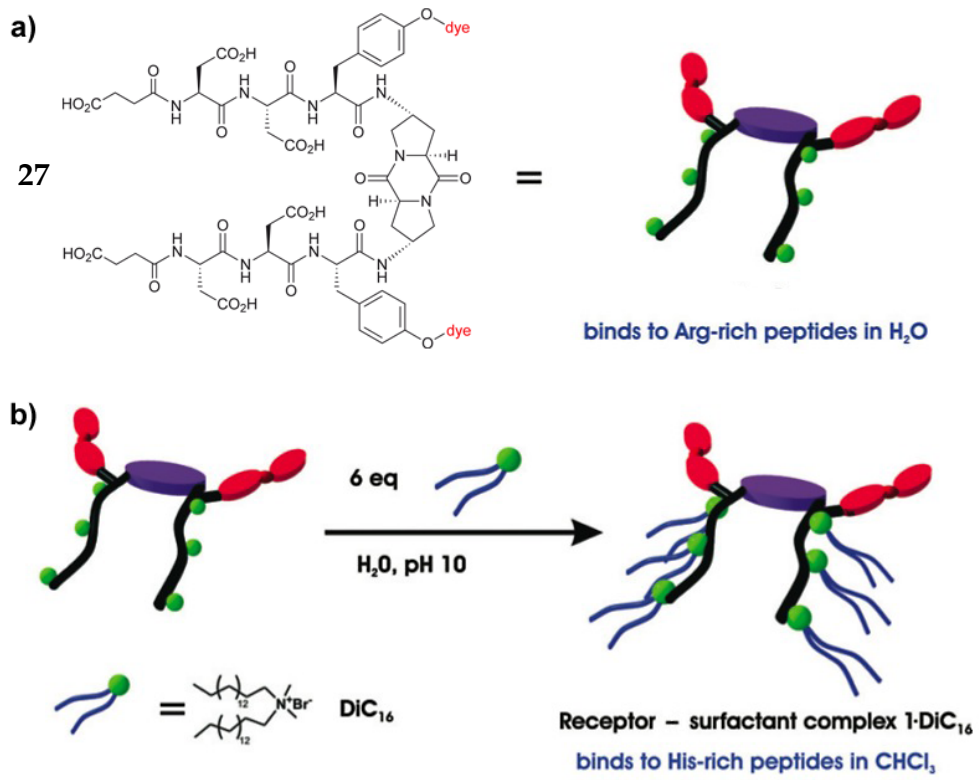

Figure 3.26: *The addition of a surfactant to the diketopiperazine receptor **27** led to the formation of a complex with different peptide binding properties.*[318]

An interesting new binding motif for the sequence selective recognition of peptides was developed and investigated by *Urbach et al.* His work is based on cucurbit[8]uril (Q8), a water soluble eight-membered macrocycle with a hydrophobic cavity and two constricted portals fringed with carbonyl groups.[158,159] It can bind cationic guests in aqueous solution with equilibrium association constants up to 10^{12} M^{-1} by the inclusion of hydrophobic groups inside the cavity, while forming cation-dipole interactions between the positively charged ammonium groups and the carbonyl portals.[160] *Urbach* showed, that these unique structures allow a charge mediated discrimination of tripeptides containing tryptophane either at the N-terminal, the internal or the C-terminal position.[161] The Q8 was demonstrated to bind Trp-Gly-Gly with an affinity constant of 1.3×10^5 M^{-1}, with 6-fold specificity over Gly-Trp-Gly, and with 40-fold specificity over Gly-Gly-Trp. A similar sequence selectivity was observed by *Inoue et al.* with zwitterionic dipeptides.[162] It was possible to show that cucurbit[7]uril recognized the peptide sequence of Phe-Gly over Gly-Phe as well as Tyr-Gly over Gly-Tyr and Trp-Gly over Gly-Trp, showing a clear selectivity for N-terminal aromatic amino acids.

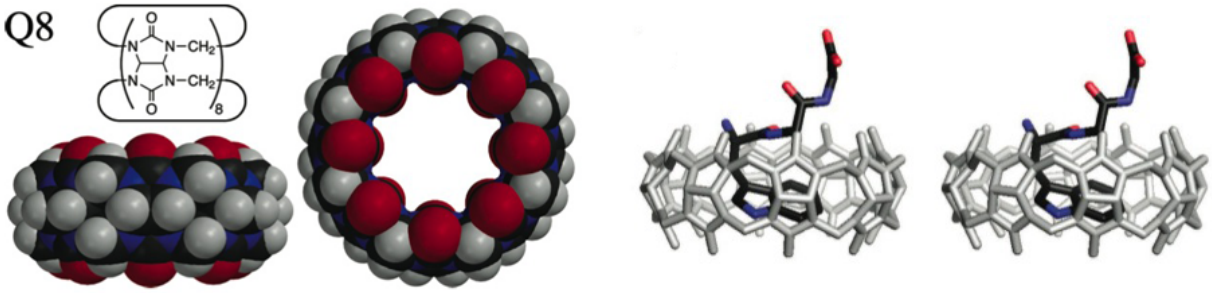

Figure 3.27: *Structure of cucurbit[8]uril (Q8), which is able to bind peptides depending on the amino acid sequence (left); Crystal structure of Q8 with Trp-Gly-Gly within the central cavity (stereo-view on the right).*[319]

These structures are also able and big enough to accommodate the simultaneous inclusion of two aromatic guests within the cavity. Cucurbit[8]uril for example was able to bind Phe-Gly-Gly in a 1:2 complex with a high binding constant of 10^{11} M^{-2}.[159] A recent publication reported the utilization of this approach for the multivalent recognition of tryptophane containing oligopeptides. *Urbach* prepared peptide-based scaffolds functionalized with up to three aromatic anchor groups (red squares in Figure 3.28 on page 41) which were used to direct the non-covalent assembly with Q8 molecules.[158] The resulting self-assembled multivalent receptor was able to bind in a discrete divalent fashion to a peptide with one to three tryptophan residues. In addition an affinity gain of 30 to 280-fold was observed due to multivalency effects.

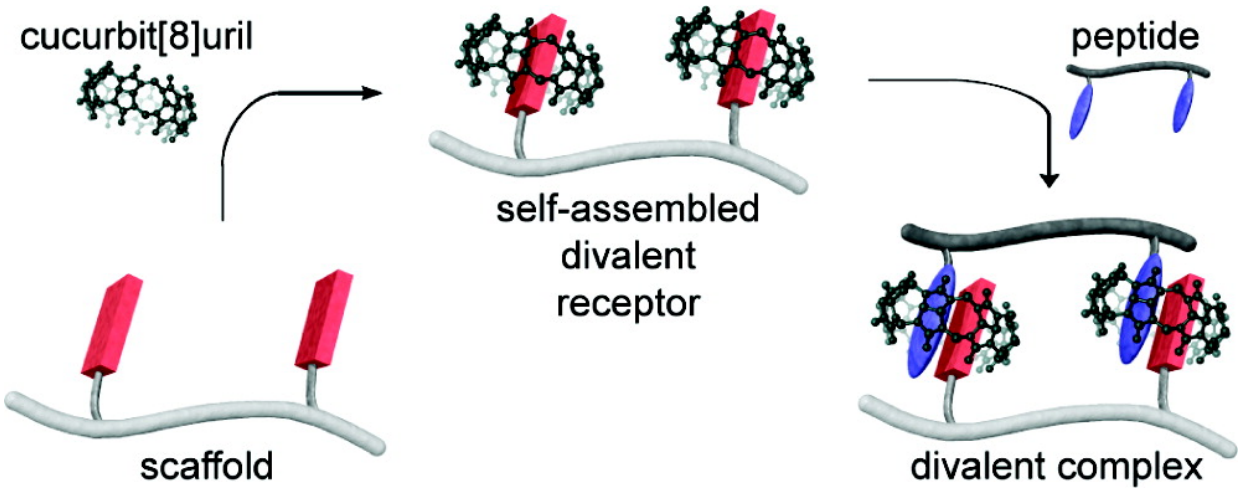

Figure 3.28: *Schematic illustration of a self-assembling receptor based on cucurbit[8]uril. A divalent scaffold presenting aromatic groups (in red) recruits two equivalent of Q8. The resulting receptor binds in a divalent fashion to a peptide with two tryptophan groups (in blue).*[320]

Cucurbiturils represent simple, yet effective receptors for the strong and selective recognition of peptides. Therefore they are a new and interesting model system which mimics the recognition of small peptides by enzymes and antibodies. There are also some metal based receptors known for the selective recognition of peptides. Due to the more remote relevance to this thesis, they are only briefly mentioned here. Interesting examples in the literature are the copper based receptors of *König*,[163] the organometallic chemosensors of *Severin*,[164] and the bowl or cage shaped receptor systems of *Fujita*.[165,166]

In summary, the selective molecular recognition of peptides with high affinity is still a very challenging area of research. However, the numerous different approaches in the literature helped to increase the knowledge about these complex binding events. In continuation of the peptide recognition, the next chapter will advance the multivalent approach to more complex systems and will present some examples of supramolecular receptors for the recognition of protein surfaces.

3.3.4 Protein Surface Recognition

In general, the possibilities of interactions with proteins can be divided into two groups, depending on the topology of the recognized surface. One is the interaction with deep buried concave areas within the protein, which are often of hydrophobic nature and shielded from water and big molecules. On the opposite, the surface of the protein can also act as point of interaction. The exterior area is usually flat, exposed and in direct contact with water. Two typical examples for both cases are the interaction between biotin (yellow) bound to streptavidin[92,93] (Figure 3.29, left) and the interaction of barnase with its polypeptide inhibitor barstar (yellow),[167–169] respectively (Figure 3.29, right).

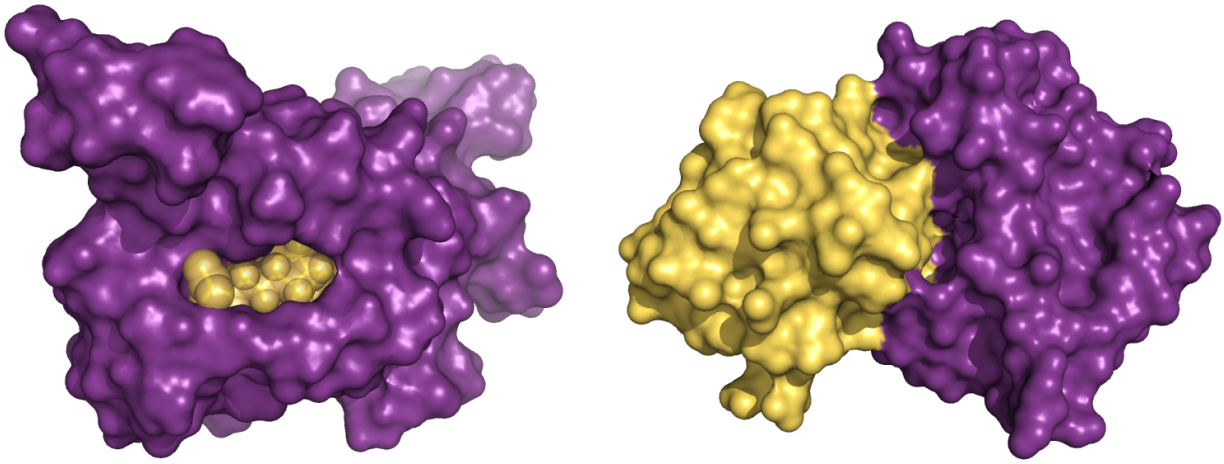

Figure 3.29: *Biotin bound to the active site of streptavidin (left complex); Interaction of barnase with its polypeptide inhibitor barstar (yellow) (right complex).*

Both complexes have very high dissociation constants of 10^{-15} M (for the biotin complex) and 10^{-14} M (for the barnase complex). However the interaction is very different in these examples. The tight binding of biotin-streptavidin complex is based on the formation of multiple hydrogen bonds and van der Waals interactions in a well-defined cavity of streptavidin, leading to the almost complete bury of the biotin in the protein interior (cf. Figure 3.11 on page 26). On the other side, the protein-protein interaction between barnase and barstar is mainly based on the electrostatic interaction of four acidic residues on the flat surface of barstar (yellow) that effectively binds towards a positively charged surface patch, representing the active site of barnase. These examples illustrate that, depending on the protein target, the possible interactions are very complex and demand well designed and matching partners. Protein surfaces are in particular challenging targets because of their relatively large solvated surfaces (typically around 1500 $Å^2$) as compared to the well-defined pockets seen in active sites of enzymes.

The following section will provide a short overview of different strategies for the protein surface recognition with designed receptors.[170–173] These molecules can help to study protein-protein interactions, that play crucial roles in a number of biological processes, from intercellular communication to programmed cell death.[174–176] Often, the protein binding areas are not evenly distributed across the surface, but instead are focused on hot spots.[177] Hence, scientists concentrate on the design of supramolecular and usually multivalent scaffolds to interact with the surface of proteins in a selective and efficient way. Figure 3.30 provides an overview of possible multivalent scaffolds.

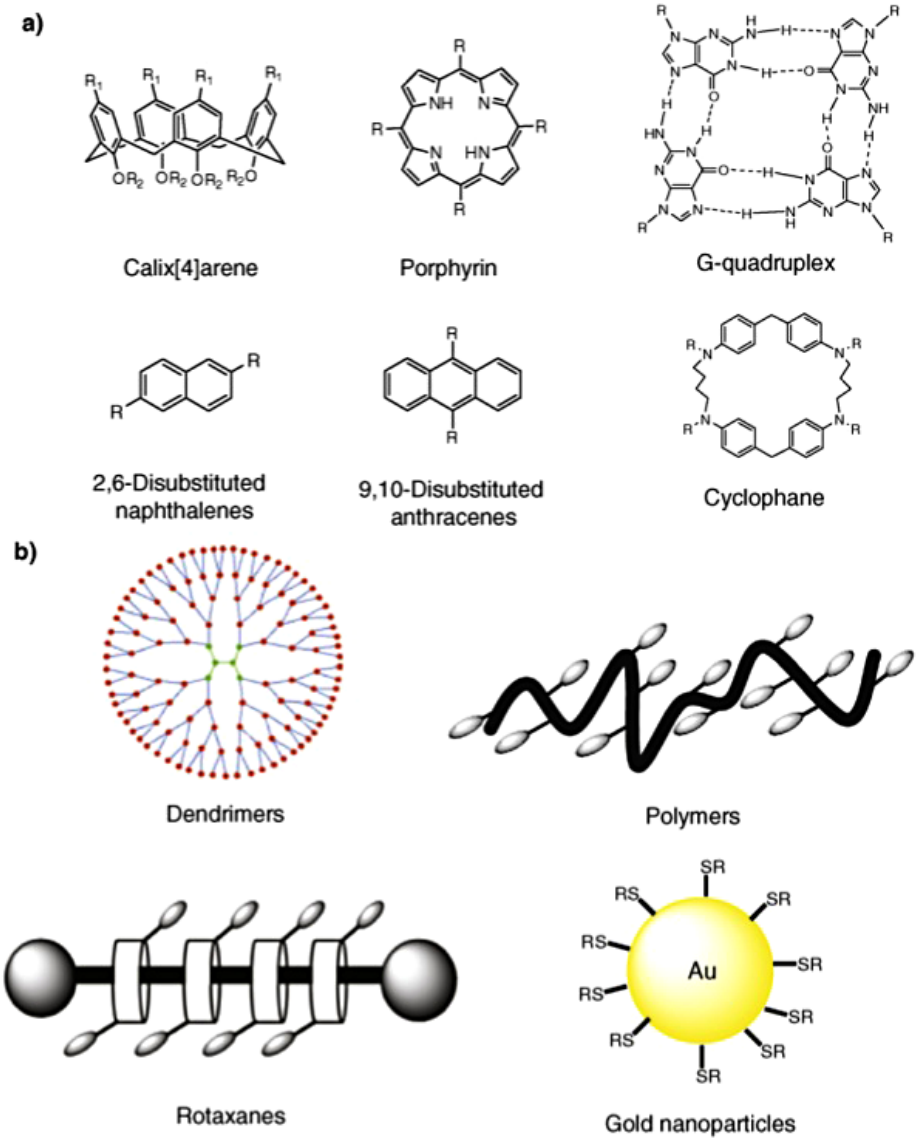

Figure 3.30: *Overview of multivalent scaffolds, including (a) low-valency examples based on aromatic moieties and (b) high-valency frameworks for supramolecular interactions with biological structures through multivalent contacts.*[321]

Calixarenes are among the most common used scaffolds. The valency of these macrocycles, obtained by the oligomerization of phenol and formaldehyde, can be easily varied from 1 to 8. Its structure can be described as semirigid cone with a wider upper and more narrow lower rim, that can easily be functionalized with a variety of groups for a molecular recognition. For example, *Hamilton et al.* arranged four peptide loops around the central core of a calix[4]arene. By varying the sequence of the loop regions a range of differently functionalized receptor surfaces, approximately 400 Å in area were prepared. It was possible to show that these receptors can function as potent inhibitors of chymotrypsin by binding to the surface of the protein and covering the active site. The competitive inhibitor had a K_i value of 0.81 μM.[178]

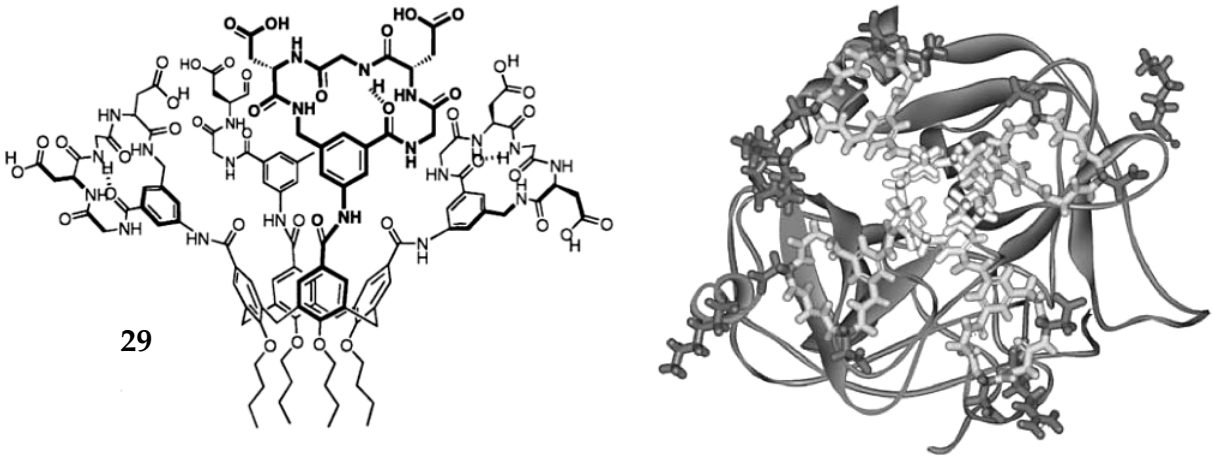

29

Figure 3.31: *Artificial calixarene based receptor for the recognition of the chymotrypsin surface (left); Calculated structure of the chymotrypsin-calixarene complex.*[322]

Mendoza and *Giralt* recently investigated a calix[4]arene with four cationic guanidiniomethyl groups to stabilize the tetramerization domain of the tumor suppressor protein p53, which helps to "clear out" cells with damaged DNA. In its active form, p53 protein is a tetramer, linked at the tetramerization domain which stabilizes the structure. However, many cancer patients suffer from structural mutations in this domain, leading to destabilization and loss of activity. Previous studies on synthetic tetraguanidinium ligands (**30**)[179] as well as arginine-rich peptides showed already that it is possible to specifically interact with the protein.[180] The linear molecules were able to bind to anionic patches on the surface of the p53 tetramerization domain with high affinity (K_D values of 50 μM and 8.4 μM, respectively).

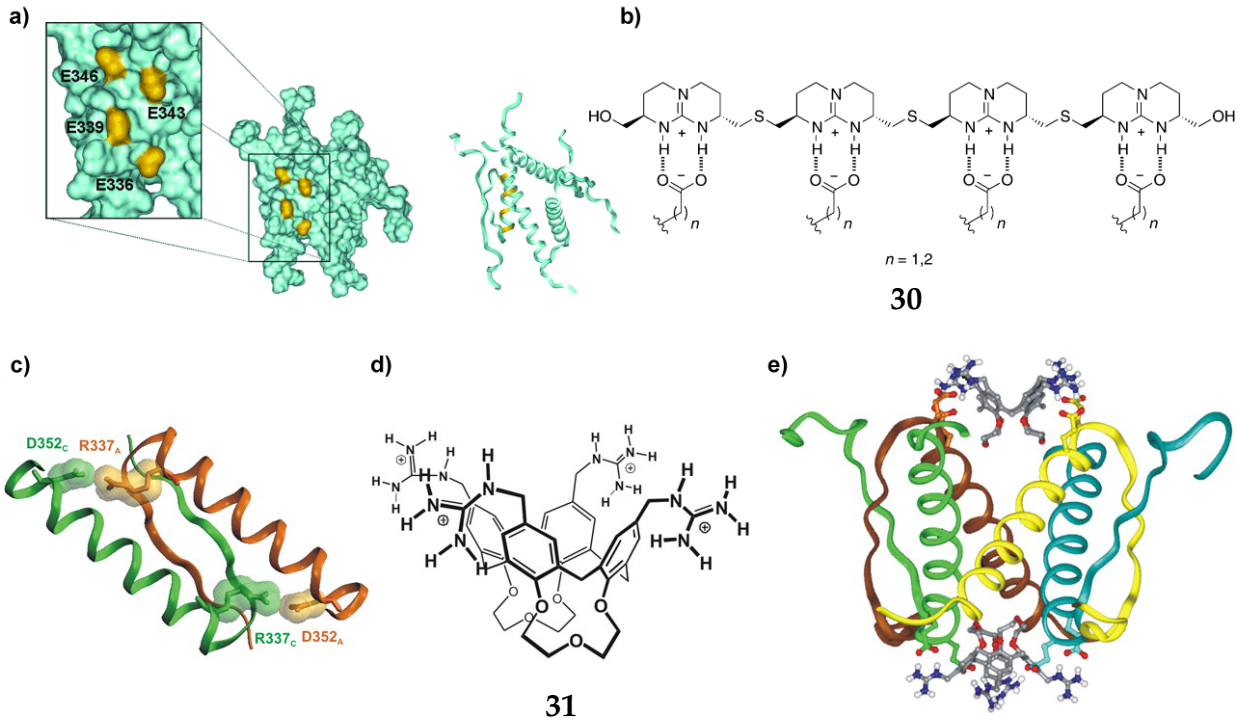

Figure 3.32: *a) p53 tetramerization domain with helical peptides containing anionic residues (gold); b) Chemical structure of the tetraguanidinium ligand* ***30*** *and the interaction with aspartate and glutamate residues of p53; c) Two of the Arg-Asp interactions which are lost in mutant p53-R337H, hence leading to instability; d) Calix[4]arene ligand* ***31****, designed to stabilize the tetramerization domain of p53; e) Tetramerization domain with two molecules of ligand* ***31*** *showing the interactions of the guanidinium groups with the exposed glutamates on the surface of p53.*[323,324]

In recently published work of *Mendoza* and *Giralt* these results were picked up and led to the design of the calix[4]arene **31** equipped with cationic guanidinio groups capable to hold together the four monomers of the mutated p53 proteins and recovering the tetramer integrity as in the wild-type structure.[181] Both electrostatic interactions of the wider upper rim of the calixarene and hydrophobic binding of the lower rim led to the formation of a structurally and thermally stabilized non-covalent 2:1 complex with the protein. Two molecules of calixarene bound sequentially in a cooperative manner with dissociation constants of K_{D1} = 130 μM and K_{D2} = 65 μM.

Another target that is recently under increased investigation are potassium channels and the selective regulation of the ion transport. Potassium channels are tetrameric membrane proteins that selectively transport K^+-ions across cellular membranes and represent a major target in biomedical research.[182,183] Any regulation of the ion stream

can control elementary cellular processes and represents a promising target for the treatment of e.g. neurological disorders and autoimmune diseases.

Trauner et al. designed a multivalent molecule based on a porphyrin scaffold with four cationic side chains in order to block the entrance of the ion channels.[184] Crystal structures of several potassium channels of the K_v1x class identified common aspartate or glutamate anchors at the entrance area of the channels. Calculations predicted these areas as promising points for the attachment of the blocking scaffold (Figure 3.33). Competitive binding assays revealed several porphyrins with nanomolar affinities that can partially block the entrance of the channels in a reversible way. For example, for cationic porphyrin **32** a high binding affinity was observed (K_i = 0.013 μM), whereas anionic porphyrins had no effect.

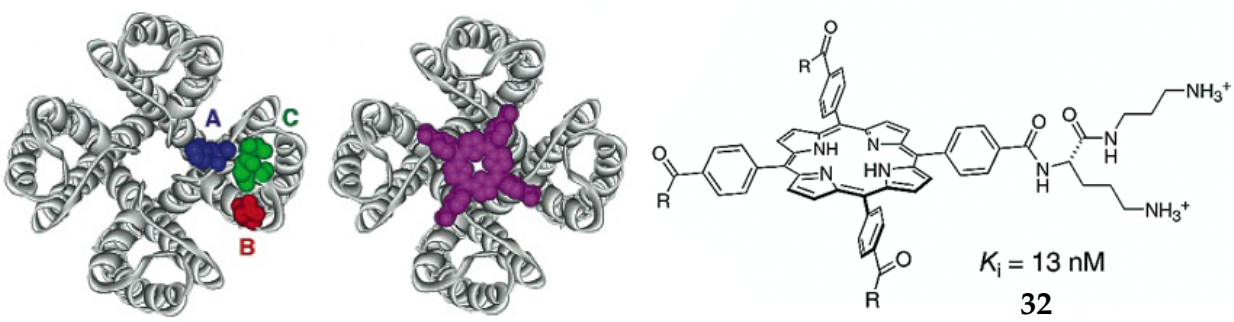

Figure 3.33: *Top view on the crystal structure of a potassium channel. The red, blue and green positions highlight the proposed anchor points for the cationic porphyrin (purple, **32**).*[325]

However, the initially proposed model of interaction was recently revised with the results of *Baldus et al.* They showed with the help of solid-state NMR spectroscopy and molecular dynamics, that the porphyrins do not sit like a lid on top of the channel, but are oriented in parallel to the channel axis.[185] Only one positively charged porphyrin arm is penetrating into the selectivity filter where the protonated amine favorably interacts with K^+ binding site (Figure 3.34). This explained also the previous observation that the ligands did not completely block the ion stream even at high concentrations.

This incomplete blocking of the extracellular entrance to the channel pore caused *Trauner et al.* to redesign the inhibitor structure. In cooperation with *Mendoza* similar guanidinylated calix[4]arenes as previously reported (compound **31** on page 45) but with free phenolic OH groups at the lower rim were tested.[186] The conical form of the cal-

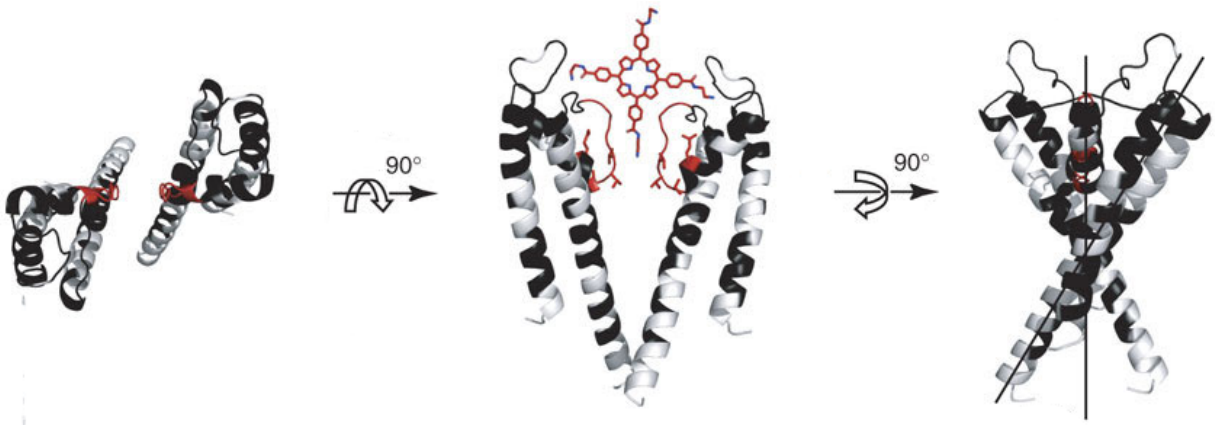

Figure 3.34: *Top and side view of the revised upright interaction of porphyrin* ***32*** *with ion channels.*[326]

ixarene was more likely to complement the shape of the outer pore entrance. The first test revealed an reversible mode of inhibition, however with no increased activity over the porphyrins and still no complete blockage.

Porphyrins seemed especially interesting because of their unique structural features which perfectly match the morphology of many protein-protein interfaces as pointed out by *Goodsell et al.*[187] He found that many proteins feature similar recognition interfaces, such as single hydrophobic surface areas surrounded by polar groups. These paradigm was picked up successfully by many groups in their design of scaffolds for the recognition of protein surfaces. In particular the small heme protein cytochrome *c* (Cyt *c*) attracted many studies, due to its interesting surface properties. Cyt *c* is a highly basic protein (p$I \approx 10$) and plays key roles in electron transfer and apoptosis.[188,189] An important recognition area on the surface of Cyt *c* involves a hydrophobic patch centered on the solvent exposed heme unit that is surrounded by basic lysine and arginine residues.[190] This area was in the main interest for many surface receptors equipped with acidic recognition elements (Figure 3.35 on page 48).

Imbrahim et al. investigated in detail the binding of a simple octaacid porphyrin (**33**) to the surface of Cyt *c* (compound **a)** in Figure 3.35).[191] The chemical shift analysis of a 1:1 complex resulted in a binding constant of 0.07 mM. 2D NMR correlation spectroscopy and docking simulations suggested that the protein-porphyrin complex exists in a dynamic ensemble with no distinct specificity for only one surface patch. Enhanced specificity can be obtained with the introduction of peptide side chains.[196,197]

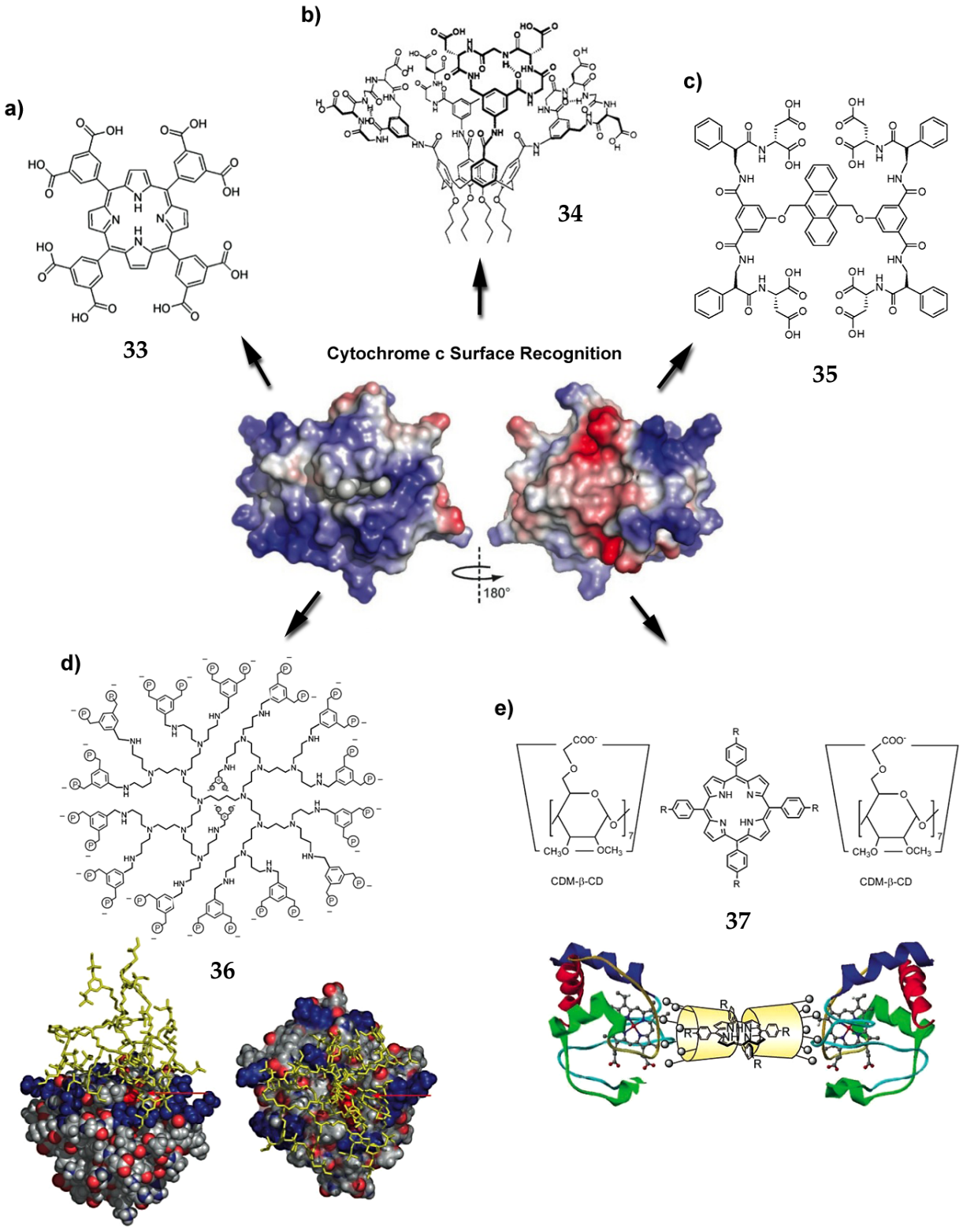

Figure 3.35: *Overview of different approaches for the surface recognition of cytochrome c (center). Blue represents basic (+) areas and red acidic (-) electrostatic potentials on the surface of the protein.[327,328] a) Ibrahim et al.[191] b) Hamilton et al.[192] c) Hamilton et al.[193] d) Schrader et al.[194] e) Ishida et al.[195]*

A similar antibody mimic based on a calix[4]arene linked to four constrained peptide loops (**34**) was synthesized and analyzed by *Park* and *Hamilton* (compound **b)** in Figure 3.35).[192,198] Each of the four cyclic hexapeptides contained two negatively charged asparagines to complement the cationic and hydrophobic regions on the surface of Cyt *c*. The large surface area of **34** allows strong binding to a complementary surface on cytochrome *c*, which is presumably close to the heme region. The 1:1 complex resulted in a binding constant of 3×10^8 M^{-1}. In addition it was possible to show that this surface recognition inhibits the reduction of the Fe(III) cytochrome *c* by ascorbate, and also the binding of the cytochrome *c* peroxidase.[199]

Hamilton also described new aromatic receptors based on an anthracene scaffold (**35**) (compound **c)** in Figure 3.35).[193] The fluorescent and hydrophobic core was functionalized with a variety of acidic groups for the electrostatic interaction with the surface of not only cytochrome *c*, but also α-lactalbumin, myoglobin and RNase A. FRET studies revealed that cooperative electrostatic interactions over a large surface area dominate the binding with low micromolar affinity. In the case of Cyt *c* a binding affinity of K_D = 0.30 μM was observed for compound **35**.

The well-defined but also versatile and derivatizable structure of dendrimers was also utilized for the surface recognition of proteins. The macromolecular-branched compounds with an inner core and physicochemical properties resembling those of biomolecules, gained increased popularity as multivalent frameworks for the study and modulation of biological events on protein surfaces. For example *Schrader et al.* synthesized dendrimeric bisphosphonates for the complex formation with several basic proteins, such as histone, trypsin, BSA and also Cyt *c* (compound **d)** in Figure 3.35).[194] The results illustrated that the weak interaction of a bisphosphonate monomer—especially in water—can be turned into a powerful receptor by applying multivalent structures (e.g. for histone H1 K_D = 0.25 μM). Similar results were published by *Tsukube*[200] and for glycopeptide dendrimers by *Jezek*.[201]

Finally, a ternary supramolecular complex involving a meso-tetraarylporphyrins, tethered by two polyanionic cyclodextrins (CD), also has been shown to recognize the surface of Cyt *c* (compound **e)** in Figure 3.35).[195] The work of *Ishida et al.* was the first ternary complex of Cyt *c*, a supramolecular receptor and an additional guest that is bound to the receptor. The aim of this project was to probe the potential of a selective modification of protein functions, depending on the third guest.

Some of the more "exotic" scaffolds are the examples from *Hayashida et al.*[202,203] They synthesized several large supramolecular receptors based on the combination of a cyclophane with four negatively charged resorcinarene-units. These compounds exhibited potent recognition capabilities toward histone, a small basic protein (pI = 10.8) of eukaryotic chromatins with high concentrations of lysine and arginine on its surfaces. The binding constant of the resorcinarene tetramer **38** with histone (1.3×10^7 M^{-1}) was 31-times larger than that of a resorcinarene monomer, which represents a distinct influence of multivalency effects. In addition the dansylated version **39** showed selective fluorescence sensing capabilities for histone.[204] Recently, a novel rotaxane-type receptor (**40**) was synthesized.[205] The movable and rotatable tetramer **38** acts again as histone-binding site, whereas the fluorophores (fluorescein and rhodamine) on the central axle composed of a 2,6-disubstituted naphthalene derivative function as histone-sensors. For the first time these compounds also enabled the FRET detection of histones.

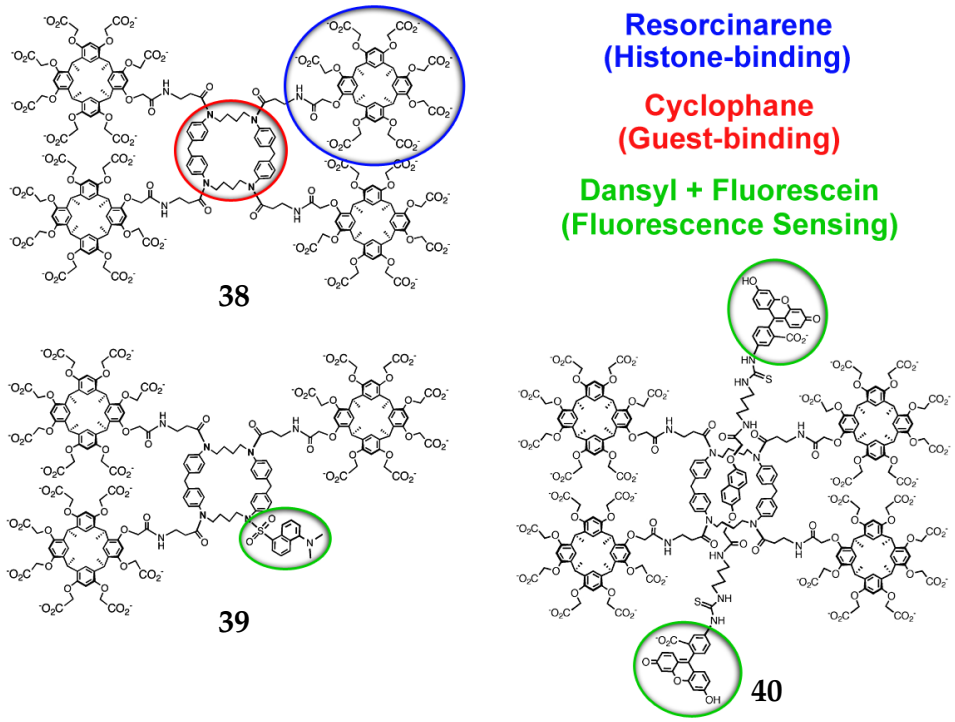

Figure 3.36: *Examples of cyclophane-based resorcinarene tri- and tetramers for the surface recognition and fluorescence sensing of histones.*[329]

In conclusion, this short survey provides an overview of the most recent and successful strategies for the recognition of protein surfaces. It clearly demonstrates that the use of a multivalent design is very advantageous, if not essential for high binding affinities and a selective recognition. The choice of the central scaffold and the surface interacting

parts of the receptor are decisive for the binding activity. Currently the focus of research is on the combination of hydrophobic and electrostatic interactions which allows dissociation constants up to the nano-molar range. The development for future receptors will certainly continue to include new scaffolds and recognition elements that function under physiological conditions. This may include more detailed structural designs that not only complement the surface characteristics but also have an effect on the functions of the proteins, beyond sensing and covering properties. In particular enzymes—as special class of proteins—are interesting due to their important role in biochemical reactions. Hence, the following chapter will present some of their unique biomolecular functions and potential methods to inhibit the catalytic activity. Especially the unique properties of the serine protease tryptase will be in focus. The inhibition of its enzymatic activity will be the target of the final project of this thesis.

3.4 Artificial Peptides as Enzyme Inhibitors

Enzymes are proteins that are very important in many in physiological processes due to their enormous catalytic efficiency. Enzymatic reactions typically proceed at rates more than millions of times faster than the corresponding uncatalyzed reactions. The possible catalyzed reactions are very versatile and include different types, such as hydrolysis, transfer of functional groups, polymerization, oxidation, reduction or dehydration, to mention only the most common classes of enzymatically mediated chemical reactions. Enzymes are highly specific in terms of binding their substrates and catalyzing reactions. One way to regulate the enzyme activity is to use substances that can influence the binding of substrates and/or change the turnover number of catalyses reaction. These substances that interact with enzymes and decrease in this way their activity are called inhibitors.

The following sections will focus on proteases—also known as peptidases or proteinases—which belong to the class of enzymes that catalyze the hydrolysis of peptide bonds. Of particular interest will be the serine protease β-tryptase, its special structural features and known approaches for the inhibition of its catalytic activity involved in many allergic and inflammatory disorders.

3.4.1 General Aspects of Enzyme Inhibition

3.4.1.1 Enzyme Kinetics

In enzyme-catalysed reactions an inhibitor often acts by binding to the enzyme in various ways, thus diminishing the rate of its chemical reaction. Many inhibitors structurally resemble the actual substrates of the enzymes and can be used to probe the chemical and conformational nature of the enzyme. In order to understand the complex interactions during enzyme inhibition, several kinetic mechanisms must be considered, all following the Michaelis-Menten model. This basic theory describes a enzymatically catalyzed reaction with two reactions steps:

$$\mathrm{E} + \mathrm{S} \underset{k_{-1}}{\overset{k_1}{\rightleftharpoons}} \mathrm{ES} \xrightarrow{k_2} \mathrm{P} + \mathrm{E} \tag{3.5}$$

At first, the enzyme (E) forms a complex (ES) with a substrate (S), which then subsequently decomposes again into the enzyme and the product of the reaction (P).

The rate constants for the individual steps are k_1, k_{-1} and k_2 and define the Michaelis constant K_m:

$$K_m = \frac{k_{-1} + k_2}{k_1} \tag{3.6}$$

Assuming rapid equilibrium between reactants (enzyme and substrate) and the enzyme-substrate complex results then in the basic equation of enzyme kinetics, the Michaelis-Menten equation:

$$v_0 = \frac{V_{max}[\mathrm{S}]}{K_m + [\mathrm{S}]} \tag{3.7}$$

The Michaelis–Menten equation relates the initial reaction rate v_0 to the substrate concentration [S] and the maximum reaction rate V_{max}. The corresponding graph is a hyperbolic function and for example visually describes the K_m value as the substrate concentration at which the reaction rate is half-maximal (Figure 3.37, left).

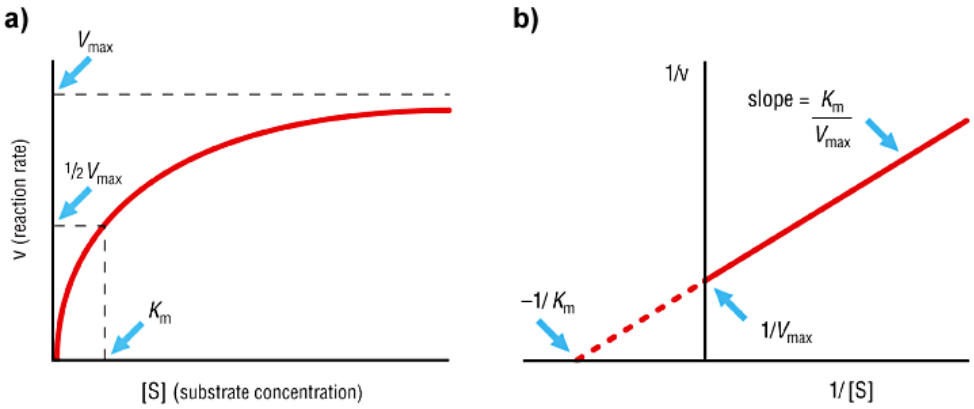

Figure 3.37: *a) Graph of rate against total substrate concentration for a typical enzyme-catalyzed reaction; b) Lineweaver-Burk or reciprocal kinetic plot of 1/v against 1/[S].*[330]

There are several methods for determining the values of the parameters K_m and V_{max} of the Michaelis-Menten equation. The classical ones are using the linearization of the Michaelis-Menten equation (Figure 3.37, right), e.g. the Lineweaver-Burk plot, the Eadie-Hofstee diagram and the Hanes-Woolf plot. Today, nonlinear curve-fitting procedures are preferred, because they allow more accurate results.[206]

Depending on the enzyme and the chemical nature of the inhibitor molecule, two types of inhibition are possible: the irreversible and the reversible inhibition. Irreversible inhibitors bind to the enzyme in a covalent way and can not be removed. In contrast, reversible inhibitors interact with enzymes in a non-covalent way with the help of hydrogen bonds, hydrophobic or electrostatic interactions. These inhibitors generally do not undergo any chemical reactions when bound to the enzyme and can be easily removed by dilution, ultrafiltration or dialysis experiments.

Reversible enzyme inhibitors can be classified as competitive, non-competitive or uncompetitive, according to their effects on K_m and V_{max}. The following short description of these different effects will focus on competitive and non-competitive interactions, due to the higher relevance for this thesis. A competitive inhibitor is any compound which closely resembles the chemical structure and molecular geometry of the substrate. The inhibitor competes for the same active site as the substrate molecule which can be described with the following reaction scheme:

$$\begin{array}{l} \mathrm{E} + \mathrm{S} \underset{k_{-1}}{\overset{k_1}{\rightleftharpoons}} \mathrm{ES} \xrightarrow{k_2} \mathrm{P} + \mathrm{E} \\ + \\ \mathrm{I} \\ k_3 \uparrow\downarrow k_{-3} \\ \mathrm{EI} + \mathrm{S} \longrightarrow \text{ no reaction} \end{array} \tag{3.8}$$

In contrast, a non-competitive inhibitor is a compound that interacts with the enzyme, but usually not at the active site. The non-competitive inhibitor can either react remote from or very close to the active site. Figure 3.38 (on page 55) summarizes the different type of interactions and depicts the corresponding Lineweaver-Burk plots.

3.4.1.2 Enzyme Assays

There are several enzyme assays known, all measuring either the consumption of substrate or production of product over time. The following descriptions will focus on fluorometric assays which measure the change in the fluorescence caused by a cleaved substrate during the catalytic enzyme reaction.

Two methods are known for the determination of inhibition constants, the dilution assay of *Kitz and Wilson*,[207] and the continuous assay by *Tian and Tsou*.[208] In a dilution

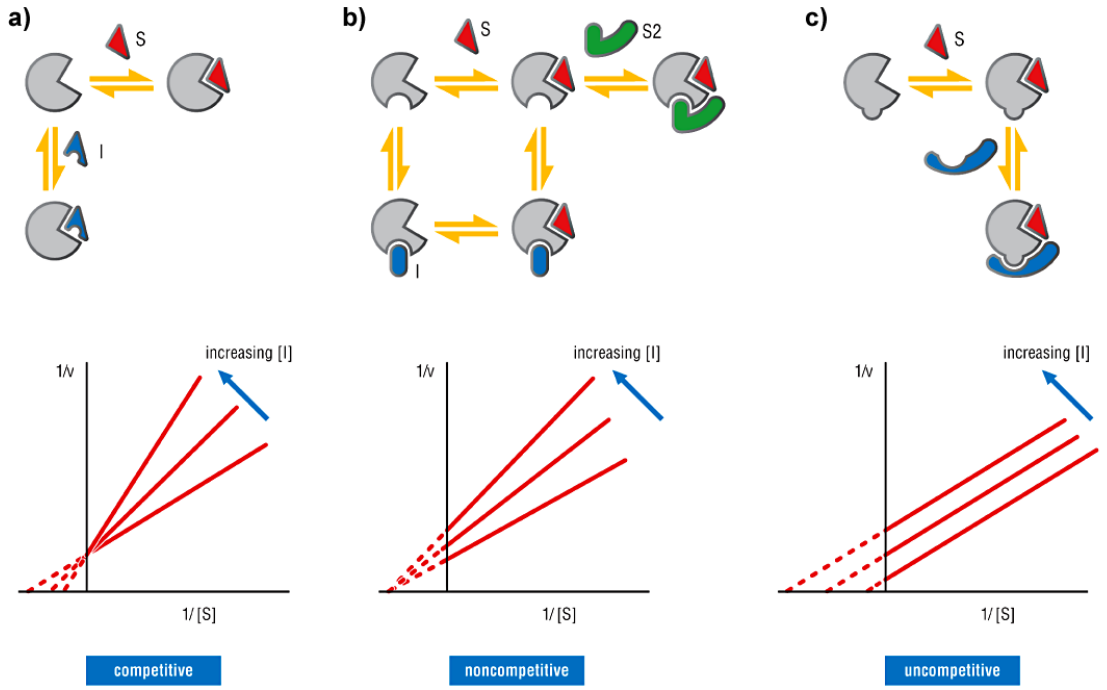

Figure 3.38: *Comparison of competitive, non-competitive and uncompetitive enzyme inhibition (inhibitor = I, blue; substrate = S, red). Below, the corresponding Lineweaver-Burk plots are shown.*[330]

assay the enzyme and inhibitor are incubated under steady-state conditions (i.e. compared to the enzyme, there is an excess of inhibitor and substrate resulting in a steady [ES] during the reaction). Then, in defined intervals, samples are taken from the enzyme reaction and the residual enzyme activity is measured. A more convenient and faster method is the continuous assay, allowing the determination of the reaction rate in one assay. Therefore, the enzyme is added to a mixture of substrate and inhibitor. Then the product released from hydrolysis of the substrate is measured as a function of time. Again, it is important to have steady-state conditions to reduce the possibility of a enzyme activity reduction caused by a too small substrate concentration. The measurement itself should be in the initial velocity region of the enzymatic reaction which is the linear range at the beginning of the experiment, where less than 10 % of the substrate has been converted to product. The initial rate experiment is the simplest to perform and analyze, being relatively free from complications such as back-reaction and enzyme degradation and is the most common used type of experiment in enzyme kinetics.

During the assay the increase of fluorescence over time (due to product generation) is measured and results in linear curves with varying slopes. A higher inhibition concentration and strong inhibitors result in smaller slopes (v_i) compared to the measure-

ment without inhibitor (v_0), respectively (Figure 3.39, right). One way to determine the dissociation constant K_i of the reaction is to measure these slopes at different inhibitor concentration. According to the Dixon equation,[209]

$$v_i = \frac{v_0}{1 + \frac{[\mathrm{I}]}{K_i}} \tag{3.9}$$

with v_i and v_0 as enzyme activities with and without inhibitor, it is possible to determine K_i from the plot of v_0/v_i against the varying inhibitor concentrations (Figure 3.39, right).

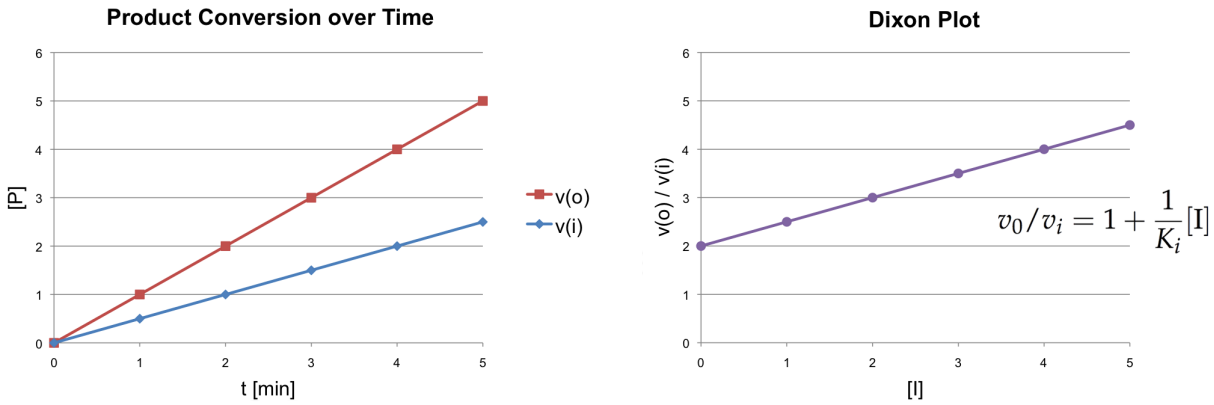

Figure 3.39: *Measurement of the product conversion over time. The slope of the curve is reduced upon the addition of inhibitor (left); Linear analysis of the inhibition with the help of the Dixon plot (right).*

Modern programs like Grafit® allow the direct nonlinear regression analysis of the obtained data to determine K_i and IC_{50}. For a non-competitive inhibition both values are the same. However, if the inhibitor is in competition with the substrate for the same binding site, the substrate concentration has to be considered for the calculation of K_i. Therefore, first the apparent K_{iapp} is calculated by nonlinear regression analysis and corrected to zero substrate concentration. With the known (or determined) K_m value of the substrate-enzyme combination it is possible to determine the "true" K_i with the following equation:

$$K_i = \frac{K_{iapp}}{1 + \frac{[\mathrm{S}]}{K_m}} \tag{3.10}$$

The dissociation constant K_i is independent from the substrate concentration and its affinity to the enzyme, thus allowing an easy comparison between literature known inhibitors.

The above mentioned procedures describe enzyme assays where all participants, such as enzymes, substrates, and inhibitors are in solution. Most of the time the setup of choice for enzyme assays is based on a fluorescent or absorbance readout in microtiter plates. This continues to be the typically laboratory method for measuring enzymatic activity both in academia-type screenings and also in high throughput screenings (HTS) performed in industry.[210]

These techniques in solution can be merged with recent advances in solid-phase peptide synthesis and combinatorial chemistry, a useful technology that allows the simultaneous synthesis of a large number of different compounds. Using the split and mix synthesis, it is for example possible to synthesize large one-bead one-compound (OBOC) peptide libraries.[211,212] Such peptide libraries can then be used to screen enzymatic substrates and inhibitors or biomolecule-binding peptides.[213,214] A commonly used method for these screenings is to incubate a fluorescence-labeled biomolecule with the immobilized library and visually identify beads that display compounds able to bind the target (Figure 3.40).[215]

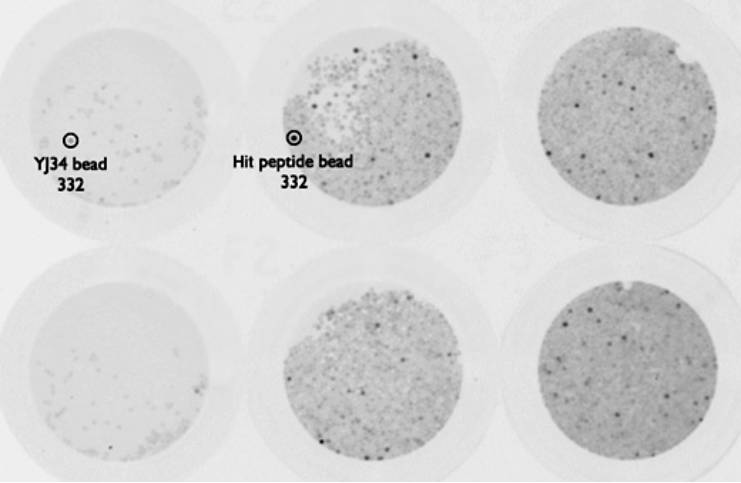

Figure 3.40: *Example of the screening of a combinatorial OBOC library under the microscope for potential hits.*[331]

The top-hit beads are then isolated with a needle or tweezer under a microscope and are further analyzed, e.g. by mass spectrometrical methods.[216,217] However, this method allows only a qualitative analysis of the best compounds and the discrimination between hit and no-hit.

One requirement for an "on-bead" enzyme screening is the bio-compatibility of the used polymer beads. The choice of solid support is crucial and depends on the types of reactions to be carried out as well as the screening methods to be employed. The resin beads must exhibit good swellability in both aqueous and organic solvents, low nonspecific protein binding, and good mechanical stability. Purely polystyrene based solid supports are generally unsuitable for the direct on-bead screening, due to the loss of enzyme activity in the polymer, poor swelling properties in polar media and the consequent exclusion of biomolecules from the hydrophobic core of the polymer. Resin types with a polystyrene core, grafted with polyethylene glycol chains (PEG), such as ArgoGel or TentaGel (Figure 3.41, left) exhibit better swelling properties while still being mechanically stable.[218,219] However, like many polystyrene-based resins they exhibit broad-wavelength autofluorescence, which interfers with fluorescence assays.[220]

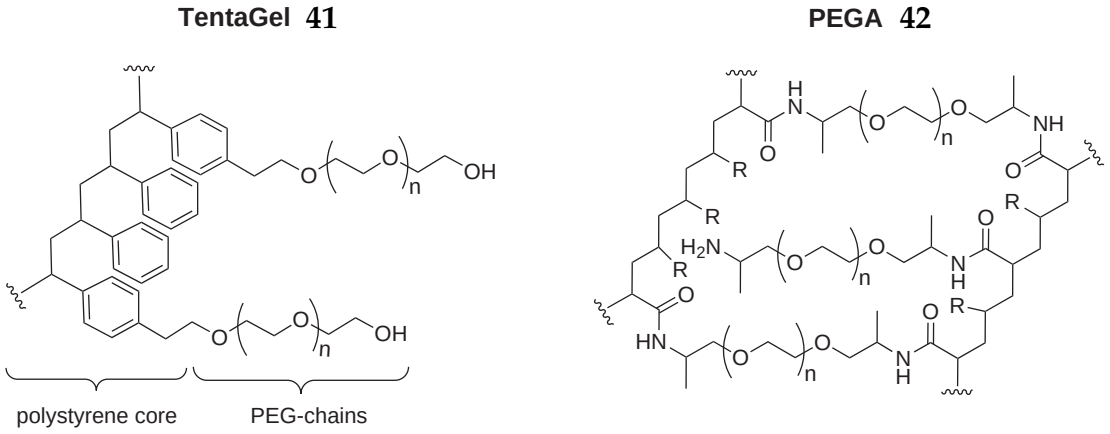

Figure 3.41: *Polyethylene glycol (PEG) functionalized types of resin for on-bead enzyme assay.*

An interesting hybrid resin similar to TentaGel is HiCore resin. It is a core-shell type resin with low non-specific protein binding that was successful applied by *Park et al.* in an enzyme-linked on-bead colorimetric assay.[221,222]

The best properties for on-bead screenings of enzymes offer solely PEG-based resins, such as PEGA, POEPS, POEPOP or ChemMatrix. In particular the PEGA resin has been widely used in both peptide synthesis and the solid phase synthesis of oligosaccharides (Figure 3.41, right). The resin material is designed to provide a complete hydrophilic support, and has excellent swelling properties in aqueous buffers allowing the permeation by enzymes.[223–225] PEGA resin also showed no nonspecific binding in protein-binding studies.[213,226] Hence, PEGA resin can be utilized for the synthesis of com-

binatorial compound libraries, followed by the direct screening in a variety of assays. *Machon* recently summarized interesting applications of on-bead screenings in his PhD thesis.[227]

Machon also reported the development of a new on-bead screening method for the identification of falcipain-2 and rhodesain inhibitors. For the first time it was possible to perform a simultaneous and quantitative screening of a library containing 150 peptidic inhibitors.[227] The new screening assay allowed a discrimination of the absolute inhibition in percent of *all* library members. Therefore, a defined amount of inhibitor-functionalized PEGA resin—previously synthesized in IRORI MikroKans[228] with a split-and-mix technique—was transfered in microtiter plates and incubated will the proteases. Compared with studies in solution an increased incubation time of 12 hours was necessary.

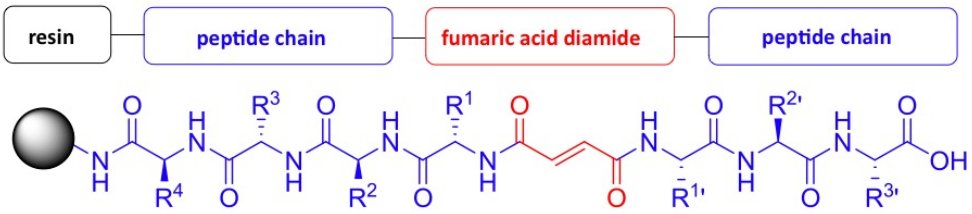

P4	P3	P2	P1	P1'	P2'	P3'
Val	Val Ala Leu	Leu Ile Phe Chg Phg	Gln Asn C1-Ac Ala Phe	Gly Ala	Gly	Phe

Figure 3.42: *Combinatorial library of falcipain-2 and rhodesain inhibitors, synthesized on PEGA resin and screened in a new on-bead screening assay.*[227]

With this fast and direct screening it was possible to obtain important information about the influence of amino acids at different positions of the inhibitor. The best inhibitors were resynthesized in solution and generated low micro-molar IC_{50}-values for the inhibition of the two cysteine proteases.

In summary, a direct on-bead screening of combinatorial peptide libraries allows a fast and quantitative analysis of *all* library members. In particular the comparison of the obtained data offers information, which is not available—or only with huge effort—in traditional enzyme screenings in solution.

3.4.2 The Serine Protease β-Tryptase

Tryptase is part of the serine endopeptidase family and has a chymotrypsin-like activity. According to the official nomenclature, proteases (or peptidases) can be classified into the subgroup of hydrolases which act on peptide bonds (EC-subclass 3.4). Proteases are globular, water-soluble proteins that function as enzymes and regulate many physiological processes. They can be divided into four big classes: serine proteases, cysteine proteases, aspartic proteases, and metallo-proteases (Figure 3.43).

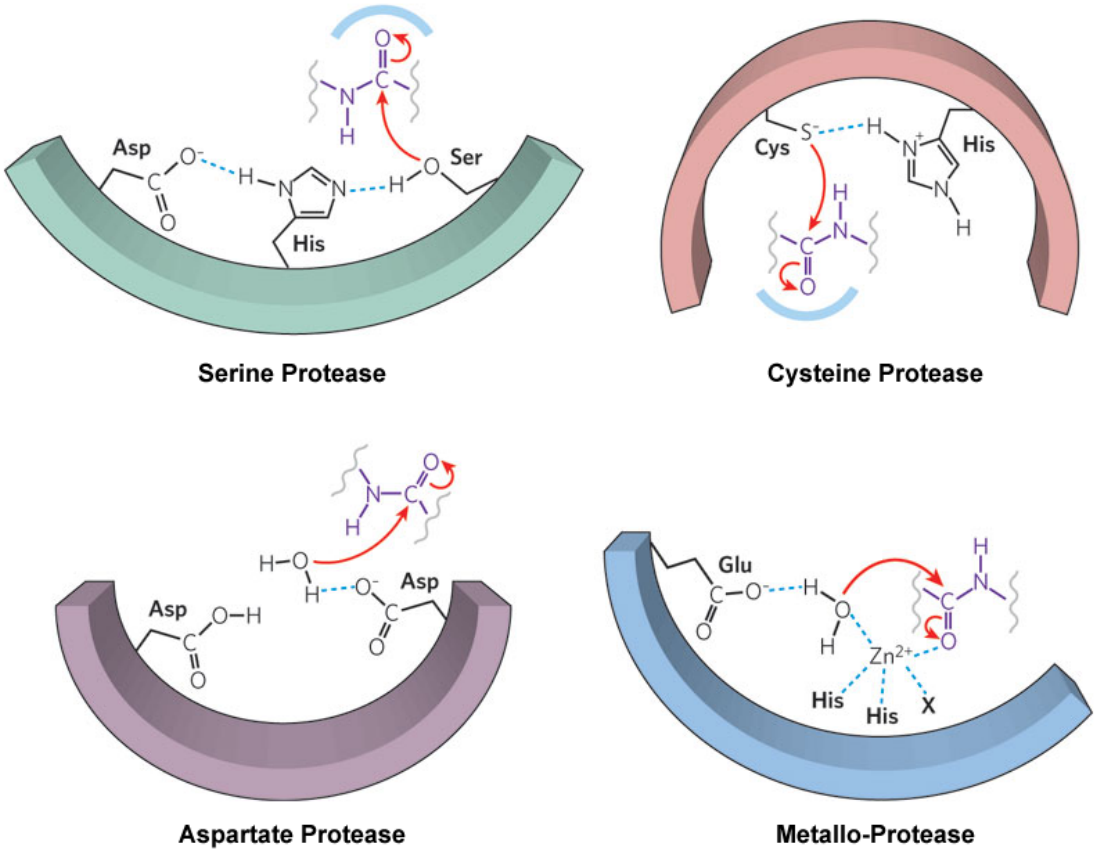

Figure 3.43: *Overview of the catalytic active sites of different proteases.*[332]

Serine and cysteine proteases feature similar cleavage mechanisms based on a structural feature called catalytic triad. It refers to a set of three amino acid residues found inside of the proteins active sites, which are directly involved in the catalytic step. In the case of serine proteases, the amino acids asparagine (Asp), histidine (His), and serine (Ser) are involved in the protease mechanism. The histidine—with the aid of the proton-withdrawing aspartate—acts as a powerful base and deprotonates the serine hydroxyl group. This allows the following nucleophilic attack on the carbonyl carbon of

the substrate and the cleavage of the peptide bond. A water molecule then reprotonates the histidine, and the remaining hydroxyl-ion attacks the carbonyl carbon resulting in a peptide with free C-terminus. Then, the cleaved peptide leaves the active site by diffusion. Also important for these reaction steps is a characteristic feature called oxyanion hole, which helps with the coordination of the substrate and stabilizes several tetrahedral transition states of the catalytic reaction. In the case of tryptase, the oxyanion hole is formed by the amides of Gly-193 and Ser-195 and the catalytic triad consists of the residues Ser-195, His-57 and Asp-102, resulting in an active cleavage site with a preference for lysine and arginine at the P1' position of the substrate.[229] Per definition by *Schechter* and *Berger*, the cleavage site positions of the substrate are between P1-P1'.[230] All amino acid residues in the N-terminal direction of the cleaved peptide bond are called P2, P3, P4, etc. The C-terminal end of the peptide is likewise incremented (P1', P2', P3', etc.). In an analogous way the cleavage sites of the protease are referred as S1 and S1' pocket, respectively.

The active site of tryptase is similar to other trypsin- and chymotrypsin-like proteases. However, tryptase clearly distinguishes itself from other serine proteases as it is resistant to most proteinaceous inhibitors. Initially only substances of small molecular weight, such as leupeptin or benzamidine were found as competitive inhibitors of tryptase.[231,232] This special behavior among serine proteases can be explained by the unique structure of tryptase.[233–236]

Tryptase has a tetrameric structure arranged in a ring-like structure with a total weight of approx. 134000 Da (Figure 3.44 on page 62). Tryptase is only enzymatically active in this form consisting of four non-covalently linked monomers. Each of the quasi-identical four subunits (A, B, C, and D) carries one active enzymatic site facing towards a central pore. Therefore, the tetramer displays an almost perfect 222 symmetry in the crystal structure with three 2-fold rotation axes.[233] The tryptase monomers interact with their neighbors via various non covalent contacts. The monomer combinations A+B and D+C, which are connected by only weak hydrophobic interactions, are additionally stabilized by heparin. This acidic polysaccharide can bind to positively charged residues on both interfaces, thereby connecting them (Figure 3.45 on page 62).

Within the pore the four negatively charged S1 binding pockets are displayed in defined spatial distances (see Figure 3.44, right). It is important to mention, that the four active sites are not on a plain layer, instead they can rather be visualized on the corners

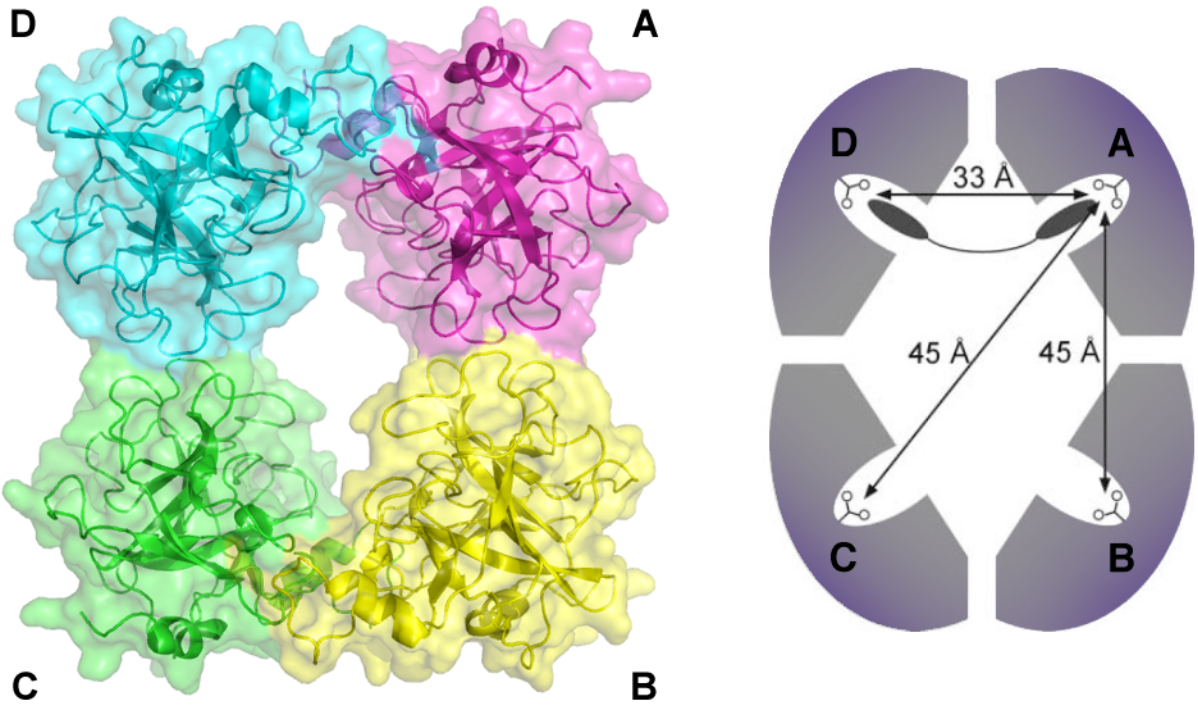

Figure 3.44: *Tetrameric structure of tryptase (PDB-code: 1A0L) with four active sites facing the inner pore.*[333]

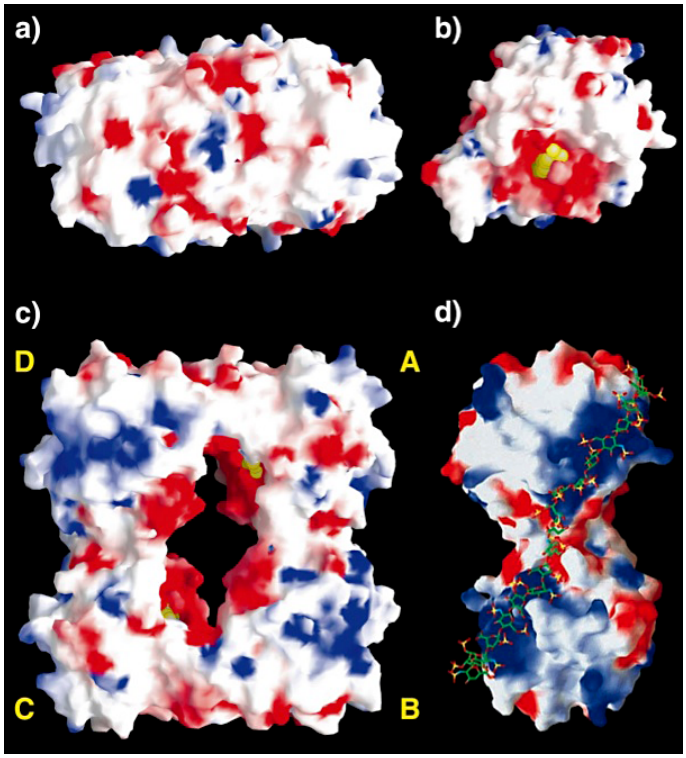

Figure 3.45: *Solid-surface illustration of tryptase indicating areas of positive (blue) and negative (red) electrostatic potential. The yellow molecule represents the small inhibitor 4-amidinophenylpyruvic acid (APPA); a) Top-view onto the DA homodimer; b) Tryptase monomer as seen from the middle of the central pore; c) Tryptase tetramer; d) Side-view of the AB homodimer stabilized by a heparin molecule.*[334]

of a distorted tetrahedron (twisted by approx. 30° from the tetramer axis). Hence the accessibility from the central pore is not equally distributed. The surroundings of the active sites are clustered with negatively charged residues, thus providing a point of interaction with basic compounds (Figure 3.45 on page 62). However, the access to the active sites is severely limited by the size of both openings to the pore. The entrances are approx. 40 × 15 Å wide, compared to the inner pore size of approx. 50 × 25 Å. These restrictions have an influence on possible inhibitors, which will be discussed in the following chapter (3.4.3).

Human tryptase derives from lung[237] and skin[238] tissue and exists in several isoenzymes (α_{1-2}, β_{1-3}, and mMCP-7-like).[23] β-Tryptase was identified to be the main derivate expressed in mast cells, whereas α-tryptase occurs—to a lesser extend—mainly in basophils.[239,240] β-Tryptase is stored in secretory granules in the mast cells and represents, with an amount of 10–35 pg per mast cell, 25 % of the total protein content of the cell, and 90 % of their granules.[240] In the human body, mast cells are present in most tissues in the vicinity of blood vessels, and are especially prominent near the boundaries between the outside world and the internal milieu, such as the skin and the lungs. The stimulation of mast cells with antigens (allergens), mediated by IgE or other stimuli, results in an increased release of tryptase (together with other inflammatory mediators) into the blood stream.[241] Eventually, this causes bronchoconstriction and the development of airway hyperresponsiveness, typical symptoms of an allergic reaction or asthma attack.[242,243]

On a molecular level tryptase interacts with different peptides and activates other proteins. For example, it degrades several neuropeptides, such as vasoactive intestinal peptide (VIP) and peptide histidine-methionine (PHM),[244] activates prekallikrein, and generates kinins,[245,246] all important mediators in the development of inflammatory disorders. As a consequence, tryptase inhibitors have become the subject of studies as potential therapeutic agents. Therefore, the following chapter will describe different structural approaches for the inhibition of β-tryptase.

3.4.3 Methods for the Inhibition of β-Tryptase

In contrast to almost all serine proteinases, there are no known natural inhibitors of tryptase in humans.[247] However, since the publication of the crystal structure in 1998

by *Sommerhoff* and *Bode*,[233] a rising number of synthetic inhibitors have been reported. In general, the discovered tryptase inhibitors can be classified into three groups, heparin antagonists, proteinaceous structures and low molecular weight inhibitors.

Heparin antagonists: The class of heparin antagonists exploits the unique requirement of tryptase, to be only enzymatically active in the tetrameric form. As previously mentioned, the structure of tryptase is stabilized by the presence of heparin. Therefore, it was shown that compounds, which are able to bind heparin can inhibit the protease. The general interpretation of these findings was, that the compounds compete with the tryptase to bind heparin. This causes the destabilization of the tetramer, followed by the fragmentation into four monomers without cleavage activity. Interestingly, the destabilized, inactive tetramer-intermediate can be reactivated by the addition of heparin, whereas this is not possible with inactive monomers.[248,249] Kinetic studies confirmed in most of the cases an irreversible and non-competitive mode of inhibition.[23]

One of the first reported compounds was antithrombin, a small protein known to inactivate thrombin by the interaction with heparin.[250] Later, many polycationic substances of varying molecular sizes followed. For example lactoferrin, a 78 kDa cationic protein released by neutrophils, was shown to inhibit tryptase in a non-competitive way with an IC_{50} value of 24 nM.[251] The studies also reveled, that lactoferrin had no activity towards proteases, which do not require heparin for stabilization, such as trypsin, thrombin or plasmin. Other cationic proteins with inhibition potential are myeloperoxidase (IC_{50} = 16 nM)[252] and protamine (IC_{50} = 56 nM).[253] The latter is a small arginine-rich protein (4500 Da), which is clinically used as heparin antagonist to neutralize its anticoagulant effect after surgery. But also synthetic compounds showed inhibitory effects, such as polybrene (5–10 kDa, hexadimethrine bromide)—also used in the reversal of heparin therapy—with an excellent IC_{50} value of 3.6 nM.[253] Recently, synthetic poly-Lys and poly-Arg as well as linear octapeptides were shown to have inhibition effects up to IC_{50} values of 1 nM. However, the exact mechanism of interaction remained uncertain in these experiments.[254]

In summary, these various types of polycationic heparin antagonists represent an interesting and highly potent class of inhibitors. However, the relative large molecular size and the high charge density limits their potential as therapeutic for tryptase-related inflammatory diseases.

Proteinaceous inhibitors: A small protein, named Leech-derived tryptase inhibitor (LDTI) is the only known, active-site directed proteinaceous inhibitor.[255] It is a 46 amino acid residue protein (4700 Da) isolated from the medical leech *Hirudo medicinalis*. It inhibits tryptase in the nanomolar range (K_i = 1.4 nM), but also trypsin (K_i = 0.9 nM) and chymotrypsin (K_i = 20 nM).[255] The exact mode of interaction with tryptase is not known, but it is suggested that LDTI occupies two of the four active sites. However, it is controversially discussed, if the protein is too big to enter the central pore.[234] Computational modeling studies, based on the solution structure of LDTI and the crystal structure in complex with trypsin,[256] describe a possible position within the central cavity (Figure 3.46).[234]

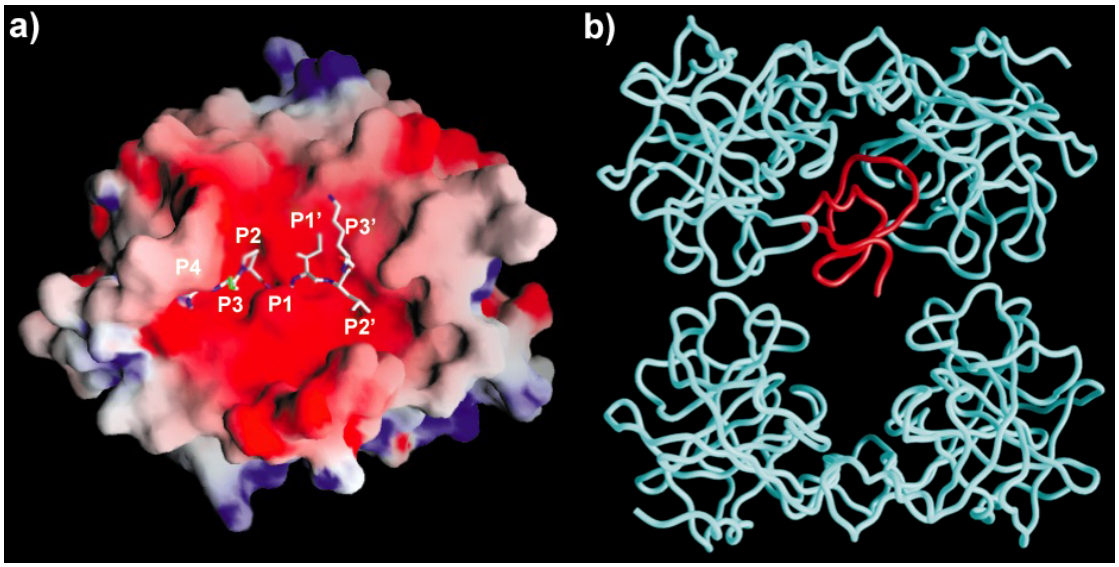

Figure 3.46: *a) Illustration of the electrostatic surface potential of trypsin in complex with the binding loop of LDTI. View towards the acidic active site of trypsin; b) Model of the proposed interaction between LDTI and the tryptase tetramer.*[334,335]

Low molecular weight inhibitors: The biggest group of tryptase inhibitors represent small synthetic inhibitors, which are able to enter the central pore and interact in a competitive way with the active site. The common low molecular weight inhibitors of trypsin-like serine proteases, such as leupeptin (**43**) and p-aminobenzamidine (p-Ab, **44**) also inhibit tryptase in the micro-molar range (K_i = 1.0 μM and 65 μM) (Figure 3.47 on page 66).[248] One of the first monovalent inhibitor, that went into a clinical trial for the treatment of asthma was APC-366 (**45**). However, the success of the studies was very moderate with slight beneficial effect, due to the weak and slow inhibition properties (K_i = 0.3–450 μM).[257] It was also no selectivity over other serine proteases, such as trypsin or thrombin observed.[258]

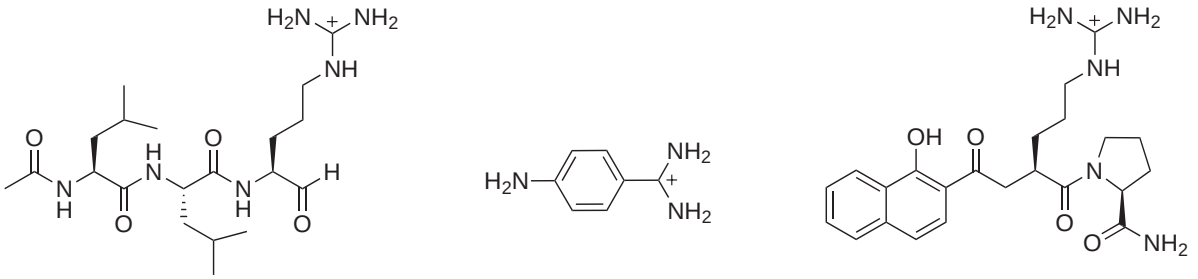

leupeptin
43

p-Ab
44

APC-366
45

Figure 3.47: *Small monovalent inhibitors of tryptase.*

The knowledge of the tryptase crystal structure led to the discovery of a new class of inhibitors, the (quasi)symmetric dibasic inhibitors. The principle design is based on two inhibiting entities, which are linked by spacers of various length. This allows the simultaneous binding into two neighboring active sites within the central pore. The beneficial influence of the multivalent effect led to highly active inhibitors in the nano-molar range. For example, the compound AMG-126737 (**46**) (K_i = 90 nM), which bears two benzamidine functions was shown to inhibit the development of airway hyperresponsiveness in guinea pigs with an ED_{50} of 0.015 mg/kg.[241] In addition the inhibitor also featured a 10- to 200-fold selectivity versus other serine proteases.

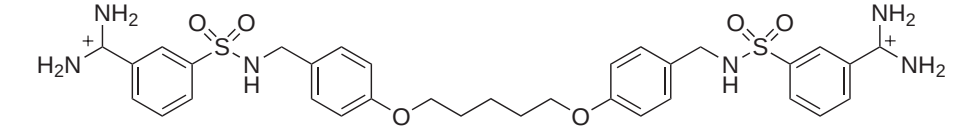

AMG-126737
46

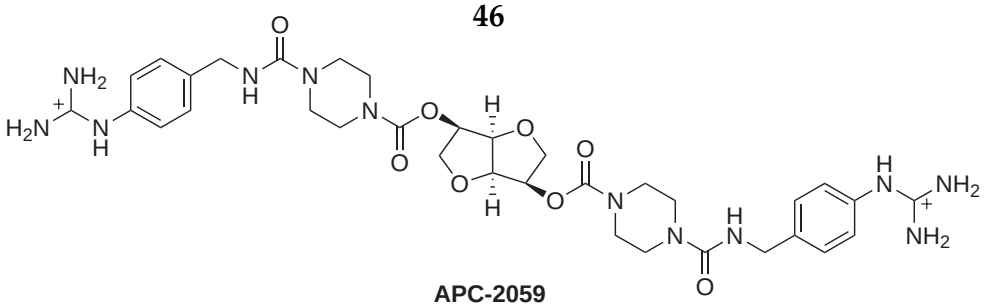

APC-2059
47

Figure 3.48: *Examples of dibasic inhibitors for the simultaneous binding in two S1 active sites of tryptase.*

For the next generation of dibasic inhibitors the linker structure was systematically varied to obtain the optimal length and rigidity for the interaction with two active sites.

Rice et al. investigated several competitive and reversible inhibitors based on heterocyclic and aromatic scaffolds and different linker sizes.[259,260] The compound APC-2059 (**47**) has a length of 33 Å, which corresponds to the shortest distance separating two binding pockets in tryptase (cf. Figure 3.44 on page 62). APC-2059 demonstrated not only high inhibition efficiency (K_i = 0.1 nM) and selectivity over other serine proteases, but also very good pharmacokinetics and safety properties in a phase II clinical trial.[261]

A combinatorial library of similar inhibitors based on a central diketopiperazine scaffold was investigated by *del Fresno et al.*[262] *Diez et al.* successfully synthesized an aminolactam-derived library with dibasic inhibitors in the low micro-molar range.[263] An interesting variation of the central scaffold was reported by *Schaschke et al.*[264] It was possible to link two aminomethyl benzene groups to a rigid cyclodextrin scaffold resulting in 10^4-fold higher selectivity for tryptase (K_i = 0.6 nM) over trypsin (K_i = 4.8 μM). This example demonstrated the advantages of entropically favored scaffolds, but also highlighted the limitations due to possible enthalpic strains as a result of bidentate binding events.

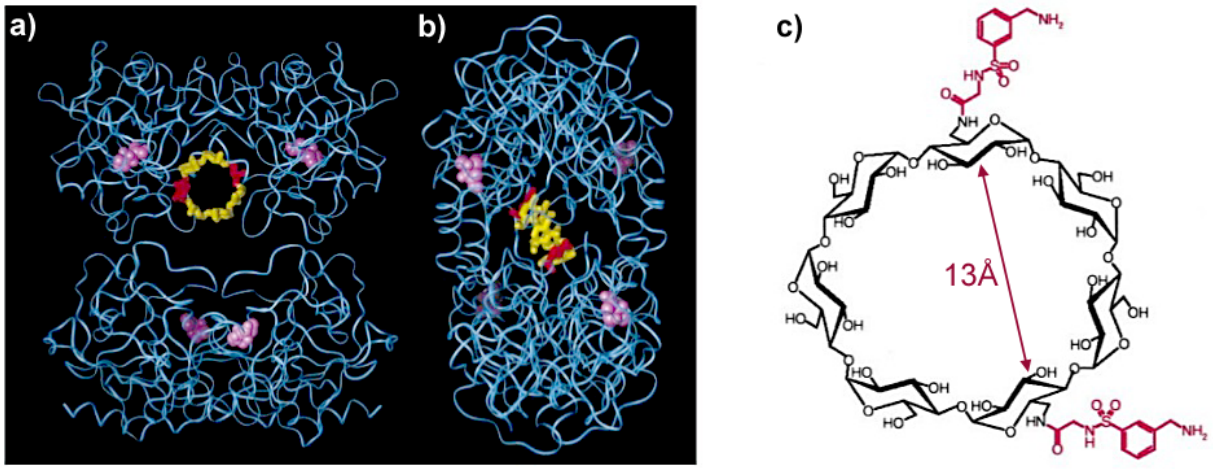

Figure 3.49: *a) Ribbon representation of the β-tryptase tetramer with β-cyclodextrin, positioned in the central pore between the tryptase subunits A and D. Asp-189 at the bottom of each S1 pocket is shown in magenta; b) Top view on tryptase subunits A and D; c) Structure of functionalized β-cyclodextrin scaffold.*[336]

Cunsolo et al. reported the investigation of a similar circular scaffold. They synthesized calix[8]arene-based ligands with eight basic amino acid residues for a selective tryptase inhibition. The best inhibitors had K_i-values between 2 and 80 nM, however a conclusive mode of inhibition could not be reasoned.[265] To some extent, a rapid inactivation of

tryptase was observed, what led to the conclusion that the ligands also interact with the stabilizing heparin. On the other side, also signs of competitive inhibition were observed. Furthermore, the exact site of interaction between the inhibitor an the protease is still unclear. The size of the calixarene may not allow a complete uptake into the central pore. Therefore, only a general description of an interaction with the acidic area close to the active sides was proposed.

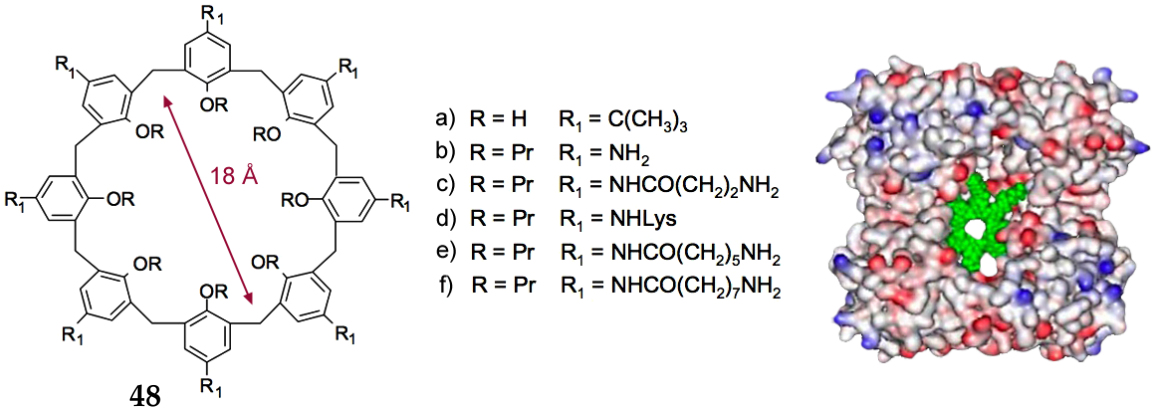

Figure 3.50: *Multivalent calixarene scaffold with eight basic residues (left); Proposed representation for the complex between tryptase and inhibitor (**48**d, green CPK model)(right).*[337]

Scarpi et al. focused their research on linear peptides as tryptase inhibitors. In particular, they investigated the sequence SCTKSIPPQCY from the binding loop of the Bowman-Birk inhibitor (BBI), a protein that is known to inhibit chymotrypsin-like proteases, but not tryptase. The smaller peptide fragment, however, is able to enter the central pore and interact with the active sites. In studies of different N- and C-terminal functionalized BBI-peptides K_i-values up to 1.0 nM were obtained.[266] *Spichalska et al.* investigated a combinatorial library of linear heptapeptides as inhibitors and observed inhibition in the micromolar range (K_i = 30–100 μM).[267] They based their experiments on reports, that β-tryptase has an enhanced substrate specificity for positively charged residues in positions P1 and P3, whereas positions P2 and P4 display a broader specificity.[268]

In summary, the previous examples demonstrate, that enzymes are interesting and still challenging targets for the search of new potent inhibitors . In particular, β-tryptase represents an attractive serine protease, due to its unique tetrameric structure and the restricted entrance to its active sites. Especially the heterogeneous arrangement of the electrostatic potential on the surface of β-tryptase may allow—beyond the active site regions—a variety of different interactions with artificial peptide receptors.

CHAPTER 4

RESULTS AND DISCUSSION

4.1 Understanding the Molecular Recognition of Small Peptides

The first part of this thesis focused on the experimental elucidation of the actual complex structure between small peptide sequences. Especially of interest was the interaction between the peptide receptor CBS-Lys-Lys-Phe-NH_2 (**1**) and the tetrapeptide N-Ac-D-Glu-D-Glu-D-Glu-D-Glu-OH (**49**) (Figure 4.1 on page 70). This complex is known to show strong electrostatic interactions and therefore is perfect for in-depth studies which may help to optimize the receptor design further. The synthesis of both receptor and substrate were already published previously.[9,269] To have substantial amount of material for the following studies, the synthesis was further optimized for a larger scale. Especially a fast and easy purification process was introduced, using reversed phase HPLC (with MeOH/H_2O + TFA as solvent) to obtain the high purity needed for NMR and Raman experiments.

All previous assumptions about a possible complex structure (of similar structures) originated from computational calculations.[8,269] The following chapters will describe several methods to validate these conclusions with the help of NMR and Raman spectroscopy methods and will also introduce, based on the gained knowledge, a new way to screen combinatorial receptor libraries.

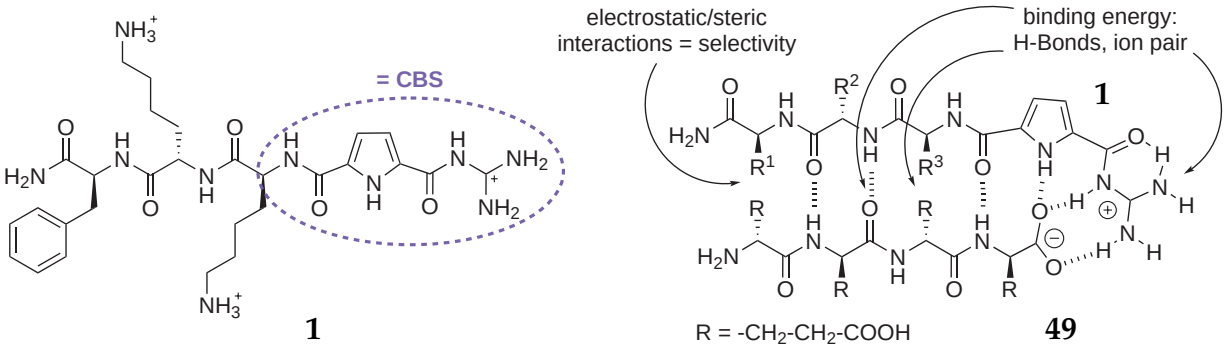

Figure 4.1: *Structure of the artificial peptide receptor CBS-Lys-Lys-Phe-NH_2 (**1**) (left); Schematic representation of the complexation between receptor **1** and the tetrapeptide N-Ac-D-Glu-D-Glu-D-Glu-D-Glu-OH (**49**) (right).*

4.1.1 Discussion of NMR and Raman Experiments in Solution as Part of External Cooperations

NMR experiments: Due to the biological relevance, all NMR experiments were performed if possible in pure water or DMSO with powerful high-resolution NMR measurements techniques. In a cooperation with *Prof. Sebastian Schlücker*, formerly Department of Physical Chemistry, University of Würzburg; now Department of Physics, University of Osnabrück and *Prof. Tobias Ulmer*, Department of Biochemistry and Molecular Biology of the Keck School of Medicine, University of Southern California (USA) several NOESY, ROESY and TOCSY experiments were done by PhD student *Stephan Niebling* from the *Schlücker* group. The NOESY spectra were measured on a *Bruker Ultrashield* spectrometer (700 MHz) with cryo sample holder and the TOCSY spectra with a *Varian* spectrometer (400 MHz). Both, receptor **1** and tetrapeptide **49** were measured in a 1:1 stoichiometry at a concentration of 1.5 mM.

With these experiments it was possible to gain some very interesting information about the structural conformation of each compound. Unfortunately no unambiguously assignable correlation peaks between the two compounds could be detected in water or DMSO. This could be due to the high flexibility of the complex and the very competitive solvent conditions. The analysis of the NOESY and TOCSY data revealed that both compounds most likely are in a stretched all-trans conformation in DMSO, which would confirm the predicted β-sheet conformation (see Figure 4.1). This can be explained with the correlation peaks in the NOESY spectrum, showing that the H_α-protons interact more with the amide proton of the subsequent amino acid than the own one. Another in-

dication are the strong NOE-cross peaks in the receptor spectrum between the pyrrole C-H (at 7.5 ppm) and the nearby guanidinium amide N-H (at 11.95 ppm), revealing the spatial proximity of these two protons (see Figure 4.2).

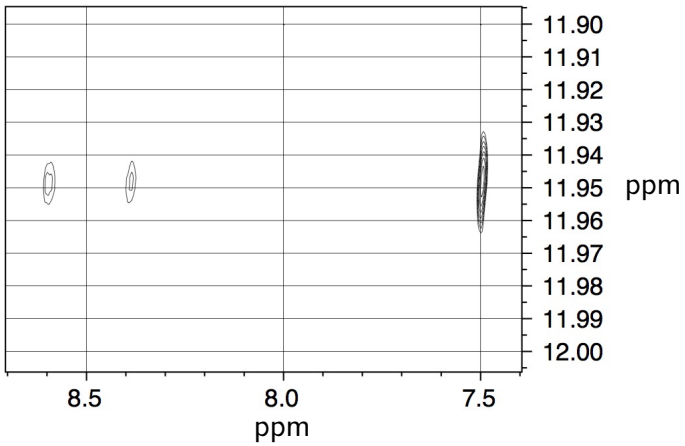

Figure 4.2: *A strong correlation peak of the pyrrole C-H (at 7.5 ppm) with the guanidinium N-H (at 11.95 ppm) is an indication for an all trans conformation of receptor* ***1*** *(also visible are the weaker interactions of the guanidinium NH_2-groups (at 8.4 and 8.6 ppm) with the guanidinium N-H).*

This conformation, called out-out (left, Figure 4.3), is more favorable (8.4 kJ/mol) than the out-in conformation, necessary for a complexation of the free carboxylate in water.[270] However, this aspect does not contradict the initial conception of a carboxylate binding of the receptor and the tetrapeptide, as shown in Figure 4.1. At least in DMSO the observed complex structure might prefer a complete β-sheet structure over the additional complexation of the free carboxylate. However, due to the different binding conditions in water and the relative low rotation barrier of 8.4 kJ/mol the initial perception of the carboxylate complexation can be still assumed.

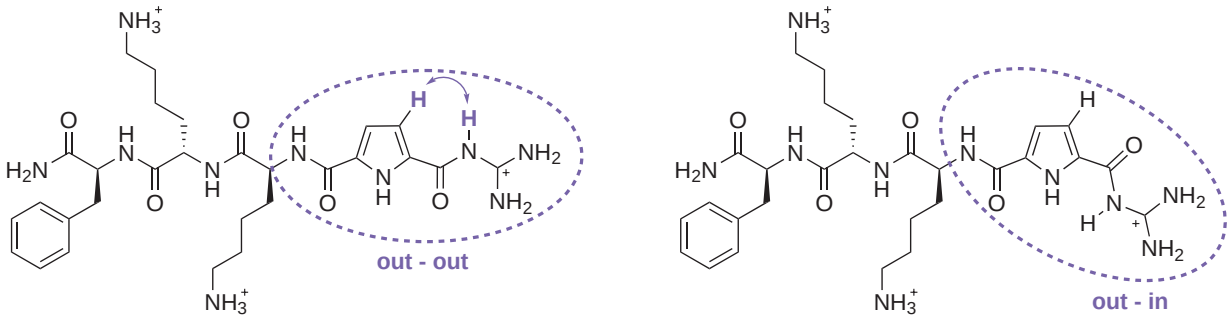

Figure 4.3: *The proton of the guanidine N-H is in close proximity to one of the pyrrole C-H in the "out-out" conformation (left); the energetically more demanding but favorable conformation for the complexation of a free carboxylate is called "out-in" (right).*

Nevertheless, the complete elucidation of the complex structure in water was not accomplished as a whole by NMR methods due to the competitive conditions in polar solvents. But it was possible to gain essential information about the individual conformation of the binding partners.

Raman experiments in solution: In order to obtain further information about the influence of the carboxylate binding site in the peptide receptor (**1**) a more sensitive method was applied. The Raman spectroscopy overcomes the limitations of NMR involving sensitivity and susceptibility to unfavorable dynamics. Our cooperation partners, the group of *Prof. Sebastian Schlücker* performed resonance Raman scattering experiments,[57] a special technique that is capable of monitoring the complexation between CBS-based receptors and tetrapeptides without the need of external labels. For this project, in addition to the peptide receptor CBS-Lys-Lys-Phe-NH_2 (**1**) also the model system CBS-NH_2 (**52**) was synthesized by me and purified with reversed phase chromatography. The synthesis was accomplished with a short solid phase synthesis using Rink-amide resin (Scheme 4.1). Boc-protected CBS-OH was attached with standard coupling conditions to the resin. After the cleavage with 95 % TFA the previous free acid function had been transformed into an amide.

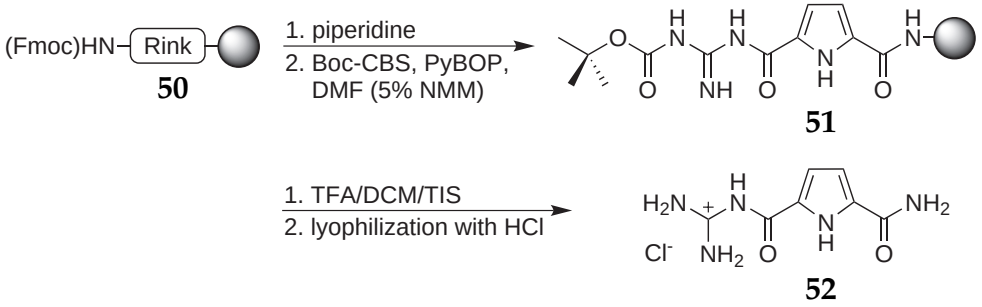

Scheme 4.1: *Synthesis of the model system CBS-NH_2 (**52**) as structural minimized form of receptor **1**.*

The following descriptions summarize the results of the Raman measurements in solution, obtained by *Prof. Schlücker* and his coworkers.[271,272] The peptide receptor (**1**) shows a strong and characteristic electronic absorption at 298 nm in UV (see Figure 4.4), which is due to the CBS subunit of the receptor. Thus, choosing an UV excitation wavelength in electronic resonance with the guanidiniocarbonyl pyrrole cation allows the selective monitoring of the interaction of the CBS of **1** with the carboxylate of peptide

substrate **49**. Because of the enormous signal enhancement in resonance Raman scattering it was possible to perform Raman spectroscopic experiments with receptor **1** in the submillimolar range combined with the advantage of selectively enhancing Raman scattering from the CBS subunit.

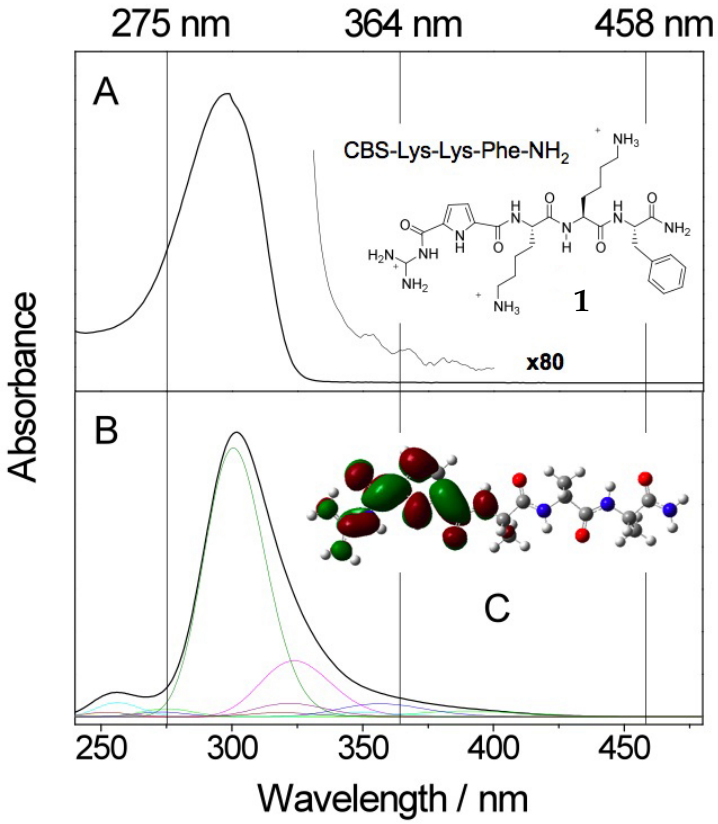

Figure 4.4: *(A) Experimental electronic absorption spectrum of the receptor CBS-Lys-Lys-Phe-NH_2 (**1**); (B) TD-DFT calculated electronic absorption spectrum of the model system CBS-Ala-Ala-Ala-NH_2; (C) Molecular orbital of CBS-Ala-Ala-Ala-NH_2 involved in the most intense electronic transition at 298 nm in (B).*[338]

The following pictures show the Raman spectra recorded for a 0.5 mM aqueous solution of the neat receptor **1** and several mixtures with increasing amount of the tetrapeptide **49** (II-IV) at pH 6. The addition of only half an equivalent of the tetrapeptide **49** to the receptor **1** already leads to significant changes in the corresponding UV resonance Raman spectra (see Figure 4.5, left). A depiction of the difference Raman spectrum of the 1:2 mixture and the neat receptor shows pronounced and specific spectral differences (Figure 4.5, right). For example, the isolated Raman band (A) at 1702 cm^{-1} exhibits changes in both wavenumber position and intensity (vibration of the CBS subunit containing

C=O stretching contributions). The largest spectral intensity changes are observed for region (B) around 1480 cm^{-1}, in which ring modes of the pyrrole part occur.

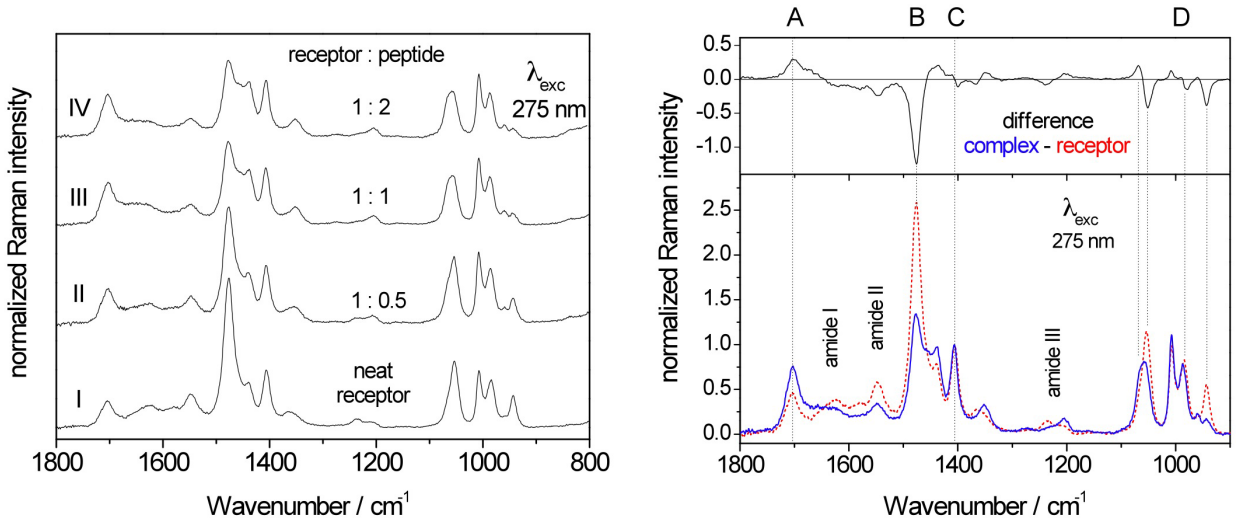

Figure 4.5: *(left) Normalized UV resonance Raman spectra of CBS-Lys-Lys-Phe-NH_2 (**1**, I) and its mixture with different equivalents of tetrapeptide N-Ac-D-Glu-D-Glu-D-Glu-D-Glu-OH (**49**, II-IV); (right) Normalized UV resonance Raman spectra of **1** (solid blue line) and its 1:2 mixture with the tetrapeptide **49** (dashed red line) and its difference spectrum.*[338]

Therefore these experiments demonstrate that it was indeed possible to selectively monitor the carboxylate binding to the CBS by using UV resonance Raman spectroscopy. In addition they confirm the importance oft the CBS for the molecular recognition of such peptides in water.

A quantitative interpretation of the changes observed in the experimental UV resonance Raman spectra of the receptor **1** upon complexation requires a detailed characterization of the receptor itself. For an assignment of its individual bands the comparison with a calculated spectra of receptor **1** is helpful. However, due to the structural complexity of **1** and the fact that the main changes happen, as mentioned, in the CBS unit, CBS-NH_2 (**52**) was chosen as a model system for that. A quantum chemical calculation on high level in a water environment revealed the theoretical Raman spectra of two possible conformers (see Figure 4.6 on page 75). The differences in both peak positions and intensities clearly demonstrate the capability of Raman spectroscopy to distinguish between the conformers.

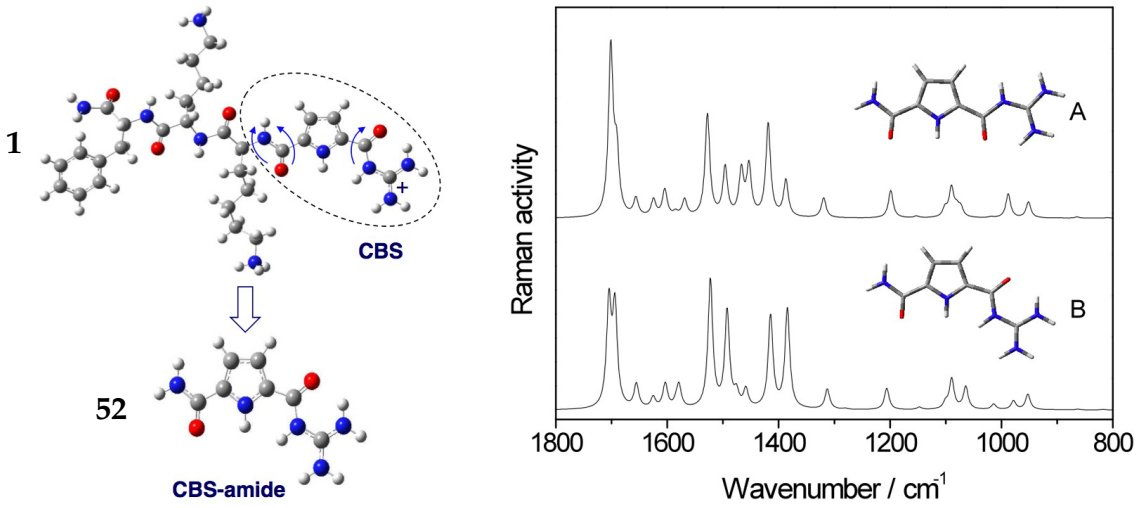

Figure 4.6: *Calculated Raman spectrum of model receptor* ***52*** *in its two conformers A and B.*[338]

But not only the conformation of the CBS, also the protonation state has influence on the Raman spectra. So, in order to determine the individual spectral contributions from the protonated and neutral CBS species, pH-dependent Raman studies on the small model receptor CBS-NH_2 (**52**) and the larger peptide receptor CBS-Lys-Lys-Phe-NH_2 (**1**) were performed in a pH range of 6 to 7. The pK_a of the CBS-unit—as previously determined with titration experiments—is around 6.5, therefore the recorded spectra contain characteristic signals from both CBS species in different proportions. The received spectra at pH = 6–7 were then analyzed with a mathematical method called non-negative matrix factorization (NMF), which helps to separate the "mixed" spectral contribution of the protonated and neutral receptor species. This allows the spectra prediction at a pH of 2 and 10, i.e. it is possible to calculate the Raman spectra of the peptide in its completely protonated as well as the entirely deprotonated form. Control experiments with Raman measurements at pH = 2 and 10 indeed confirmed that in the case of both compounds (**52** and **1**) the calculated spectra were almost identical with the measured ones (see Figure 4.7 on page 76 for compound **1**).

In summary these results show that with the help of the UV resonance Raman spectroscopy it was possible to gain significant information about the receptor structure and its change during the complexation of a possible substrate. In particular the influence of the CBS was clarified with this method, which has in terms of structural information many advantages over fluorescence spectroscopy.

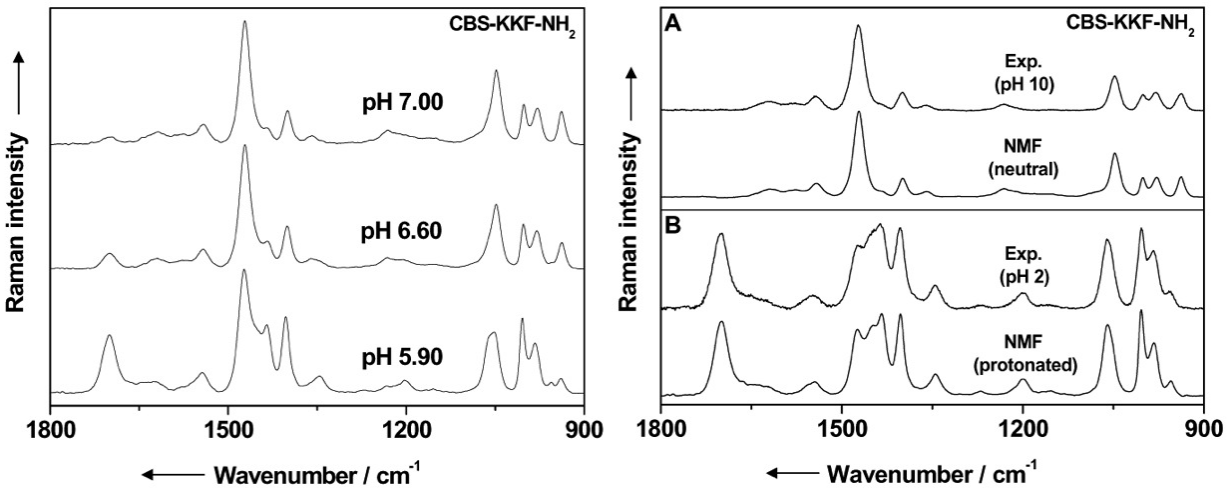

Figure 4.7: *(left) UV Raman spectra of CBS-Lys-Lys-Phe-NH_2 (**1**) in water at pH values above and below the pK_a of the CBS-unit (6.5), which had the main contributions in the spectra; (right) (A) Experimental UV Raman and NMF-derived component spectrum of **1** at pH 10 assigned to the neutral CBS species; (B) The same spectra set at pH 2 assigned to the protonated CBS-species.*[339]

4.1.2 Development of a New On-Bead Screening Method Based on SERS

The results described in the previous chapter illustrate the feasibility of Raman spectroscopy for the examination of supramolecular interactions. Based on the results of these thorough investigations in solution the approach was extended to a direct and label free spectroscopic detection of solid phase bound compounds which are often found in combinatorial libraries. In general, the solid support—in most cases a modified polystyrene resin—has a loading of typically some 100 pmol per bead. Due to this low loading it is rather difficult to analyze the solid-phase bound compound directly. But with the help of a method called surface enhanced Raman scattering (SERS) it is possible to detect structural information of compounds bound to a single polystyrene bead within few seconds. This is possible due to noble metal nanoparticles that tremendously enhance the Raman signals up to a factor of 10^{14} but only of those molecules which are close to their surface (Figure 4.8 on page 77).

As a proof of concept for this completely new detection method, the artificial peptide receptor CBS-Lys-Lys-Phe-NH_2 (**1**) was analyzed but this time bound to a solid sup-

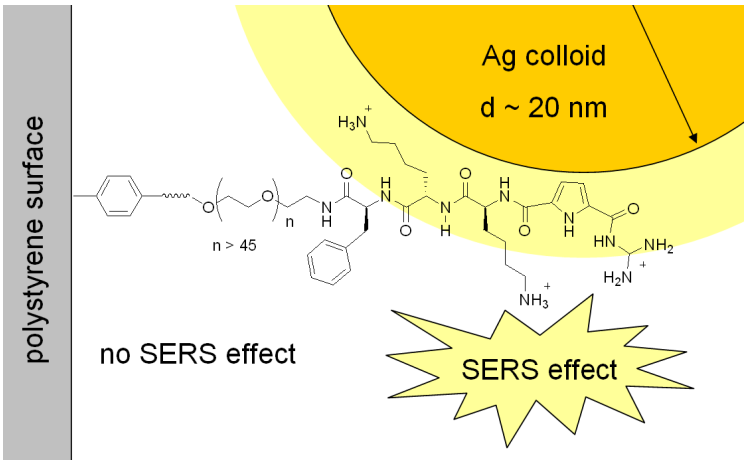

Figure 4.8: *Silver colloidal particles lead to a tremendous enhancement of the Raman signal of an immobilized peptide receptor.*[340]

port (**55**). Therefore the receptor was synthesized on TentaGel resin, a polystyrene based resin that has long polyethylene glycol chains on the surface for good swelling properties in polar solvents like water. The synthesis of CBS-Lys-Lys-Phe-TentaGel (**55**) was performed under analogous conditions as **1**. The same amino acids as well as the standard coupling conditions with PyBOP and NNM in DMF could be applied. However, due to the high acid stability of the resin, the peptide remains on the solid support during the final deprotection step with 95 % TFA (Scheme 4.2).

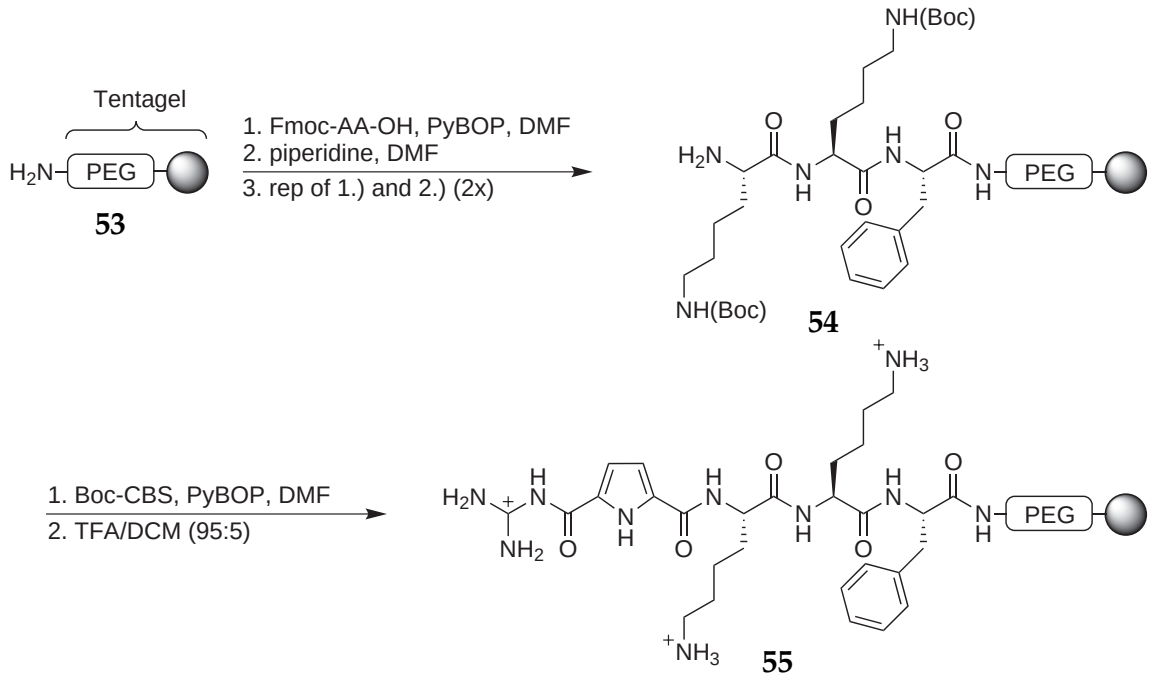

Scheme 4.2: *Synthesis of the immobilized form (**55**) of the artificial peptide receptor CBS-Lys-Lys-Phe-NH_2 (**1**), which is attached to TentaGel resin.*

Our cooperation partner, the group of *Prof. Sebastian Schlücker*, provided the silver nanoparticles and performed the Raman experiments. The colloidal solution of silver nanoparticles was mixed with the swollen TentaGel resin **55** which was already functionalized with the peptide sequence as mentioned before.[273] As the size of the silver nanoparticles used here is around 10000 times smaller than the size of the TentaGel beads (see Figure 4.9), the silver particles can only interact with small areas on the surface of the solid support. Hence, the nanoparticles only "see" the peptide which is attached via long polyethylene glycol chains (M $\approx$ 2000 g·mol^{-1}, n = 45), but they do not sense the underlying polystyrene matrix.

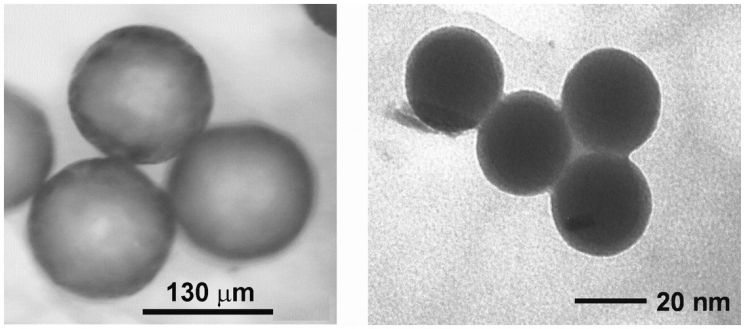

Figure 4.9: *Microscopic image of the polystyrene beads (TentaGel) which can be functionalized with peptides (left); TEM image of the silver nanoparticles used for the SERS effect. The nanoparticles are around four orders of magnitude smaller than the polystyrene beads (right).*[340]

Under these conditions, we were able to directly record a Raman spectrum of about 50 femtomole of **55** still attached to the TentaGel bead within a few seconds (upper spectrum, Figure 4.10 on page 79). A qualitative comparison with the conventional Raman spectrum of **1** in a 20 mM aqueous solution, which takes around 30 minutes to record, showed a close match of the signal sets and no spectral contributions from the polystyrene support (lower spectrum, Figure 4.10). Hence, this method of on-bead detection using SERS is about a factor of 10^6–10^7 more sensitive than a conventional Raman spectrum recorded in solution—based on the comparison of the detected amount on bead and in solution—and takes only a few seconds compared to minutes in the later case (for a complete description of this approximation, see calculation in ref.[273]). Therefore, a direct and label free detection of molecules bound on a solid phase is possible even with the standard resins and the rather low loadings conventionally used in solid phase synthesis.

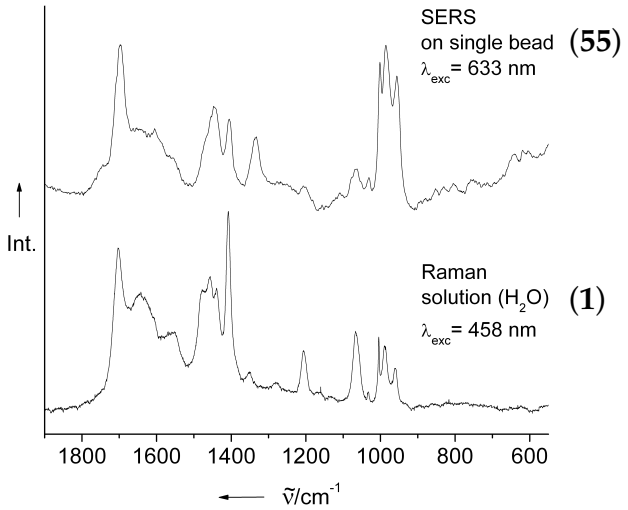

Figure 4.10: *The SERS spectrum measured on one bead resembles the conventional Raman spectrum recorded in solution.*[340]

To probe the reproducibility of this method, spectra from different beads as well as from different surface spots on one bead were recorded. In all cases essentially the same SERS spectrum was obtained for **55** (left spectrum, Figure 4.11). In addition receptor **1** was also synthesized on a different sort of bead, the PAM resin (see Chapter 7.3 for experimental data). This resin lacks the polyethylene glycol linker and is purely based on polystyrene. The spectrum quality is not as good as with TentaGel but the characteristic Raman signals are also clearly visible (right spectrum, Figure 4.11). Hence, the method is not limited to TentaGel even though it works best if the compounds under analysis are more distant from the polystyrene matrix.

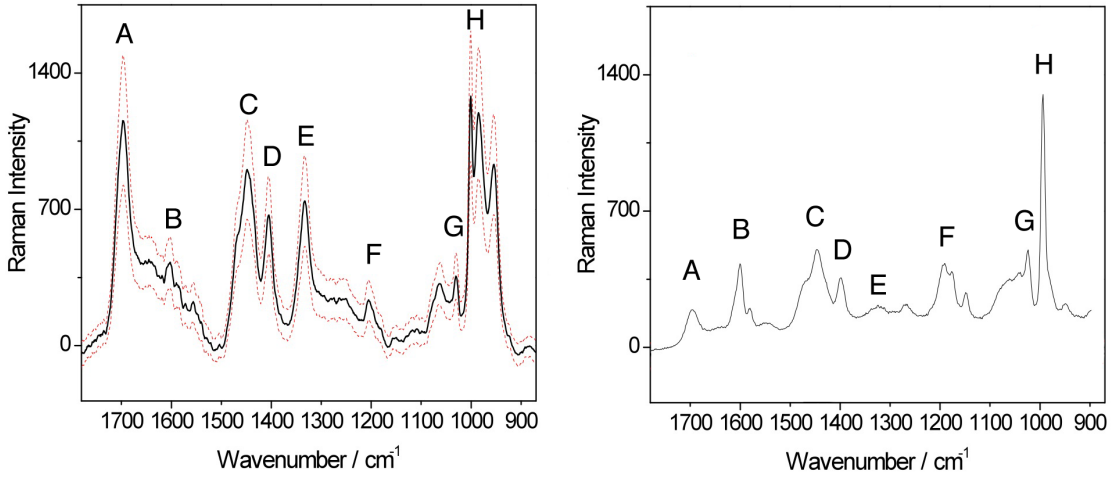

Figure 4.11: *(left) Solid line in black: mean SERS spectrum for **1** on TentaGel resin calculated from a Raman point microspectroscopic mapping experiment (36 spectra) on a single bead; (right) SERS spectrum of **1** on PAM resin with similar bands (A-H).*[340]

First attempts to monitor the complex formation between with **55** and the tetrapeptide N-Ac-D-Glu-D-Glu-D-Glu-D-Glu-OH (**49**) were not successful. The origin of the problem was the pH value (2.5) necessary for the aggregation of the nanoparticles. Under these conditions the tetrapeptide was fully protonated (i.e. no free carboxylates) and therefore could not built up the electrostatic interactions necessary for the complex formation.

In order to test if this Raman technique is capable to distinguish between different compounds attached to a solid support, the SERS spectrum of a structurally related compound but with completely different amino acids in the tripeptide part was also recorded. The sequence CBS-Ala-Ile-Val was synthesized under similar conditions as before on TentaGel (**56**). Then again a Raman spectrum was recorded. Differences in the SERS spectra of the two compounds (Figure 4.12) are clearly visible, indicating that indeed a Raman spectroscopic differentiation and identification of immobilized compounds is possible.

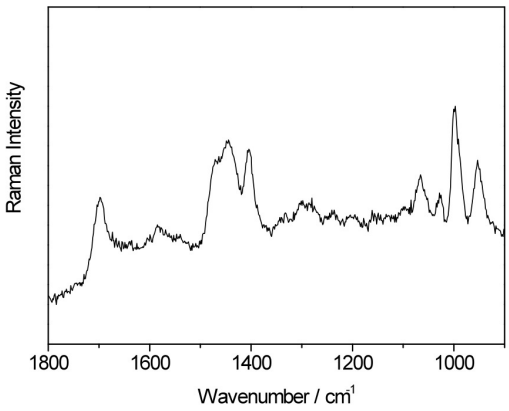

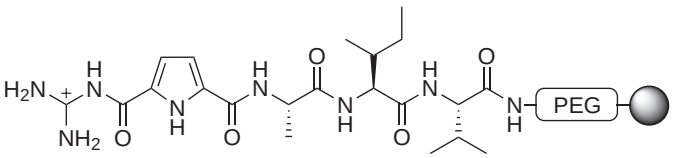

56

Figure 4.12: *SERS spectrum of compound CBS-Ala-Ile-Val on TentaGel (**56**) which just differs in the tripeptide part compared with compound **55**. The spectrum exhibits characteristic differences when compared with the spectrum of **55** (Figure 4.11).*[340]

In summary, this was the first time that a direct detection of a compound attached to a single polystyrene bead using surface enhanced Raman scattering (SERS) was achieved. Therefore, the method allows to distinguish between different compounds based on the differences in their Raman spectra. This opens, for example, the possibility for an easy and fast structure determination and identification during a solid phase synthesis. This method might also help to detect spectral changes upon complex formation with another molecule in an on-bead screening experiment. Hence, this completely new

approach could improve the scope of the well established high-throughput screenings used by industrial and academic laboratories all around the world. It could be used in biochemical and pharmacological tests, not only to rapidly identify active compounds, but also to immediately provide an insight into the structural changes happening during the screening.

4.1.3 Conclusion and Outlook

The first part of this thesis focused on the analysis and the understanding of the non-covalent interaction between small peptide sequences. It was possible to gain important information about the structural arrangement of the small artificial peptide sequence CBS-Lys-Lys-Phe-NH_2 (**1**) with the help of NMR and Raman spectroscopical methods. Several aspects of this receptor molecule were investigated, in particular the conformational behavior of the CBS group responsible for its dominant binding properties. Therefore, especially the prominent spectroscopical features of the guanidiniocarbonyl pyrrole were analyzed in different solvents with different pH values. Based on these results it was possible to apply the gained knowledge and develop a completely new method for the detection of immobilized peptide sequences using silver nano particles. With the help of the SERS effect it was possible to distinguish between the structure of different peptide sequence still bound a single resin bead. This technique surpasses in many areas the solid state NMR, which is not sensitive enough and requires much more material.

However, the actual investigation of the non-covalent interactions in a supramolecular complex still remains very challenging. In particular polar solvents and flexible molecules complicate the analysis. The results of this thesis lay the foundations for the future understanding of the detailed structural interactions of supramolecular complexes. Especially the complex interactions and the individual contributions of the amino acids have to be analyzed in detail. The main focus for future Raman experiments should be on the unambiguous assignment of all spectral bands, in particular during a complexation process to monitor the structural changes, e.g. information about the spatial arrangement of the amino acid side chains and the behavior of the peptidic backbones. First steps were already done with the Raman experiments in solution and the qualitative monitoring of the complex formation. Also SERS experiments revealed differences in the obtained spectra of the peptide receptors. However, it was not possible to monitor the complex formation due to the existing pH value (2.5) necessary for the aggregation

of the nanoparticles. Future preparation techniques may allow the right pH adjustment in the physiological range, eventually leading to the structural analysis of the on-bead complexation.

Further methods for the determination and the analysis of the complex formation in solution may include the mass-spectrometrical analysis of strong peptide complexes and crystallization experiments. Isothermal titration calorimetry (ITC) experiments to determine the thermodynamic parameters of the complex formation are also of interest. This method not only allows the direct measurement of the binding affinity (K) but also the enthalpy changes (ΔH), Gibbs energy changes (ΔG) and entropy changes (ΔS).

4.2 The Synthesis of Tailor-Made Oligopeptides for Biological Recognition Events

The following chapter describes various experiments to investigate the interaction of small oligopeptides with biological relevant structures. Especially the different structural designs to enhance the activity for the given biological target will be described in detail. The search for efficient peptides included several modifications in the structural composition, e.g. the addition of solubility and fluorescence groups. But also the exchange of individual amino acids and changes in the spatial arrangement apart from normal linear peptides were under investigation.

4.2.1 Design of a Binder for Alzheimer's related β-Amyloid Fibrils

In cooperation with the group of *Prof. Jerry Yang*, UC San Diego (USA) it was the aim to investigate the possible binding of the peptide receptor CBS-Lys-Lys-Phe-NH_2 (**1**) to the free C-terminal peptide sequence (VVIA) of β-amyloid (Aβ) fibrils. As mentioned before, this receptor has a high binding affinity towards free carboxylates and therefore came into consideration as a possible molecule that can interact with the amyloid fibrils.

All experiments were carried out by myself during a research exchange visit in San Diego, where it was possible to apply a special screening method developed by the group of *Prof. Yang*. The used ELISA-based assay is described schematically in Figure 4.13 on page 84 and in detail in the literature.[109] The only difference to the known procedure was the used buffer solution. Instead of PBS buffer (phosphate buffered saline) at pH = 7.4, tris-buffer at pH = 6 was used. This new base was picked to avoid a possible interaction of the phosphate in PBS with the CBS of the receptor. The pH was chosen to ensure the deprotonation of the guanidino group in the receptor.

The basic procedure of the assay starts with the coating of 96 well plates with freshly prepared Aβ-fibrils. Then the inhibitor, in our case the peptide receptor, was added and incubated over night. In the next step, the receptor-coated fibrils were treated with a monoclonal anti-Aβ IgG. Finally, the interaction of the anti-Ab IgG with the receptor-coated Aβ fibrils was quantified with an ELISA-based assay using a UV-Vis spectroscopic readout.

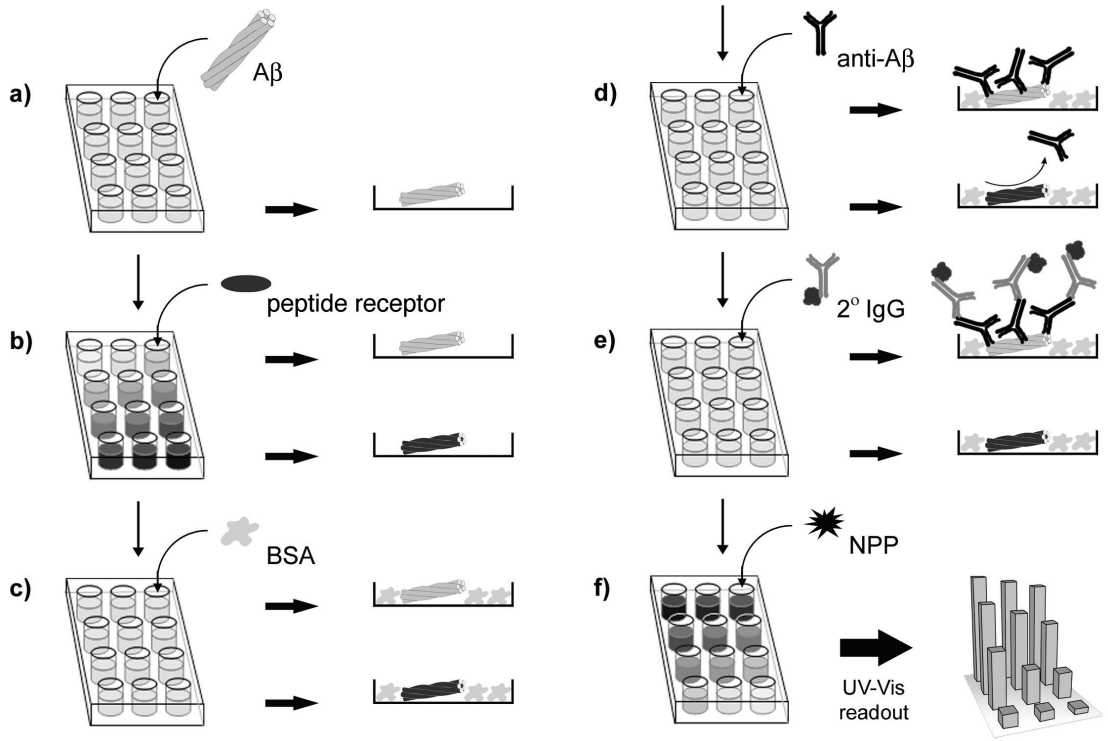

Figure 4.13: *Illustration of the ELISA-based assay to test the inhibition of IgG-amyloid interactions by coating the surface of* Alzheimer's*-related Aβ-fibrils with small peptides.*

For the first tests several already known and in our group available peptide receptors were chosen (Table 4.1 summarizes the results). Only receptor **1** and **57** show an inhibition effect at concentrations around 40-50 mM. Due to problems with the solubility in the buffer, receptor **58** could only be tested at low concentrations (< 10 mM) and exhibited no effect.

Table 4.1: *Initial tests of different peptide receptors as inhibitors for the interaction of proteins with Aβ (1–42) fibrils.*

No.	Receptor	Fibrils	c(Receptor)	Observation
1	CBS-Lys-Lys-Phe-NH_2	Aβ (1–42)	50 mM	inhibition effect
57	CBS-Lys-Tyr-Lys-NH_2	Aβ (1–42)	40 mM	inhibition effect
57	CBS-Lys-Tyr-Lys-NH_2	Aβ (1–42)	2.5 mM	no effect
58	CBS-Val-Val-Val-NH_2	Aβ (1–42)	1 mM + DMSO	no effect

These first promising results led to the additional determination of the IC_{50} value of receptor **1**. Also a possible specificity between Aβ 1–40 and Aβ 1–42 was tested, respec-

tively. Both amyloid peptides are biological relevant and have different C-terminal sequences. Unfortunately, an accurate confirmation of the IC_{50} was not possible because of solubility limits at higher concentrations, but the results suggest values around 100 mM (Figure 4.14).

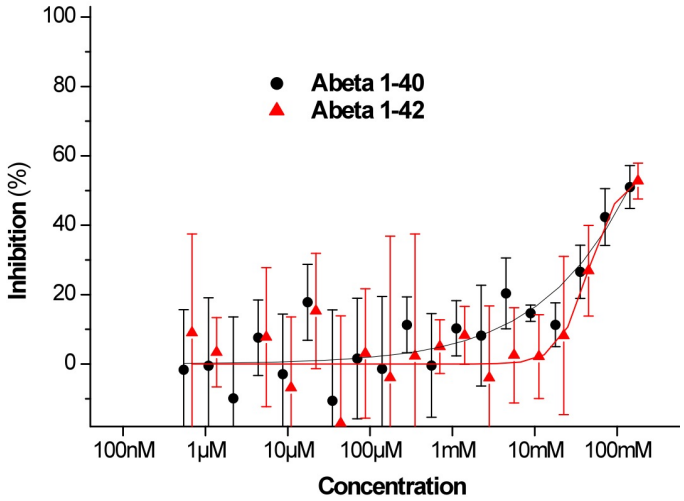

Figure 4.14: *Receptor **1** associates with both forms of Aβ (1–40) and (1–42) at similar concentrations (c > 10 mM). The IC_{50} value is approx. 100 mM.*

It was not possible to observe a selective interaction with one of the two C-terminal sequences of the fibrils. The lack of specificity might the result of secondary interactions with the fibrils (van der Waals forces, polar forces). Hence, a determination of the complete mode of interaction was not possible. However, it was possible to show that already small and simple peptide receptors like **1** can interact with biomolecules like amyloid fibrils. Certainly, the affinity and specificity had to be increased. This led to the design and synthesis of the following peptide systems, hopefully featuring a higher activity.

59

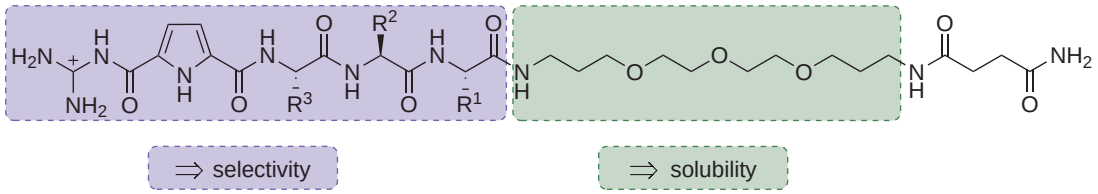

Figure 4.15: *Schematic representation of receptor **59** (R^1 = Phe, R^2 = R^3 = Lys) with an additional triethylene glycol chain for better solubility in polar solvents.*

The first new peptide system CBS-Lys-Lys-Phe-TEG-NH_2 (**59**) is a variation of **1** with an additional triethylene glycol chain for better solubility (Figure 4.15). The synthe-

sis starts with Rink amide resin and the attachment of succinic anhydride, which is necessary to convert the initial amine function of the resin to an acid function. Then the triethylene glycol group was introduced with the coupling of 1,13-diamino-4,7,10-trioxatriadecane, followed by three amino acids, coupled under standard solid phase peptide synthesis conditions. As the last building block the Boc-protected guanidiniocarbonylpyrrole carboxylic acid (CBS) (**64**) was attached. In the final cleavage step from the resin also all side chain protecting groups of the amino acids and the CBS were removed. After dry freezing with added hydrochloric acid, compound **59** was obtained as a colorless solid (Scheme 4.3).

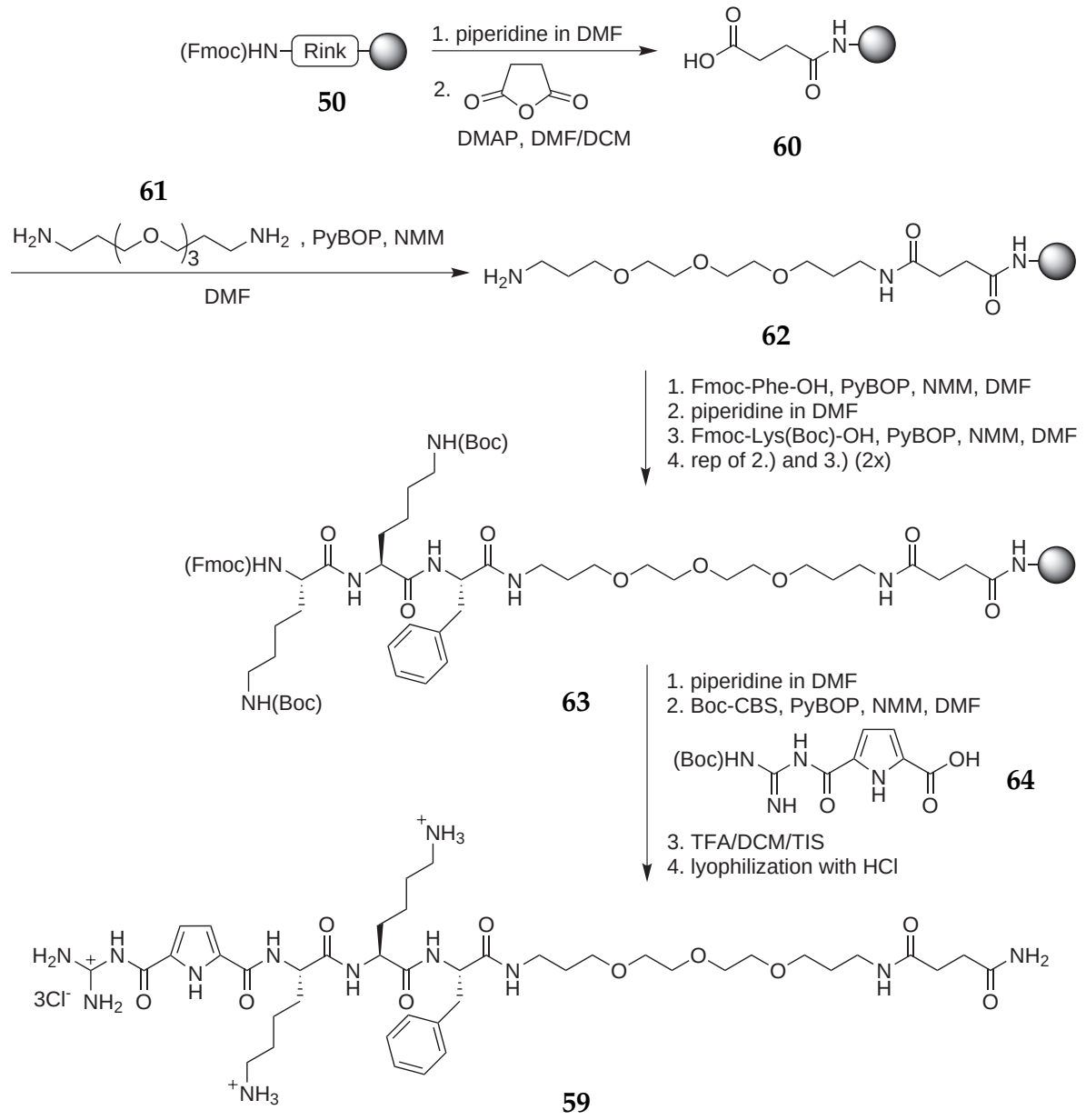

Scheme 4.3: *Synthesis of CBS-Lys-Lys-Phe-TEG-NH_2 (**59**) with hopefully better solubility and biological activity.*

The next attempt was to investigate an increase of binding affinity with the help of a multivalent structure. Therefore **1** was synthesized as trivalent structure (**65**) based on one common scaffold (Figure 4.16).

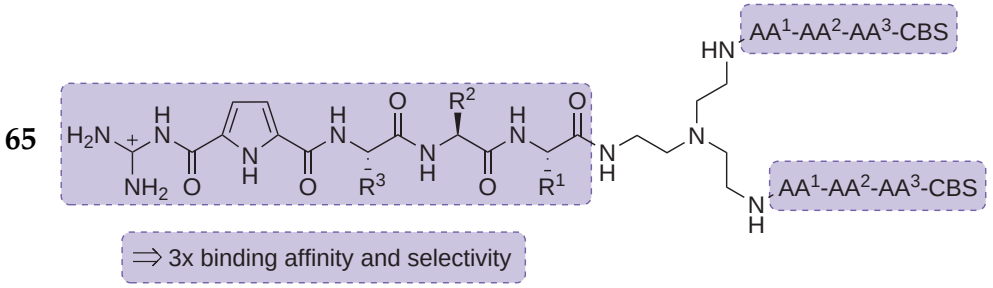

Figure 4.16: *Schematic representation of receptor **65** (R^1 = Phe, R^2 = R^3 = Lys) attached to a trivalent scaffold for a higher affinity.*

To introduce a flexible and simple trivalent scaffold, tris-(2-aminoethyl)-amine (TREN) (**67**) was chosen. It was coupled in a single reaction with three equivalents of compound **66** under standard coupling conditions in DMF over night in solution. After the coupling all protecting groups were removed with the help of a 1:1 mixture TFA in DCM (Scheme 4.4 on page 88).

All functional groups of the monomeric form of the peptide receptor (**66**) had to be protected except the acid function. To avoid any alternative reactions (i.e. the reaction with itself) the Boc-group was chosen as a protecting group for all amines. With this strategy only the amines of TREN would react with the peptide receptor. Compound **66** was synthesized with a solid phase peptide procedure similar to CBS-Lys-Lys-Phe-NH_2 (**1**). The only difference is the free carboxylic acid at the C-terminal end of the final peptide and the fact that even after the cleavage from the resin all Boc-protecting groups must be preserved. Both requirements could be achieved with the use of SASRIN resin (Super Acid Sensitive ResIN).[274,275] Due to the high acid sensitivity of its linker it is possible to cleave any compound from the resin already with 1 % TFA (in DCM), a harmless amount for any used protecting group. The cleavage mixture was collected by filtration into a flask containing pyridine to scavenge the TFA. This procedure had to be repeated several times to ensure a complete cleavage from the resin. Finally, all solvents were removed and the product purified by reversed-phase MPLC (Scheme 4.4 on page 88).

With the synthesis of **59** and **65** it was possible to introduce two new substructures of the initial peptide receptor **1**. First tests already revealed an increased solubility of **59**

in water which presumably leads to a higher activity in the bioassays. Unfortunately it was not possible yet to test these substances for their activity linked to Aβ fibrils due to time constraints. However, with the successful synthesis of the trivalent peptide system the way for more multivalent structures was paved. In particular it was hoped to benefit from the unique features of multivalent systems (described in Chapter 3.2) as an antimicrobial agent. Several of these branched systems were synthesized and examined as described in the following chapter.

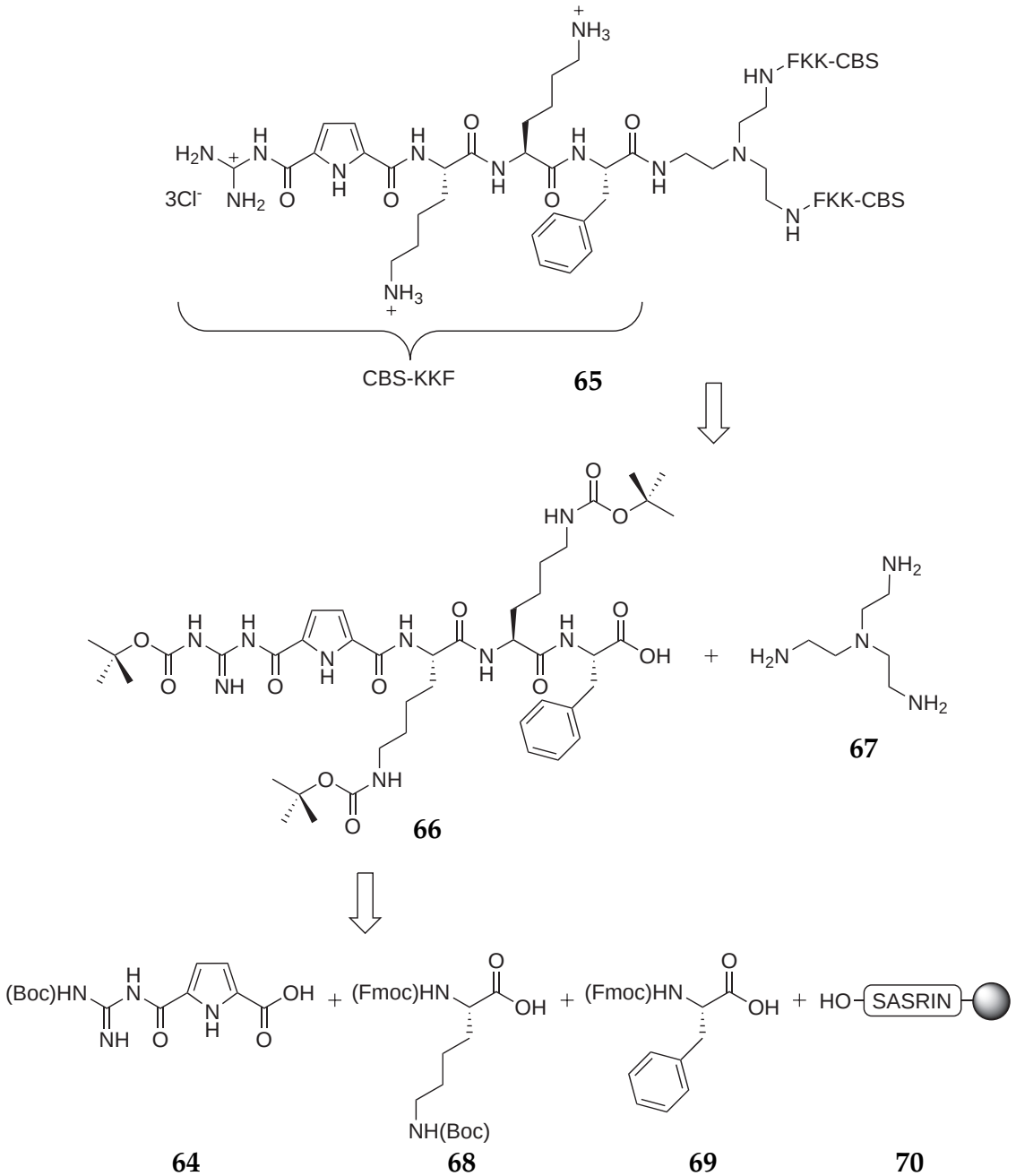

Scheme 4.4: *Synthesis of trivalent peptide receptor (CBS-Lys-Lys-Phe)$_3$TREN (**65**) with TREN (**67**) as branching element.*

4.2.2 Fluorescence Labelled Peptides as Biomarkers

Peptide receptors on the basis of the guanidiniocarbonyl pyrroles have previously shown that they are interesting for the investigation of biochemical processes, or more generally to the qualitative as well as quantitative analysis of peptide mixtures. So far we found low-molecular receptors which already show *in vitro* an impressive affinity and selectivity to biologically relevant model peptides. However, in respect of an *in vivo* application the affinities should be increased about one to two powers of ten, into the sub-micro molar range. A promising strategy is the multivalent approach already mentioned in the previous chapter.

In particular, this approach might be interesting to study the use of artificial peptide receptors for a related field of interest, the interaction with biological membranes. Small peptides bearing several positive charges are known to have the remarkable feature to pass readily through nonpolar membranes of cells and also enter tissues. Especially arginine rich peptides with a basic structure in combination with a few hydrophobic amino acids such as tryptophan and phenyl alanine show transmembrane activity (see Chapter 3.3.2 on page 31). Therefore, the previously mentioned structures such as CBS-Lys-Lys-Phe-NH_2 (**1**) and its variations (**59** and **65**) might be interesting candidates due to their similar types of amino acids (accumulation of positive charges, artificial arginine analog, aromatic amino acid). In particular we were interested in the membrane interaction with Gram-positive and negative bacteria. During the synthesis of the cell wall of Gram-positive bacteria, linear peptidoglycans are crosslinked involving the tetrapeptide sequence D-Glu-L-Lys-D-Ala-D-Ala-OH, which is also the point of attack of the important antibiotic vancomycin. *Schmuck et al.* demonstrated that the tris-cationic receptor **1** efficiently binds this peptide sequence in buffered water.[269] However, it is unknown how this receptor might interact with the real membrane of bacteria.

For the investigation of this kind of interaction fluorescence labelled forms of the receptors are necessary to detect the molecules and a possible translocation process across the different membrane types. For this purpose a fluorescence label in form of a dansyl group was attached via a spacer to the C-terminal end of the receptor (Figure 4.17).

The synthesis of the dansyl labelled receptor **71** (short form: CBS-KKF-(Dns)) was achieved with standard solid phase peptide chemistry starting with the attachment of the first amino acid on Rink amide resin (Scheme 4.5 on page 91). Therefore, a specially

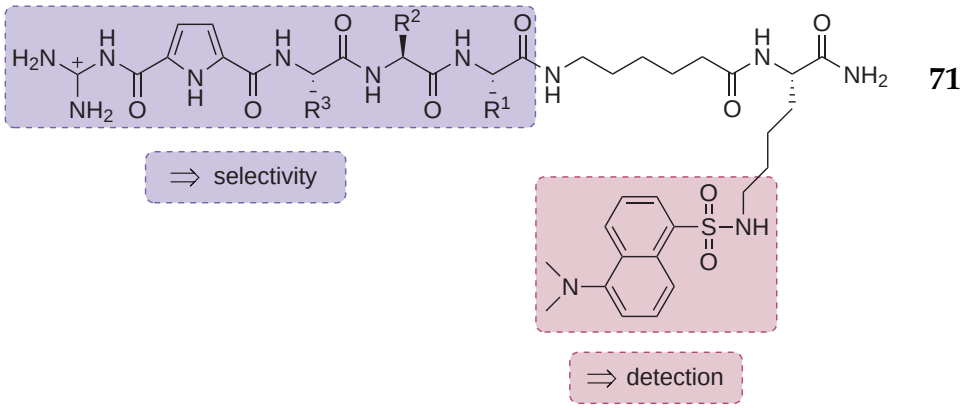

Figure 4.17: *Fluorescence labelled form of the initial peptide receptor* ***1*** *(R^1 = Phe, R^2 = R^3 = Lys).*

protected form of lysine was chosen. It has a base labile Fmoc-protecting group at the α-amino function and an acid labile Mtt-protecting group for the amino function in the side chain. This orthogonal protecting group allows the selective deprotection of the side chain with 1 % TFA in DCM followed by the introduction of the dansyl group. Thereafter the Fmoc group was cleaved with piperidine and the spacer aminocaproic acid was coupled to the free amine under the same conditions as normal amino acids. The following tripeptide and the guanidiniocarbonylpyrrole carboxylic acid were attached under standard conditions for SPPS as previously described (see also Scheme 4.3 on page 86). The product **71** was cleaved from the solid support by shaking the resin with a mixture of 50 % TFA in DCM.

To study also the differences and possible advantages of a multivalent structure, the known peptide receptor **1** was attached to a common template, a lysine trimer (see Figure 4.18 on page 92). Hence, the new receptor design (**75**) features a tetrameric structure with four side chains for the linkage of **1**. Again, a fluorescence label for an easy detection was integrated in the structure.

The synthesis of the multivalent peptide receptor **75** started the same way as the monovalent form **71**. After the insertion of the dansyl label the attachment of amino acid **76** followed, a two times Fmoc-protected form of lysine (see Scheme 4.6 on page 93). This allowed the simultaneous deprotection of both protecting groups in the following step and the introduction of the first branching. Amino acid **76** was then again coupled to the resin, but this time with twice the equivalents as before. The resulting compound **77** had now four positions for the attachment of the peptide sequence of receptor **1**. Thereafter,

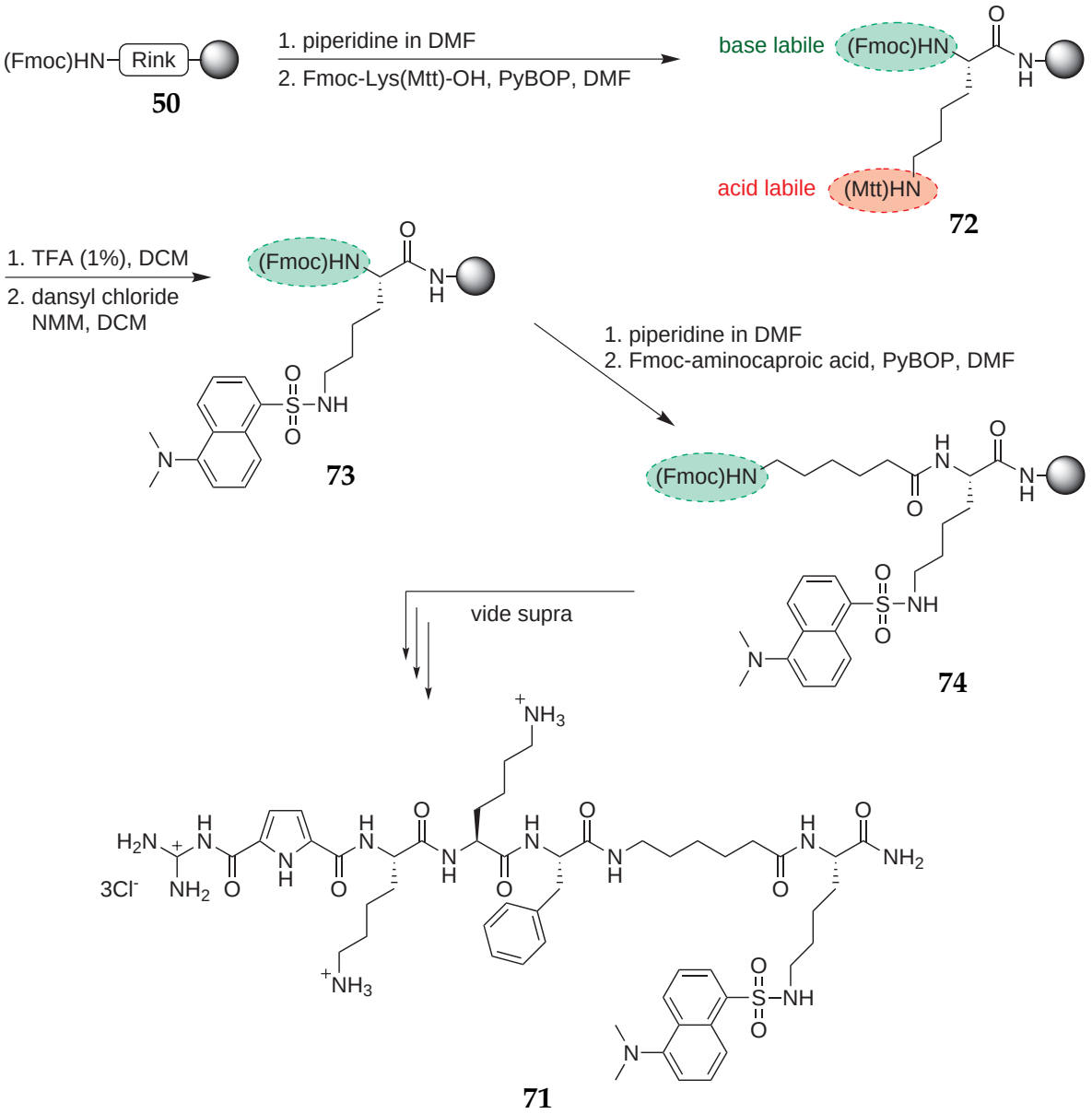

Scheme 4.5: *Synthesis of CBS-Lys-Lys-Phe-aminocaproicacid-Lys(Dansyl)-NH_2 (short form: CBS-KKF-(Dns), **71**) with an additional fluorescence label for an easy detection.*

the product was treated with a mixture of 50 % TFA in DCM which led to the cleavage from the Rink amide resin and the simultaneous removal of all protecting groups. After the dry freezing with added hydrochloric acid, the compound **75** (short form:* (CBS-KKF)$_4$-(Dns)) was obtained as a colorless solid (Scheme 4.6 on page 93).

* The following abbreviation scheme is used for all tetravalent peptides in this thesis: [(*peptide sequence in each of the four side chains*)$_4$]-[*optional insertions into the lysin scaffold*]-[*optional dansyl label*].

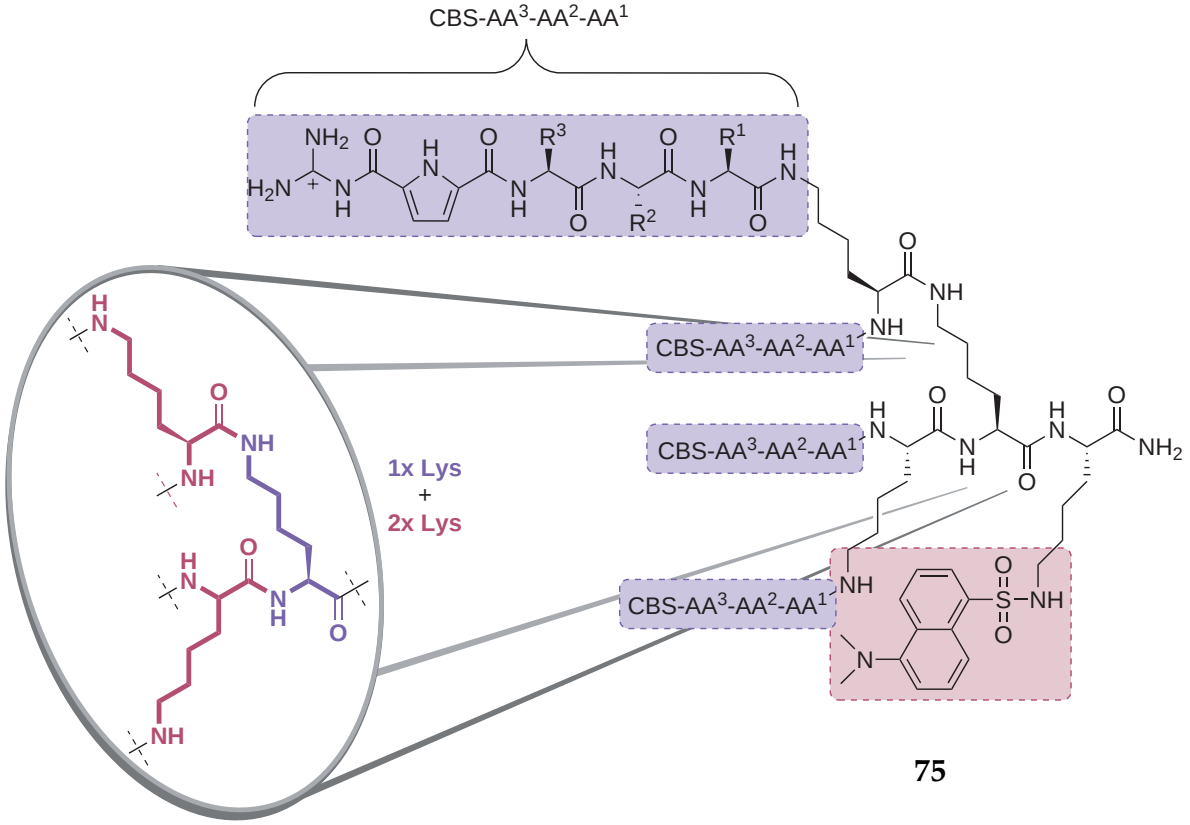

Figure 4.18: *Schematic representation of tetravalent receptor* ***75*** *(R^1 = Phe, R^2 = R^3 = Lys). The branching element is a lysine trimer (highlighted in the circle).*

The fluorescence labelled compounds **71** and the multivalent form **75** were then tested in cooperation with the group of *Prof. Bradley Smith*, University of Notre Dame (USA) for their membrane crossing potential. Therefore, the effect of both peptides on the Gram-positive bacterium *Staphylococcus aureus* (strain NRS11) and the Gram-negative bacterium *Escherichia coli* (strain UTI89) was evaluated. To determine the concentration at which fluorescence staining of the bacteria can be detected, overnight cultures of each respective bacteria were treated with varying concentrations of peptide. The peptides were dissolved in double-distilled H_2O at concentrations ranging from 1 mM to 5 mM. 10 μL of the peptide solution was then added to bacteria suspended in 1 mL of TES buffer (pH = 7.4) yielding final concentrations ranging from 10 to 50 μM. The staining, which occurred at various concentrations, was evaluated using fluorescence microscopy. The minimum concentration at which fluorescence was observed in bacterial membranes was 50 μM for peptide **71** and 45 μM for peptide **75** in the Gram-positive bacterium

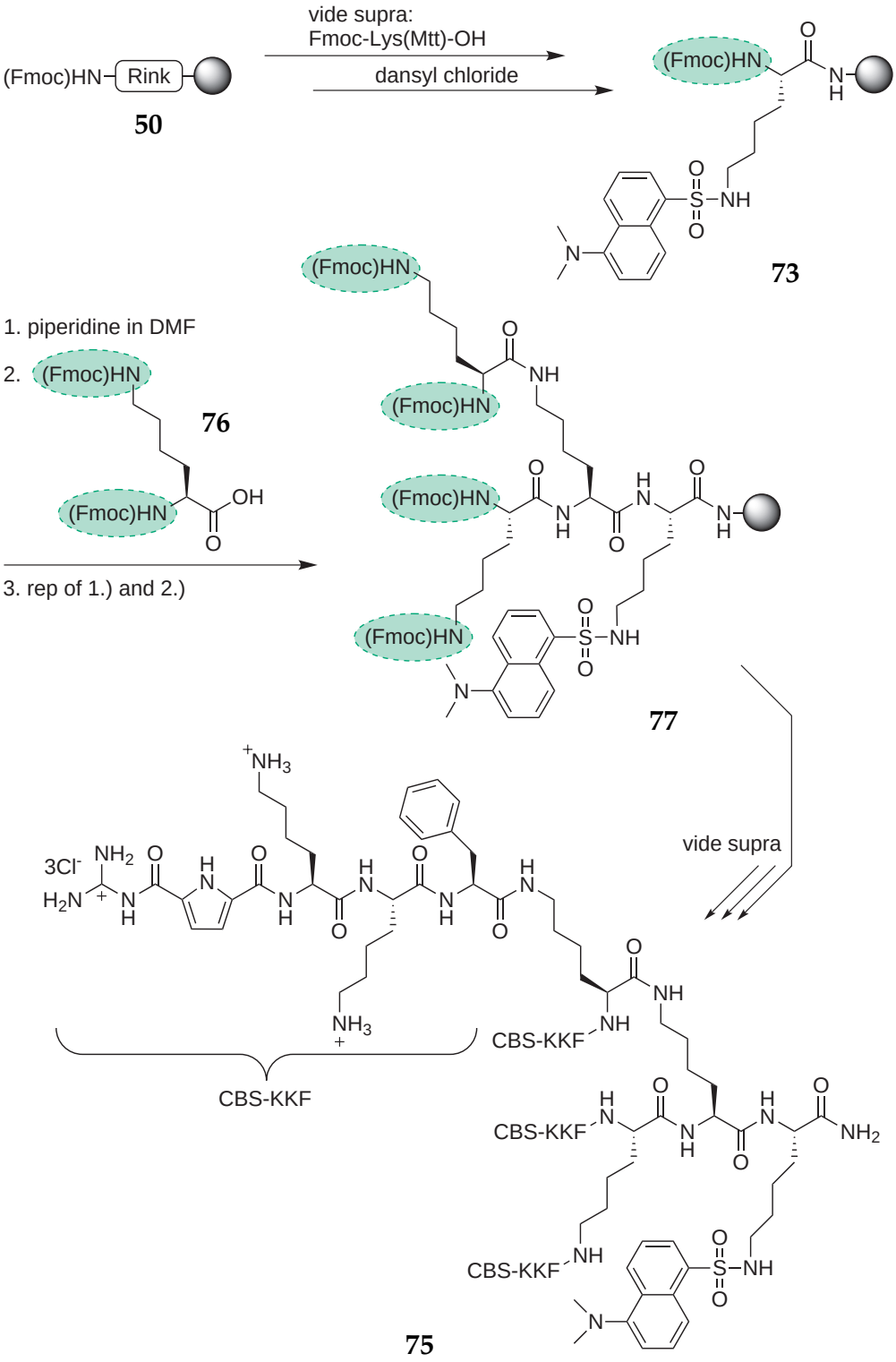

Scheme 4.6: *Synthesis of (CBS-Lys-Lys-Phe)$_4$(Lys)$_2$Lys-Lys(Dansyl)-NH$_2$ (**75**) (short form: (CBS-KKF)$_4$-(Dns), cf. text for abbreviation scheme) the tetravalent form of receptor **1** with an additional fluorescence label for an easy detection.*

S. aureus while staining of the Gram-negative bacterium *E. coli* occurred at the lower concentrations of 30 μM and 34 μM for peptides **71** and **75**, respectively (Figure 4.19 and 4.20 on page 95). As a positive control, bacteria were also treated with a compound containing a fluorescent dansyl group conjugated to a bis-Zn(II)-dipicolylamine ligand which targets anionic lipids in the membrane of bacteria and apoptotic cells.[138] Using this compound, staining is apparent at 10 μM in both *S. aureus* and *E. coli*.

Results for *S. aureus*: Both peptides **71** and **75** show the same staining pattern in *S. aureus* cells. Fluorescence is not localized to the membrane of the cells, but is seen constant throughout the cells indicating the internalization of the peptide (Figure 4.19). The membrane structure of each bacterium is different and therefore the likely determinant of the staining pattern. The Gram-positive membrane is rather simple with only one lipid bilayer, but has compared to a Gram-negative membrane a thicker peptidoglycan layer. However, the effect of the peptidoglycan seemed to be minimal as internalization of both peptides was seen. It is plausible that both peptides are endocytosed upon association with the membrane, which would explain the appearance of the probes inside the cell.

Results for *E. coli*: In contrast to *S. aureus* cells, a preferred membrane staining can be seen with both peptides (Figure 4.20). The Gram-negative bacterial membrane is more complex with two lipid bilayers, a thin peptidoglycan layer and a covering of lipopolysaccharides (LPS) which contain large amounts of anionic sugars. Therefore, the binding to the lipopolysaccharides on the Gram-negative outer membrane seems most likely, as it carries negative charges. If the probes were entering inside the outer lipid membrane of *E. coli*, it would be possible that endocytosis of the peptide can be seen as it was in *S. aureus*. However, as that is not seen, it is probable that they do not penetrate into the periplasm of the cell wall and are blocked (maybe even sterically) by the large and branched O-antigens of the LPS.

Comparison mono vs. tetravalent peptide: The fluorescence is greater in the monovalent probe for both bacteria, which is an indication, that the monovalent peptide (**71**) is more versatile as a detection probe because of its smaller size and therefore enters the cell wall more easily. However, it cannot be ruled out that the tetravalent peptide is binding with higher affinity and proximity, because possible self-quenching processes may reduce the fluorescence.

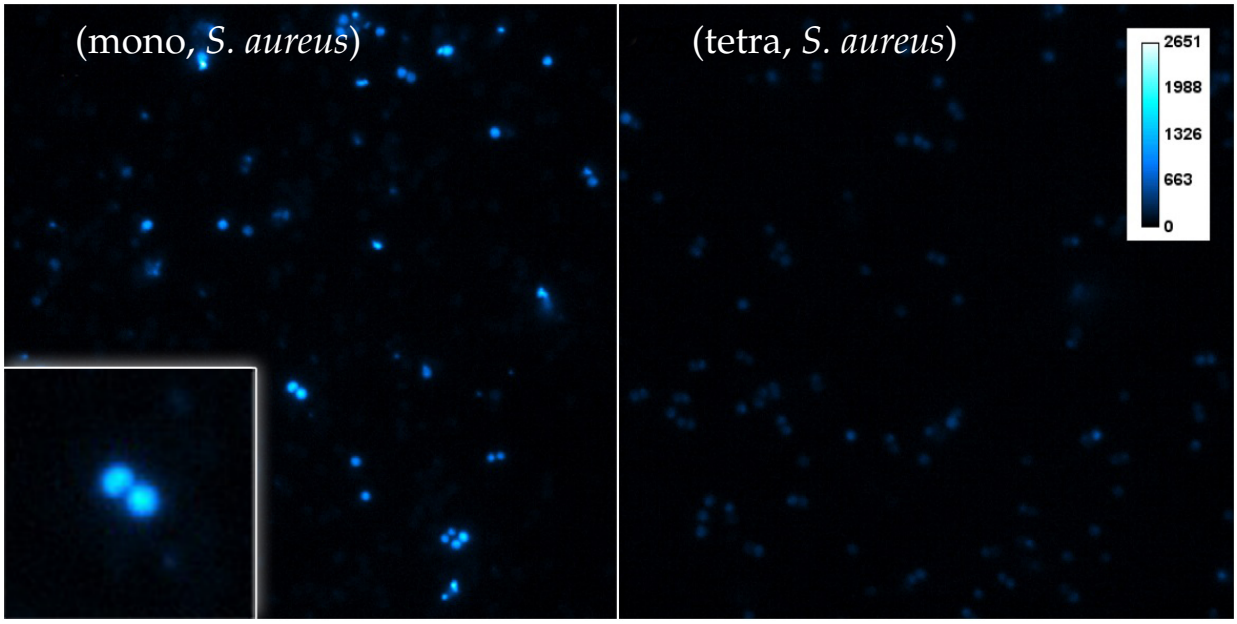

Figure 4.19: *Fluorescence microscopy of* ***Staphylococcus aureus*** *NRS11 treated with monovalent (**71**) and tetravalent (**75**) dansyl-conjugated peptides. The minimum concentration at which fluorescence is observed in bacterial membranes is 50 μM for peptide **71** and 45 μM for peptide **75**. Scale bar is indicative of number of photons at specific pixels.*

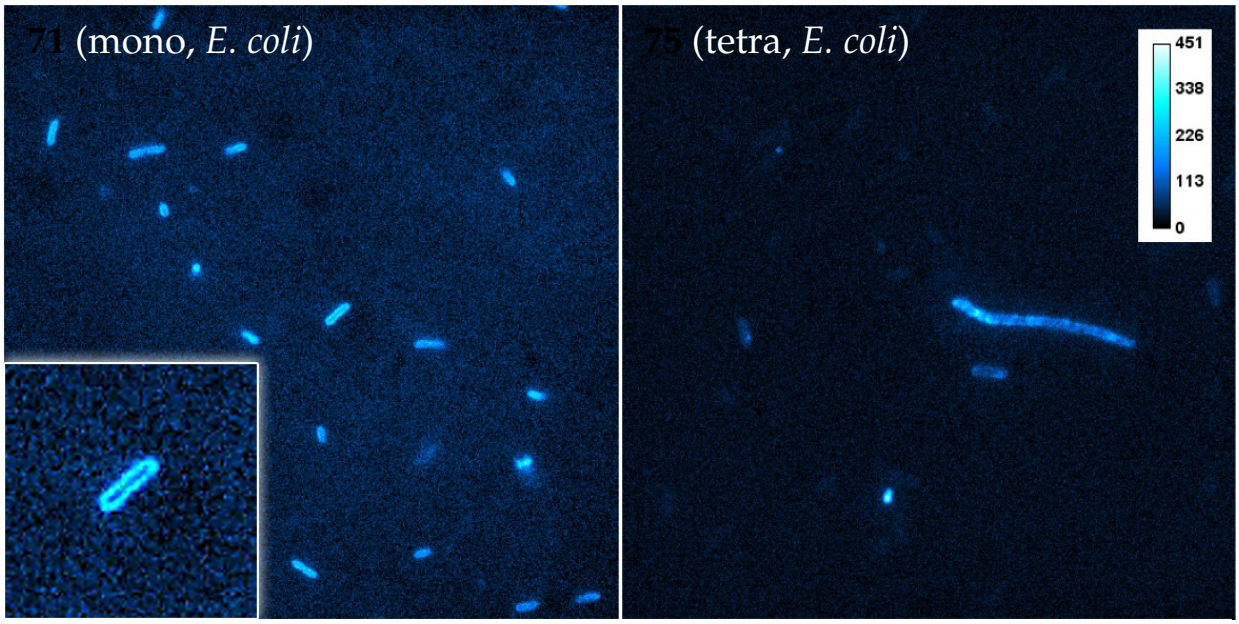

Figure 4.20: *Fluorescence microscopy of* ***Escherichia coli*** *UTI89 treated with monovalent (**71**) and tetravalent (**75**) dansyl-conjugated peptides. The minimum concentration at which fluorescence is observed in bacterial membranes is 30 μM for peptide **71** and 34 μM for peptide **75**. Scale bar is indicative of number of photons at specific pixels.*

In conclusion, it was indeed possible to show for the first time that peptide structures on the basis of receptor **1** can interact with the cell walls of Gram-positive and Gram-negative bacteria. In the case of ***Staphylococcus aureus*** (positive) even an internalization throughout the whole cell was observed, whereas in case of ***Escherichia coli*** (negative) only the membrane was stained (Figure 4.21). Due to the complexity of the cell wall in *E. coli* not only an internalization was hindered, also the fluorescence in general was much lower than with *S. aureus*. In comparison, the monovalent peptide (**71**) seems to be more efficient than the tetravalent (**75**) due to its smaller size. The amount of synthetic peptides that must be used for good fluorescent staining is still relatively high compared with the dansylated Zn-ligand used as positive control. But this is not unexpected due to the fact that the latter probe is metal based, which has intrinsically a higher binding affinity than interactions solely based on hydrogen bonds and electrostatic attraction. The mechanism of binding or internalization of peptides (**71**) and (**75**) are still unknown, but these first results are very promising and will help to design better probes in the future.

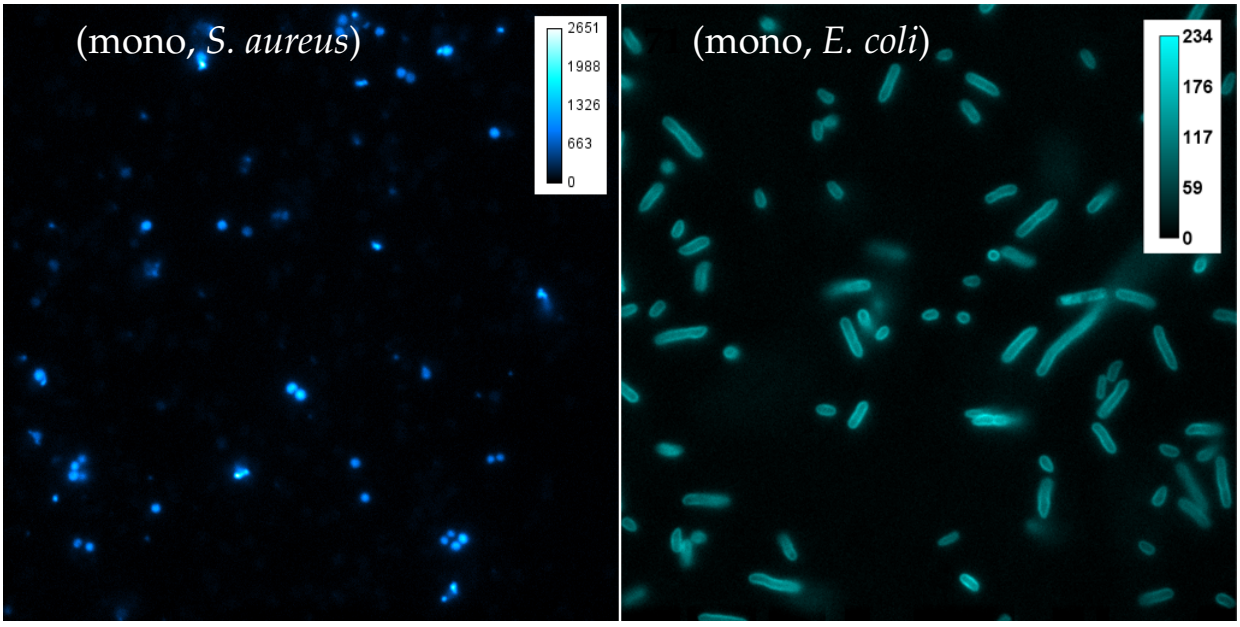

Figure 4.21: *In the case of* ***S. aureus*** *the monovalent peptide* ***71*** *was internalized (left), whereas at* ***E. coli*** *bacteria only the membrane was stained (right).*

4.2.3 Mono- and Multivalent Peptides as Antimicrobial Agents

The previously described tests showed that the newly introduced peptides indeed interact with different bacteria types. However, these tests focused on the membrane activity and revealed no information about their potential as antibacterial agent. This could be accomplished in cooperation with the Institute for Molecular Infection Biology of the University of Würzburg where the compounds were tested for their antimicrobial activity. In detail they tested the antibacterial potential, the ability of bacterial biofilm inhibition, the antiparasitic activity and evaluated the effects on macrophages.

The main focus was on the comparison of the bioactivity between the monovalent (**71**) and multivalent peptide (**75**). In addition, some new multivalent peptide systems with hopefully increased activity were also synthesized. Especially the influence of the multivalent scaffold and the use of additional guanidiniocarbonyl pyrrole binding motifs were investigated. The variations are summarized in Figure 4.22.

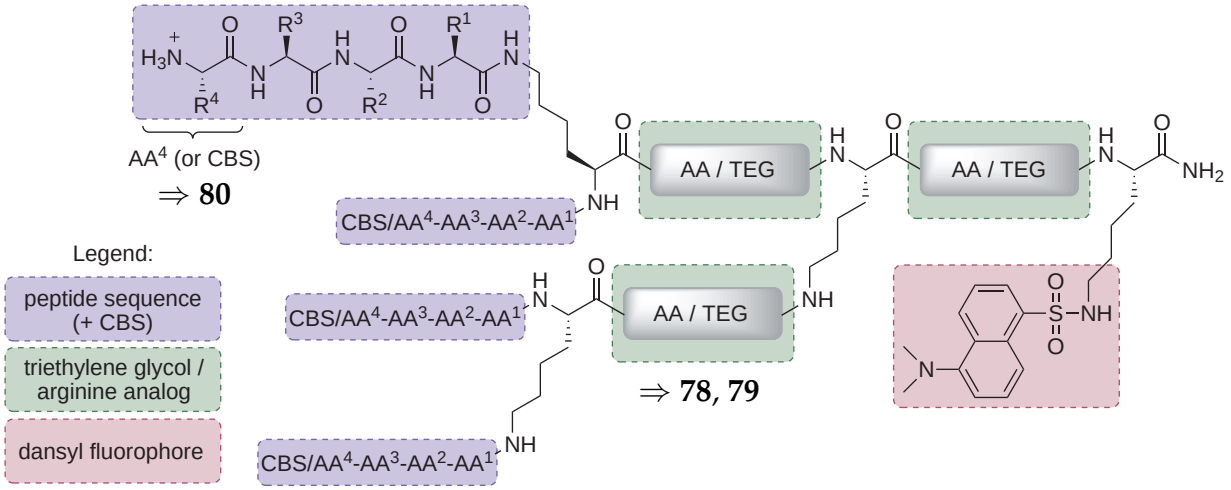

Figure 4.22: *Schematic representation of different variations of the multivalent peptide structures to increase the antimicrobial activity. One attempt was to incorporate triethylene glycol chains into the lysine scaffold to increase the solubility (compound **78**, Schemes 4.7, 4.8), or arginine analogs to test additional carboxylate binding sites (CBS) (compound **79**, Schemes 4.9, 4.10). But also the exchange of the CBS with arginine in the four side chains was examined (compound **80**, Figure 4.23 on page 102).*

The first receptor (CBS-KKF)$_4$-TEG-(Dns) (**78**) had the same peptide sequence (CBS-Lys-Lys-Phe) in each of the four side chains as the previously mentioned multivalent peptide **75**. The only difference were the extra triethylene glycol (TEG) chains within the lysine scaffold, which should increase the hydrophilicity and the flexibility of the structure. The synthesis started again with Rink amide resin followed by the attachment

of the first Mtt-protected lysine and the dansyl label (see Scheme 4.7). The incorporation of the TEG group was performed as previously described for compound **59** (on page 86): first succinic anhydride was added to convert the initial amine function to an acid function; then the triethylene glycol group was introduced with the coupling of 1,13-diamino-4,7,10-trioxatriadecane. The unprotected product **82** was then coupled with the two times Fmoc-protected form of lysine (**76**) which introduced the first branching in compound **83**.

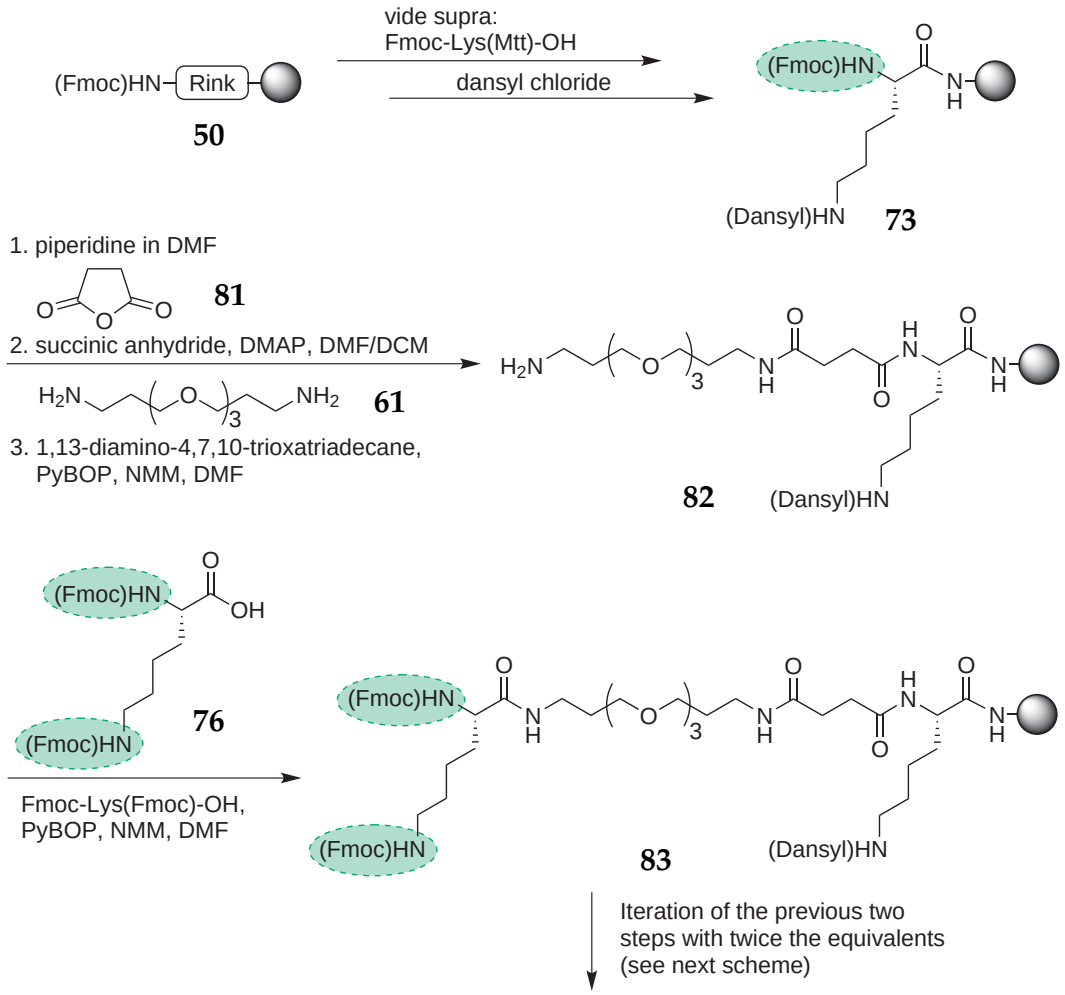

Scheme 4.7: *First part of the synthesis of compound **78**, a more hydrophilic form of previously synthesized receptor **75**.*

After the deprotection of the two Fmoc-groups with piperidine the last three steps, the attachment of succinic anhydride, TEG and Fmoc-Lys(Fmoc)-OH were repeated, but this time always with twice the equivalents to produce two side chains (see Scheme 4.8). The four times Fmoc-protected compound **84** was then ready for the attachment of the tripeptide and the guanidiniocarbonylpyrrole carboxylic acid as previously described

(e.g. Scheme 4.3 on page 86). After the cleavage from the resin with 50 % TFA (in DCM) and dry freezing with hydrochloric acid, the compound **78** was obtained as a colorless solid (Scheme 4.8).

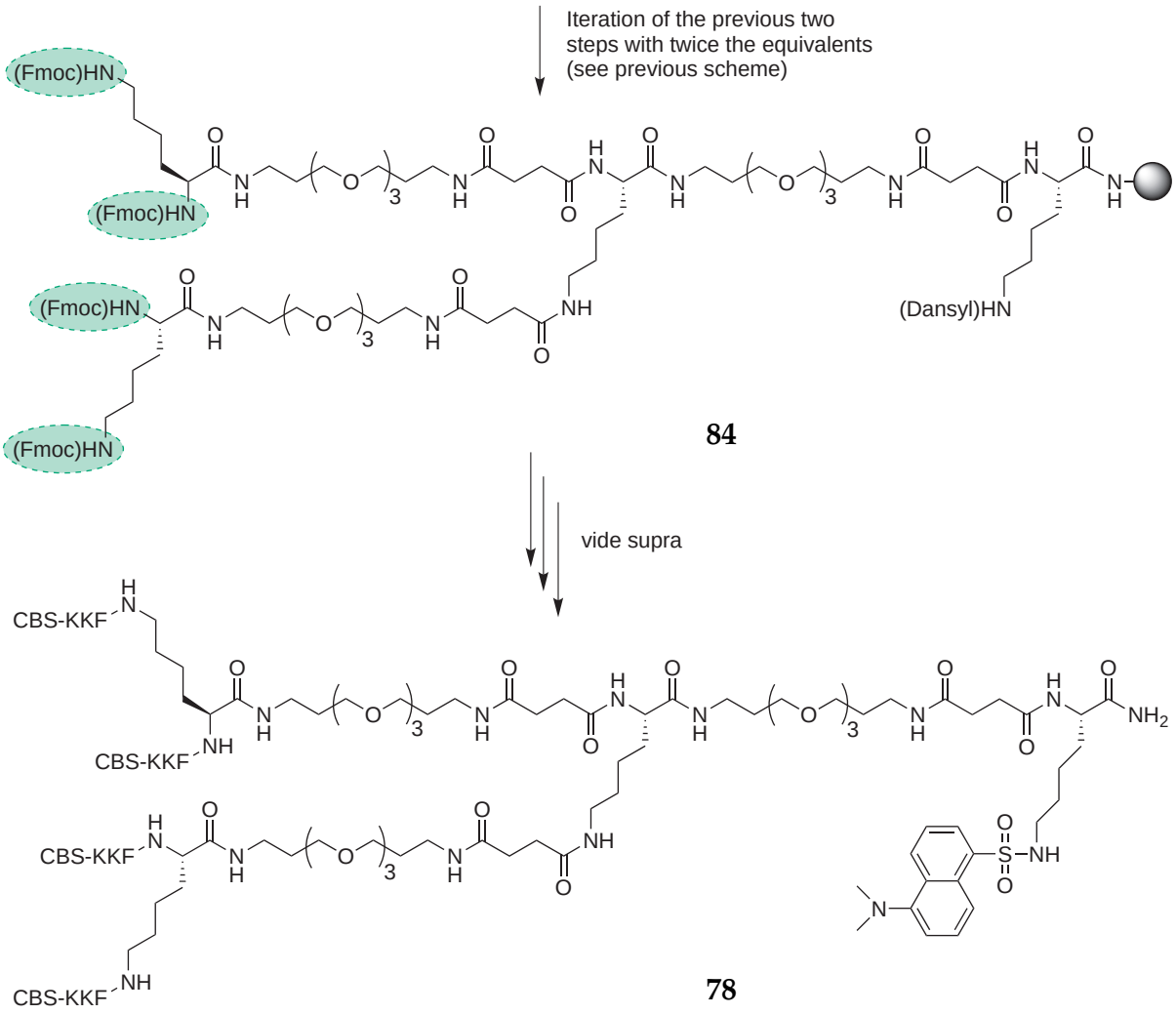

Scheme 4.8: *Second part of the synthesis of compound **78**, a more hydrophilic form of previously synthesized receptor **75**.*

The synthesis of the second receptor $(CBS\text{-}KKF)_4$-pyArg-(Dns) (**79**, on page 101) showed similarities to the previous described receptor (**78**). The only difference is the replacement of the TEG-linker with a Boc-protected arginine analog (**85**) in the lysin scaffold (see Scheme 4.9 on page 100 and Scheme 4.10 on page 101). The new building block was incorporated the first time right after the first dansylated lysine (**73**) and the second time after the first lysine branching, now with twice the equivalents.

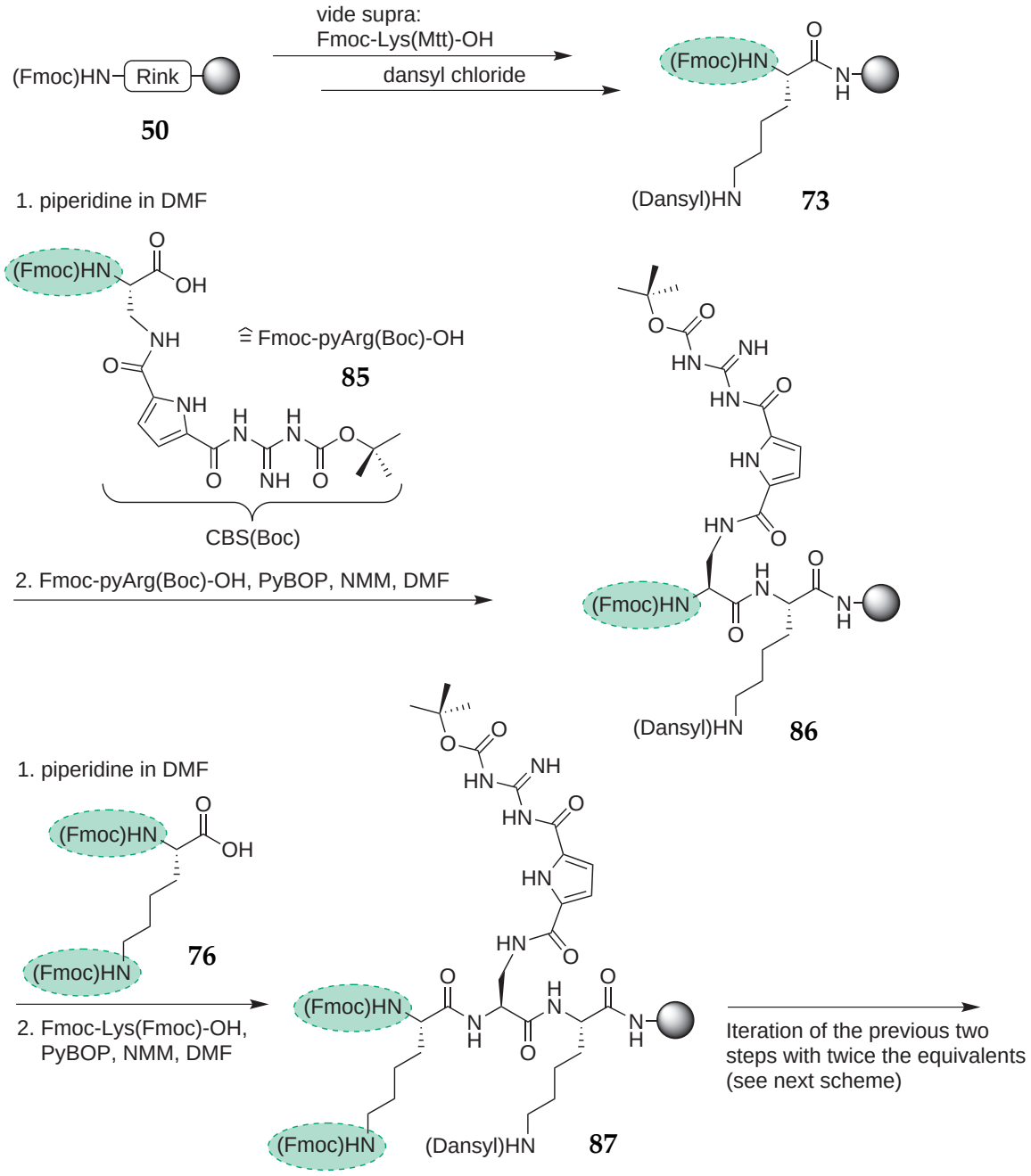

Scheme 4.9: *First part of the synthesis of compound **79**, a compound additional with arginine analogs to test the influence of the carboxylate binding sites.*

The arginine analog was developed in the *Schmuck* group and is an artificial amino acid based on the guanidiniocarbonylpyrrole carboxylic acid.[276] The N-terminal amine is Fmoc-protected, allowing to use the arginine analog (**85**) like a "normal" amino acid in SPPS. The incorporation into the lysine scaffold increased the number of positive charges and provided additional binding options for carboxylates.

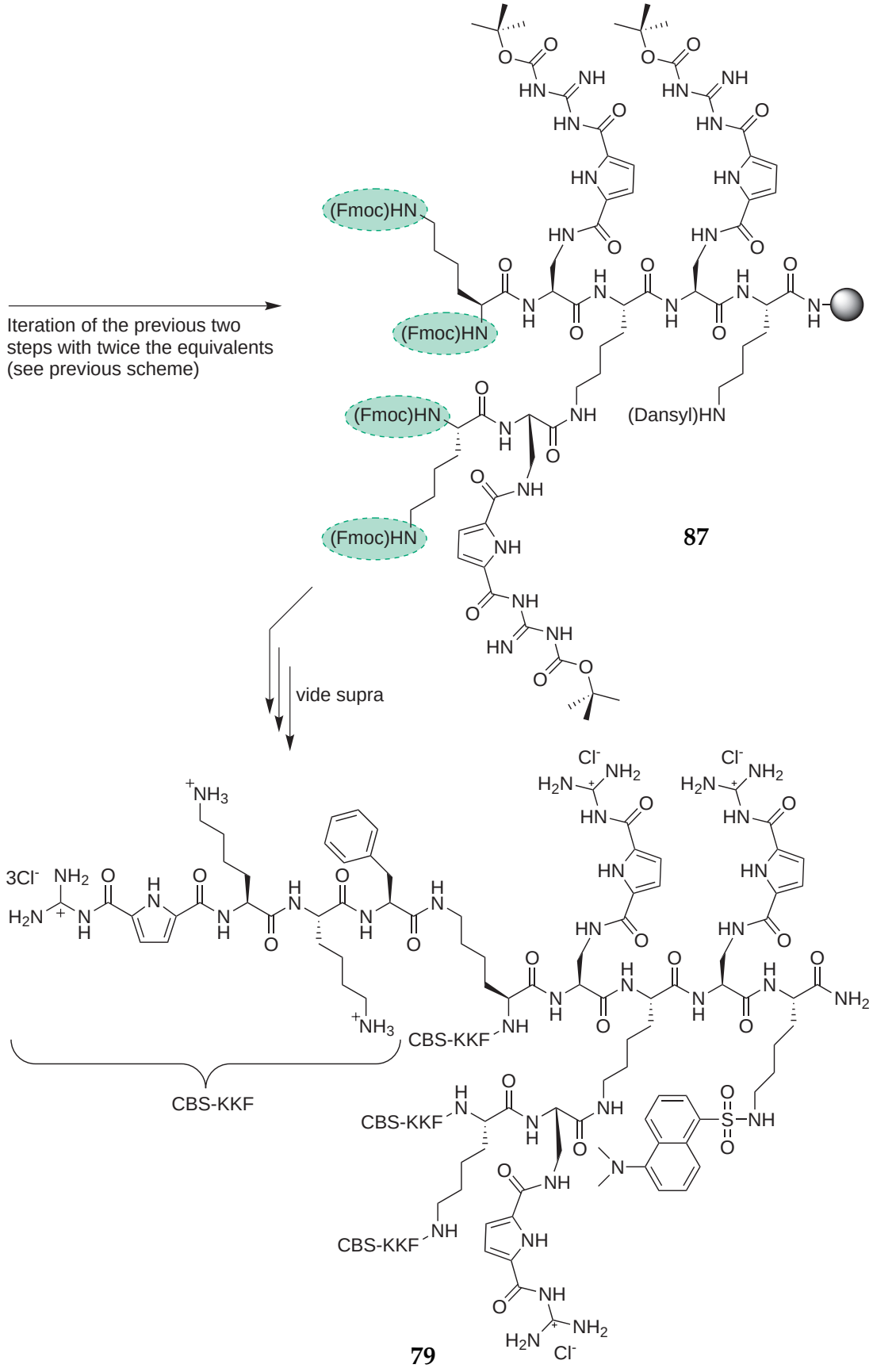

Scheme 4.10: *Second part of the synthesis of (CBS-KKF)$_4$-pyArg-(Dns) (**79**), a compound with additional arginine analogs to test the influence of the carboxylate binding sites.*

The third and last new compound in this series of fluorescence labelled multivalent peptide receptors was $(RKKF)_4$-(Dns) (**80**, Figure 4.23). The basic structure resembled the initial receptor **75** with the difference that the N-terminal CBS groups in all four side chains were replaced with arginine (Arg = R). The idea was to examine the general influence of the guanidiniocarbonyl pyrroles in biological systems. The synthesis of **80** is identical to **75** up to the last step (cf. page 93). As side chain protection group for arginine, the Pbf group was chosen which could also be removed in the final cleavage step with 50 % TFA in DCM (Figure 4.23).

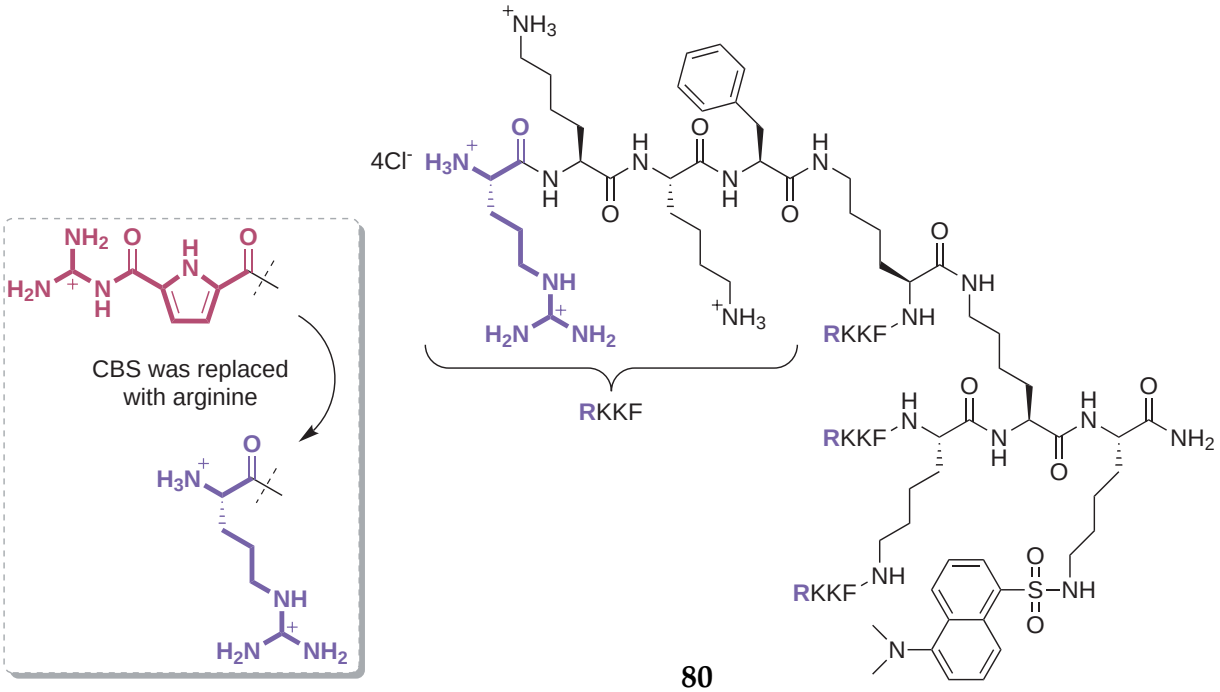

Figure 4.23: *Structure of multivalent receptor $(RKKF)_4$-(Dns) (**80**) where the N-terminal CBS groups in all four side chains of initial receptor **75** were replaced with arginine.*

These five compounds (overview in Figure 4.24 on page 103) were then tested by our cooperation partners of the Institute for Molecular Infection Biology for their activity against several microbes. They provided the tests procedures against two types of parasites. The first was *Trypanosoma brucei brucei* (*T. brucei brucei*), a parasite species that causes the nagana pest, also called animal african trypanosomiasis, which is most important in cattle. The disease is transmitted by the tsetse-fly and is closely related to human african trypanosomiasis (also called sleeping sickness) caused by the parasites *T. brucei gambiense* and *T. brucei rhodesiense*. Furthermore it was possible to test the

synthesized compounds against the protozoan parasites of the species *Leishmania major* (*L. major*) which are causing a disease called leishmaniasis. The pathogen is transmitted by the bite of female phlebotomine sandflies and induces severe skin sores and also damages to spleen and liver.

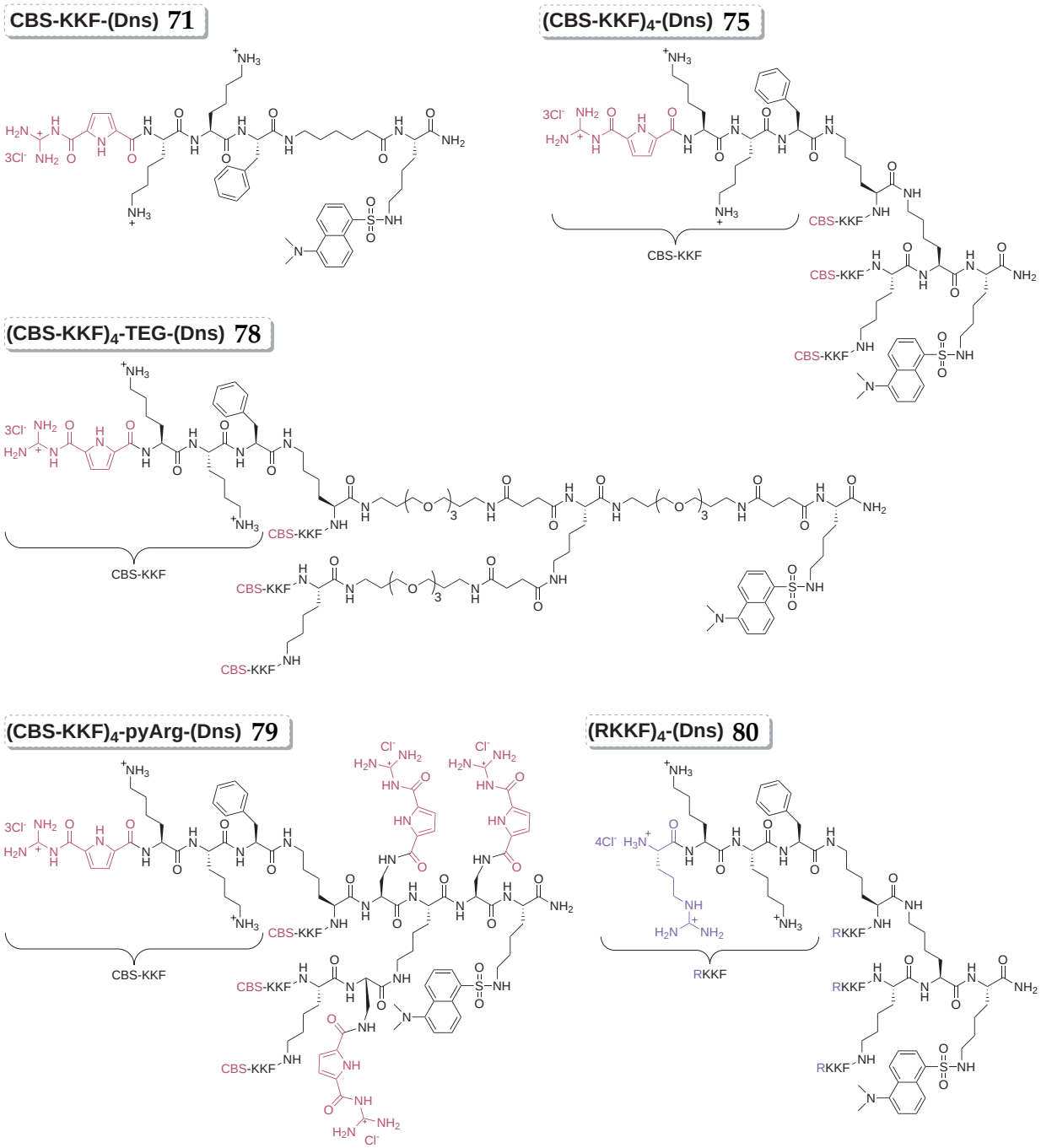

Figure 4.24: *Overview over all structures tested for their antimicrobial activity (incl. short form of the names for an easy comparison with the test results).*

In a second series of tests the potency of the peptides against disease related bacteria strains was investigated. Among the pathogens were Gram-negative bacteria of the strain *Pseudomonas aeruginosa* (no. 3) and *Escherichia coli* (strain 536), as well as the Gram-positive *Staphylococcus*-species *S. aureus* (strain 325 and 8325) and *S. epidermidis* (strain RP 62). During the tests the minimum inhibitory concentration (MIC) was measured, indicating the lowest concentration that is necessary to inhibit the visible growth of the bacteria after overnight incubation. A substance is called inactive when the MIC is higher than 160 μM. Besides these tests also the biofilm inhibition was investigated. Biofilms are the most common mode of bacterial growth in nature and are highly resistant to antibiotics. In particular they are medically relevant in relation to infections caused by indwelling medical devices such as catheters, implants and respiratory tubes. To test a possible inhibition of growth, the optical density of a biofilm caused by *S. epidermis* was determined and compared to an untreated reference. In the case of 100 % inhibition, the minimal necessary peptide concentration was denoted. The following paragraphs will summarize and discuss the obtained data.

Results of bioactivity against parasites: The tetravalent compounds (CBS-KKF)$_4$-(Dns) (**75**) and (RKKF)$_4$-(Dns) (**80**) exhibit for both parasites the highest activity with IC$_{50}$-values in the low micromolar range (Table 4.2). Unfortunately, both are also toxic at the same concentrations to macrophages, the human reference material. The results revealed, that the C-terminal exchange of the CBS unit with arginine has in these tests no influence on the biological activity.

Table 4.2: *Results of the test on antiparasitic activity and the effects on macrophages. The half maximal inhibitory concentration (IC$_{50}$) is a measure of the effectiveness of a compound.*

No.	Compound	*L. major* IC$_{50}$ [μM]	*T. brucei brucei* IC$_{50}$ [μM]	Macrophages IC$_{50}$ [μM]
71	CBS-KKF-(Dns)	>100	26.1	>100
75	(CBS-KKF)$_4$-(Dns)	**2.4**	**3.7**	3
78	(CBS-KKF)$_4$-TEG-(Dns)	7.9	25.6	25
79	(CBS-KKF)$_4$-pyArg-(Dns)	3.4	10.2	**33**
80	(RKKF)$_4$-(Dns)	**1.3**	**3.1**	3

The direct comparison between (CBS-KKF)$_4$-(Dns) (**75**) and (CBS-KKF)$_4$-TEG-(Dns) (**78**) illustrated that the additional TEG linker had no positive, but rather a negative in-

fluence on the activity, especially on *Trypanosoma b. b.* In the same way the additional artificial arginine analogs had no positive consequence (cf. (CBS-KKF)$_4$-(Dns) (**75**) with (CBS-KKF)$_4$-pyArg-(Dns) (**79**)). However, in both cases with the modified lysine scaffold, an enhanced selectivity was observed between *Leishmania* and *Trypanosoma* parasites. In particular noticeable is the clearly reduced toxicity towards macrophages. The most interesting result was the direct comparison between the monovalent receptor CBS-KKF-(Dns) (**71**) and the multivalent counterpart (CBS-KKF)$_4$-(Dns) (**75**). While the increase of activity against the *Trypanosomes* can be explained due to the direct proportional gain of valency, a disproportionate activity jump stood out in the case of the *Leishmania* (from IC_{50} = >100 to 2.4 μM). This example emphasizes the distinct influence of the multivalent effect for the antimicrobial activity. It is considerable high in the case of the *L. major* species and therefore also exhibits an unexpected selectivity of the receptors.

Results of bioactivity against bacteria: The tests regarding the growth and biofilm inhibition of various Gram-negative and Gram-positive bacteria revealed only an activity in the strains of *Staphylococcus epidermis* (Table 4.3). There is again a remarkable difference between the MIC of CBS-KKF-(Dns) (**71**, 80 μM) and (CBS-KKF)$_4$-(Dns) (**75**, 10 μM) caused by the multivalent effect. Additionally, the multivalent receptor featured a 100 % biofilm inhibition already at a very low concentration of 10 μM. The monovalent receptor required for the same inhibition the 16-fold concentration (160 μM) (Table 4.4).

Table 4.3: *Results of the test on antibacterial activity. The minimum inhibitory concentrations (MIC) were determined using the broth microdilution method.*

		Minimum Inhibitory Concentration [μM]				
		S. aur.	***S. aur.***	***S. epiderm.***	***E. coli***	***P. aerugin.***
No.	**Compound**	**325**	**8325**	**RP 62**	**536**	**Nr. 3**
71	CBS-KKF-(Dns)	160	160	80	160	>160
75	(CBS-KKF)$_4$-(Dns)	>160	>160	10	n.d.	n.d.

Table 4.4: *Results for the test on biofilm inhibition.*

		Biofilm Inhibition in % (μM)
No.	**Compound**	***S. epiderm.* RP 62**
71	CBS-KKF-(Dns)	100 (160)
75	(CBS-KKF)$_4$-(Dns)	100 (10)

Interestingly, in the case of *S. aureus* and *E. coli* no antibacterial activity was observed. This might be an advantage in respect to the membrane activity of the mono- and multivalent peptides. As previously reported (see Chapter 4.2.2 on page 89), some of the peptides feature internalization properties. Therefore, the minimal interference with the viability of these bacteria strains makes them interesting as molecular probes and translocation vectors.

Summary of antimicrobial tests: In the present study, the activities of one mono- and several multivalent peptides were compared against the growth of parasites, pathogenic bacteria and macrophages. Doing so, the multivalent systems demonstrated in some cases a remarkable increase of activity beyond the expected fourfold enhancement. Especially in the case of the parasites the IC_{50} values were brought down to the low micro molar range. Also, in some cases a selectivity in the toxicity towards macrophages were observed, caused by only small changes in the peptide structure. Therefore, with this study it was possible to gain precious information about the influence of small structural changes in the peptide receptors for their antimicrobial activity.

4.2.4 Conclusion and Outlook

The second part of this thesis focused on the tailor-made design and synthesis of small artificial peptide receptors and the investigation of their activity towards several biological targets. The aim was to advance from the analytical understanding of the peptides described in Chapter 4.1 to the investigation of their value in biological relevant applications. The compounds contain guanidiniocarbonyl pyrroles as specific binding sites for carboxylates and were all synthesized in different modifications to enhance the activity depending on the type of target. With the help of solid phase synthesis techniques it was possible to synthesize successfully several hydrophilic and fluorescence active peptides, both in mono- and multivalent forms (see Figure 4.15, 4.16 and 4.24).

In cooperation with the University of San Diego it was possible to show that already the small compound (**1**) can influence physiological relevant peptide-protein interactions, like the binding of antibodies to the surface of amyloid fibrils. However, the selectivity and the affinity of the peptide can still be optimized. One way would be the combination with an already well known and studied binder of the fibrils. Among others, derivatives of Congo red and thioflavine T (ThT) are used as fluorescent dyes for the detection of amyloid fibrils. They are known to bind in a nonselective but strong

way to the fibrils. A structural combination with the previously described compound **1** or a modification might lead to both selectivity and affinity for the surface covering approach. A possible structural candidate could be the combination with the BTA, the neutral derivate of ThT (Figure 4.25). The attachment of additional ethylene glycol chains are also of interest, because they would not only increase the solubility but also might help to mask and cover the surface of the fibrils.

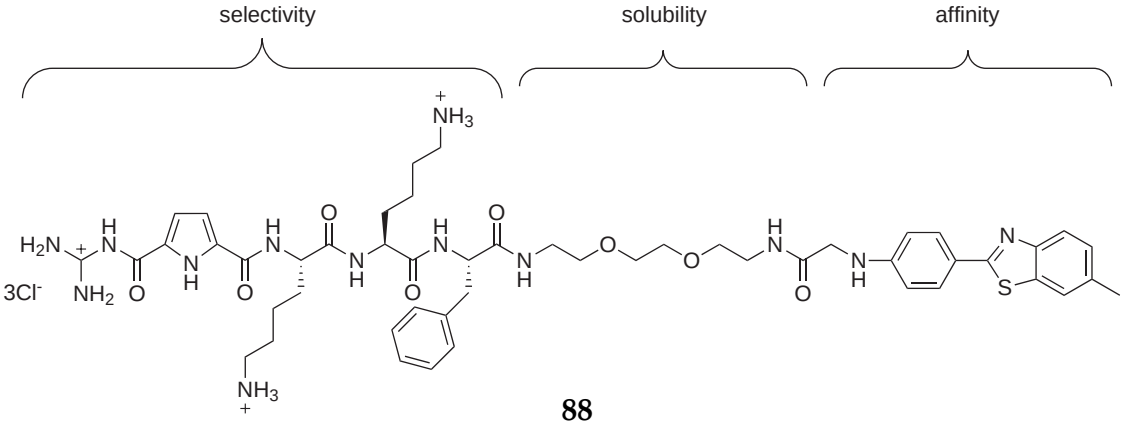

Figure 4.25: *Structural combination of peptide receptor **1** with BTA, a small compound known to cover the surface of Aβ fibrils. The adduct might help to increase the selectivity and affinity of this approach.*

During the tests in San Diego the first ideas for multivalent structures with increased binding affinity arose. Hence, this approach would also be very interesting for the covering of the Aβ fibrils. The multiple attachment of several identical binding units to one common template has already been demonstrated to be very successful in this thesis. Several tetravalent structures were examined for their antimicrobial activity and as biomarkers. The fluorescence labelled probes successfully demonstrated for the first time that the CBS-based peptides indeed interact with the cell wall of bacteria and even get internalized in the case of Gram positive bacteria. The exact mechanisms of interaction may not be known yet, but these results were very promising. Subsequent antimicrobial test revealed that tetravalent systems indeed showed in some cases IC_{50} values the low micro molar range. But even more interesting, a comparison with the monovalent analogs uncovered a remarkable increase of activity beyond the expected fourfold enhancement. This rises the question if maybe the activity can be increased even more with an octameric structure? Also, the analysis of using different variations in the peptidic side chains or the comparison of altered scaffolds would be interesting. These tests are especially important for the development of bioactive structures with a pharmacokinetical compatibility favorable for humans.

4.3 Multivalent Peptides as Potent Inhibitors for β-Tryptase

The previous chapter showed that small peptides can indeed interact efficiently with biological relevant targets. Starting with the physico-chemical investigation of the interaction with small model peptide systems, the following experiments focused already on more complex systems such as cell membranes, bacteria and microbes. Actually it was possible to show that the synthesized mono- and multivalent peptides have an effect on specifically chosen targets. However, due to the complexity of the investigated systems it was difficult to elucidate the exact mechanism of interaction. Hence, these tests focused more on the application of the synthesized peptides and provided a first prove of concept that it is possible to influence biological systems.
The following project will concentrate on a more tailor-made approach to control non-covalent interactions and will focus on a special recognition event, the inhibition of the serine protease β-tryptase. The idea was to extend the already very comprehensive knowledge about the molecular recognition of small peptide systems to more complex, but well defined biological systems. The protein x-ray crystal structure of β-tryptase is known since 1998[233] and the unique structural features are well examined. This set the basis for a completely new surface based approach for the inhibition of the catalytic cleavage activity of the protease.
The protein surface of tryptase displays a p*I*-value around 5.0 to 6.6, therefore offering only a mild tendency to be negatively charged.[277] However, the surface features some highly acidic "hot spots" with clusters of negatively charged amino acids. These are mainly arranged at the entrance to the central pore and around the active cleavage sites. Force field calculations already provided an orientation of how the previously mentioned multivalent and mainly positively (basic) charged peptides might interact with the protein (Figure 4.26 on page 109). This blockage would then inhibit the enzyme activity due to the limited accessibility of possible substrates.

As already stated in Chapter 4.2.1, it was possible to demonstrate that artificial receptors have an influence on physiological relevant peptide-protein interactions, as for example the binding of antibodies to the surface of Aβ fibrils. Therefore, these peptides were chosen again for the initial inhibition tests. Again, as basic structure of a possible inhibitor a second generation poly-lysine dendrimer was chosen. The four terminal side chains contained a tripeptide sequence with an additional N-terminal CBS

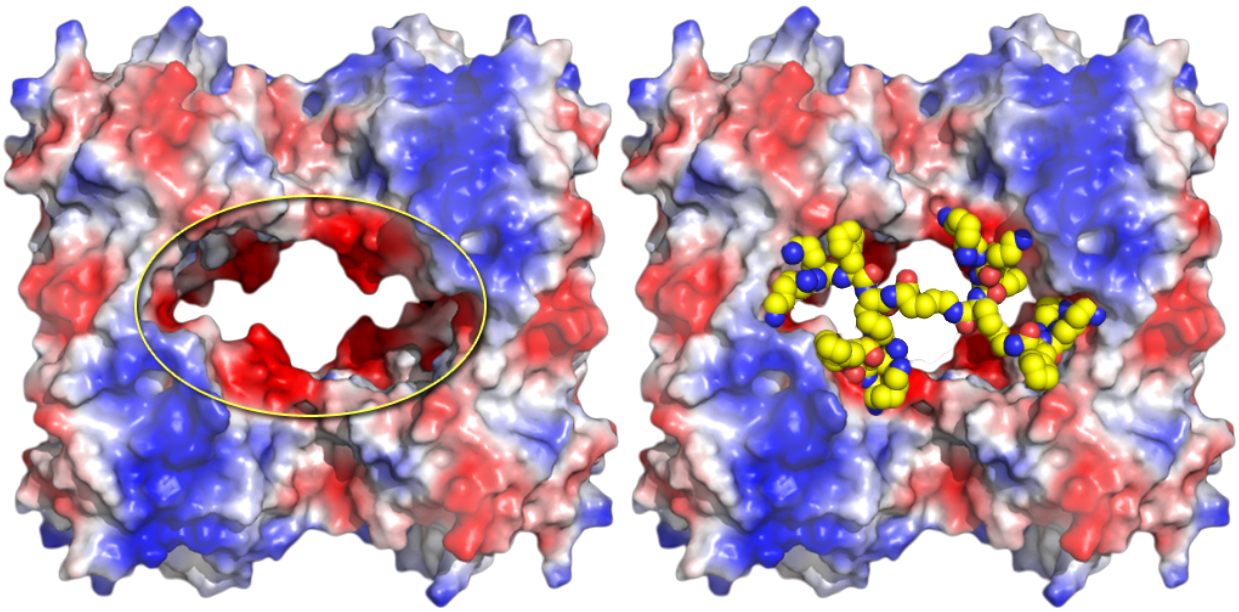

Figure 4.26: *The surface of tryptase features some highly acidic "hot spots" with clusters of negatively charged amino acids especially around the central pore (left); a multivalent and mainly positive (basic) charged peptide might interact with the acidic areas and block the entrance to the enzyme (right).*

unit. The proteolytic stability of this small dendrimer should be sufficient to resist any cleavage activity of the tryptase. Recent studies on the possible proteolysis of peptide dendrimers revealed that even small branched compounds are stable upon treatment with trypsin and chymotrypsin.[278] In addition the complex structure of tryptase with the deep buried active sites is known to be responsible for a reduced and selective enzymatic activity, compared to the more accessible cleavage sites of trypsin.[233,266,267] The following chapter will describe the synthesis and the screening of different peptide systems as new and efficient inhibitors for β-tryptase.

4.3.1 Development of a New Surface Based Inhibition Method

The first peptidic inhibitors chosen for the tests featured the already well known peptide sequence CBS-Lys-Lys-Phe. Both the monovalent (**1**) and the multivalent form (**90**) were synthesized this time without the dansyl label, which would have no effect and need in this series of experiments. The comparison with the monovalent version was necessary to measure the multivalent effect, which in these experiments was proposed to be not only helpful but essential for an effective inhibition of tryptase. The synthesis of **1**

has been described already earlier. The preparation of $(CBS\text{-}KKF)_4$ (**90**) was similar, but shorter than the one of $(CBS\text{-}KKF)_4$-(Dns) (**75**, on page 93) due to the lack of the dansyl label. The synthesis started on Rink amide resin and continued with the direct attachment of the double Fmoc-protected lysine. This step was then repeated to result in the four times branched lysine scaffold (**89**). The following three amino acids and the CBS group were attached as previously reported (Scheme 4.3 on page 86). Then the product was treated with a mixture of 95 % TFA in DCM which led to the cleavage from the Rink amide resin and the simultaneous removal of all protecting groups. After dry freezing with hydrochloric acid, the compound **90** was obtained as a colorless solid (Scheme 4.11).

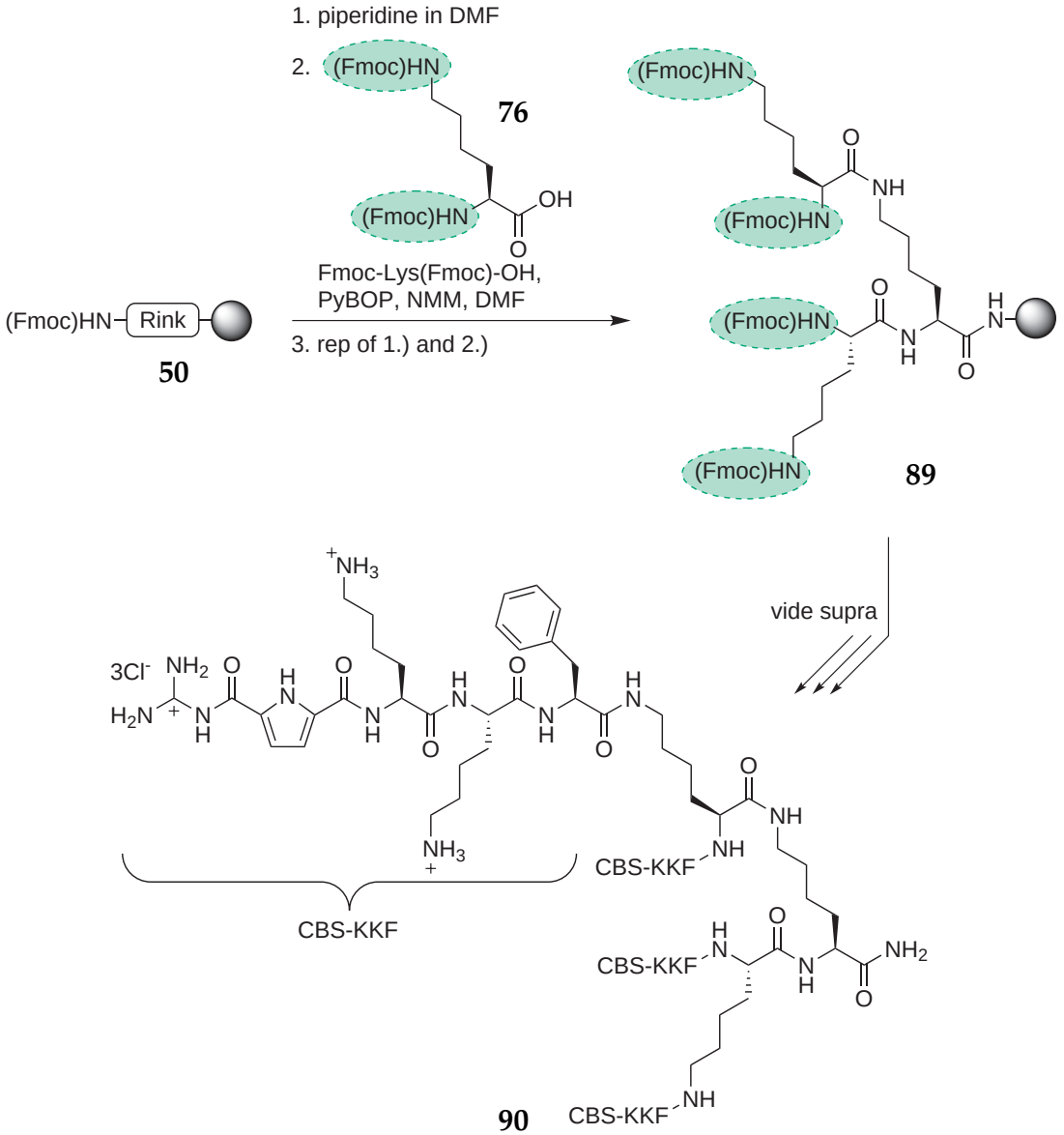

Scheme 4.11: *Synthesis of $(CBS\text{-}KKF)_4$ (**90**), as a possible multivalent inhibitor of the serine protease β-tryptase.*

For comparison also an alternative version with a different composition of the tripeptide was synthesized. Therefore, the amino acids tryptophan, histidine and arginine were chosen. They were interesting due to their mixture of aromatic and cationic properties. Again, both a monovalent (CBS-WHR, **91**) and a tetravalent form ((CBS-WHR)$_4$, **92**) were synthesized in order to measure the multivalent effect. The synthesis of was performed in an analog way as for **1** and **90**. *Tert*-butyloxycarbonyl (-Boc) was used as side chain protection group for histidine and tryptophan, and 2,2,4,6,7-pentamethyldihydrobenzofuran-5-sulfonyl (-Pbf) was chosen for arginine. All protection groups were removed in the final cleavage step from the resin with 95 % TFA. Figure 4.27 provides an overview of the first four inhibitors used in the enzyme assay which will be described in the following paragraphs.

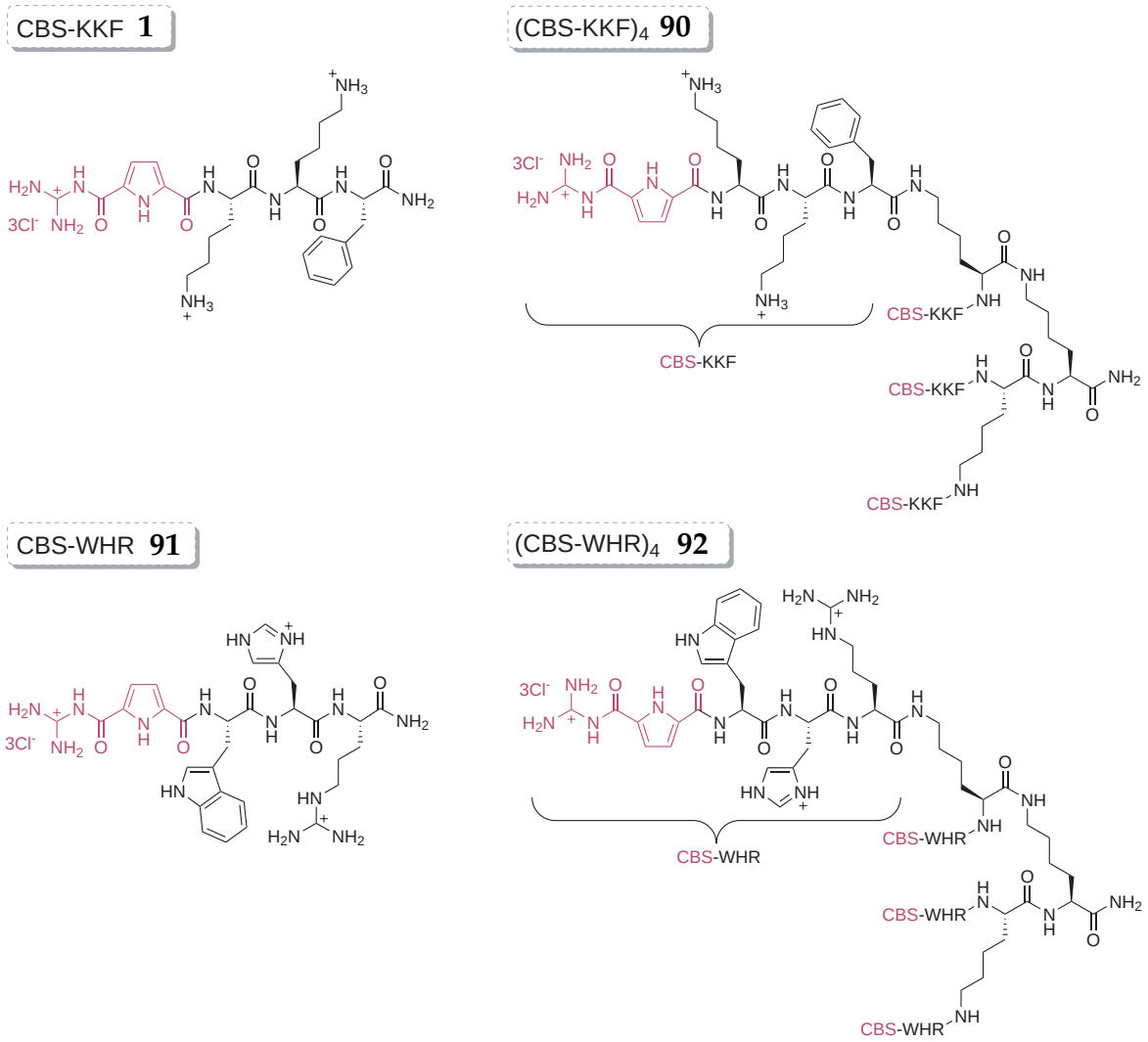

Figure 4.27: *Overview over several mono- and multivalent structures (incl. CBS-unit) tested for their potential as inhibitor of β-tryptase (incl. short form of the names for an easy comparison with the test results).*

The theoretical background information about the principles of the enzyme assay was already described in Chapter 3.4.1. The following section will explain the modifications to the known literature procedures,[254,260,262,263,265–267,279,280] applied to the specific project requirements of this thesis project.

Enzymes: As previously mentioned, the tetrameric structure of β-tryptase is kept together by heparin, a negatively charged polysaccharide (see Chapter 3.4.2). In the absence of heparin (or of high salt concentration *in vitro*) tryptase rapidly dissociates into inactive monomers. However, it was necessary in our tests to clarify if the polycationic peptides only interact with the heparin (and therefore disrupt the enzyme and cause a non-reversible inhibition) or if they indeed interact with the active sites and/or the acidic patches on the protein surface of tryptase (and therefore cause a reversible inhibition). To overcome this problem two commercially available forms of β-tryptase were purchased from *Promega*:

- rhSkin β-tryptase: heparin-stabilized
- rhLung β-tryptase: heparin-free, stabilized by a high concentration of NaCl (2 N)

Both enzymes had to be aliquoted for a comfortable use during the enzyme assays. Therefore, they were diluted to a concentration of 0.1 mg/ml resulting in 50 vials, each containing 2 μg of protein (50 $\times$ 20 μL). The details of the formulation mixture are described in the experimental chapter of this thesis (7.5.1 on page 208). It was important that the formulation for the rhLung β-tryptase contained no heparin. The optimal concentration of the enzyme used in the assay had to be determined prior to the tests. Therefore, the enzyme was measured at different dilutions without inhibitor until the slope of the linear graph representing the product conversion over time was between 15 and 30 (cf. Chapter 3.4.1.2 on page 54).

Substrate: Tryptase is known to cleave small synthetic ester or peptide substrates with Arg or Lys in the C-terminal P1 position. Therefore, the enzymatic activity of both tryptase types was determined with the help of a chromogenic substrate (Tos-Gly-Pro-Arg-AMC) (Scheme 4.12 on page 113). The released free AMC (7-amino-4-methylcoumarin) was measured using a fluorescence spectrophotometer with a microplate reader unit at 380 nm excitation / 460 nm emission wavelength.

Screening method: Kinetic experiments to determine the inhibition parameters were carried out in white 96 well plates. Thus, kinetic assays (at 25 °C) were started by adding

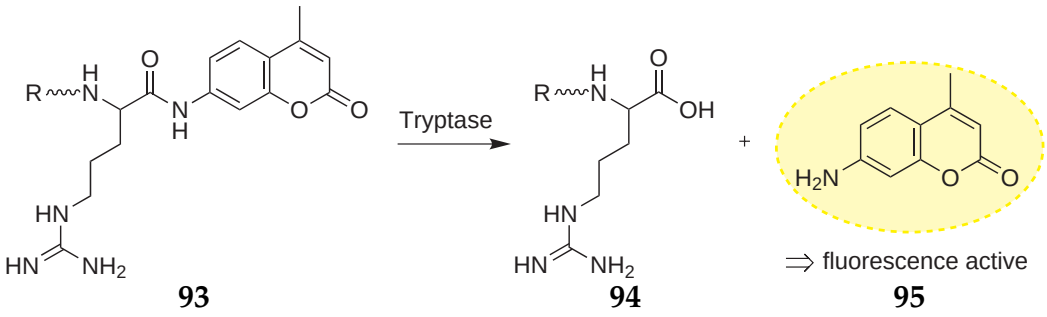

93 **94** **95**

Scheme 4.12: *Enzymatically cleavage of the fluorescence labelled substrate Tos-Gly-Pro-Arg-AMC (**93**).*

the enzyme to a Tris-HCl buffer at pH = 7.4, containing additionally Triton-X (to minimize aggregation) and NaCl. In the case of rhSkin β-tryptase the buffer also contained heparin in order to stabilize the enzyme. Then the inhibitor was added at a concentration of 100 μM in DMSO and finally the chromogenic substrate. The tryptase activity was measured by monitoring the absorbance change for 10 min, and the initial slope was determined by linear regression analysis. All assays were performed in duplicate. To reveal the potential as an inhibitor, all synthesized peptides were tested with this fixed concentration of 100 μM at first. If the inhibition was higher than 80 % also the half maximal inhibitory concentration (IC_{50}) and the absolute inhibition constant (K_i) were determined at varying inhibitor concentrations. Depending on the inhibition activity it was necessary to make a dilution series of the inhibitor stock solution to obtain final concentrations in the range between 1000 μM and 0.01 μM. The resulting data was then processed with Exel® and Grafit® to obtain the kinetic parameters.

To adjust the inhibition constants, the used substrate concentrations and the affinity of the substrate to the enzyme, the individual Michaelis constant (K_m) for the combination tryptase/Tos-GPR-AMC had to be determined, because this combination was not literature known. Therefore, the rate of the enzymatic reaction was measured at different substrate concentrations (0–1000 μM), always with a fixed enzyme concentration and without inhibitor. Then, with the help of Grafit®, the kinetic parameters were determined, using the Michaelis-Menten equation. The obtained K_m-value was 368 μM. Now it was possible to determine the independent initial inhibition constant K_i for each of the inhibitors.

In order to guarantee the applicability of all the previously described assay methods, a literature known inhibitor was chosen to test if the K_i-value was reproducible under

these new conditions. For comparison p-aminobenzamidine (**44**) was chosen, which showed a K_i of 65 μM in tests of *N. M. Schechter*.[248] Using the above described procedure a K_i of 57 μM was obtained, which is very near to the literature and a prove for the reproducibility of the developed assay conditions.

Screening results: The following table 4.5 will summarize the screening results for the four initial inhibitors (**1**, **90**, **91** and **92**). For a direct comparison both forms of tryptase were used for the determination of the inhibition constants to study the influence of heparin on the inhibition. Due to the fact that the previously determined K_m is relatively high the difference between K_i and IC_{50} is relatively small. Hence, the table only displays the K_i and not the corresponding IC_{50}-values.

Table 4.5: *Inhibition of β-tryptase by mono- and multivalent peptide structures carrying a CBS-unit at the C-terminal positions (without dansyl label). (rhSkin β-tryptase (heparin-stabilized), rhLung β-tryptase (heparin-free), n.d. = not determined).*

No.	Compound	**rhSkin β-Tryptase** K_i [μM]	**rhLung β-Tryptase** K_i [μM]
1	CBS-KKF	24.25 ± 7.88	33.52 ± 6.76
90	$(CBS\text{-}KKF)_4$	**0.28 ± 0.15**	**0.45 ± 0.0097**
91	(CBS-WHR)	80.82 ± 19.01	n.d.
92	$(CBS\text{-}WHR)_4$	**8.95 ± 0.01**	n.d.

Comparing the results it becomes apparent that heparin has no influence on the inhibition. Both the monovalent peptide **1** and the multivalent peptide **90** exhibit almost similar K_i-values for freshly prepared rhSkin and rhLung tryptase, respectively. However, it was observed that the heparin free tryptase lost a noticeable amount of activity when stored over night in buffer, even frozen. Therefore, only the heparin stabilized rhSkin β-tryptase was used for the following experiments within this project.

But most prominent is the difference in inhibition activity compared depending on the valency of the peptides. In both cases the multivalent peptides exhibit an inhibition beyond the four-fold increased value. In the example of **92** the inhibition is 9x better, in the case of **90** the inhibition is even 87x better than with the monovalent counterpart (cf. Figure 4.28 on page 115). Also the very low value of **90**, which is already in the medium nanomolar range, is extraordinary and therefore can be classed with literature known inhibitors (see Chapter 3.4.3 on page 63).

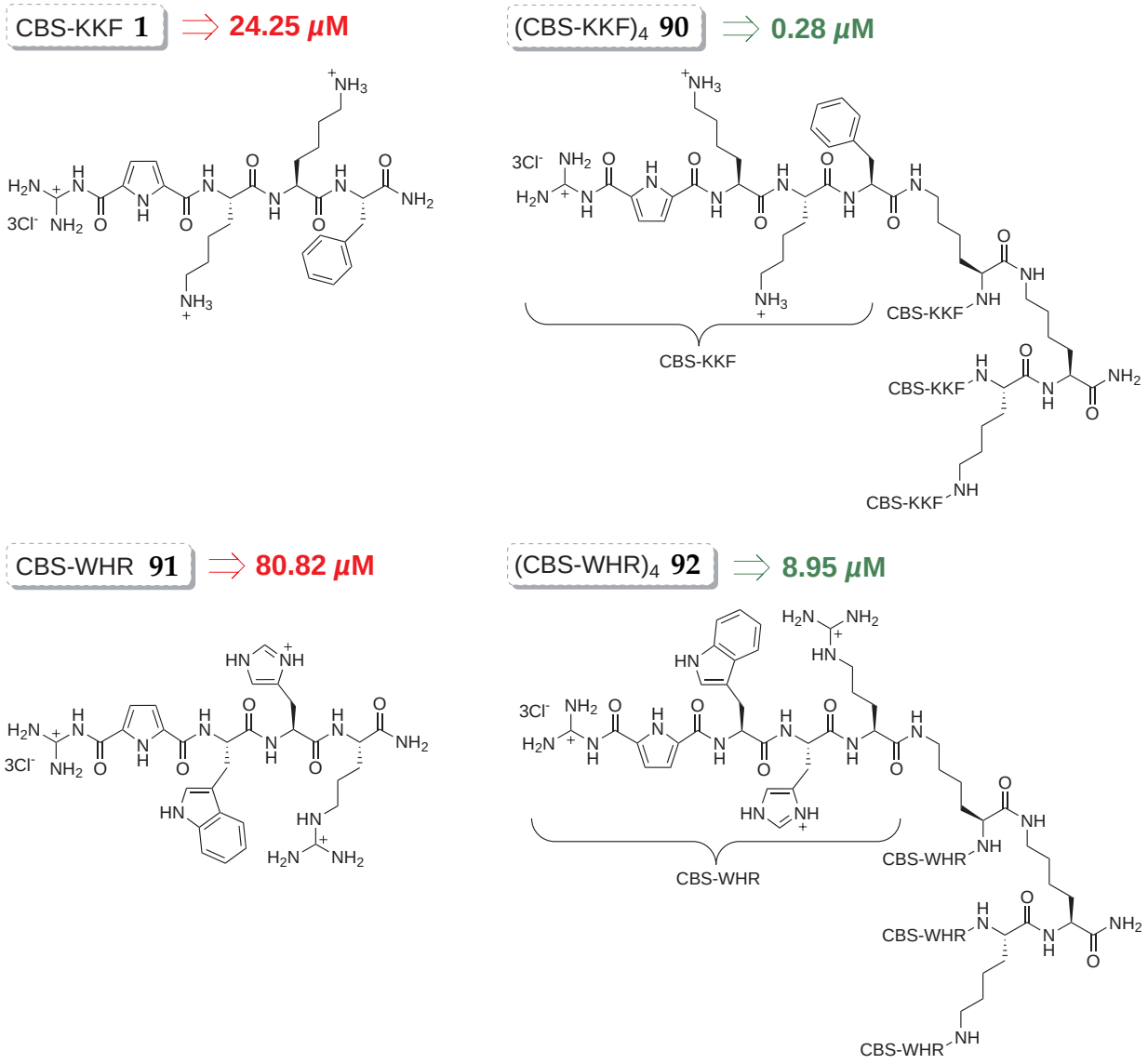

Figure 4.28: *The tetravalent compounds feature a 9x (**92**) and 87x (**90**) better inhibition (K_i-value) than the monovalent counterpart.*

These results suggest that the multivalent structures indeed have a different binding mode than the smaller monovalent inhibitors, which are probably in direct competition with the substrates in the four binding pockets. However, to elucidate the complete inhibition mode, especially to determine if the multivalent structures indeed cover the entrance to the central pore, additional experiments were necessary. The previous tests illustrated that already small changes in the tripeptide sequences can have a huge influence on the inhibition activity. Therefore, it was the idea to synthesize more varieties of the tetravalent compounds and the best and fastest way to do that is with the help of the combinatorial chemistry. Hence, the following chapter will explain the design, synthesis and screening of a combinatorial library of 216 inhibitors.

4.3.2 On-Bead Screening Assay of a Combinatorial Inhibitor Library

Prior to the screening of the combinatorial library of inhibitors careful considerations had to be made. Next to the design of the individual members, in particular the technical standpoint had to be investigated. Previous screenings of combinatorial inhibitor libraries were often based on a cleavage of all members from the resin, followed by an often time and substance consuming workup and the screening in solution. The second alternative was an on-bead screening, followed by the manual picking under the microscope of the most prominent candidates. Then the selected beads had to be analyzed mass spectrometrically and the resulting inhibitor resynthesized in solution.[281] For the screening in this thesis a new approach was applied, based on a similar screening method introduced by *Machon*.[227] With an on-bead screening method it is possible to minimize the steps from the synthesis to the inhibition results in a direct and easy way. The advantage of the new technique is a simultaneous readout of the total inhibition of *all* library members. This is different from known on-bead assays which allow no quantitative but only a qualitative "good or bad" answer. Therefore, the tryptase would have to be incubated with the still resin bound inhibitors, followed by a fluorescence screening similar to the tests in solution.

As a polymer carrier for the inhibitors PEGA resin was chosen. It exhibits the best biocompatibility due to its chemical structure and the perfect swelling properties in polar solvents like water. The resin is also very resistant towards the treatment with TFA. Therefore, the protecting groups in the side chains of all amino acids can be the same as during the synthesis in solution. They can all be removed in the final deprotection step still leaving the multivalent peptides attached to the solid support. A further advantage of this resin are the very good swelling properties in water and buffer solutions, allowing biomolecules an easy interaction with the functionalized groups on the resin. Hence, the peptides should have enough freedom of movement to interact with the tryptase.

The design of the individual members of the combinatorial library was chosen accordingly to the previous inhibitors **92** and **90**, but with some minor changes (Figure 4.29 on page 117). The C-terminal CBS-units were replaced with an amino acid, resulting in a tetrapeptide of natural amino acids in each of the four side chains. The inhibitor structure ought to be kept as simple as possible to avoid any problems during the synthesis of the library. Especially the use of the artificial arginine analog (**85**) was observed to cause sporadic problems in the synthesis of complex structures with SPPS techniques.

Therefore, the use of standard Fmoc-protected and (also important) proteinogenic amino acids was preferred. Due to the anticipated binding area, the surface around the central pore of the tryptase, it was expected that the main interaction at the inhibitor molecule will be in the outer regions of the four side chains. Therefore, all of the library members carried in the first position after the lysine scaffold an additional glycine, which allows enough flexibility and particularly length of the side chains to interact with the enzyme. Additionally, the introduction of spacer residues such as glycine between the lysine core and the peptide sequence may also reduce an inhibitory interchain aggregation.[282,283]

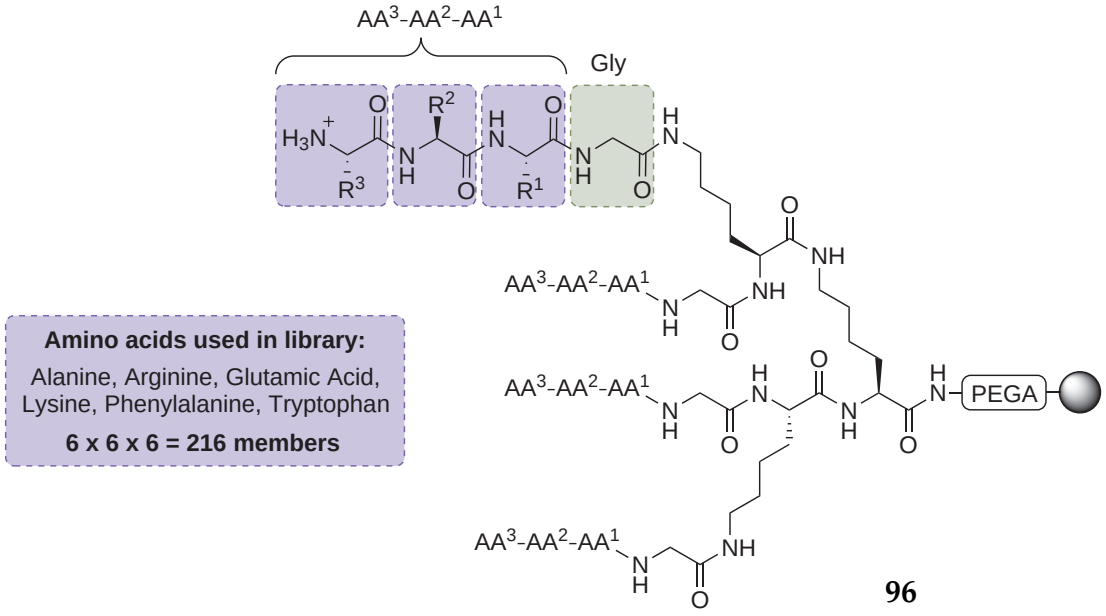

Figure 4.29: *Design of a combinatorial library of 216 inhibitors immobilized on PEGA resin. Every side chain has the same sequence of amino acids. The last three positions for amino acids at the C-terminal sequence are combinatorial varied with six amino acids each.*

Each of the four side chains had the same sequence of amino acids. Different sequences would have required a more complicated protecting group strategy. The complexity of the system would have also led to an undesired difficult interpretation of the mode of inhibitor with the anyway symmetrical enzyme. For each of the three combinatorial varied positions, 6 different amino acids were chosen (all in their natural L-form): lysine (K, **97**), arginine (R, **98**), tryptophan (W, **99**), glutamic acid (E, **100**), phenylalanine (F, **69**) and alanine (A, **101**). They were selected because they cover a wide range of different properties, such as basic (+), acidic (-), aromatic and aliphatic characteristics (Figure 4.30 on page 118). Therefore, the results of the screening should be different enough to discriminate between specific inhibition trends. As side chain protecting groups for

amines the Boc (**103**) and Pbf (**104**) groups were chosen and for the acid of glutamic acid the *tert*-butyl ester (**103**). All of them are acid labile and should be removed in the final TFA treatment step.

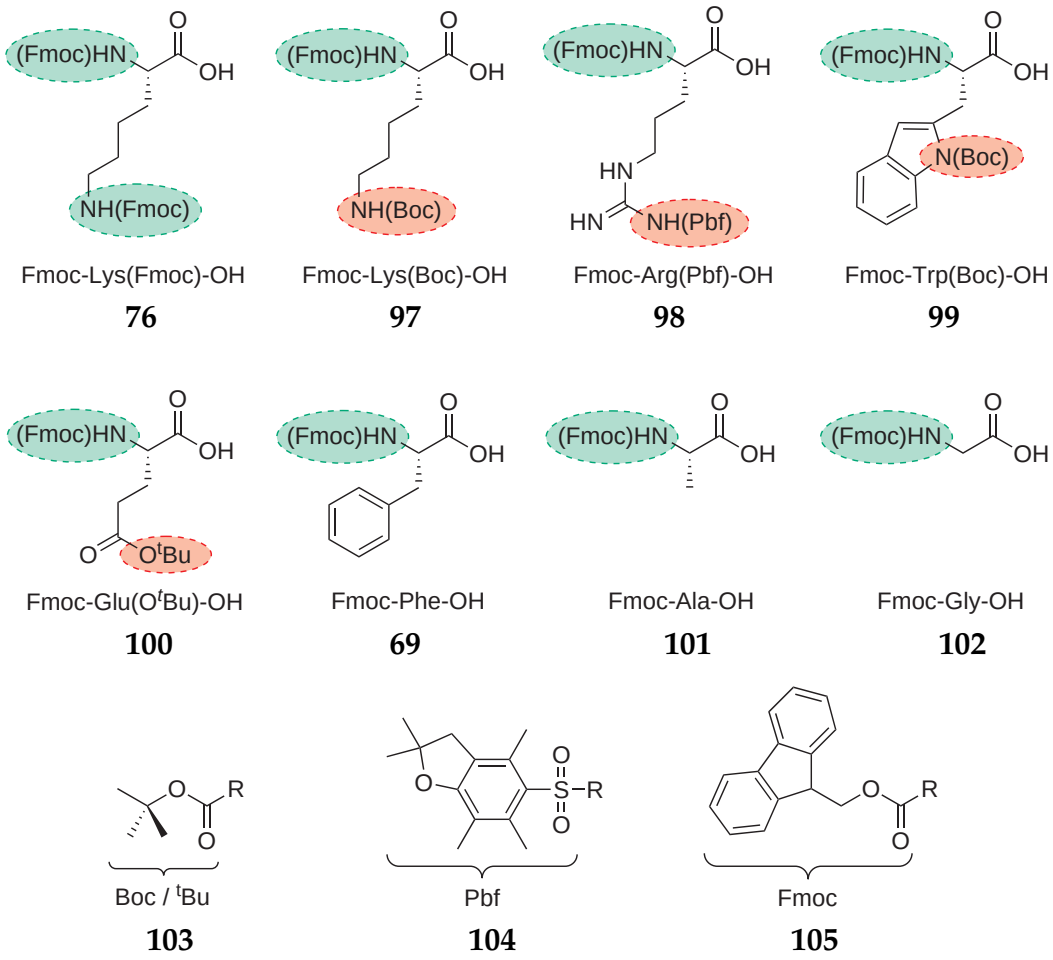

Figure 4.30: *Amino acids and protecting groups used in the synthesis of the combinatorial inhibitor library (**96**).*

Synthesis of a sample inhibitor: Prior to the synthesis of the library it was necessary to check the feasibility of the inhibitor synthesis with one sample inhibitor. The acid stability of the PEGA resin did not permit a cleavage of the peptide from the resin and a direct analysis of the resin bound peptides is not possible with enough accuracy. Hence, the test synthesis was performed on Rink amide resin, which is related but shows neither high acid stability nor swelling properties in water. With this resin it was possible to synthesize the test inhibitor $(KKFG)_4$ (**106**) with the identical amino acids as in the following library. During the synthesis a positive Kaiser test was used to monitor the coupling conditions and guaranteed an almost quantitative attachment of the amino acids. In several systematic test experiments the synthesis conditions were optimized and the structure of **106** was determined with different spectroscopical methods.

The synthesis of $(KKFG)_4$ (**106**) was performed under similar conditions as for $(CBS\text{-}KKF)_4$ (**90**, on page 110). The first reactions—including the assembly of the lysine scaffold **89**—were the same. The following tetrapeptide sequence, starting with glycine, was attached with the help of PyBOP as coupling reagent and DMF containing 3 % NMM. All amino acids and reagents were added with 10 equivalents to ensure a complete coupling in all four positions. The final cleavage and workup steps were identical as previously described (Scheme 4.13).

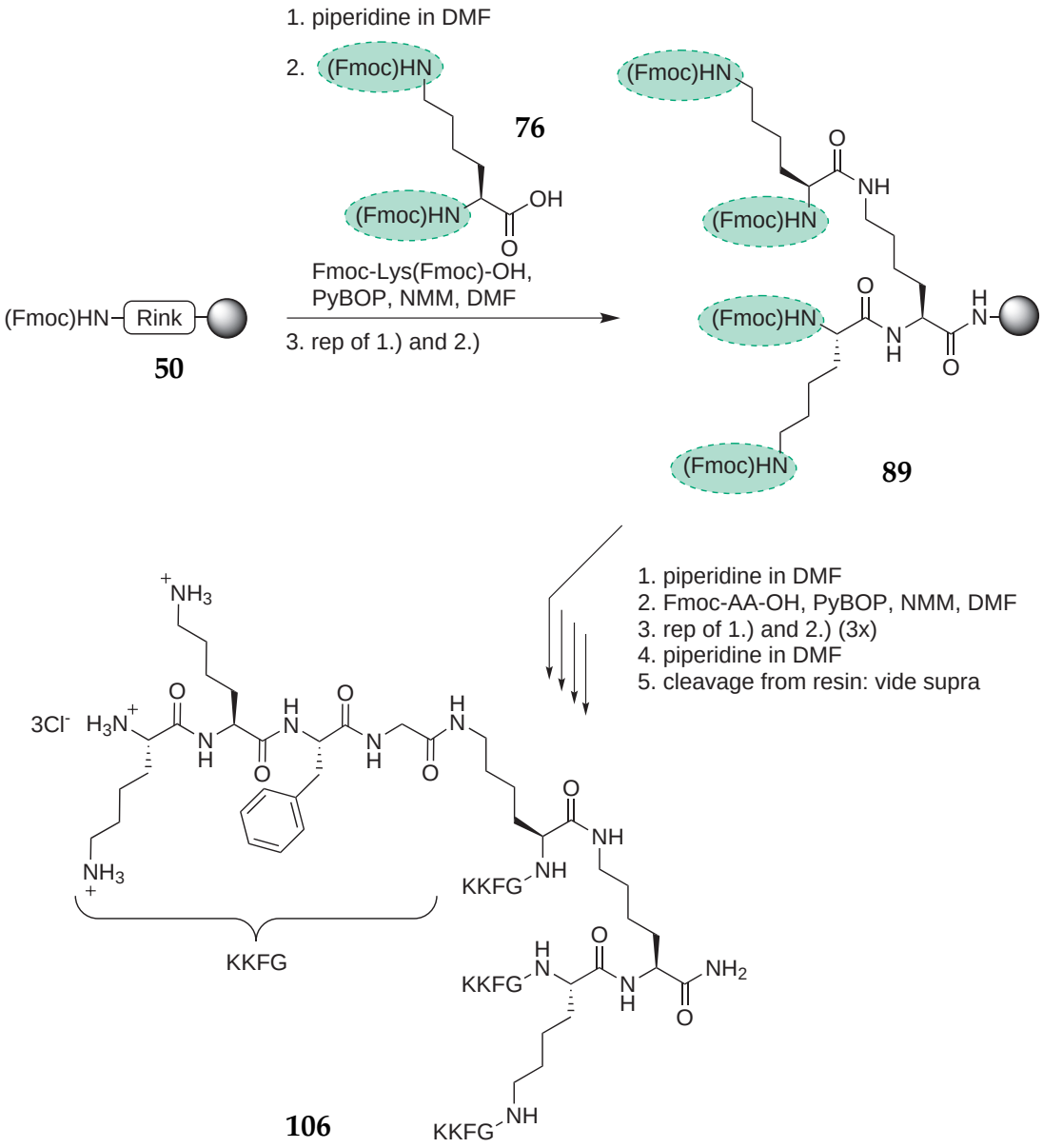

Scheme 4.13: *Synthesis of the test inhibitor ($(KKFG)_4$, **106**) on Rink amide resin to test the reaction conditions and the structural composition of the cleaved peptide prior to the synthesis of the combinatorial library.*

This compound (**106**) was then tested for its inhibition activity against rhSkin β-tryptase in solution. It exhibits a good K_i-value of 0.63 μM. Compared to the previously screened inhibitor **90** the new compound is able to inhibit in the same range of activity. Hence, the changes in the inhibitor design resulted in an equivalent good inhibitor, but this time solely based on natural amino acids.

Synthesis of the combinatorial library: With the successful test synthesis of one member of the intended library it was possible to start the synthesis of the combinatorial library with the "split and mix" technique,[284–286] using a radio frequency tagging technology.[228] The receptor library was synthesized on amino-PEGA resin, that had to be dried prior use because it is very hygroscopic. To distribute the resin equally to the 216 *IRORI MicroKans* of the combinatorial library it was suspended in a mixture of DCM and hexan. Due to the fact that the resin had the same density as the mixture (isopycnic principle) it was possible to handle the resin as a "solution" and therefore to portion it out in small fractions with an micropipette. Then all micro-reactors were equipped with an *IRORI AccuTag* radio frequency chip and scanned with the computer according to the *IRORI* synthesis software.

The first two steps of the synthesis were similar to the one of the test inhibitor **106** (Scheme 4.13 on page 119). They were performed in big glass reactors that can contain and shake up to 80 *MicroKans*. The commercial available PEGA resin carries no Fmoc group and can therefore directly be coupled with the first amino acid. Due to the increased solvent volumes and the limited mobility of the resins in the *MicroKans*, the washing steps were longer than for the test inhibitor. Additionally, each reaction step was repeated twice to ensure a complete coupling. After every reaction two *MicroKans* were opened and a small amount of resin was subjected to a Kaiser test.

As first amino acid after the lysine scaffold glycine was introduced in all library members, i.e. as before, all *MicroKans* were agitated with the same reagents. The first combinatorial step was the attachment of AA^1 directly after glycine in all of the four side chains (see overview in Figure 4.29 on page 117). Therefore, prior to the coupling step the 216 *MicroKans* were split according to the *IRORI* software in six separate portions for the introduction of the following six amino acids: lysine, arginine, tryptophan, glutamic acid, phenylalanine and alanine. All amino acids were coupled under standard conditions, this time with 10 equivalents to ensure a complete coupling. After the successful coupling and the removal of the Fmoc group of all library members, the previous procedure including splitting and redistributing into six portions was repeated again for the introduction of the second (AA^2) and third (AA^3) combinatorial varied position in the

library. In the final step the C-terminal Fmoc group was removed followed by the deprotection of all amino acid side chain protecting groups with 95 % TFA for 2×2 hours without any detachment of product from the resin. The results of a literature search for the necessary TFA treatment times were inconclusive,[225,287] therefore they were determined prior to the synthesis of the library in a series of stability experiments. The tests proved that the integrity of the resin is guaranteed up to 15 h at a concentration of 95 % TFA. The minimal time necessary for the complete cleavage of all side chain deprotection groups was determined as 2 h. With the successful synthesis of this combinatorial library of 216 different inhibitors it was now possible to arrange the screening against the β-tryptase to find the amino acid sequence necessary for the best inhibition.

Screening of the combinatorial library: The screening of the immobilized inhibitor library still bound to PEGA-resin against rhSkin β-tryptase was performed under similar conditions as the screening in solution (see page 112). However, some of the steps during the performing of the assay had to be slightly changed due to the limited reactivity of the resin bound inhibitors. Prior to the screening resin samples of all members had to be weighted into small glass vessels and mixed with a defined amount of DMSO. This method, to use an isopycnic solution, allowed the distribution of an equal amount of resin into the preassigned positions in white well plates. The preparation procedure for the incubation of the inhibitors with the enzyme is following the same order of addition as during the screening in solution (vide supra). Starting with buffer, then the isopycnic solution of inhibitor and the enzyme were added. Each well had to be mixed thoroughly with a multichannel pipette, because it was important to ensure that each resin sample had the same definite contact with the enzyme-mixture. Then the well plates were incubated for 20 hours at room temperature, permitting the immobilized inhibitors enough time to interact with the tryptase. The screening was performed the following day in the same order as the initial preparation of the well plates, to ensure the same incubation time for all samples. After the addition of the substrate with a multichannel pipette all vials were mixed and immediately subjected to the measurement of the fluorescence activity. With this method it was possible to determine the absolute inhibition of all library members within a period of approx. 6 hours.

The following chapter will describe the results of the on-bead screening assay and will discuss some interesting trends of inhibition depending on the peptide sequence, that will help to understand the mode of inhibition. Additional experiments will also assist to elucidate the inhibition type (competitive vs. non-competitive) and if the inhibitors have any protein selectivity.

4.3.3 Elucidation of the Inhibition Mode

The on-bead screening assay revealed that it was indeed possible to cover a huge range of inhibition with the broad choice of different amino acids in the library. The following graph is a representation of all library members in order of their absolute inhibition (Figure 4.31). The spectrum of inhibition ranges from 95 % for the best and 10 % for the weakest inhibitor.

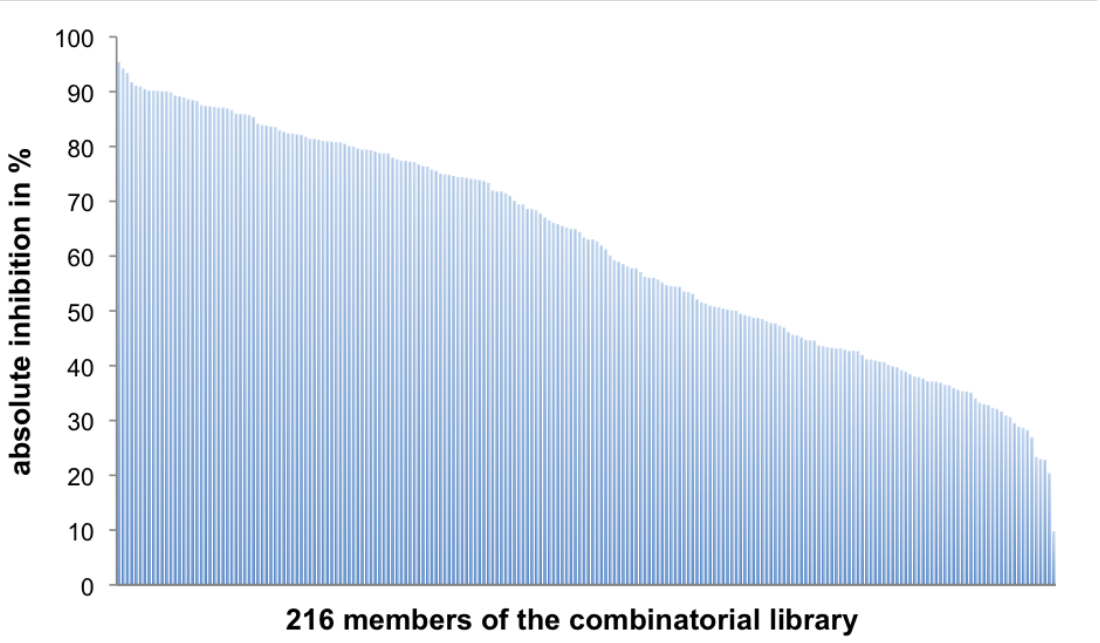

Figure 4.31: *Overview of the total inhibition of all 216 library members ranging from 95 % for the best and 10 % for the weakest inhibitor.*

A complete list of all inhibitors with their individual peptide sequence and the observed inhibition can be found in the appendix (Appendix D.1 on page 239) The following table 4.6 (on page 123) shows an excerpt of the ten best inhibitors, all with an inhibition above 90 %. The best inhibitor with an absolute inhibition of 95 % is $(RWKG)_4$ (**107**). The previously synthesized test inhibitor **106** can be found on the 35th place with an absolute inhibition of 84 %.

The high frequency of basic amino acids in the ten best inhibitors immediately indicates their essential role for the inhibition. A counting of all the basic amino acids (Lys + Arg) among the 30 possible positions in these ten inhibitors led to a remarkable result of 20 appearances. Also no glutamic acid or alanine can be found there, suggesting that they are not beneficial for the inhibition.

Table 4.6: *Excerpt of the ten best inhibitors of the on-bead screening (with AA^3 as terminal amino acid).* The inhibitors are listed in descending order of their absolute inhibition (in %).*

No.	AA^3	AA^2	AA^1	AA^0	Inhibition (%)
107	Arg	Trp	Lys	Gly	95
108	Lys	Trp	Lys	Gly	94
109	Trp	Lys	Phe	Gly	93
110	Phe	Arg	Lys	Gly	92
111	Lys	Arg	Arg	Gly	91
112	Phe	Lys	Arg	Gly	91
113	Lys	Trp	Arg	Gly	90
114	Lys	Phe	Arg	Gly	90
115	Lys	Lys	Trp	Gly	90
116	Phe	Trp	Lys	Gly	90

For the following in-depth discussion of the individual contribution of every amino acid, the 216 inhibitors were divided into four blocks containing 54 members each. The best inhibitors in the first block of 54 inhibitors are referred to as "Top 25 %", followed by the next blocks "Top 25 – 50 %" and "Top 50 – 75 %". The group of 54 library members with the lowest inhibition is called "Top 75 – 100 %". Figure 4.32 on page 124 provides a first overview of the whole library and the importance of individual amino acids depending on their position. Each amino acid has its own color code and is marked upon its occurrence in the inhibitor. The figure is divided into seven columns each representing the whole library with the best inhibitors on top and the worst on the bottom. The dotted pattern represents the PEGA resin (on the right) and therefore an orientation point for the attachment of the amino acids. The lysine scaffold and the glycine as first amino acid in every side chain were omitted in this presentation to simplify matters. Therefore, only the three combinatorial varied positions are visible, starting with AA^1 right after the resin, followed by AA^2 as second and AA^3 as third marker on the left.*

As it is clearly visible, the frequency of the basic amino acids is much higher in the "Top 25 %". The first column on the left depicts the combination of lysine and arginine

* As previously mentioned, the amino acid residues are numbered according to their synthesis steps. This special notation scheme is used systematically throughout the thesis.

(grey) and emphasizes the importance of these amino acids in the best 50 % of the inhibitors. On the opposite, the column on the right shows the occurrence of glutamic acid (blue), which is almost not evident in the best inhibitors. Tryptophane (pink), phenylalanine (purple) and alanine (green) do not seem to have a special location preference, they occur widely spread in both strong and weak inhibitors. In general, lysine and arginine—the basic amino acids—are the most important amino acids in order to obtain strong inhibition (cf. also Figure 4.33 on page 125).

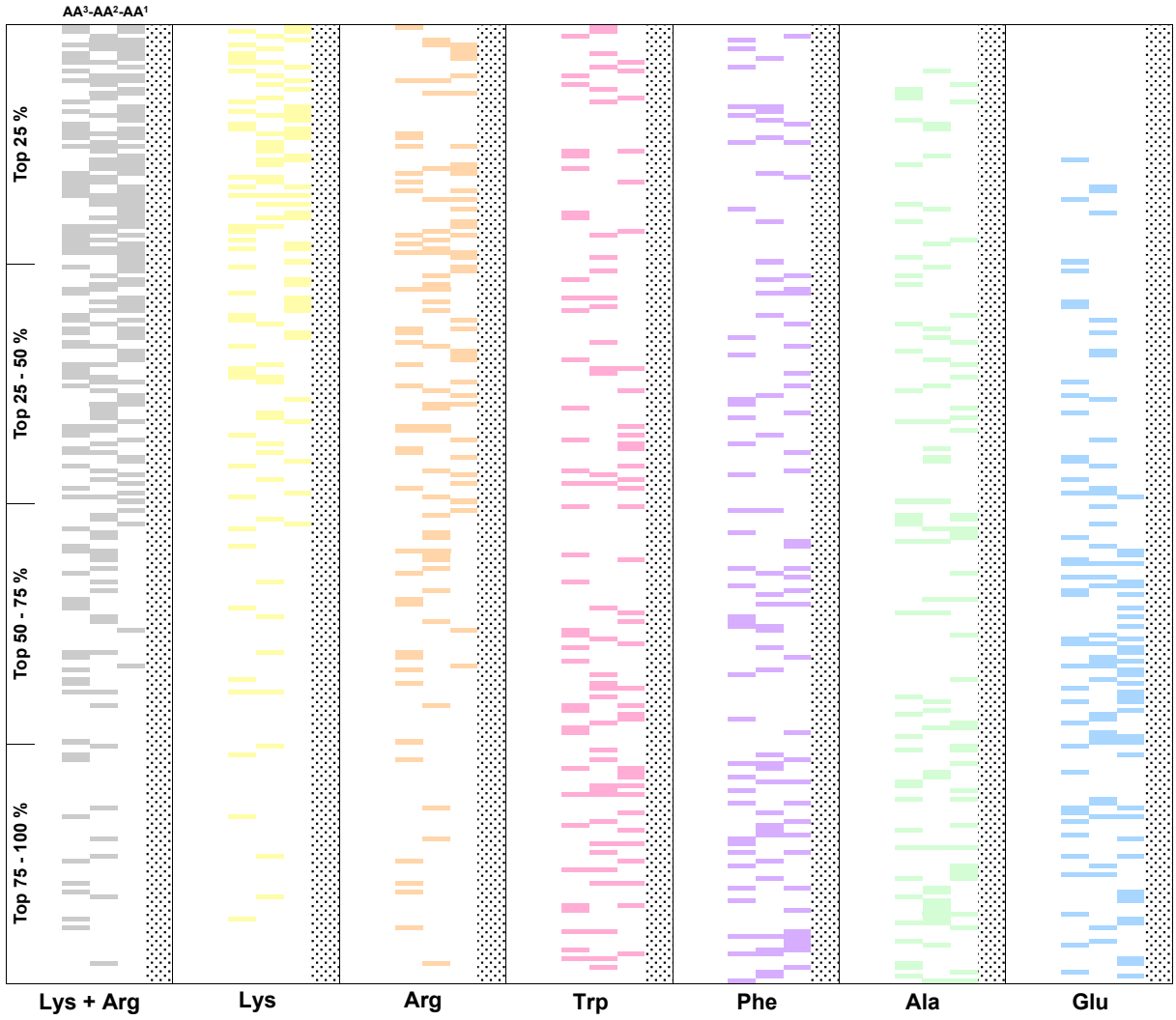

Figure 4.32: *Overview of the screening results of all library members. Each amino acid has its own color code and is marked upon its occurrence in the inhibitor. The dotted pattern represents the PEGA resin, followed by the combinatorial varied positions AA^1 to AA^3. The inhibitor activity is descending from the top and is divided into for blocks of 54 inhibitors each (e.g. "Top 25 %").*

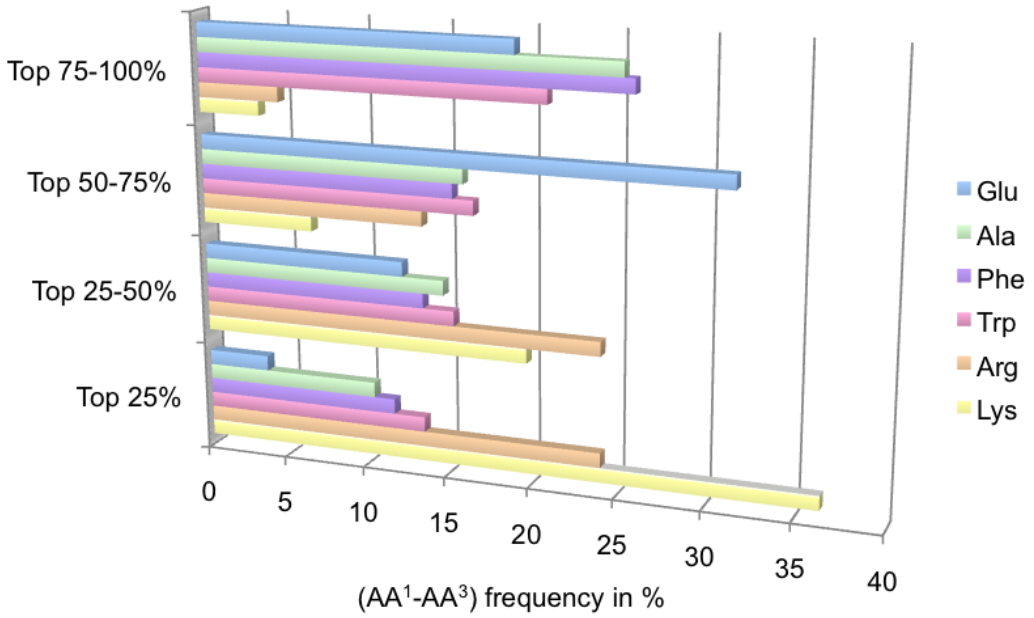

Figure 4.33: *General importance of the individual amino acids in each four inhibition blocks, with no discrimination between the positions AA^1-AA^3 (x-axis: frequency of occurrence in %). Especially in the best 54 inhibitors (Top 25 %) lysine and arginine are the most important amino acids and necessary for strong inhibition.*

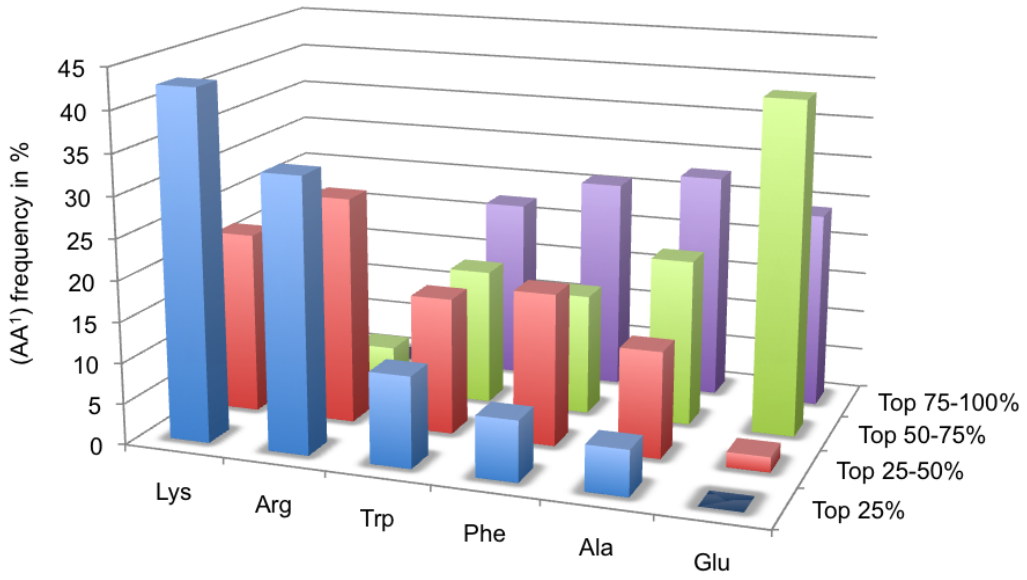

Figure 4.34: *Importance of the individual amino acids in position AA^1 (y-axis: frequency of occurrence in %). Looking at the best 25 % of the inhibitors, lysine and arginine are the predominant amino acids in this position. Together, they occur in three-quarters of the best block of inhibitors.*

Unexpected and very interesting is the surprising significance of the combinatorial varied position AA^1. It seems that the choice of amino acid already at this position is crucial for a good inhibition. Is there e.g. a glutamic acid, the chance of high inhibition is very low, even if two cationic amino acids are following (cf. Figure 4.32 and 4.34). The distribution of lysine or arginine in position AA^2 and AA^3 is rather scattered over all library members (with a slight higher frequency in the Top 50 %). In comparison lysine is a little bit more important than arginine in terms of high inhibition in general.

The inhibition is particularly high when basic amino acids are combined with aromatic amino acids. For comparison, all combinations of three cationic amino acids within each arm (lysine and/or arginine) are among the "Top 25 %", but they are not *the best* inhibitors. For example the sequence Lys-Lys-Lys is ranked on the 35th place and Arg-Arg-Arg even on the 52nd place. However, looking again at the ten best inhibitors an astonishing accumulation of basic (boldface) and aromatic amino acids can be observed (see Table 4.7). They all contain *only* lysine, arginine, tryptophan or phenylalanine. In particular the combination of two basic amino acids with one phenyl alanine (this combination occurs 3×) or with one tryptophan (4×) shows a noticeable cumulation. Especially the combination with tryptophan on position AA^2, surrounded by basic amino acids seems to be very efficient (compounds **107** (1st), **108** (2nd) and **113** (7th place), grey highlighted).

Table 4.7: *The combination of two basic amino acids (boldface) with one aromatic amino acid shows a noticeable cumulation among the ten best inhibitors, in particular with tryptophan on position AA^2 (grey highlighted).*

No.	AA^3	AA^2	AA^1	AA^0	Inhibition (%)
107	**Arg**	Trp	**Lys**	Gly	95
108	**Lys**	Trp	**Lys**	Gly	94
109	Trp	**Lys**	Phe	Gly	93
110	Phe	**Arg**	**Lys**	Gly	92
111	**Lys**	**Arg**	**Arg**	Gly	91
112	Phe	**Lys**	**Arg**	Gly	91
113	**Lys**	Trp	**Arg**	Gly	90
114	**Lys**	Phe	**Arg**	Gly	90
115	**Lys**	**Lys**	Trp	Gly	90
116	Phe	Trp	**Lys**	Gly	90

On the first look this selectivity may seem like a similar effect that was reported by *Craik et al.* They investigated linear peptides, that act as competitive inhibitors and bind *into* the active sites of tryptase.[268] As previously mentioned, they observed an enhanced substrate specificity for lysine and arginine in positions P1 and P3 of the inhibitors. They also reported a preference for asparagine in position P2, which would—assuming our inhibitors would also bind into the active sites—correspond to the position AA^2 in our library. However, we observed in this position a cumulation of Lys, Arg, Try and Phe, which represented in the screening of *Craik* the *least* activity at P2 among 19 tested amino acids. Hence, based on this information the probability is very low that our peptides bind to the active sites. It is more likely that the combination of basic and aromatic amino acids is necessary for the recognition of the acidic patches on the surface of tryptase.

In summary, this on-bead screening confirmed, that basic amino acids are essential for a strong inhibition of β-tryptase. Additionally, it was discovered that already the choice of the amino acid at the first combinatorial varied position after the lysine scaffold is crucial for the inhibition result. This unexpected finding was only possible to reveal with the help of this combinatorial approach. Hence, this library provided interesting knowledge about the structure-reactivity relationship during the surface recognition in a fast and easy way, that would otherwise only have been possible in a far more extensive and time-consuming study in solution.

Synthesis in solution: As mentioned before, the test inhibitor $(KKFG)_4$ (**106**) previously synthesized in solution exhibits an absolute inhibition of 84 % in the library and a K_i-value of 0.63 μM in solution. However, the best inhibitor in the on-bead screening was $(RWKG)_4$ (**107**) with an absolute inhibition of 95 %. Hence it was of high interest to test this compound also in solution. This led to the synthesis of **107** on Rink amide resin as previously described. In addition, also the corresponding monovalent inhibitors of both library members were synthesized: KKFG (**117**) and RWKG (**118**). These three new compounds were then screened for their inhibition potential against β-tryptase. Figure 4.35 on page 128 provides an overview of the obtained K_i-values. As predicted by the results of the on-bead screening, compound **107** ($(RWKG)_4$) has indeed the best K_i-value (0.17 μM) so far. Its inhibition is almost 4-times better than the one of the previously synthesized compound **106**. But even more remarkable is the comparison with the monovalent counterparts. In the case of the peptide sequence Lys-Lys-Phe-Gly, the tetravalent inhibitor is 750$\times$ better, with the best amino acid combination Arg-Trp-Lys-Gly even 1800$\times$ better than the monovalent analog. These exceptional results strengthen

the assumption that the mode of inhibition is indeed depending on a multivalent interaction based on a steric blocking of the entrance to the central pore of the β-tryptase.

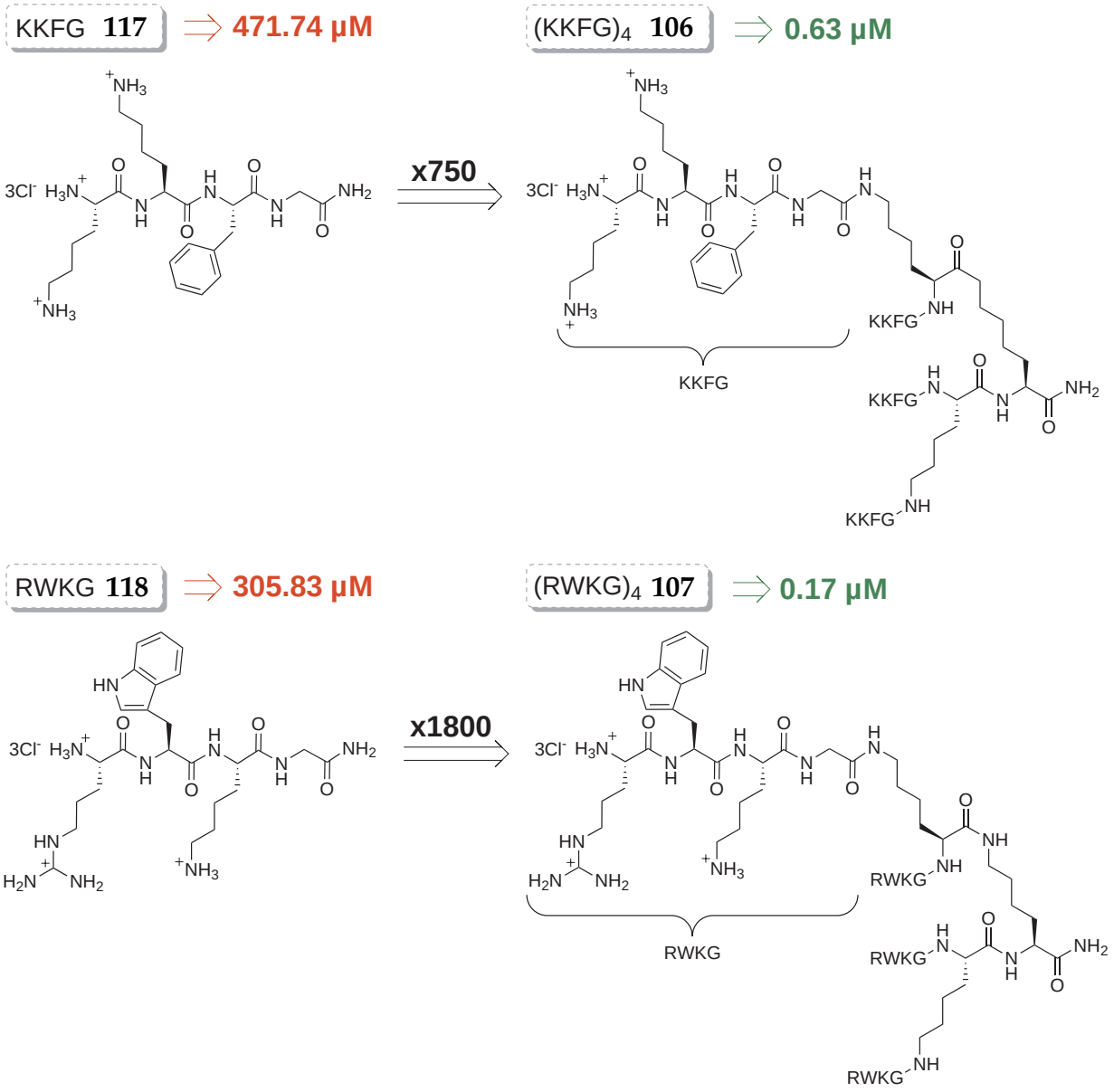

Figure 4.35: *Both of the multivalent compounds **106** and **107** are part of the combinatorial library and were resynthesized in solution, together with their monovalent analogs. The tetravalent compounds feature a 750x (**106**) and 1800x (**107**) better inhibition (K_i-value) than the monovalent counterparts, respectively.*

To obtain a detailed understanding of the mode of interaction, the previous results were further investigated and verified with several experiments in solution. The following series of experiments will focus on the investigation of the general protein selectivity, the reversibility and the kinetic classification of the tryptase inhibition.

Test on protein selectivity: Human tryptase is part of the superfamily of (chymo)-trypsin-like serine proteases. The proteolytic active form of tryptase is, as mentioned before, the tetrameric structure. However, the tryptase monomer is surprisingly similar in fold to the serine proteases trypsin and chymotrypsin, which are both digestive enzymes. Of the 245 amino acid residues of the monomer, 168 and 162 are topologically equivalent to those of trypsin and chymotrypsin, respectively. The active site of the tryptase monomer is very similar in structure to that of trypsin and not suitable to confer specificity. In particular, the S1 pocket is nearly identical to that of trypsin and well suited to accommodate both P1 arginine and lysine residues. Chymotrypsin cleaves peptides at the carboxyl side of tyrosine, tryptophan, and phenylalanine which fit into a "hydrophobic pocket" in the enzyme. Hence, the active site of trypsin is very similar to the one of the tryptase monomer, whereas for chymotrypsin only the general structure is similar to the tryptase monomer but not the active site.

Because of these similarities both enzymes were used for inhibition experiments with the four previously mentioned mono- and multivalent peptides (see page 128). Whereas the monovalent tetrapeptide compounds might have an inhibition effect due to their related structure to known trypsin inhibitors, the multivalent compound should exhibit no or only little beneficial effects for an inhibition at all. The assay conditions were similar to the ones for tryptase, with minor changes in the buffer and the used chromogenic substrates (cf. Chapter 7.5.1 on page 208). Again p-aminobenzamidine (p-Ab) was used as literature known inhibitor to test the assay conditions. The compound is known to inhibit trypsin, but not chymotrypsin. This could be reproduced with our assay conditions. It was possible to measure a K_i of 5.29 μM which is very similar to the literature known value of 7 μM.[280] These calibration experiments allowed the direct comparison of the inhibition between tryptase, trypsin and chymotrypsin. Table 4.8 on page 130 summarizes the results of the screening.

In conclusion, both mono- and multivalent compounds show no inhibition of trypsin and chymotrypsin at all. The monovalent structures seem to have no effect on the two new proteases, indicating that the peptide sequences have a low affinity for the closely

Table 4.8: *Two multivalent library members and their monovalent counterpart were tested for their protein selectivity. For comparison trypsin and α-chymotrypsin were chosen, due to their similarities with the tryptase monomers.*

No.	Compound	rhSkin β-Tryptase K_i [μM]	Trypsin K_i [μM]	α-Chymotrypsin K_i [μM]
44	p-Ab	56.97 ± 8.25	5.29 ± 0.80	>1000
117	KKFG	471.74 ± 31.27	>1000	>1000
106	$(KKFG)_4$	0.63 ± 0.02	>1000	>1000
118	RWKG	305.83 ± 50.22	>1000	>1000
107	$(RWKG)_4$	0.17 ± 0.02	>1000	>1000

related active sites of trypsin and tryptase. This would be in agreement with the previously mentioned results of *Craik* concerning the substrate selectivity.[268] But most importantly, the very high inhibition of the multivalent compounds **106** and **107** cannot be reproduced with trypsin or chymotrypsin. Hence, this dominant enzyme selectivity in the range of the factor >6000 is a very strong indication that there is a mode of inhibition depending on the tetrameric structure of tryptase. Also, there should be indeed an interaction with the entrance to the central pore or the surrounding of the active sites and not a direct binding to the cleavage sites.

Test on reversibility of inhibition: The next experiments focused on the reversibility of the β-tryptase inhibition. Reversible inhibitors bind to the enzymes through weak non-covalent interactions and do not form any chemical bonds or reactions with the enzyme. Thus the enzyme-inhibitor complex should rapidly dissociate in contrast to irreversible inhibition. The peptide inhibitors used in this thesis are unlikely irreversible inhibitors, however these tests are necessary to eliminate the possibility that the observed inhibition is only based on the decomposition of the enzyme.

The reversibility of the tryptase inhibition was tested in a dialysis experiment using a custom-built dialysis device. Therefore, a dialysis separation tube permeable for everything smaller than 12 to 14 kDa was clamped into the device separating a continuous stream of buffer solution from small cavities on top of the instrument. In these chambers mixtures of tryptase and inhibitor in buffer were added. Then, every two hours a 100 μL sample was taken from the cavities and submitted to the standard fluorescence inhibitor assay to determine the activity of the enzyme. The underlying principle of this exper-

iment is, that a reversible inhibitor will be "washed out" by the continuous stream of buffer and the enzyme will be reactivated over time. Again for this test, the four previously used mono- and multivalent inhibitors were analyzed. Both monovalent peptides **117** and **118** show a clear reversible behavior based on the regeneration of the tryptase activity. It was possible to observe the following average enzyme activities, which were measured over a period of eight hours (similar values for both peptides): 24 % (start), 25 % (after 1h), 46 % (after 2h), 58 % (after 4h), 70 % (after 6h), 76 % (after 8h). However, no distinct regeneration of the enzyme was observed for the multivalent peptides **106** and **107** (change of enzyme activity over 8h: 0.1 % to 2 %). A reason for that could be the high binding affinity of the peptides. It is known that some reversible inhibitors bind so tightly to their target enzyme that they show kinetics similar to irreversible inhibitors.[288,289]

To elucidate this uncertainty a second experiment was performed. In this test tryptase was treated again with mono- and multivalent peptides for 5 minutes, followed by the addition of excess heparin. If the inhibition is reversible, then the cationic peptides should favor the interaction with heparin over the enzyme, resulting in a reactivation of the tryptase activity.[254] All experiments were performed in a parallel duplicate where instead of heparin in buffer, buffer alone was added to the vials. Both vials were mixed and again incubated for 5 minutes before the final addition of the substrate and the fluorescence readout. In the case of the multivalent peptide a 20–30 % recovery of tryptase activity was observed, whereas the monovalent peptides showed no reactivation. This might be explained by the small size and therefore only weak interactions of the monovalent compound with heparin. In contrast the multivalent molecules are big enough to interact with heparin. Hence, this test showed that the inhibition of β-tryptase by multivalent polycationic peptides could be partly reversed by adding excess heparin, proving that the inhibition is reversible.

In conclusion, the two described test methods revealed that both mono- and multivalent peptides inhibit tryptase in a reversible and non-destructive way. They do not damage the active tetrameric form of tryptase. Also the enzyme can be reactivated with an excess of heparin after the inhibitor addition.

Classification of enzyme inhibition: So far all experiments led to the assumption that the inhibition mechanism of the multivalent peptides is based on a steric blocking of the active sites. The following experiments will focus on the determination of the exact type of inhibition, typically classified into three main types: competitive, uncompetitive and non-competitive inhibition (see Chapter 3.4.1.1 on page 52). With this information it was possible determine if the inhibitors bind into the active sites of tryptase. Therefore, these tests helped to explain where the inhibitors interact with the enzyme. Two types of experiments were carried out, a simple and fast preliminary test and an elaborate and more precise test.

For the first experiment the IC_{50} and K_i of one monovalent (CBS-KKF, **1**) and two multivalent systems ((CBS-KKF)$_4$, **90** and (KKFG)$_4$, **106**) were determined at different substrate concentrations of 200 and 400 μM (normally 50 μM). If there is a change of the IC_{50}-value upon the increase of the substrate amount, then this is an indication for a competitive inhibition mode where the peptides have to compete with the substrate for the active sites inside of the tryptase. If there is no change, then a non-competitive inhibition mode can be assumed. Table 4.9 on page 132 summarizes the test results.

Table 4.9: *First experiment for the determination of the inhibition type: measurement of the IC_{50} values at varied substrate concentration. A change of the IC_{50} is an indication for a competitive inhibition type, no change for non-competitive.*

No.	Compound	**c(S) = 50 μM** **IC_{50} [μM]**	**c(S) = 200 μM** **IC_{50} [μM]**	**c(S) = 400 μM** **IC_{50} [μM]**	
1	CBS-KKF	27.25 $\pm$ 8.90	34.98 $\pm$ 1.17	65.83 $\pm$ 22.88	$\rightarrow$ **change**
90	(CBS-KKF)$_4$	0.28 $\pm$ 0.15	0.19 $\pm$ 0.18	1.16 $\pm$ 0.38	$\rightarrow$ **no change**
106	(KKFG)$_4$	0.63 $\pm$ 0.02	0.83 $\pm$ 0.028	1.18 $\pm$ 0.25	$\rightarrow$ **no change**

The IC_{50}-values increase only for the monovalent peptide **1** (with a constant K_i at the same time), whereas the values for the multivalent peptides remain relatively constant. This is an indication that the small monovalent peptides compete with the chromogenic substrate for the active sites within the tryptase cage. The results of the multivalent peptides lead to the assumption that there is a non-covalent inhibition, where the peptides interact with the enzyme on the surface or the surrounding of the active sites, but not actually *in* the active sites.

The second and more detailed test to elucidate the mode of enzyme inhibition was a similar experiment as the K_m determination (see page 113). Therefore, the rate of the enzyme reaction was measured at different substrate concentrations (0–1000 μM) and a fixed enzyme concentration, but this time also the inhibitor **106** ($(KKFG)_4$) was added at different concentrations ([I] = 1, 10 and 100 μM) instead of DMSO during the tests. The type of inhibition was determined with the interpretation of the resulting *Lineweaver-Burk* (Figure 4.36) and *Hanes-Woolf* plots (Figure 4.37 on page 134) as well as the non-linear regression fits (Figure 4.38 on page 134). In comparison with literature known inhibitors, all three plots show the graphic renditions indicative for a non-covalent inhibition. The double-reciprocal *Lineweaver-Burk* representation shows plots that have no common intersection on the y-axis, as it would have been in the case of competitive inhibitors. Also the *Hanes-Woolf* plots are not parallel, as caused by competitive inhibitors. In the non-linear representation the K_m-values are constant and the saturation curves tend to get parallel and reach different V_{max}-values. With the increase of the inhibitor concentration, the maximal reaction speed cannot be reached any more. In contrast, V_{max} would have been reached at all inhibitor concentrations during a competitive inhibition.

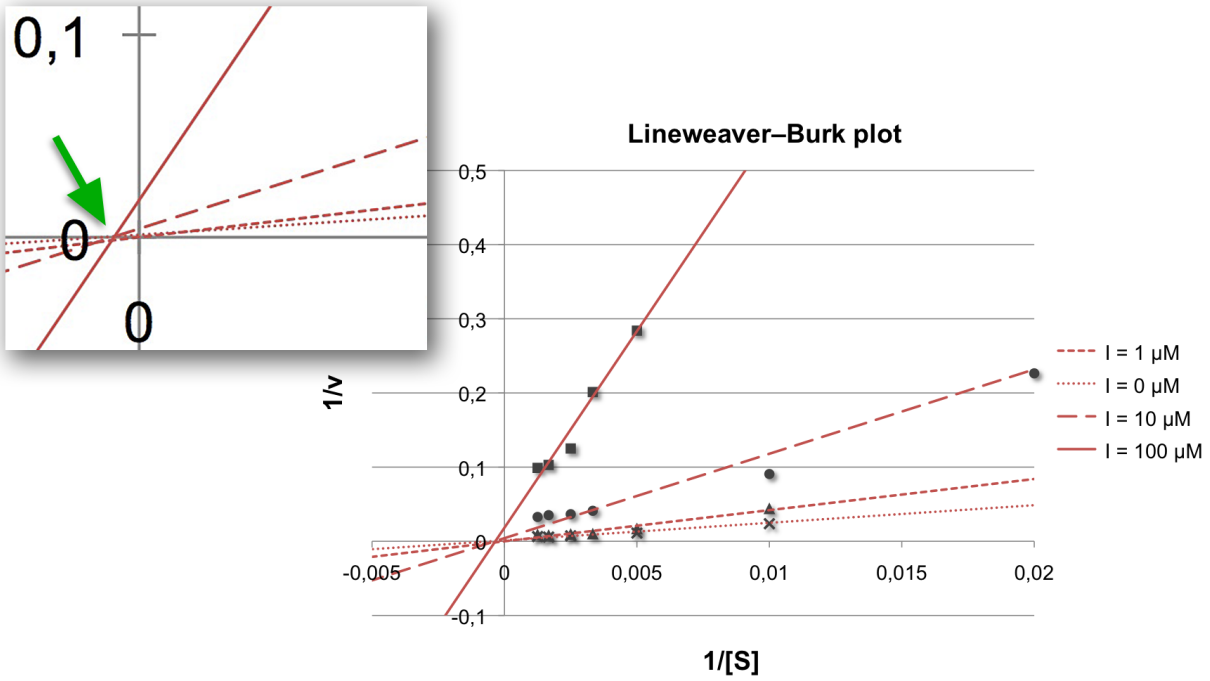

Figure 4.36: *Depiction of the enzyme kinetics of the multivalent inhibitor* ***106*** *with the help of the Lineweaver-Burk representation. The plots at different inhibitor concentration have a common intersection that is not on the y-axis. This is an indication for a non-competitive inhibition.*

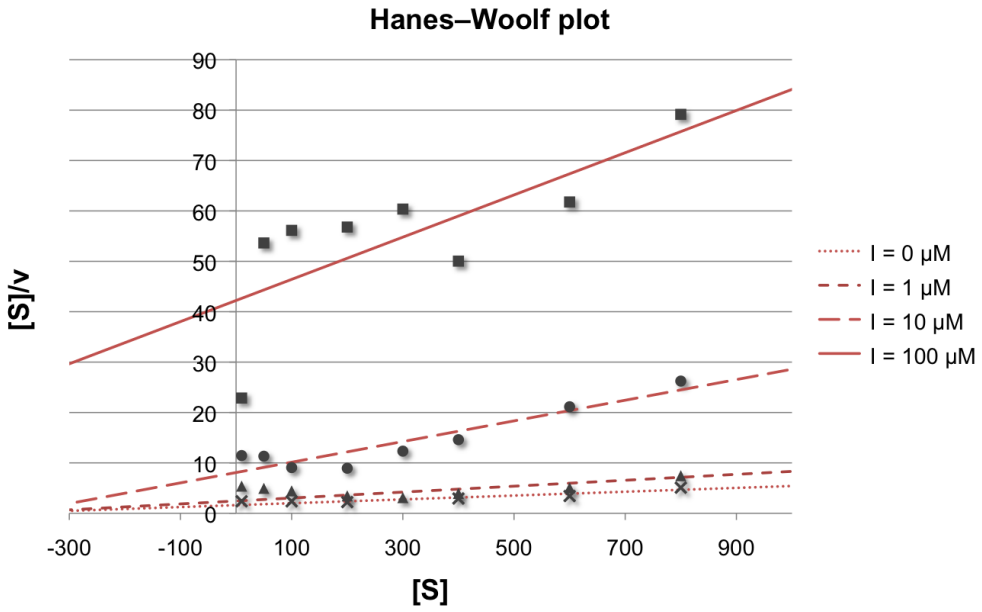

Figure 4.37: *Depiction of the enzyme kinetics of the multivalent inhibitor* ***106*** *with the help of the Hanes-Woolf representation. The ratio of the initial substrate concentration [S] to the reaction velocity v is plotted against the substrate concentration [S]. The plots are not parallel, as would be produced by competitive inhibitors.*

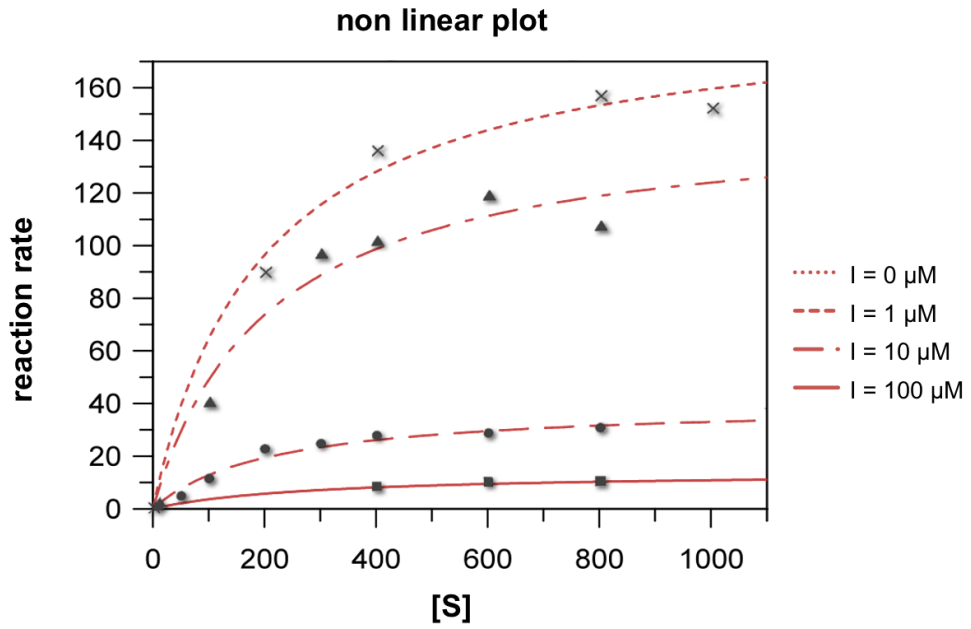

Figure 4.38: *The non-linear representation of the enzyme kinetics illustrates that with increasing inhibitor concentration the maximum reaction velocity cannot be reached anymore. This is an indication for a non-competitive inhibition.*

In conclusion, it was possible to prove with these experiments that the multivalent inhibitors are not in direct competition with the substrate, hence they do not bind into the active cleavage sites buried deep inside of the tryptase. Therefore, the multivalent inhibitors are the first non-competitive and at the same time reversible inhibitors. So far all non-competitive inhibitors for tryptase were heparin antagonists and thus destabilized the active tetrameric enzyme structure in an irreversible matter.

These findings led to the most likely model that the inhibitors sterically block the accessibility to the active sites. Computational calculations with *MacroModel* endorsed this concept and helped to visualize a possible three-dimensional representation of the interaction between the inhibitor and the tryptase (Figure 4.39 and Figure 4.40 on page 136). The illustrations show the binding of the multivalent inhibitor **106** to the acidic area around the central pore. This region has an accumulation of acidic amino acids and attracts the basic amino acids of the inhibitor. Figure 4.40 illustrates all aspartic and glutamic acids on the surface of the tryptase, ten of them (6×Asp, 4×Glu) are in the area around the entrance to the central pore. The calculations revealed that it is indeed possible to saturate all of these acid functions with the inhibitor **106**, thus forming a tight "molecular plug"-like structure that is sealing the central pore.

Summary of the inhibitor studies: These in-depth studies revealed the details of the unusual binding and inhibition mechanism depending on the composition of the peptide arms. Up to now most of the literature known inhibitors are designed to fit into the binding pockets of the active sites of tryptase and bind in a competitive way. To the best of my knowledge, the described multivalent peptides are the first non-competitive and at the same time reversible inhibitors. The comparison with the monovalent form reveals in some cases an exceptional 1800-fold increase of activity, proving the importance of the multivalent design. In addition, there is a high selectivity against other serine proteases, such as trypsin or chymotrypsin in the range of >6000. The attractive results of this project are important for the understanding of the molecular mechanisms by which proteins interact with small molecules and with each other, in general. They also help to gain new insights for possible drug candidates against tryptase-related allergic and inflammatory diseases such as asthma.

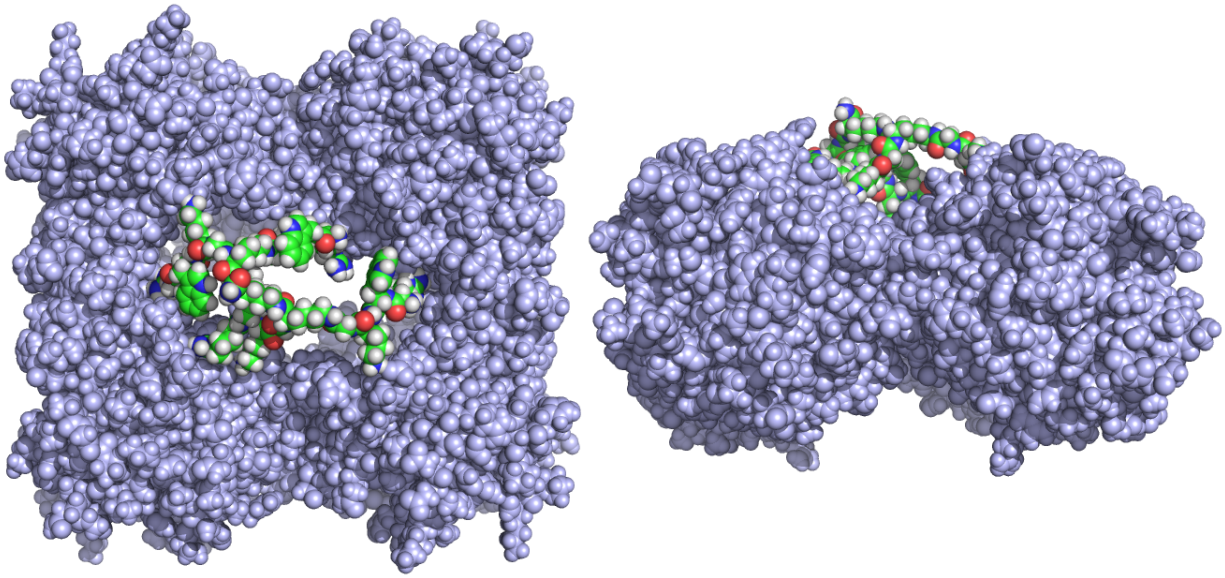

Figure 4.39: *Computational calculation of the interaction between the multivalent inhibitor* ***106*** *and tryptase. The peptide spans over the central pore of the tryptase, thus limiting the accessibility to the active sites.*

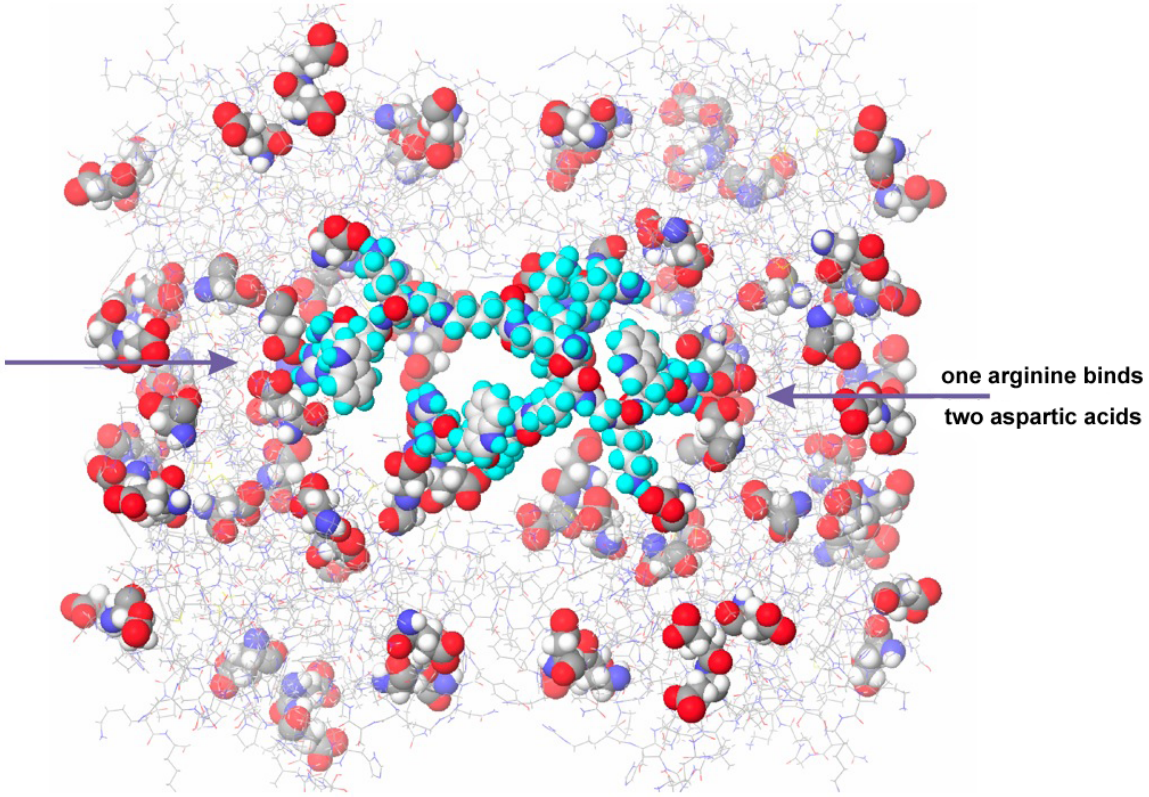

Figure 4.40: *The multivalent inhibitor* ***106*** *saturates all aspartic and glutamic acids in the area around the entrance to the central pore (only the aspartic acids of the tryptase surface are highlighted).*

4.3.4 Conclusion and Outlook

The final project of this thesis combined the gained knowledge of the previous research work and focused on a complex recognition event. It was possible to take a step forward from the successful recognition of small oligopeptides to the complex interaction with protein surfaces. A newly developed on-bead assay allowed the screening of a combinatorial library of 216 multivalent inhibitors of β-tryptase. This method provided a fast and easy way to reveal the best possible inhibitor composition and confirmed the effectivity of small and tailor made libraries designed for specific targets. The best inhibitor $(RWKG)_4$ (**107**) with a K_i-value of 0.17 μM has already proven to have the best amino acid composition. Compared with the monovalent analog (**118**) its inhibition is 1800$\times$ higher, a clear signal that the multivalent approach is crucial for an effective blockage of the active centers. This inhibition process should now also be investigated with ITC experiments to determine the thermodynamic parameters of the complex formation. Unfortunately, it was not possible to run these tests during this thesis, due to time constrains.

One unexpected finding of the screening was, that already the first combinatorial varied position right after the lysine branching is very important. Hence, possible improvements should not focus on longer side chains, but rather on variations in the branching scaffold. For example, a version containing a β-alanine spacer at the α-amine of lysine can produce a branching unit (**119**) that has symmetrical arms (Figure 4.14 on page 138).[290] In order to limit the flexibility of the branched lysine template, ornithine (**120**),[291] the lower homolog of lysine, as well as even more constrained diamino acids like the 2,3-diaminopropionic acid (Dap, **121**) can be used.[278,292]

Also very interesting would be the exchange of the amino acids in the four side chains with unnatural amino acids, such as β-amino acids[293,294] or D-amino acids,[295,296] as it is often done for linear peptides. This might lead to an increased proteolytic stability and to different inhibition results.

In general, the investigated multivalent peptide structures of this thesis might also be attractive for the investigation of their interaction with further biological targets, such as nucleotides or proteins which also feature negative surface patches or a general acidic behavior. Examples might be pepsin (pI = 1.0), ferredoxin (pI = 2.5), amyloglucosidase (pI = 3.5) or bovine serum albumin (pI = 4.8).

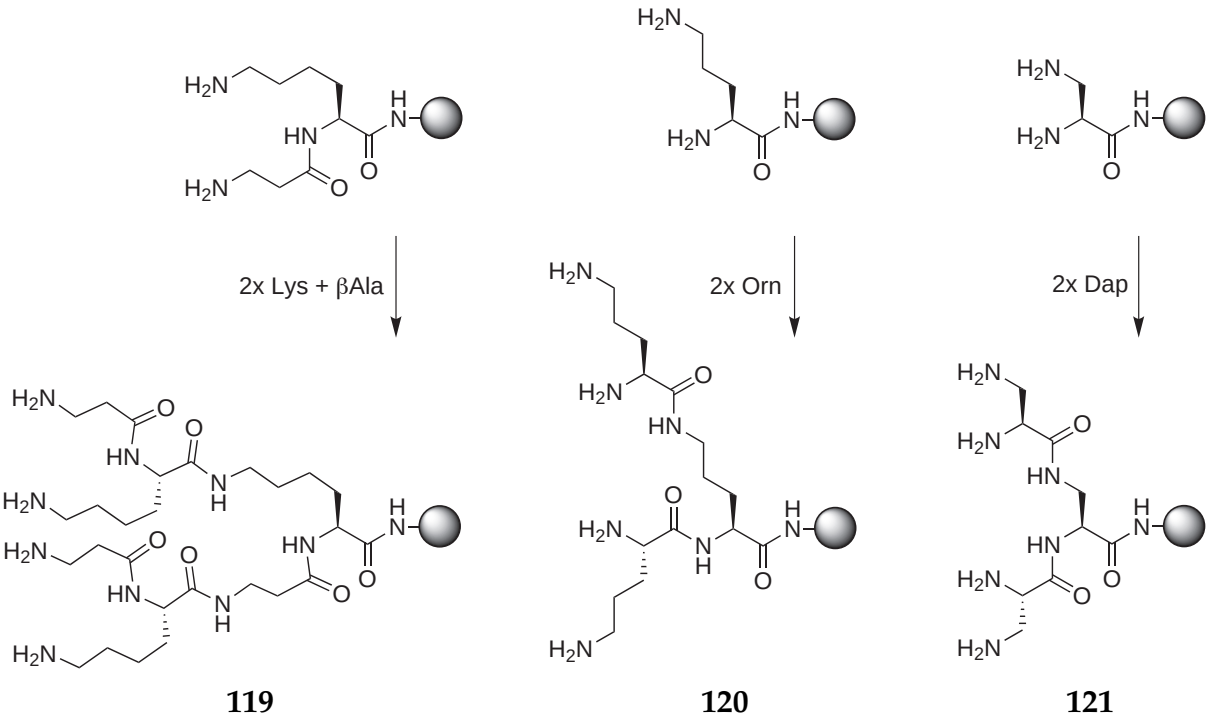

Scheme 4.14: *Possible variations of the lysine scaffold include symmetrical dendrons (**119**) or more rigid and constrained templates (**120, 121**).*

Looking ahead to even more distant projects in the future, one very interesting application would be the use of multivalent structures as molecular anchors for proteins. If the surface binding to proteins can be increased by some orders of magnitude one can think of chemical modifications to produce structurally defined connections between two proteins. Such bis-proteins would then provide the basis for a systematic analysis of protein-protein interactions.[297] In addition the use as a surface based "biotin-equivalent" may be a future application, where the multivalent structures could be utilized for the non-covalent attachment of synthetic macromolecules to the surface of proteins.[298] They could also serve as adhesive molecules which can stick to specific proteins in order to induce their assembly, or stabilize for example microtubules against their depolymerization.[299] In summary, these projects might help to obtain a better understanding of protein interactions and would support the application of proteins and peptides as therapeutics.

CHAPTER 5

SUMMARY

The main focus of this thesis was the synthesis and analysis of multifunctional oligopeptides. The study of their non-covalent interactions with various counterparts revealed interesting new results, leading to both methodological and application related progress. The following summary will recap the most important discoveries.

5.1 Insights into the Binding Mode of Small Peptides

The first project of this thesis concentrated on the in-depth analysis of the peptide receptor CBS-Lys-Lys-Phe-NH_2 (**1**) to acquire a better understanding of its binding mode upon complexation with a substrate. The sensitive spectroscopical methods required a high purity of **1**. This led to an optimized synthesis on a large scale followed by an extensive purification process to meet the necessary demands. In cooperation with the Department of Physical Chemistry of the University of Würzburg it was possible to obtain high resolution 2D NMR spectra in DMSO. They revealed that at least in DMSO a β-sheet like structure is favored, with the CBS group in its energetically more stable out-out conformation. The structural analysis was refined with the help of resonance Raman experiments in water. Therefore, characteristic electronic absorption areas were utilized for the selective monitoring of the CBS group and the interaction with the carboxylate groups of the tetrapeptide N-Ac-D-Glu-D-Glu-D-Glu-D-Glu-OH. This method allowed

the pH dependent analysis of **1** and a detailed description of the structural changes during the complexation, demonstrating the advantages over UV and fluorescence experiments.

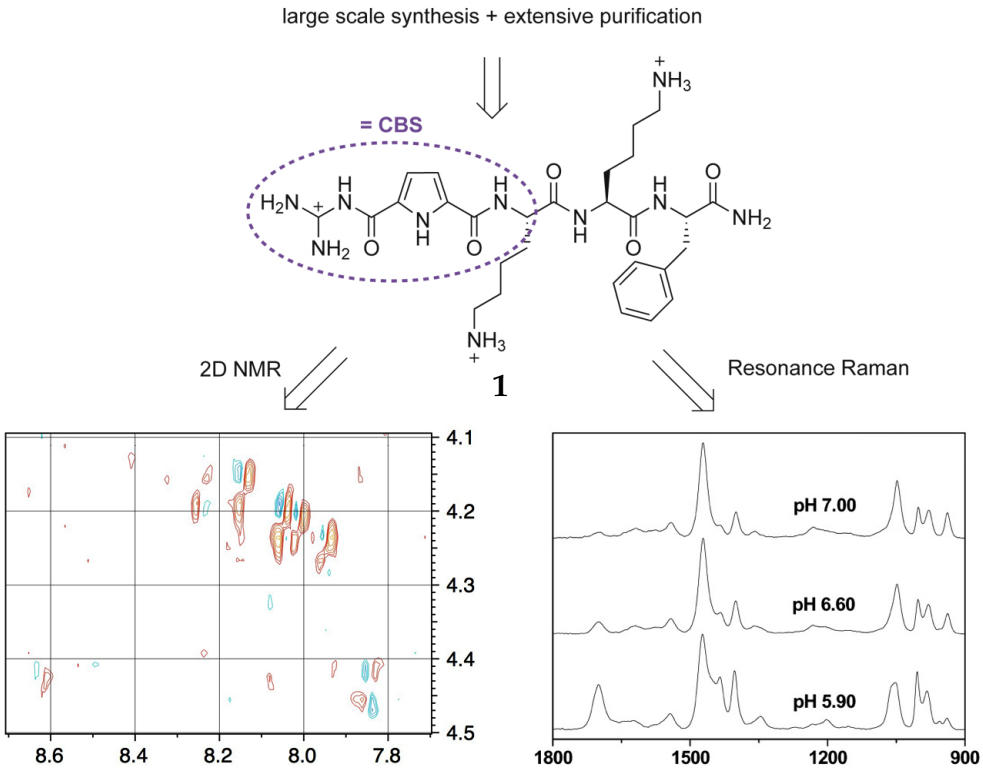

Figure 5.1: *With the help of high resolution 2D NMR and resonance Raman experiments it was possible to obtain important information about the structural properties of* ***1****.*

These results led—in cooperation with the group of *Prof. Sebastian Schlücker*—to the development of a direct and label free spectroscopic detection of immobilized compounds which are often found in combinatorial libraries. This new screening method utilizes the advantages of the surface enhanced Raman spectroscopy and allowed for the first time a surface mapping of a single polystyrene bead for the identification of peptides in femtomolar concentrations. Therefore, compound **1** was successfully synthesized on TentaGel resin and incubated with silver nanoparticles, necessary for the SERS effect. A comparison with the Raman spectrum in solution showed a close match of the signal set (Figure 5.2 on page 141). Hence, this method allows a very fast and sensitive detection of resin bound compounds. The development of this promising new approach set the starting point for future experiments to enable on-bead library screenings and to investigate the complex formation of immobilized compounds.

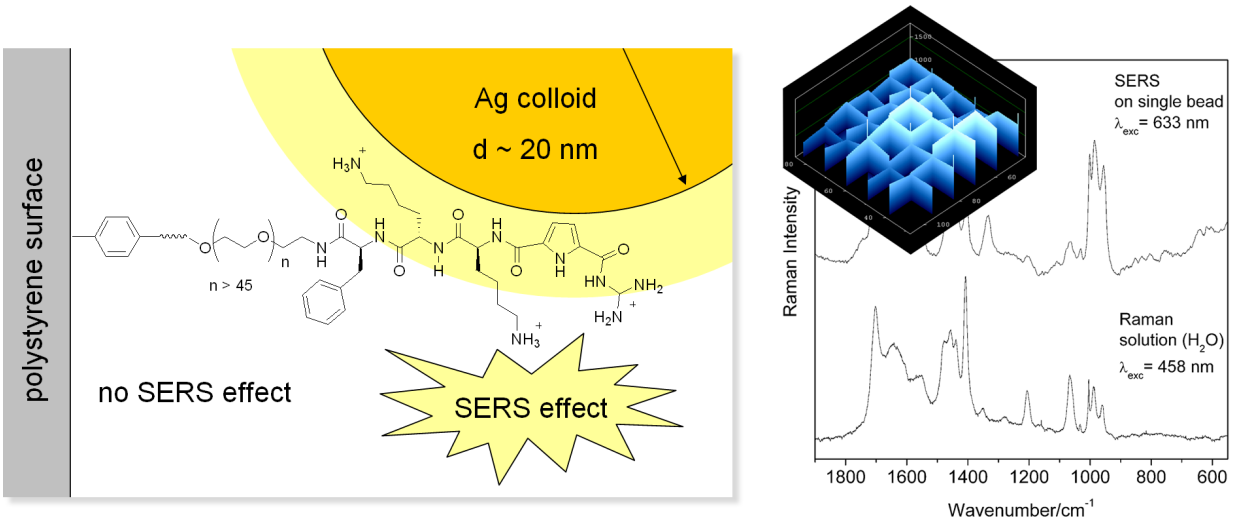

Figure 5.2: *Utilizing the SERS effect it was possible to develop a new surface based screening method for the detection of immobilized compounds (left). The mapping of single resin beads resulted in reproducible Raman spectra, almost identical with experiments in solution (right).*

5.2 Mono and Multivalent Peptides as Efficient Tools for the Recognition of Biological Relevant Structures

After the comprehensive analysis of the basic structural features of the small receptor **1** in the first part of this thesis, the second big block focused on its *in vitro* evaluation using biological relevant targets. Therefore, several different modifications of the initial peptide structure **1** were synthesized. The list of changes featured the dansyl groups for an easy detection, ethylene glycol chains for better solubility and artificial arginine analogs for additional carboxylate binding sites. Tri- and tetrafunctional scaffolds provided extra variation possibilities and allowed the additional investigation of branching and multivalence effects (Figure 5.3 on page 142).

These modifications provided a molecular toolkit for the tailor made synthesis of structures individually designed for the respective target. The first tests addressed the interaction with *Alzheimer's* related amyloid fibrils. It was possible to show that already small and simple peptide receptors like **1** can interact with biomolecules such as amyloid fibrils. A modified ELISA assay demonstrated that it is possible to inhibit the protein-amyloid interactions via the coating of the surface of Aβ-fibrils with IC_{50}-values around 100 mM. During these experiments, the successful SPPS syntheses of tri- and tetravalent

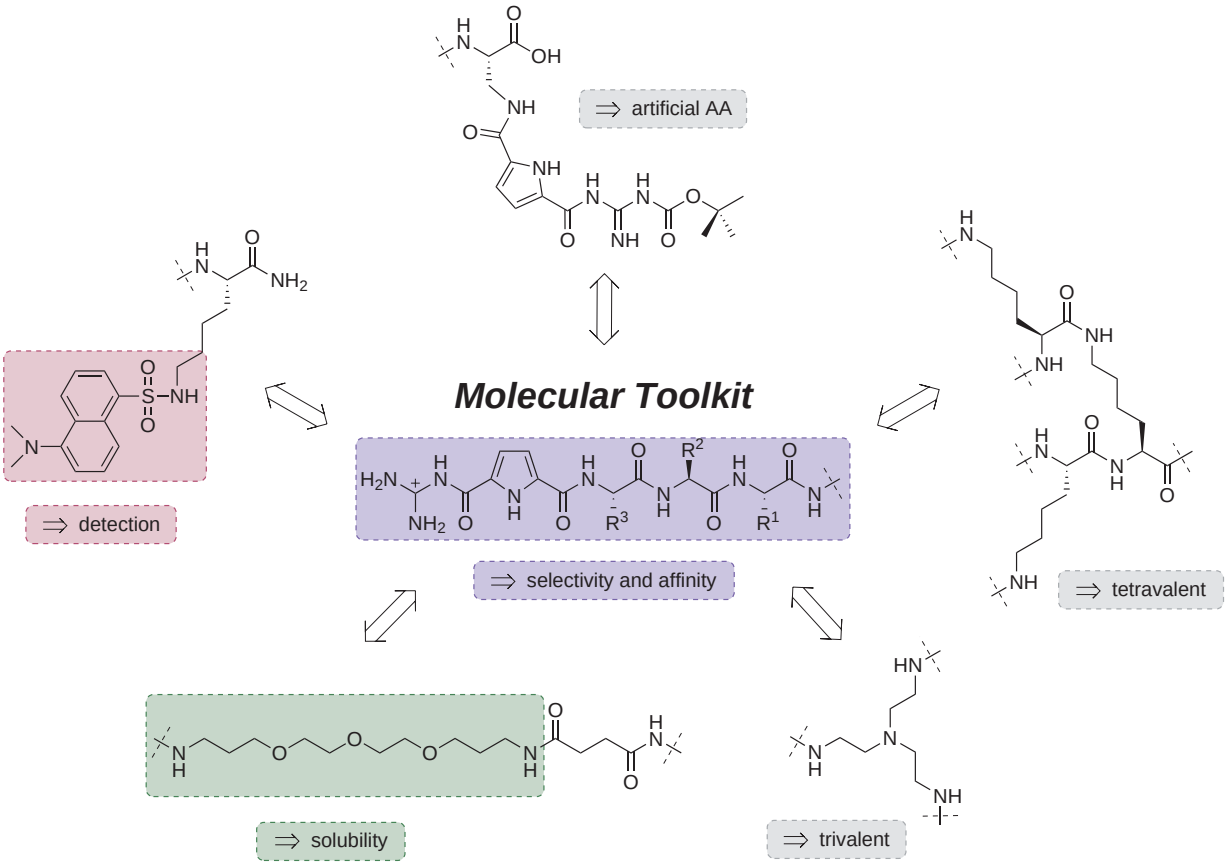

Figure 5.3: *Several modifications of the initial peptide receptor* ***1*** *were synthesized with SPPS techniques and tested for their biological activity.*

systems were achieved. The comparison of the multivalent form with the corresponding monovalent version was then under special investigations. These concentrated mainly on the interaction with various bacteria strains, as well as with different parasites. To localize the compounds within the organisms, the synthesis of fluorescence labelled versions was achieved. Cooperations with two external groups showed for the first time that peptide structures containing the artificial CBS group can specifically interact with biological material. The group of *Prof. Bradley Smith* revealed, for example, some interesting activity trends for the membrane penetration of Gram-positive and -negative bacteria. In the case of *Staphylococcus aureus* an internalization of the peptides **71** and **75** throughout the whole cell was observed at concentrations between 45 and 50 μM, whereas in case of *Escherichia coli* only the membrane was stained (30 – 34 μM). This difference can be explained with the diverging complexity of the cell walls, and is already an indication of a selective interaction with the membrane.

In addition, several compounds were tested by the Institute for Molecular Infection Biology of the University of Würzburg for their antibacterial activity. Depending on the

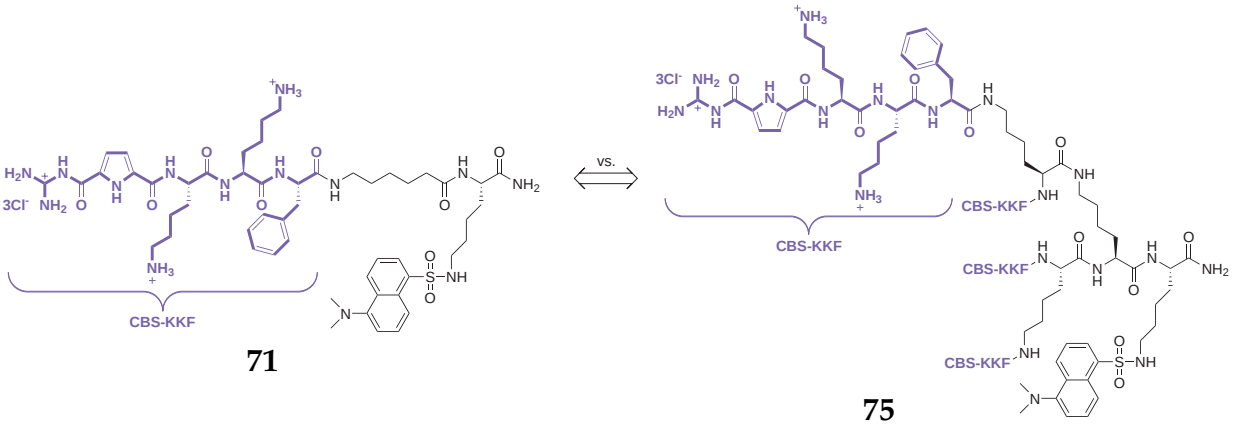

71 **75**

Figure 5.4: *Structural comparison of the monovalent peptide **71** with its multivalent counterpart **75**.*

structure of the peptides, significant differences were observed in direct comparison. For example, the tetravalent peptide **75** (with an MIC of 10 μM against *S. epidermis* bacteria) is eight times more active than the monovalent peptide **71** (80 μM) (Figure 5.4 and Table 5.1). This trend continues with the antiparasitic activity, where IC_{50}-values in the low micromolar range were observed. The beneficial multivalency effect appeared in particular at *Leishmania* parasites, where a disproportionate activity jump from IC_{50} = >100 to 2.4 μM attracted attention.

Table 5.1: *The results of the test on antiparasitic and antibacterial activity revealed a remarkable increase of activity beyond the expected fourfold enhancement.*

Biological Target	**Compound No. 71 CBS-KKF-(Dns)**	**Compound No. 75 $(CBS\text{-}KKF)_4$-(Dns)**
S. epiderm. – MIC [μM]	**80**	**10**
S. epiderm. – Biofilm Inh. in % (μM)	**100 (160)**	**100 (10)**
L. major – IC_{50} [μM]	**>100**	**2.4**
T. brucei brucei – IC_{50} [μM]	**26.1**	**3.7**
Macrophages – IC_{50} [μM]	>100	3

These results were refined with the synthesis of several variations of the multivalent compounds. This thorough evaluation of the biological activity generated precious information about the influence of small structural changes in the peptide receptors. Especially the distinct influence of the multivalency effect and the acquired synthetic skills led to the development of an advanced non-covalent recognition event, as described in the final project of this thesis and summarized in the following section.

5.3 New Surface Based Approach for the Inhibition of β-Tryptase

The last part of this thesis discussed the development of a novel inhibitor for the serine protease β-tryptase based on a tailor-made surface recognition event. It was possible to study and analyze the complex interaction with the unique structure of tryptase, that features a tetrameric frame and four catalytic cleavage sites buried deep inside of the hollow structure. However, the point of attack were not the four binding pockets, as mostly described in the literature, but rather the acidic areas around the cleavage sites and at the two circular openings. These should attract peptides with basic residues, which then can block the accessibility to the active sites. The basic idea for this inhibition of the cleavage activity was simple and compelling, but had to be carefully elaborated. Preliminary tests and calculations revealed that branched tetrameric structures similar to compound **75** are big enough to sterically block the entrance to the central pore. Hence, a combinatorial library of 216 tetravalent peptide compounds was synthesized to find the best structural composition for the non-covalent inhibition of β-tryptase (Figure 5.5).

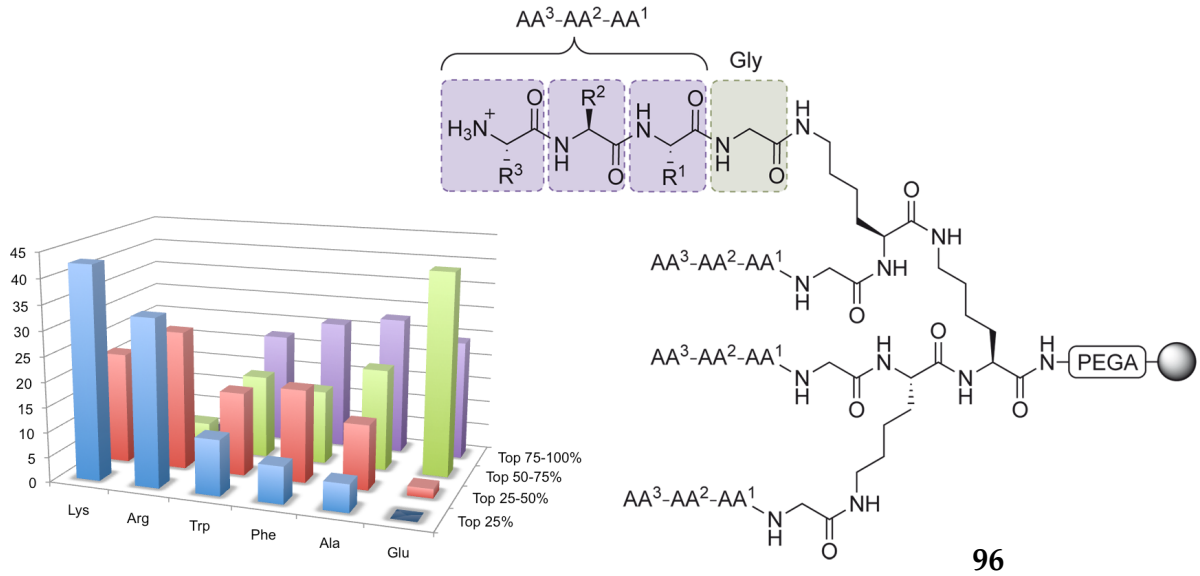

Figure 5.5: *For the search of new inhibitors of the β-tryptase, a synthetic library of 216 compounds was synthesized on PEGA-resin, containing three combinatorial varied positions in each of the four side chains of* ***96****. The screening revealed a total inhibition range between 10 and 95 %, with a distinct trend for the accumulation of basic amino acids in the best inhibitors.*

For the screening of the library (**96**) a new on-bead assay was applied. With this method a simultaneous readout of the total inhibition of *all* library members was possible, thus allowing a fast and direct investigation of the still resin bound inhibitors. This provided the advantage to retrieve structural trends and the comparison of individual K_i-values, beyond the qualitative information normally obtained from the analysis of single beads. The screening revealed, that the presence of basic amino acids (Lys and Arg) in the four side chains of the peptides are indeed essential for a good inhibition. A rather unexpected discovery was the fact, that already the choice of amino acid in the first combinatorial varied position after the lysine scaffold is crucial for the inhibition.

The compound **107** with the peptide sequence Arg-Trp-Lys-Gly in each of the four side chains was identified as the best inhibitor in the on-bead screening with an absolute inhibition of 95 %. A control screening in solution confirmed this result with a K_i of 0.17 μM, the highest dissociation constant measured of any compound within this thesis and also in the range of literature known inhibitors. But it is even more interesting, that in direct comparison with the monovalent analog, this inhibitor shows an exceptional 1800-fold increase of activity, which clearly supports the proposed novel mode of inhibition. This was further substantiated with tests, which demonstrated a high selectivity against other serine proteases such as trypsin or chymotrypsin in the range of >6000.

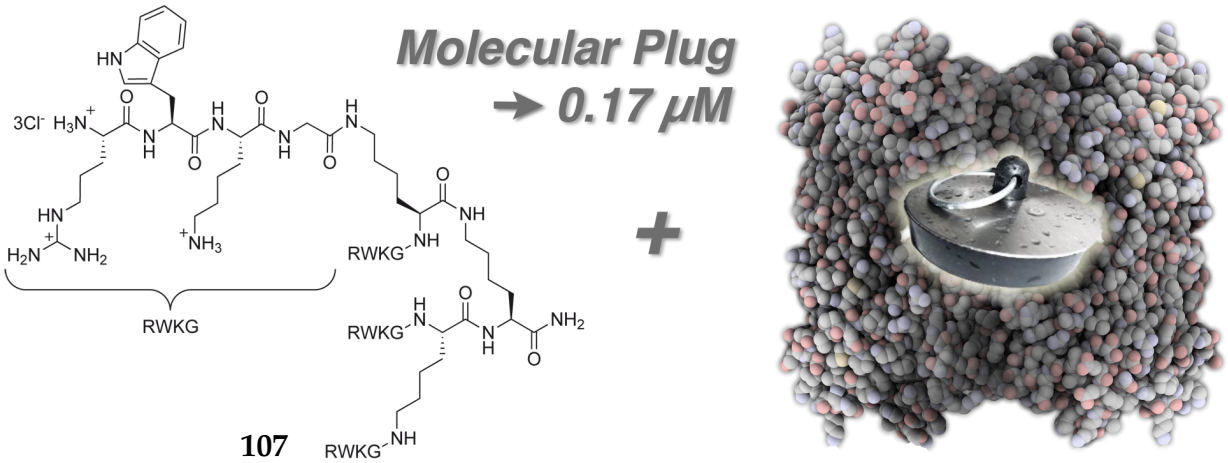

Figure 5.6: *The multivalent peptide **107** was identified as the best inhibitor of the screening (K_i = 0.17 µM). All experiments lead to the conclusion that it blocks the active sites of β-tryptase like a molecular plug and therefore inhibits the enzyme activity.*

Several additional experiments in solution unveiled the kinetics of the inhibition process. In conclusion, both mono- and multivalent inhibitors interact in a non-destructive

and reversible way with the tryptase. This was shown in dialysis experiments and heparin additions, which re-initiated the enzyme activity. A closer look at the mode of inhibition confirmed that the small monovalent compounds are competitive inhibitors, whereas the multivalent peptides feature a non-competitive inhibition process. As a result, both peptides differ in their area of interaction with tryptase. The small peptides bind to the catalytic pockets and are in competition with the substrate, whereas the sterically demanding multivalent peptides bind in a different area and might not be able to enter the central pore.

Finally, computational calculations provided a possible visualization of the plug-like interaction. The positive charged amino acids of the inhibitor **107** bind tightly to the protein surface and are able to saturate all aspartic and glutamic acids around the circular opening. Therefore, the star-like cover blocks the access of possible substrates to the inner binding pockets.

5.4 Conclusion

During this thesis significant progress in the design, synthesis and analysis of novel artificial peptide receptors was made. Starting with the supramolecular recognition of biological relevant peptide sequences and the analysis of the underlying non-covalent interactions with various state-of-the-art methods, it was possible to develop a completely new technique for the screening of combinatorial libraries based on Raman spectroscopy. This method has a clear potential for a practical application in the pharmaceutical and biotechnological industry. Using the profound knowledge in the molecular recognition of peptides by artificial hosts, gained from smaller models, eventually also the development of an innovative method for the supramolecular recognition and inhibition of enzymes was achieved.

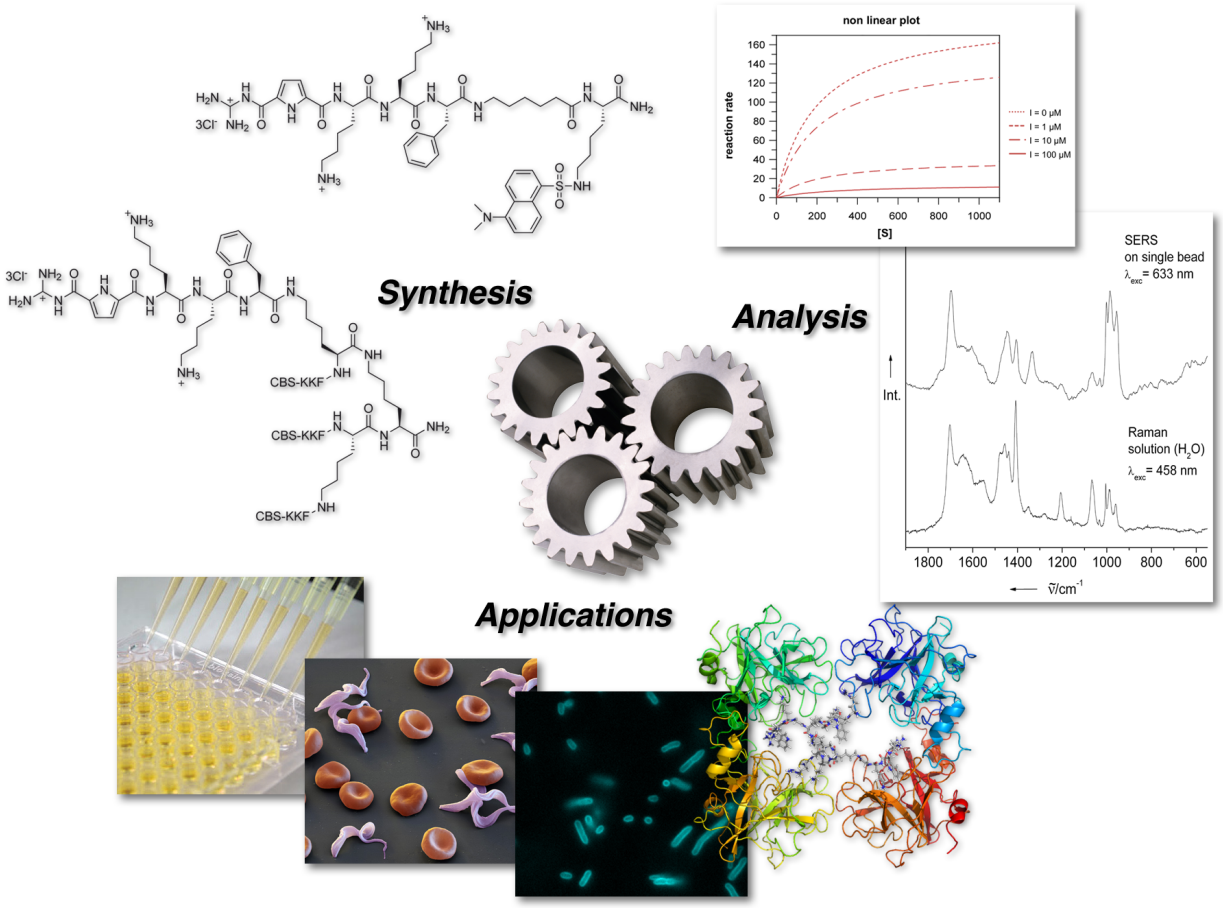

Figure 5.7: *The results of this thesis are based on the successful combination of different synthetical and analytical methods, eventually leading to interesting applications and offering an impulse for further investigations.*

In conclusion, this project represents an important contribution to the fundamental understanding of molecular recognition and offers a deeper insight in this still very challenging research area at the interface between chemistry, physics and biology. Hence, the combination of organic synthesis, modern analytical methods and innovative applications offers a starting point for the development of possible new lead structures for future drugs.

CHAPTER 6

ZUSAMMENFASSUNG

Der Hauptfokus dieser Arbeit lag in der Synthese und Analyse multifunktionaler Oligopeptide. Die Untersuchung ihrer nicht-kovalenten Wechselwirkungen mit verschiedenen Strukturen resultierte sowohl in interessanten methodischen als auch anwendungsbezogenen Fortschritten. Die folgende Übersicht fasst die wichtigsten Entdeckungen zusammen.

6.1 Einblicke in die Bindungseigenschaften kleiner Peptidsequenzen

Das erste Projekt dieser Dissertation konzentrierte sich auf die detaillierte Analyse des Peptid-Rezeptors CBS-Lys-Lys-Phe-NH_2 (**1**), um ein besseres Verständnis seines Bindungsverhaltens während einer Substratkomplexierung zu erhalten. Insbesondere die hochsensitiven spektroskopischen Methoden erforderten dabei eine hohe Reinheit von **1**. Dies resultierte in einer Optimierung der Syntheseschritte für eine Darstellung in großem Maßstab, sowie einem gründlichen Reinigungsprozess um die notwendigen Anforderungen zu erfüllen. In diesem Zusammenhang gelang es in Kooperation mit dem Institut für Physikalische Chemie der Universität Würzburg hochaufgelöste 2D NMR Spektren einer Komplexmischung in DMSO zu erhalten. Hierbei konnte gezeigt werden, dass zumindest in DMSO eine β-faltblattartige Struktur bevorzugt wird, bei der

die CBS-Gruppe in einer für sie stabileren out-out Kornformation vorliegt. Die Strukturaufklärung wurde mit Hilfe von Resonanz-Raman Experimenten in Wasser ausgeweitet. Dazu bediente man sich charakteristischer Absorptionsbanden, die eine selektive Betrachtung der CBS-Einheit ermöglichten, sowie eine Untersuchung der Wechselwirkung mit den Carboxylatgruppen des Tetrapeptids N-Ac-D-Glu-D-Glu-D-Glu-D-Glu-OH zuließen. Mit dieser Methode gelang eine pH-Wert abhängige Analyse von **1** und damit eine detaillierte Beschreibung der strukturellen Veränderung während des Vorgangs der Komplexierung. Mit diesen Test konnten die Vorteile gegenüber UV und Fluoreszenz Experimenten verdeutlicht werden.

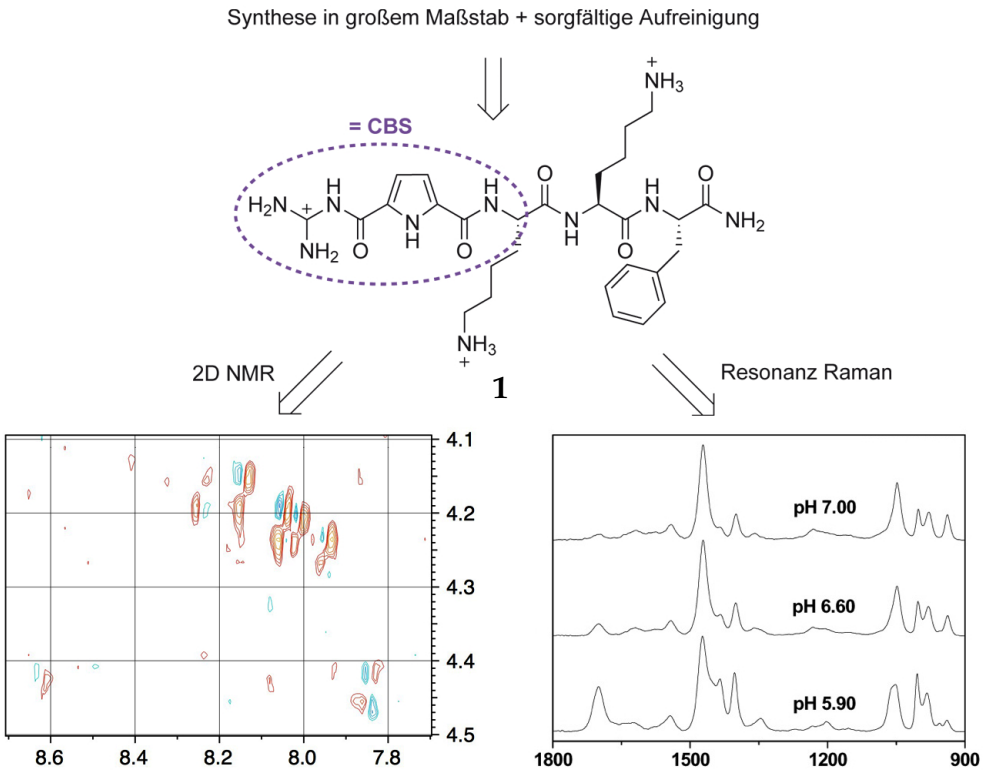

Abbildung 6.1: *Mit der Hilfe von hochauflösenden NMR- und Raman-Experimenten gelang es wichtige Informationen über die strukturellen Eigenschaften von* ***1*** *zu erhalten.*

Diese Ergebnisse führten, in Kooperation mit der Gruppe von *Prof. Sebastian Schlücker*, zur Entwicklung einer direkten und markierungsfreien spektroskopischen Methode zur Detektion festphasengebundener Substanzen, wie man sie z.B. oft in kombinatorischen Molekülbibliotheken findet. Diese neuartige Screeningmethode bedient sich der Vorteile der Oberflächen-verstärkten Raman-Streuung (SERS) und ermöglichte erstmals das Scannen der Oberfläche eines einzelnen Harz-Kügelchens und damit die Identifizie-

rung von Peptiden in femtomolaren Konzentrationen. Dazu wurde die Verbindung **1** erfolgreich auf TentaGel synthetisiert und mit kolloidalen Silbernanopartikeln inkubiert, um einen SERS Effekt zu erhalten. Ein qualitativer Vergleich mit dem konventionellen Raman-Spektrum einer Lösung von **1** bestätigte eine eindeutige Übereinstimmung der Signalbereiche (Abbildung 6.2).

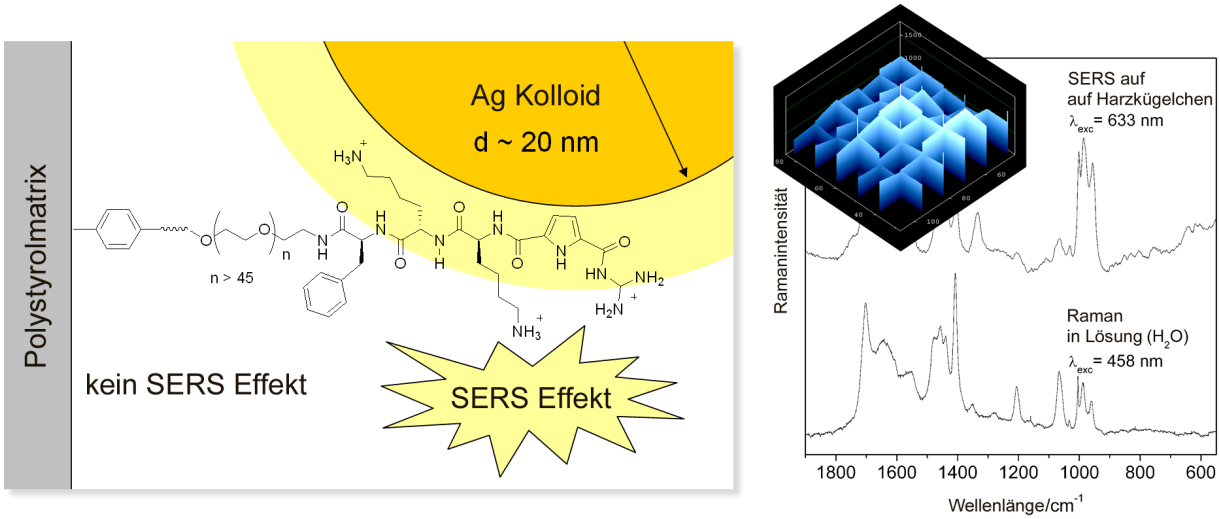

Abbildung 6.2: *Mit Hilfe der SERS Technik gelang es eine neue Oberflächen-basierte Screening Methode für Harz-gebundene Substanzen zu entwickeln (links). Das Scannen einzelner Harz-Kügelchen resultierte in reproduzierbaren Raman-Spektren die eine hohe Ähnlichkeit mit Experimenten in Lösung aufweisen (rechts).*

Zusammenfassend erlaubt diese neue Methode eine schnelle und hoch sensitive Detektion harzgebundener Substanzen. Die Entwicklung dieses viel versprechenden Ansatzes bildet die Basis möglicher zukünftiger Entwicklungen für das direkte und schnelle Screening von kombinatorischen Bibliotheken sowie für die detaillierte Untersuchung der Komplexbildung von immobilisierten Verbindungen.

6.2 Mono- und Multivalente Peptide als effiziente Werkzeuge zur Erkennung biologisch relevanter Strukturen

Nach der ausführlichen Analyse der grundlegenden strukturellen Eigenschaften des Rezeptors **1** im ersten Teil dieser Dissertation schloss sich im zweiten großen Block dessen *in vitro* Evaluierung mit Hilfe verschiedener biologisch relevanter Zielstrukturen an. Dazu wurden einige strukturell verwandte Versionen des ursprünglichen Rezeptors **1** synthetisiert. Zu den Modifikationen zählte die Einführung eines Dansyl-Labels zur einfachen Detektion, bzw. Ethylenglykolketten für eine besser Löslichkeit sowie künstliche Argininanaloga für zusätzliche Carboxylatbindungstellen. Mit Hilfe von tri- und tetravalenten Templaten konnten darüber hinaus weitere Molekülvariationen synthetisiert werden, um eventuelle multivalente Effekte zu untersuchen (Abbildung 6.3).

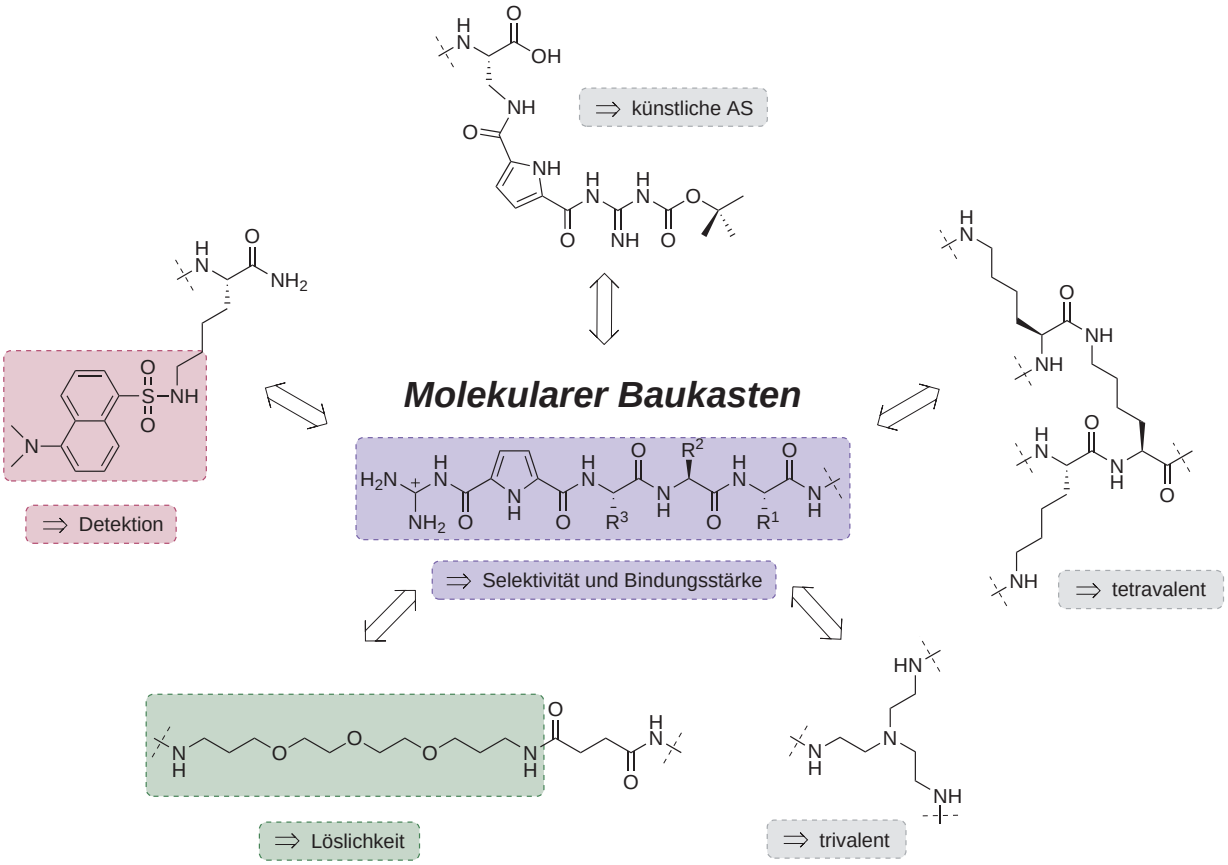

Abbildung 6.3: *Mit Hilfe von SPPS Techniken wurden verschiedene Modifikationen des ursprünglichen Rezeptor-Designs (**1**) synthetisiert und auf ihre biologische Aktivität hin untersucht.*

Dies ermöglichte die Zusammenstellung eines variablen molekularen Baukasten zur zielgerichteten Synthese von Strukturen, die individuell für ausgesuchte Ziele entworfen werden konnten. Die ersten Tests betrachteten die Wechselwirkung mit Amyloid-Fibrillen, die im Zusammenhang mit der Alzheimer-Krankheit stehen. Es konnte gezeigt werden, dass bereits kleine und einfache Peptidrezeptoren wie **1** mit biologischen Strukturen wie den Fibrillen interagieren können. Mit einem modifizierten ELISA Assay konnte hierbei gezeigt werden, dass es möglich ist Wechselwirkungen zwischen Proteinen und Amyloidstrukturen zu inhibieren. Das Bedecken der Fibrillen-Oberfläche mit **1** resultierte in IC_{50}-Werten um die 100 mM. Während dieser Arbeiten wurden erste tri- und tetravalente Rezeptorsysteme mit Hilfe der Festphasenchemie synthetisiert. In diesem Zusammenhang war insbesondere der Vergleich der multivalenten Systemen mit den entsprechenden monovalenten Peptiden von Interesse. Die Untersuchungen konzentrierten sich hauptsächlich auf die Interaktion mit verschiedenen Bakterienarten, sowie unterschiedlichen Parasiten. Um die Verbindungen in den Organismen zu lokalisieren wurden spezielle Fluoreszenz-markierte Versionen der Peptide synthetisiert. In Kooperation mit zwei externen Gruppen konnte erstmals gezeigt werden, dass Peptide mit künstlichen Argininanaloga spezifisch mit biologischem Material wechselwirken können. Die Gruppe um *Prof. Bradley Smith* konnte zum Beispiel interessante Aktivitätstrends in Bezug auf die Membrangängigkeit bei Gram-positiven sowie -negativen Bakterien feststellen. Im Falle von *Staphylococcus aureus* konnte für die Peptide **71** und **75** in einem Konzentrationsbereich von 45 bis 50 μM eine Aufnahme in Zellen beobachtet werden, wohingegen bei *Escherichia coli* Bakterien nur die Zellwand angefärbt werden konnte (30 – 34 μM). Diese Unterschiede können mit der abweichenden Komplexität der Zellwände erklärt werden und sind bereits ein deutlichen Zeichen, dass eine selektive Interaktion mit den Membranen möglich ist.

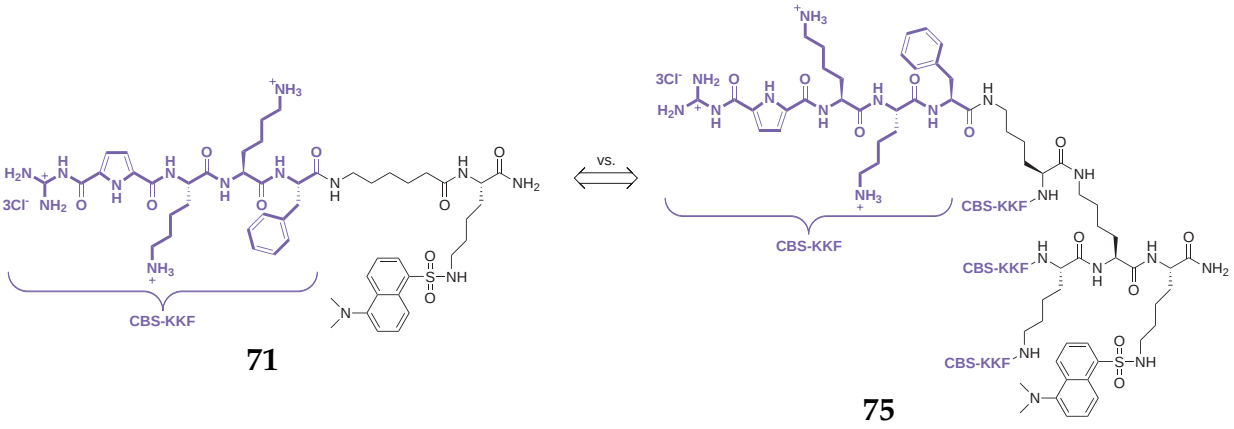

71 **75**

Abbildung 6.4: *Struktureller Vergleich zwischen dem monovalenten Peptid **71** und dem multivalenten Äquivalent **75**.*

Zusätzlich wurden einige Verbindung vom Institut für Molekulare Infektionsbiologie der Universität Würzburg auf ihre antibakterielle Aktivität untersucht. Hierbei konnten im direkten Vergleich abhängig von der Peptidstruktur signifikante Unterschiede festgestellt werden. So weist zum Beispiel das tetravalente Peptid **75** (mit einer MHK von 10 μM bei *S. epidermis* Bakterien) eine achtfach höhere Aktivität auf, als das monovalente Peptid **75** (MHK = 80 μM) (Abbildung 6.4 und Tabelle 6.1). Dieser Trend setzt sich bei der antiparasitären Aktivität mit IC_{50}-Werten im niedrigen mikromolaren Bereich fort. Die Vorteile des multivalenten Effektes treten insbesondere bei *Leishmania* Parasiten auf. Hier konnte ein überproportionaler Aktivitätssprung des IC_{50}-Wertes von >100 auf 2.4 μM beobachtet werden.

Tabelle 6.1: *Die Resultate der antibakteriellen sowie antiparasitären Untersuchungen weisen eine bemerkenswerte Zunahme jenseits der erwarteten vierfachen Aktivitätssteigerung auf.*

Biologisches Zielobjekt	**Substanz-Nr. 71 CBS-KKF-(Dns)**	**Substanz-Nr. 75 $(CBS\text{-}KKF)_4$-(Dns)**
S. epiderm. – MHK [μM]	**80**	**10**
S. epiderm. – Biofilm Inh. in % (μM)	**100 (160)**	**100 (10)**
L. major – IC_{50} [μM]	**>100**	**2.4**
T. brucei brucei – IC_{50} [μM]	**26.1**	**3.7**
Makrophagen – IC_{50} [μM]	>100	3

Durch die Synthese weiter Variationen der multivalenter Verbindungen konnten die Ergebnisse tiefergehend untersucht werden. Mit dieser detaillierten Evaluierung der biologischen Aktivität konnten somit wertvolle Informationen über den Einfluss kleiner struktureller Änderungen in den Peptidrezeptoren gewonnen werden. Insbesondere der ausgeprägte Einfluss des multivalenten Effektes und die angeeigneten synthetischen Fertigkeiten führten zur Entwicklung und Untersuchung eines komplexeren Bindungsereignisses. Im abschließenden Projekt dieser Dissertation wurde dazu der spezielle Fall einer Proteinoberflächenerkennung beschrieben. Dieser neue Ansatz der Enzymhemmung wird im folgenden Abschnitt zusammengefasst.

6.3 Entwicklung eines neuen Oberflächen-basierten Ansatzes zur Inhibierung von β-Tryptase

Der letzte Abschnitt dieser Dissertation beschreibt die Entwicklung eines neues Inhibitors der Serinprotease β-Tryptase, welche eine tetramere Struktur aufweist, in der die vier aktiven Zentren sich im Inneren eines zentralen Hohlraumes befinden. In diesem Zusammenhang gelang es die zur Inhibierung notwendige Komplexbildung, die auf einem speziell zugeschnittenen Oberflächenerkennungsprozess basiert, zu studieren und analysieren. Die Angriffspunkte waren jedoch nicht die üblicherweise in der Literatur beschriebenen aktiven Zentren, sondern Anhäufungen negativ geladener Aminosäure-Reste, die in der Umgebung der aktiven Zentren sowie in den beiden Eingangsbereichen zum zentralen Hohlraum zu finden sind. Diese sollten in der Lage sein positiv geladene Aminosäurereste anzuziehen und dazu führen, dass ein entsprechend voluminöses Peptid die Zugänglichkeit zu den aktiven Zentren einschränkt. Die grundlegende Idee dieser Inhibierungsmethode, so einfach und zugleich attraktiv sie erschien, bedurfte einer sorgfältigen Ausarbeitung. Durch Vortests und Berechnungen konnte bereits bestätigt werden, dass verzweigte tetramere Strukturen wie das Peptid **75** groß genug sind, um den Eingang zur zentralen Pore sterisch zu verschließen. Daraufhin wurde eine kombinatorische Bibliothek (**96**) bestehend aus 216 Verbindungen synthetisiert (Abbildung 6.5). Es war das Ziel, die beste strukturelle Zusammensetzung zu finden, die eine effiziente nicht-kovalente Inhibierung der Tryptase ermöglicht.

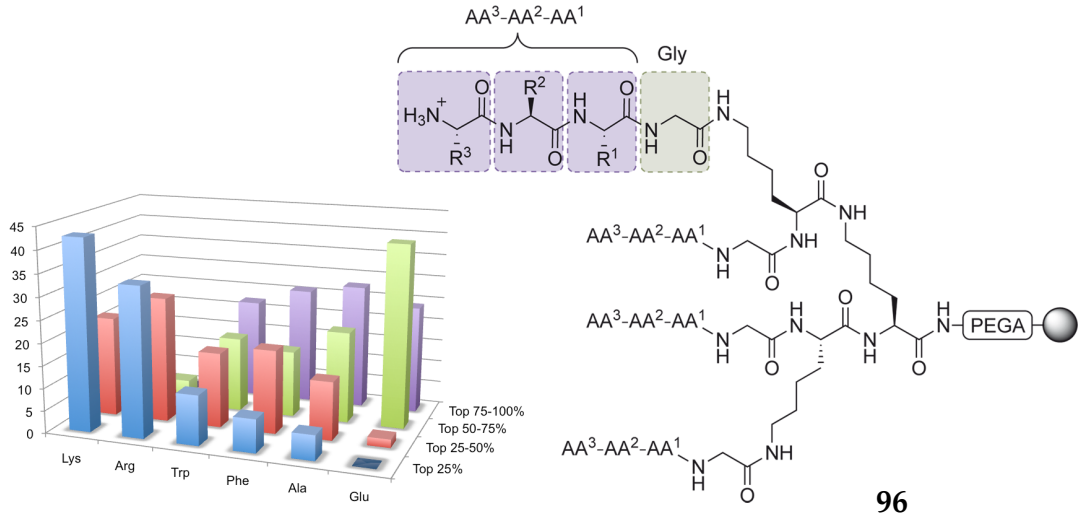

Abbildung 6.5: *Auf der Suche nach neuen Inhibitoren der β-Tryptase wurde eine 216 Mitglieder umfassende Bibliothek synthetisiert. Jeweils drei Positionen in jedem der vier Seitenarme von **96** wurde dabei kombinatorisch variiert. Das Screening ermittelte Hemmwerte im Bereich zwischen 10 und 95 % mit einer deutlichen Häufung von basischen Aminosäuren in den besten Inhibitoren.*

Für das Screening der Bibliothek (**96**) wurde ein neuartiger "on-bead" Assay angewendet. Mit Hilfe dieser Methode war ein simultanes Auslesen der absoluten Hemmwerte *aller* Bibliotheksmitglieder möglich, was somit eine schnelle und direkte Untersuchung der noch Harz-gebundenen Inhibitoren erlaubte. Dies hatte zum Vorteil, dass neben dem Aufdecken von Strukturtrends ebenso ein Vergleich aller K_i-Werte möglich war. Somit konnten weit mehr Informationen erhalten werden, als die rein qualitativen Daten aus standardmäßigen OBOC-Enzymassays. Das Screening zeigte, dass basische Aminosäuren (Lys und Arg) in den vier Seitenarmen in der Tat zu den wichtigsten Komponenten für eine gute Inhibierung gehören. Ein eher unerwartetes Ergebnis war die Entdeckung, dass bereits die Wahl der Aminosäure in der ersten kombinatorisch variierten Position nach dem Lysingerüst entscheidend ist für eine effiziente Hemmung.

Als bester Inhibitor wurde die Verbindung **107** identifiziert, die in jedem der vier Arme die Peptidsequenz Arg-Trp-Lys-Gly trägt und einen absoluten Hemmwert von 95 % aufweist. Ein Kontrollscreening in Lösung bestätigte dieses Ergebnis mit einem sehr guten K_i-Wert von 0.17 μM. Dies stellte die höchste gemessene Dissoziationskonstante im Zuge dieser Doktorarbeit dar und befindet sich im Bereich guter literaturbekannter Inhibitoren. Besonders interessant ist darüber hinaus der direkte Vergleich mit der monovalenten Vergleichssubstanz. Hier zeigt die multivalente Verbindung einen außerordentlichen 1800-facher Aktivitätssprung auf, was eindeutig für den vorgeschlagenen verschlussartigen Hemmmechanismus spricht. In zusätzlichen Tests konnte ferner eine hohe Selektivität gegenüber weiteren Serinproteasen wie z.B. Trypsin und Chymotrypsin im Bereich von >6000 festgestellt werden.

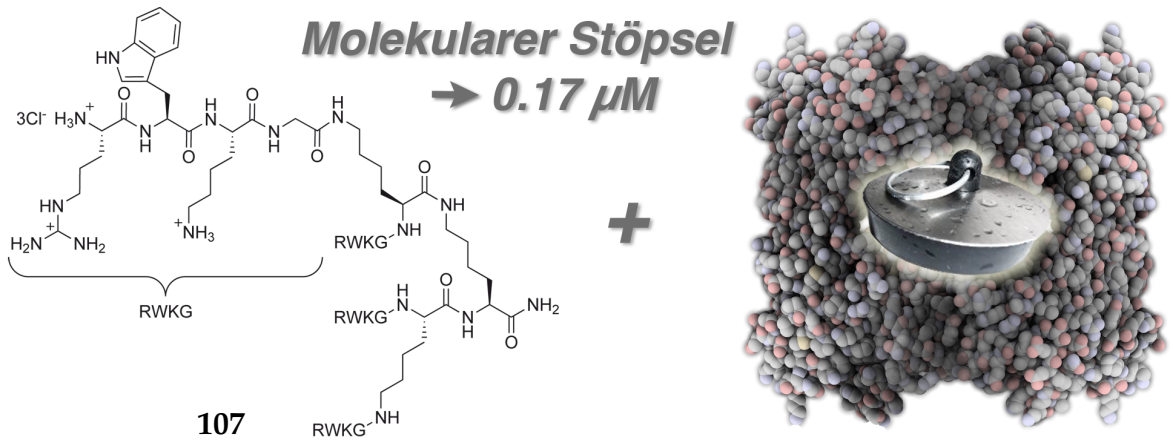

Abbildung 6.6: *Das multivalente Peptid **107** wurde als bester Inhibitor im Screening identifiziert (K_i = 0.17 μM). Alle Experimente führten zur Schlussfolgerung, dass die aktiven Zentren der β-Tryptase durch einen molekularen Stöpsel blockiert werden und somit die Enzymaktivität gehemmt wird.*

Verschiedene zusätzliche Experimente in Lösung halfen bei der Aufklärung der kinetischen Beschreibung des Hemmprozesses. Zusammenfassend lässt sich die Wechselwirkung zwischen der Tryptase und den sowohl mono- als auch multivalenten Inhibitoren als nicht-destruktiv und gleichzeitig reversibel beschreiben. Die monovalenten Peptide agieren dabei als kompetitive Inhibitoren, während die multivalenten Substanzen einen nicht-kompetitiven Hemmmechanismus aufweisen. Somit unterscheiden sich die Angriffspunkte beider Inhibitortypen in ihrer Wechselwirkung mit der Tryptase. Während die kleinen Peptide in den aktiven Zentren der Tryptase binden und somit in direkter Konkurrenz mit spaltbaren Substraten stehen, binden die sterisch anspruchsvolleren multivalenten Peptide an einem anderen Ort der Enzymoberfläche und sollten nicht in den zentralen Hohlraum eindringen können.

Abschließend konnte mit der Hilfe von Computermodellen eine mögliche verschlussartiger Wechselwirkung graphisch dargestellt werden. Die positive geladenen Aminosäuren des Inhibitors **107** binden fest an die Proteinoberfläche und sättigen alle Asparagin- sowie Glutaminsäuren die sich am Eingang zur zentralen Pore befinden. Dadurch blockt die sternartige Abdeckung den Zugang möglicher Substrate zu den inneren Bindungstaschen.

6.4 Fazit

Im Zuge dieser Doktorarbeit konnten signifikante Fortschritte im Design, der Synthese und der Analyse neuartiger künstlicher Peptidrezeptoren gemacht werden. Angefangen mit der supramolekularen Erkennung biologisch relevanter Peptidsequenzen und der Analyse der zu Grunde liegenden nicht-kovalenten Wechselwirkungen mit verschiedenen modernen Methoden, war es zusätzlich möglich ein komplett neues Screeningverfahren für kombinatorische Molekülbibliotheken basierend auf der Raman Spektroskopie zu entwickeln. Diese Methode hat ein klares Potential für eine Anwendung in der pharmazeutischen oder biotechnischen Industrie. Durch die Studie kleiner Modellsysteme gelang es wichtige Informationen über die Komplexierungsverhalten von Peptiden mit künstlichen Rezeptoren zu erhalten, die dann abschließend zur erfolgreichen Entwicklung einer innovativen Methode zur supramolekularen Erkennung und Inhibierung von Enzymen führte.

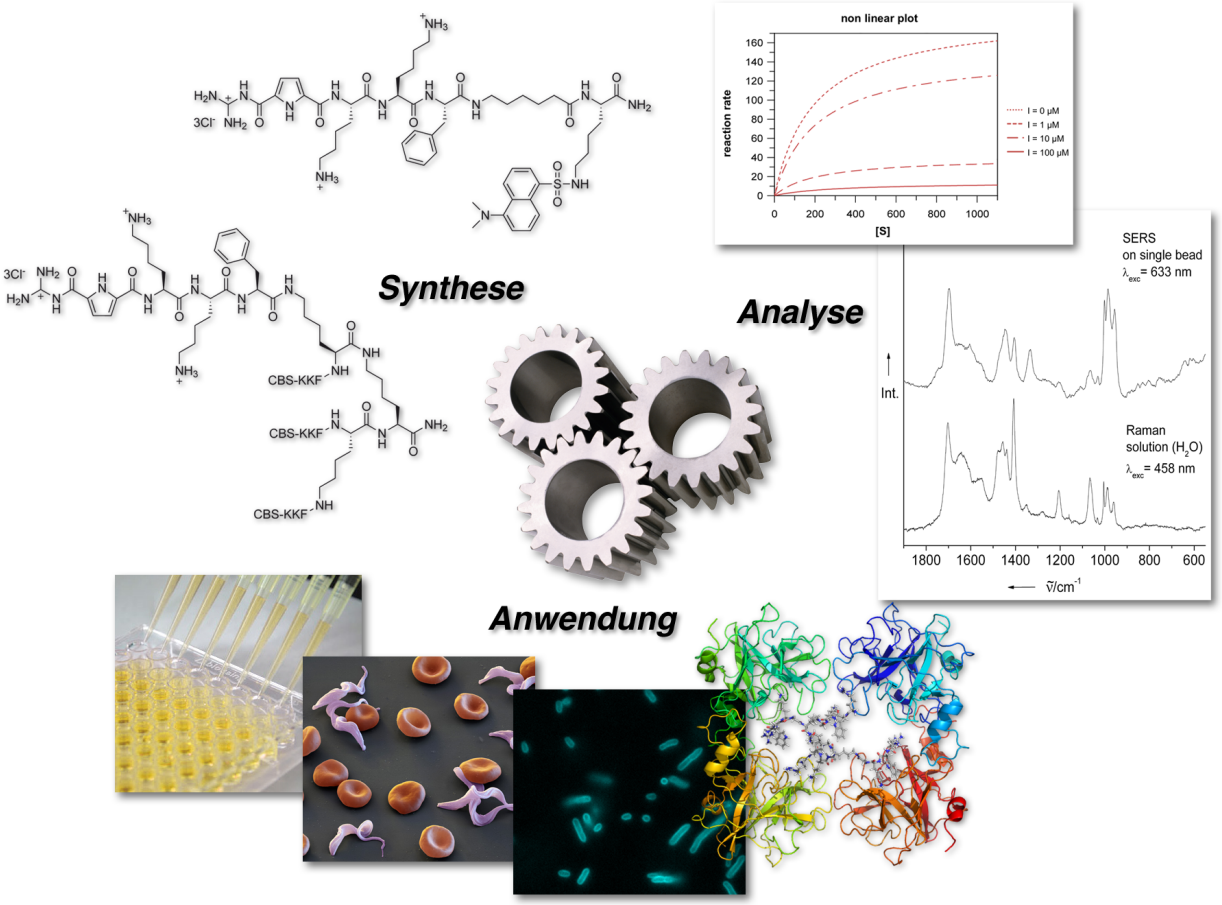

Abbildung 6.7: *Die Ergebnisse dieser Doktorarbeit basieren auf der erfolgreichen Kombination verschiedener synthetischer und analytischer Methoden. Dies führte schließlich zu interessanten Anwendungen und setzte den Impuls für weitergehende Untersuchungen.*

Zusammenfassend repräsentiert diese Forschungsarbeit einen wichtigen Beitrag für das grundlegende Verständnis der molekularen Erkennung und ermöglicht einen tiefen Einblick in dieses immer noch sehr herausfordernde Forschungsgebiet im Grenzbereich zwischen Chemie, Physik und Biologie. Die Kombination von organischer Synthese, modernen analytischen Methoden und innovativen Anwendungen stellt den perfekten Ausgangspunkt für die Entwicklung möglicher neuer Leitstrukturen zukünftiger Medikamente dar.

CHAPTER 7

EXPERIMENTAL SECTION

7.1 General Experimental and Analytical Methods

Solvents and chemicals

All solvents were dried according to literature procedures.[300] Dichloromethane and *N*,*N*-dimethyl formamide were dried by distillation from calcium hydride. Diethyl ether and tetrahydrofuran were distilled from sodium with benzophenone as indicator. Methanol was distilled from magnesium. Water for chromatographic and spectroscopic measurements was purified with a *TKA* MicroPure ultrapure water system. All other commercial reagents were purchased and used as received unless otherwise specified.

Rotary evaporation

Equipment: *Heidolph* VV2000 rotavapor and *Heidolph* WB 2000 water bath

Concentration under reduced pressure was performed by rotary evaporation at 40°C at the appropriate pressure for the solvent used.

Inert gas

Reactions with humidity-sensitive compounds were carried out under technical argon (99.998 %, purchased from *Linde*), which was dried with blue gel and calcium chloride.

Vacuum pumps

Equipment: *Vacuubrand* Diaphragm vacuum pump MZ C2
Vacuubrand Sliding vane rotary vacuum pump RD 8

Orbital shaker for peptide synthesis

Equipment: *IKA* KS 130 and KS 260 basic orbital shaker

Combinatorial synthesis of peptide library

Equipment: *Nexus Biosystems* IRORI AccuTag-100 System

The synthesis of the combinatorial inhibitor library was performed with the help of the AccuTag-100 Combinatorial Chemistry System. All compounds were synthesized in MikroKans^{TM} and equipped with radiofrequency tags. A scanning station is used during the sorting and identification of the spatially separated library members.

Lyophilization

Equipment: *Christ* Alpha 1–4 LD plus freeze dryer

All lyophilizations were performed from salt-free or ultrapure water. If necessary, the substances were dissolved in a few milliliters of methanol.

Melting point

Equipment: *Büchi* SMP-20 apparatus, according to Dr. Tottoli

All melting points were measured with open end glass capillary tubes and are not corrected.

pH measurement

Equipment: *Knick* pH-Meter 766 Calimatic

The pH-meter was calibrated with commercial available buffer standards (pH = 4.00 and pH = 7.00).

Thin layer chromatography

Equipment: *Benda* Nu-4 KL UV lamp (wavelengths: 254 nm, 366 nm)

Material: *Merck* TLC aluminium sheets, silica gel 60 F_{256} (20×20 cm plates)
Macherey-Nagel AluGRAM RP-18 W/UV_{254}

Reactions were monitored by TLC on silica gel precoated plates. Visualization of the spots was carried out by fluorescence quenching with 254 nm UV light or with the help of an acidic ninhydrin solution in ethanol (for detection of amines). The TLC elution mixtures are reported in volume percent (v/v) except otherwise stated.

Flash chromatography

Equipment: *Acros Organics* silica gel for chromatography, 0.035–0.070, 60 Å
MP Biomedicals Company, MP Silica 32–63, 60 Å

Flash chromatography was performed on silica gel with the indicated solvent mixtures on columns of different diameter and length. Solvent mixtures used for flash chromatography are reported in volume percent. Yields refer to chromatographically purified and spectroscopical pure compounds, unless otherwise stated.

Preparative "Medium Performance Liquid Chromatography" (MPLC)

Equipment: *Teledyne Isco, Inc.* CombiFlash Companion

Column: *RediSep* C-18 reversed phase (4–40g column size)

All eluents were distilled prior use. Solvent mixtures used for liquid chromatography are reported in volume percent.

Analytical "High Performance Liquid Chromatography" (HPLC)

Equipment: *Dionex* HPLC system: P680 pump, ASI-100 automated sample injector, UVD-340U UV detector

Column: *Supelcosil* LC-18 Reversed Phase, 250 mm × 4.6 mm, 5 μm
Supelcosil LC-8 Reversed Phase, 250 mm × 4.6 mm, 5 μm)
Varian Dynamax Microsorb C18, 250 mm × 21.4 mm, 60 Å, 8 μm

All eluents used for liquid chromatography were commercial available and in "HPLC - Gradient Grade" quality. Solvent mixtures are reported in volume percent.

Nuclear Magnetic Resonance (NMR)

Equipment: *Bruker* Avance 400 (^{1}H: 400 MHz; ^{13}C: 100 MHz)
Bruker DMX 600 (^{1}H: 600 MHz; ^{13}C: 150 MHz)

For standard analytical purpose ^{1}H-NMR spectra were recorded at 400 MHz and ^{13}C-NMR spectra at 100 MHz. All measurements were performed at room temperature, using DMSO-d_6 or $CDCl_3$ as solvents. The chemical shifts were measured against the solvent signal and are reported in ppm from TMS (δ scale). The coupling constants are given in Hertz. The following abbreviations for the description of the fine structure were used: s = singlet, bs = broad singlet, d = doublet, t = triplet, q = quartet, m = multiplet, br = broad signal. All assignments have been performed according to literature.[301]

Mass Spectrometry (MS)

Equipment: High resolution ESI: *Bruker Daltonik* MicroTOF focus
MALDI-TOF: *Bruker Daltonik* AutoflexTOF II LRF 50
EI and FAB: *Finnigan* Mat 900 S

Fourier Transform Infrared Spectroscopy (FT-IR)

Equipment: *Jasco* FT-IR 410 spectrophotometer

The compounds were measured either as KBr pellet or in pure form with the *JASCO* ATR-500M unit. The maxima are classified in four intensities: s (strong), m (middle), w (weak), br (broad) and are reported in [cm^{-1}].

Computational Calculations

Software: *Schrödinger* MacroModel Vers. 9.6
Software: *Schrödinger* Maestro

The unoptimized structure of the multivalent inhibitor **106** was drawn with *ChemDraw 11*. The β-tryptase input is based on a structure from the RCBS Protein Data Bank (PDB code: 1A0L). As preparation for the calculations all water molecules and substrates of the PDB crystal structure were removed. With the help of *Maestro* any lacking hydrogen atoms were added to the protein structure. The structure calculations with *MacroModel* were performed based on the forcefield OPLS 2005. Water was chosen as solvent. The resulting structures were the result of 2000 calculation cycles.

7.2 Technical Notes for Solid Phase Peptide Synthesis

7.2.1 Attachment of First Amino Acid and General Coupling Conditions

Fmoc Removal

The Fmoc protecting group was cleaved by treatment with 20 % piperidine in DMF for (2×10 mL, 20 min each). Then, the resin was washed 3× with DMF, 3× with DCM and again 3× with DMF (5–10 minutes each) to remove the last traces of piperidine. A positive Kaiser test confirmed the cleavage of the Fmoc group and the formation of the free amino function.

Resin Type: Rink Amide and PEGA

The resin was weighed out into a glass peptide synthesis vessel and allowed to swell in DMF (10 mL) for 1 h. Then, the Fmoc protection group was removed by agitation with piperidine in DMF as mentioned above. After an intensive washing cycle with DMF the resin was suspended in DMF (10 mL) containing 3 % NMM. The attachment of the fist Fmoc-protected amino acid (2.5 equiv) was accomplished with the help of a coupling activator such as PyBOP or HCTU (2.5 equiv) by shaking over night at room temperature. The last step was repeated to ensure quantitative coupling. The resin was finally filtered, washed with DMF (3×5 min) before a Kaiser test was performed. In the case of a quantitative coupling the Fmoc group was removed and the following amino acid was attached, if required.

Resin Type: Wang, PAM and SASRIN

These resin types were weighed out into a glass peptide synthesis vessel and allowed to swell in DCM/DMF (8:2, 10 mL) for 1 h. The attachment of the fist Fmoc-protected amino acid (2.5 equiv) was accomplished with the help of diisopropylcarbodiimide (DIC, 2.5 equiv), 1-hydroxybenzotriazole (HOBt, 2.5 equiv) and dimethylaminopyridine (DMAP, 0.1 equiv) by shaking over night at room temperature. This step was repeated to ensure quantitative coupling. The resin was finally filtered, washed with DMF (3×5 min) before a Kaiser test was performed. In the case of a quantitative coupling the Fmoc group was removed and the next amino acid was attached, if required, now again with the standard coupling conditions (PyBOP, 3 % NMM, DMF).

Choice of amino acids and side chain protection groups
All amino acids in this thesis were used as pure optical isomer in the L-form. If otherwise stated, the following side chain protection groups were used for amino- and carboxyl-functions: As side chain protection group for lysine, histidine and tryptophan *tert*-butyl-oxycarbonyl (-Boc) and for arginine 2,2,4,6,7-pentamethyldihydrobenzofuran-5-sulfonyl (-Pbf) was chosen.

7.2.2 Color Tests

The Kaiser test was carried out in the reactions involving resin-bonded amines. Reactions involving resin-bonded carboxylic acids were monitored by the malachite green test. When necessary, the coupling reaction was repeated until the desired test result was obtained.

Detection of free amino functions on the resin (Kaiser test)[302]
Two separate solutions of ninhydrin (1.00 g) in ethanol (10 mL) and phenol (40.0 g) in ethanol (10 mL) were prepared. A small amount of resin beads from the reaction were selected, added to a mixture of both solutions (0.5 mL each) and heated for 2 minutes at 100 °C. Resin beads with free amino functions (NH_2) turned dark blue/red, whereas beads without amino functions remained clear.

Detection of free acid functions on the resin (malachite green test)[303]
A few beads of the resin were washed several times with DCM or DMF, followed by MeOH. Afterwards 1 mL of a 0.25 % solution of malachite green oxalate (250 mg) in EtOH (100 mL) was added followed by a single drop of pure Et_3N. After 2 min at room temperature the green solution was discarded and the beads were rinsed several times with EtOH until the solution remained clear. In the presence of free acid functions (COOH) the beads were colored dark green, otherwise they remained clear.

7.2.3 Resin Cleavage and Work Up

After the final coupling step (and optional Fmoc removal), the resin was thoroughly washed (3×DMF, 3×DCM, 2×MeOH and again 3×DCM) and dried under vacuum. The peptide was then cleaved from the resin by the following protocols.

Resin Type: Rink Amide

Cleavage of the product from the resin was achieved by treatment with a mixture of TFA/DCM/triisopropylsilane (95:2.5:2.5) for 3 h. The dark cleavage mixture was collected by filtration and the resin was washed twice with pure TFA. The filtrates were combined and concentrated under vacuum to afford an oily residue. The peptide was then precipitated by adding dry diethyl ether to the oil. To obtain the colorless hydrochloride salt, the solid was dissolved in water (40 mL), acidified with hydrochloric acid (0.1 N, 4 mL) and lyophilized. This step was repeated two to five times.

Resin Type: Wang

Cleavage of the product from the resin was achieved by treatment with a mixture of TFA/DCM (50:50) for 3 h. The dark cleavage mixture was collected by filtration and the resin was washed twice with TFA. The filtrates were combined and concentrated under vacuum to afford an oily residue. The peptide was then precipitated by adding dry diethyl ether to the oil. The solid was dissolved in water (40 mL), acidified with hydrochloric acid (0.1 N, 4 mL) and lyophilized to obtain a colorless hydrochloride salt. This dry freezing process was repeated two to five times.

Resin Type: SASRIN

Due to the high acid sensitivity of the resin it is possible to preserve, e.g. Boc-protecting groups during the cleavage. To achieve this, short cleavage times and quenching compounds are necessary. In detail, this was achieved by the treatment with a mixture of TFA/DCM (1:99) for 5 min. The cleavage mixture was collected by filtration into a flask containing pyridine (2 equiv) to scavenge the TFA (1 equiv). This step was repeated five times. Then, the combined solvents were removed and the product was purified by reversed-phase MPLC (H_2O/MeOH + TEA).

7.3 Synthesis of Small Oligopeptides

7.3.1 Tripeptides Containing the CBS Building Block

Synthesis of CBS-Lys-Lys-Phe-NH_2 (1)
(short form: CBS-KKF)

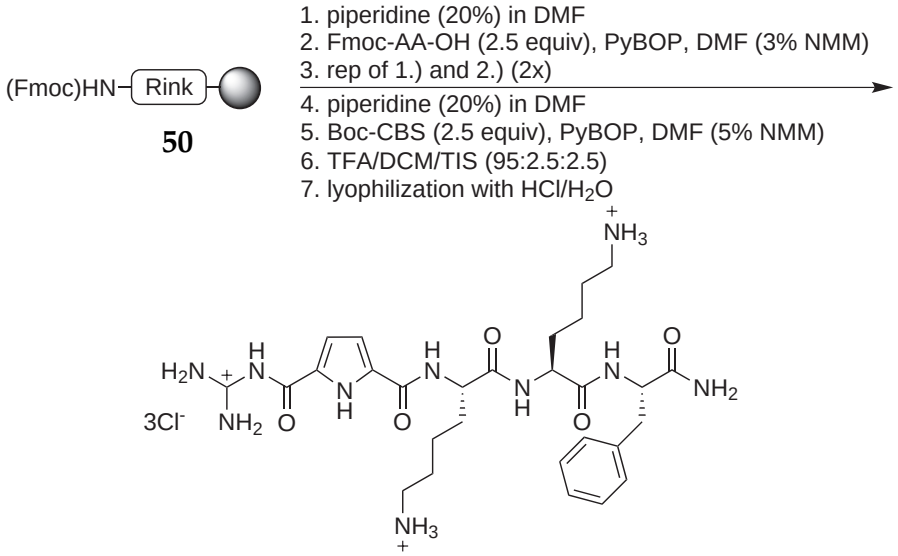

1

Rink amide resin (500 mg, 0.940 mmol/g, 470 μmol, 1 equiv) was prepared for the attachment of the first amino acid according to the general procedures (see Chapter 7.2.1 on page 165). The following three amino acids were attached under standard conditions for SPPS: Fmoc-protected amino acid (1.18 mmol, 2.5 equiv), PyBOP (611 mg, 1.18 mmol, 2.5 equiv) in DMF (10 mL) containing NMM (3 %). The mixture was shaken for 20 h to ensure quantitative coupling. After the final Fmoc deprotection the attachment of the Boc-protected 5-guanidiniocarbonylpyrrole-2-carboxylic acid[122] was performed under related conditions: carboxylic acid (467 mg, 1.18 mmol, 2.5 equiv), PyBOP (611 mg, 1.18 mmol, 2.5 equiv) and DMF containing 5 % NMM with a reaction time of 20 h. The last step was repeated to ensure quantitative coupling. The product was cleaved from the solid support according to the general procedure for the Rink amide resin (see Chapter 7.2.3 on page 166) and was further purified by RP-HPLC (MeOH/H_2O + 0.1 % TFA; 20/80).

$C_{28}H_{45}Cl_3N_{10}O_5$	708.08 g·mol^{-1}
yield:	282 mg, 398 μmol (85 %)
melting point:	247 °C (decomposition)

^{1}H-NMR (400 MHz, DMSO-d_6): δ [ppm] = 1.19–1.79 (m, 12 H, 6×Lys-CH_2), 2.60–2.80 (m, 4 H, 2×CH_2), 2.77 (m, 1 H, CH_2Ph), 2.93 (m, 1 H, CH_2Ph), 4.08–4.15 (m, 1 H, CH), 4.35–4.38 (m, 2 H, 2×CH), 6.84 (s, 1 H, py-CH), 7.03 (s, 1 H, py-CH), 7.12 (s, 1 H, NH_2), 7.17 (m, 5 H, ar-CH), 7.45 (s, 1 H, NH_2), 7.63–7.91 (br, 6 H, NH_3^+), 7.80 (d, $^3J_{HH}$ = 8.1 Hz, 1 H, NH), 8.17 (d, $^3J_{HH}$ = 7.5 Hz, 1 H, NH), 8.36 (bs, 2 H, gua-NH_2), 8.56 (bs, 2 H, gua-NH_2), 11.94 (bs, 1 H, gua-NH), 12.45 (s, 1 H, py-NH)

MPLC (RediSep C-18 Reverse Phase, 43 g): 2 min H_2O + 0.1 % TFA, then in 40 min to MeOH/H_2O 80:20 + 0.1 % TFA, 20 mL/min, τ_R = 22 min (300 nm)

HPLC prep. (*Varian* Microsorb C18, 250 mm × 4.6 mm, 5 μm): MeOH/H_2O 20:80 + 0.1 % TFA, 31 mL/min, τ_R = 12.4 min (300 nm)

The full characterization of this compound was already published in the *Schmuck* group.[269] However, it is mentioned here due to the significance and the relationship to the compounds synthesized in this thesis. In addition to the previous work it was possible to synthesize this compound on a larger scale followed by an optimized purification protocol with RP-HPLC.

Synthesis of CBS-Trp-His-Arg-NH_2 (91)
(short form: CBS-WHR)

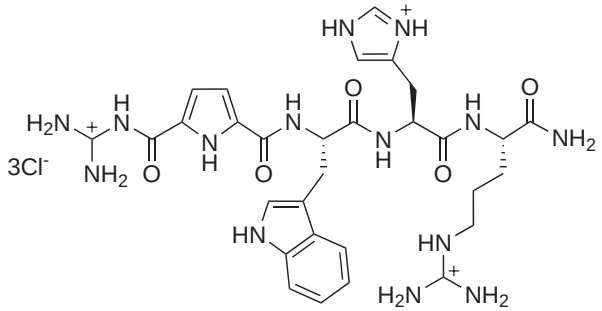

91

The synthesis of CBS-Trp-His-Arg-NH_2 (**91**) was performed under analogous conditions as previously described for CBS-Lys-Lys-Phe-NH_2 (**1**). Reaction batch: Rink amide resin (100 mg, 940 μmol/g, 94.0 μmol, 1 equiv)

$C_{30}H_{41}Cl_3N_{14}O_5$	784.10 g·mol^{-1}
yield:	39.5 mg, 50.4 μmol (54 %)
melting point:	208 °C (decomposition)

^{1}H-NMR (400 MHz, DMSO-d_6): δ [ppm] = 1.08–1.85 (m, 4 H, 2×CH_2), 2.93–3.19 (m, 6 H, 3×CH_2), 4.19 (m, 1 H, C*H*), 4.65–4.71 (m, 2 H, C*H*), 6.70–7.88 (m, 14 H, 2×His-C*H*, 5×Trp-C*H*, 2×py-C*H*), 8.09 (d, $^3J_{HH}$ = 7.6 Hz, 1 H, N*H*), 8.47 (bs, 2 H, gua-NH_2), 8.56 (bs, 2 H, gua-NH_2), 8.58 (d, $^3J_{HH}$ = 7.5 Hz, 1 H, N*H*), 8.59 (bs, 2 H, gua-NH_2), 8.75 (d, $^3J_{HH}$ = 7.5 Hz, 1 H, N*H*), 9.03 (s, 2 H, gua-NH_2), 10.76 (s, 1 H, Trp-N*H*), 12.03 (bs, 1 H, gua-N*H*), 12.40 (s, 1 H, py-N*H*), 14.21 (bs, 2 H, 2×His-N*H*)

^{13}C-NMR (100 MHz, DMSO-d_6): δ [ppm] = 24.9, 26.8, 27.4, 29.0, 39.55 (5×CH_2), 51.8, 52.1, 53.9 (3×C*H*), 110.0, 111.3, 113,4, 115.8, 116.9, 118.2, 118.4, 120.9, 123.6, 133.6 (10×ar-C*H*), 125.6, 127.1, 129.2, 132.1, 136.0, 155.4, 156.8, 158.9, 159.7, 169.6, 171.8, 173.4 (13×C_q)

MS (MALDI, DHB/HCCA 1:1, MeOH, TA50): m/z = 675.878, calculated for $C_{30}H_{39}N_{14}O_5^+$ $[M+H]^+$: 675.721

FT-IR (pure): $\tilde{\nu}$ [cm^{-1}] = 3155 (br), 1644 (s), 1549 (s), 1448 (m), 1280 (m), 1184 (w), 1085 (m), 815 (w), 743 (w)

Synthesis of CBS-Ala-Ile-Val-NH_2 (122)
(short form: CBS-AIV)

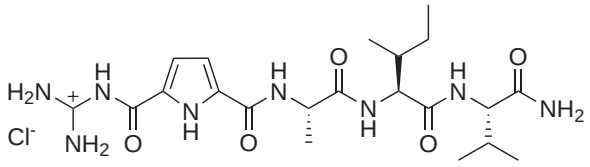

122

The synthesis of CBS-Ala-Ile-Val-NH_2 (**122**) was performed under analogous conditions as previously described for CBS-Lys-Lys-Phe-NH_2 (**1**). Reaction batch: Rink amide resin (300 mg, 720 μmol/g, 216 μmol, 1 equiv)

$C_{21}H_{35}ClN_8O_5$	515.01 g·mol^{-1}
yield:	54.4 mg, 106 μmol (49 %)
melting point:	238 °C (decomposition)

^{1}H-NMR (400 MHz, DMSO-d_6): δ [ppm] = 0.83 (m, 12 H, 3×CH_3), 1.08 (m, 2 H, Ile-CH_2), 1.29 (m, 3 H, Ala-CH_3), 1.45 (m, 1 H, Ile-CH), 1.76 (m, 1 H, Val-CH), 4.09–4.20 (m, 2 H, CH), 4.55 (m, 1 H, CH), 6.91 (s, 1 H, py-CH), 7.03 (s, 1 H, NH_2), 7.18 (s, 1 H, py-CH), 7.30 (s, 1 H, NH_2), 7.55 (d, $^3J_{HH}$ = 8.9 Hz, 1 H, NH), 8.06 (d, $^3J_{HH}$ = 8.8 Hz, 1 H, NH), 8.29 (bs, 4 H, 2×gua-NH_2), 8.57 (d, $^3J_{HH}$ = 7.2 Hz, 1 H, NH), 11.29 (s, 1 H, gua-NH), 12.52 (s, 1 H, py-NH)

^{13}C-NMR (100 MHz, DMSO-d_6): δ [ppm] = 11.0, 15.4, 17.9, 18.0, 19.3 (5×CH_3), 24.4 (Ile-CH_2), 30.6 (Val-CH), 36.2 (Ile-CH), 48.5, 57.3, 57.4 (3×CH), 113.5, 115.4 (2×py-CH), 125.6, 132.3, 155.2, 158.7, 159.7, 170.8, 172.3, 172.8 (8×C_q)

MS (pos. ESI, MeOH): m/z = 479.273, calculated for $C_{21}H_{35}N_8O_5^+$ $[M+H]^+$: 479.553

FT-IR (pure): $\tilde{\nu}$ [cm^{-1}] = 3268 (br), 2961 (w), 1681 (m), 1630 (s), 1549 (s), 1475 (w), 1300 (m), 1280 (m), 1205 (w), 1134 (w)

Synthesis of CBS(Boc)-Lys(Boc)-Lys(Boc)-Phe-COOH (66)
(short form: CBS-K(Boc)K(Boc)F(Boc)-OH)

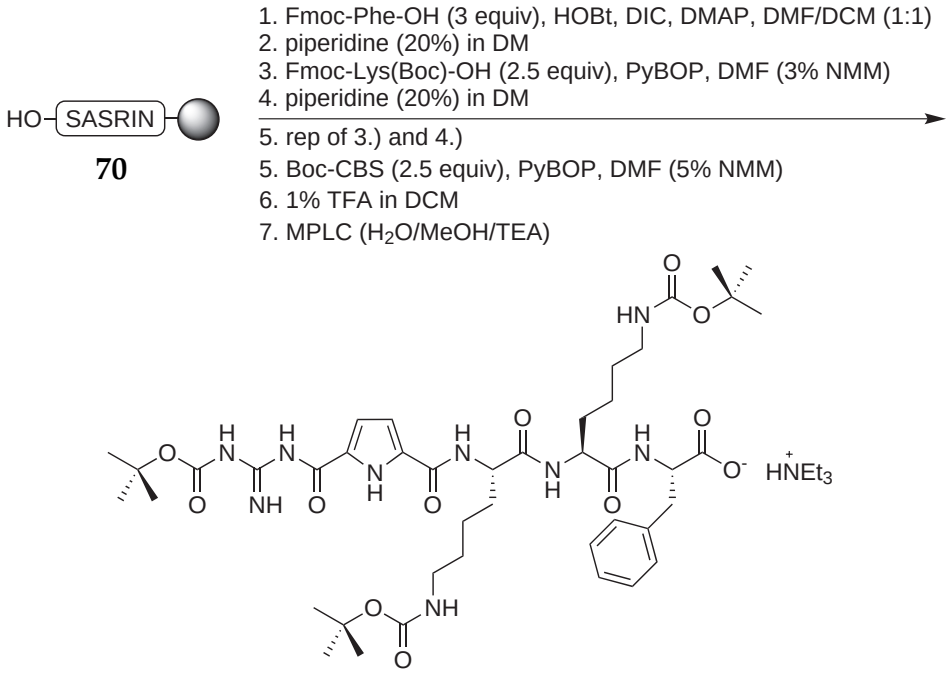

66

SASRIN resin (300 mg, 1.00 mmol/g, 300 μmol, 1 equiv) was swollen in DMF for 1 h. The first amino acid was attached under standard conditions for SPPS of Wang type resins (see Chapter 7.2.1): Fmoc-protected amino acid (0.75 mmol, 2.5 equiv), DIC (0.75 mmol, 2.5 equiv), HOBt (750 μmol, 2.5 equiv) and DMAP (30.0 μmol, 0.1 equiv) in DMF/DCM (1:1). After a reaction time of 20 h the Fmoc-protecting group was removed and the following two amino acids as well as the 5-guanidiniocarbonylpyrrole-2-carboxylic acid were attached under analogous conditions as previously described for CBS-Lys-Lys-Phe-NH_2 (**1**). The product was cleaved from the solid support according to the general procedure for the SASRIN resin (see Chapter 7.2.3 on page 166).

$C_{49}H_{80}N_{10}O_{12}$	1001.22 g·mol^{-1}
yield:	287 mg, 287 μmol (95 %)
melting point:	231 °C (decomposition)

^{1}H-NMR (600 MHz, DMSO-d_6): δ [ppm] = 1.17 (t, $^3J_{HH}$ = 10.8 Hz, NEt_3-CH_3), 1.13–1.69 (m, 12 H, 6×Lys-CH_2), 1.34 (s, 9 H, 3×Boc-CH_3), 1.36 (s, 9 H, 3×Boc-CH_3), 1.47 (s, 9 H,

3×Boc-CH_3), 2.77–2.96 (m, 6 H, CH_2Ph, 2×Lys-CH_2), 3.09 (m, NEt_3-CH_2), 4.16–4.26 (m, 1 H, C*H*), 4.33–4.49 (m, 2 H, 2×C*H*), 6.68–6.88 (m, 4 H, 2×py-C*H*, 2×N*H*), 7.15–7.32 (m, 5 H, Phe-C*H*), 7.96 (d, $^3J_{HH}$ = 11.4 Hz, 1 H, N*H*), 8.05 (d, $^3J_{HH}$ = 10.8 Hz, 1 H, N*H*), 8.39 (d, $^3J_{HH}$ = 11.4 Hz, 1 H, N*H*), 8.59 (s, 1 H, N*H*), 9.28 (bs, 4H, 2×gua-NH_2), 11.63 (bs, 1 H, gua-N*H*), 12.30 (s, 1 H, py-N*H*)

^{13}C-NMR (150 MHz, DMSO-d_6): δ [ppm] = 8.6 (NEt_3-CH_3), 22.6, 23.1, 27.5, 29.3, 31.5, 31.6, 39.6 (8×Lys-CH_2, Phe-CH_2), 27.8, 28.3 (9×Boc-CH_3), 52.3, 52.8, 53.2 (3×CH), 112.9, 115.8 (py-CH), 126.4, 128.2, 129.1 (5×Phe-CH), 137.4 (Phe-C_q), 155.5, 157.6 (2×py-C_q), 157.9, 158.2 (3×Boc-CO-C_q, 3×Boc-C_q), 158.6, 159.4 (py-CO-C_q), 171.5, 171.6, 172.7 (3×CO-C_q)

MPLC (RediSep C-18 Reverse Phase, 43 g): 2 min H_2O + 0.1 % TEA, then in 50 min to MeOH/H_2O 90:10 + 0.1 % TEA, 20 mL/min, τ_R = 21 min (300 nm)

MS (MALDI, DHB/MeOH 1:5): m/z = 899.444, calculated for $C_{43}H_{64}N_9O_{12}^-$ $[M\text{-}H]^-$: 899.022

FT-IR (pure): $\tilde{\nu}$ [cm^{-1}] = 3298 (w), 2991 (w), 2942 (w), 1669 (s), 1625 (s), 1527 (m), 1448 (m), 1395 (w), 1291 (w), 1199 (s), 1171 (s), 1127 (s), 829 (m), 801 (m), 715 (s)

Synthesis of CBS-Lys-Lys-Phe-TEG-NH_2 (59)

(short form: CBS-KKF-TEG)

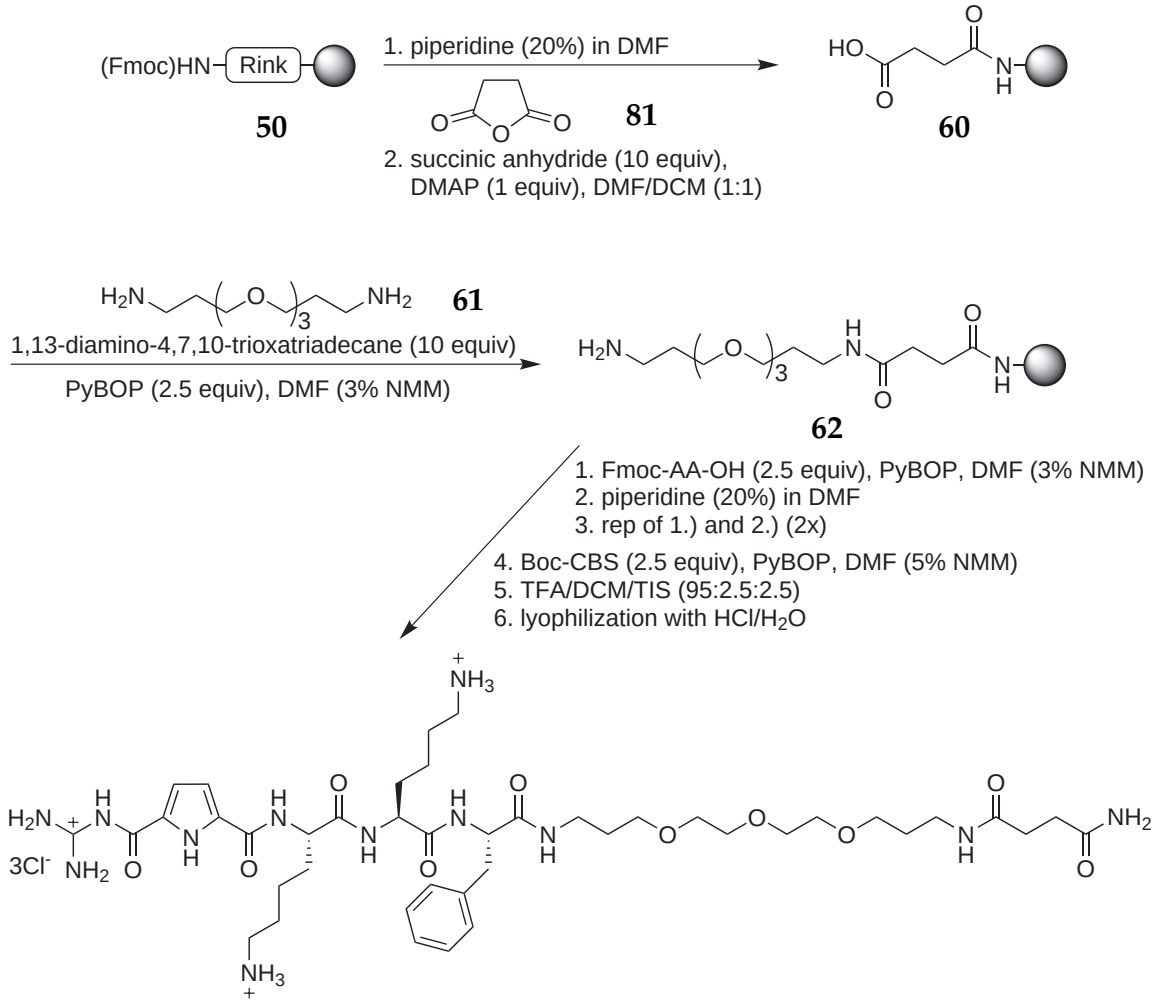

59

Rink amide resin (300 mg, 740 μmol/g, 222 μmol, 1 equiv) was prepared for the attachment of the first amino acid according to the general procedures (see Chapter 7.2.1 on page 165). For the first coupling succinic anhydride (222 mg, 2.22 mmol, 10 equiv) and DMAP (27.1 mg, 222 μmol, 1 equiv) were added in a DMF/DCM (1:1) mixture (10 mL) for 20 h. A malachite green test indicated the successful conversion to the free acid. In the next step 1,13-diamino-4,7,10-trioxatriadecane (489 mg, 2.22 mmol, 10 equiv) and PyBOP (289 mg, 555 μmol, 2.5 equiv) in DMF (10 mL) containing NMM (3 %) were added and shaken for 20 h. A negative malachite green and a positive Kaiser test confirmed the complete reaction. The attachment of the following three amino acids and the 5-guanidiniocarbonylpyrrole-2-carboxylic acid was performed under analogous conditions as previously described for the synthesis of CBS-Lys-Lys-Phe-NH_2 (**1**). The product was cleaved from the solid support according to the general procedure for the Rink amide resin (see Chapter 7.2.3 on page 166).

$C_{42}H_{71}Cl_3N_{12}O_{10}$	1010.45 g·mol^{-1}
yield:	151 mg, 149 μmol (68 %)
melting point:	220 °C (decomposition)

^{1}H-NMR (400 MHz, DMSO-d_6): δ [ppm] = 1.19–1.78 (m, 12 H, 6×Lys-CH_2), 2.61–2.79 (m, 4 H, 2×CH_2), 2.80 (m, 1 H, CH_2Ph), 2.94 (m, 1 H, CH_2Ph), 2.97–3.11 (m, 6 H, 3×CH_2), 3.20–3.51 (m, 18 H, 9×CH_2), 4.13–4.25 (m, 1 H, CH), 4.36–4.49 (m, 2 H, 2×CH), 6.69 (s, 2 H, 2×py-CH), 6.92 (s, 1 H, NH), 7.09 (s, 1 H, NH_2), 7.21 (m, 5 H, ar-CH), 7.34 (s, 1 H, NH_2), 7.59 (s, 1 H, NH), 7.77 (m, 2 H, 2×NH), 7.81–8.05 (br, 2 H, 2×NH_3^+), 8.24 (d, $^3J_{HH}$ = 7.6 Hz, 1 H, NH), 8.50 (bs, 2 H, gua-NH_2), 8.69 (bs, 2 H, gua-NH_2), 12.16 (bs, 1 H, gua-NH), 12.53 (s, 1 H, py-NH)

^{13}C-NMR (100 MHz, DMSO-d_6): δ [ppm] = 27.4, 27.9, 29.3, 30.5, 30.6, 35.6, 35.8, 38.5 (8×Lys-CH_2, 1×Phe-CH_2), 48.5, 48.6 (3×CH), 67.8, 68.0, 68.1, 69.5, 69.6, 69.7 (9×CH_2), 114.9, 115.9 (py-CH), 125.6, 126.3, 127.9, 129.2, 131.4, 137.5 (5×Phe-CH, 3×ar-C_q), 152.5 (gua-C_q), 159.0, 159.7 (py-CO-C_q), 171.2, 171.3, 173.4, 173.5, 177.7 (5×CO-C_q)

MS (pos. ESI, MeOH): m/z = 901.5255, calculated for $C_{42}H_{69}N_{12}O_{10}^+$ [M+H]$^+$: 902.0711

FT-IR (pure): $\tilde{\nu}$ [cm^{-1}] = 3178 (br), 2928 (s), 2879 (s), 1640 (s), 1549 (s), 1438 (w), 1402 (w), 1280 (m), 1255 (m), 1190 (w), 1099 (s)

Synthesis of CBS-Lys-Lys-Phe-TentaGel (55)

(short form: CBS-KKF-TentaGel)

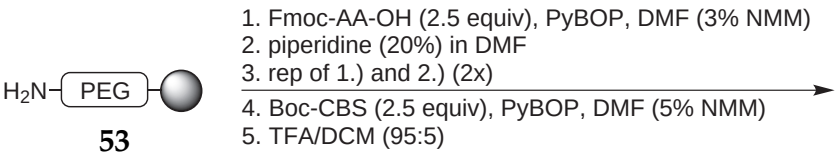

53

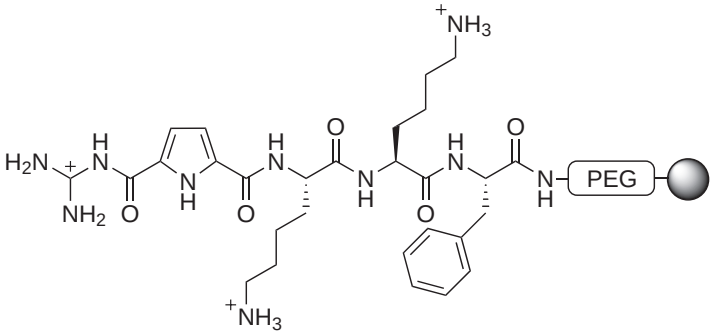

55

The synthesis of CBS-Lys-Lys-Phe-TentaGel (**55**) was performed under analogous conditions as previously described for CBS-Lys-Lys-Phe-NH_2 (**1**). The only difference was the used solid support. The synthesis on TentaGel starts without an initial Fmoc-deprotection step. Due to the high acid stability of the resin, the peptide remains on the solid support during the final deprotection step (TFA/DCM 95:5 for 3 h). *tert*-Butyloxycarbonyl (-Boc) was chosen as side chain protection group for the guanidiniocarbonylpyrrole carboxylic acid. Reaction batch: TentaGel-NH_2 resin (100 mg, 310 μmol/g, 31.0 μmol, 1 equiv)

Synthesis of CBS-Ala-Ile-Val-TentaGel (56)

(short form: CBS-AIV-TentaGel)

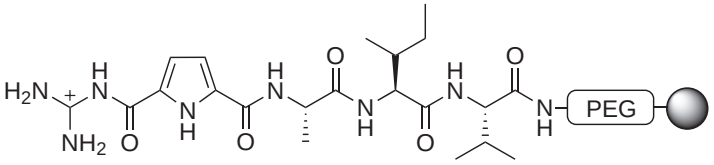

56

The synthesis of CBS-Ala-Ile-Val-TentaGel (**56**) was performed under analogous conditions as previously described for CBS-Lys-Lys-Phe-TentaGel (**55**). Reaction batch: TentaGel-NH_2 resin (100 mg, 310 μmol/g, 31.0 μmol, 1 equiv)

Synthesis of CBS-Lys-Lys-Phe-PAM (124)

(short form: CBS-KKF-PAM)

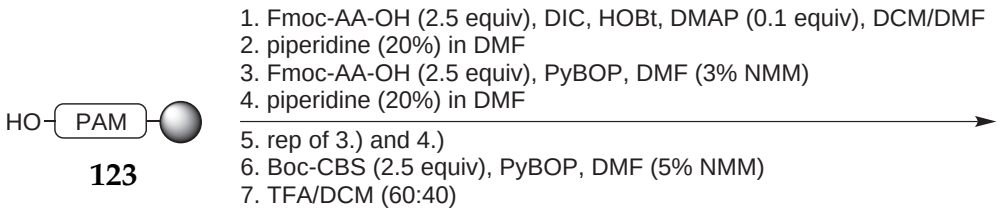

123

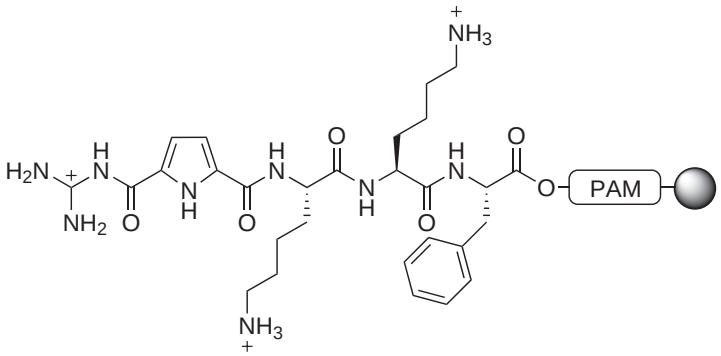

124

The synthesis of CBS-Lys-Lys-Phe-TentaGel (**55**) was performed under analogous conditions as previously described for CBS-Lys-Lys-Phe-NH_2 (**1**). The only difference was the use of PAM resin instead of Rink amide resin. The synthesis starts without an initial Fmoc-deprotection step and uses a different mixture of coupling reagents (see Chapter 7.2.1 on page 165) Due to the high acid stability of the resin, the peptide remains on the solid support during the final deprotection step (TFA/DCM 60:40). *tert*-Butyloxycarbonyl (-Boc) was chosen as side chain protection group for the guanidiniocarbonylpyrrole carboxylic acid. Reaction batch: PAM resin (100 mg, 1.00 mmol/g, 100 μmol, 1 equiv)

Special non-peptide addition: Synthesis of CBS-NH_2 (52)

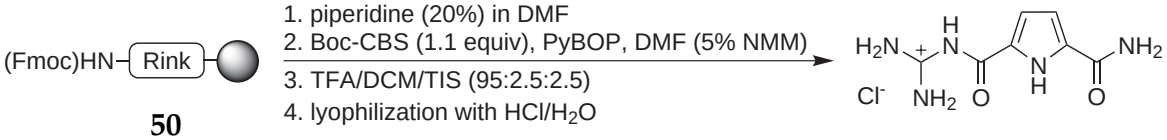

50 **52**

Rink amide resin (1.00 g, 720 μmol/g, 720 μmol, 1 equiv) was prepared for the attachment of the first amino acid according to the general procedures (see Chapter 7.2.1 on

page 165). Then the Boc-protected 5-guanidiniocarbonylpyrrole-2-carboxylic acid[122] (315 mg, 792 μmol, 1.1 equiv), PyBOP (412 mg, 792 μmol, 1.1 equiv) and DMF containing 5 % NMM was added and shaken for 20 h. The product was cleaved from the solid support by shaking the resin with a mixture of TFA/DCM/triisopropylsilane (95:2.5:2.5) for 3 h. The solvent was evaporated and the remaining oil was treated with dry diethyl ether. The precipitate was dried under vacuum and further purified by RP-MPLC (MeOH/H_2O + 0.1 % TFA; 20/80). To obtain the colorless hydrochloride salt, the solid was dissolved in water (40 mL), acidified with hydrochloric acid (0.1 N, 4 mL) and lyophilized.

$C_7H_{10}ClN_5O_2$	231.64 g·mol^{-1}
yield:	128 mg, 553 μmol (77 %)
melting point:	221 °C (decomposition)

^{1}H-NMR (400 MHz, DMSO-d_6): δ [ppm] = 6.86 (s, 1 H, py-C*H*), 7.21 (s, 1 H, py-C*H*), 7.45 (s, 1 H, NH_2), 7.91 (s, 1 H, NH_2), 8.34 (bs, 4 H, 2×gua-NH_2), 11.37 (s, 1 H, gua-N*H*), 12.30 (s, 1 H, py-N*H*)

^{13}C-NMR (100 MHz, DMSO-d_6): δ [ppm] = 112.8, 115.9 (py-*C*H), 125.5, 132.9 (2×py-C_q), 155.4 (gua-C_q), 159.6, 160.7 (py-*C*O-C_q)

MS (neg. ESI, MeOH): m/z = 194.0689, calculated for $C_7H_8N_5O_2^-$ [M-H]$^+$: 194.1713

MPLC (RediSep C-18 Reverse Phase, 43 g): 2 min H_2O + 0.1 % TFA, then in 40 min to MeOH/H_2O 80:20 + 0.1 % TFA, 20 mL/min, τ_R = 23 min (300 nm)

FT-IR (pure): $\tilde{\nu}$ [cm^{-1}] = 3178 (br), 2928 (s), 2879 (s), 1640 (s), 1549 (s), 1438 (w), 1402 (w), 1280 (m), 1255 (m), 1190 (w), 1099 (s)

7.3.2 Fluorescence Labelled Tripeptides Containing the CBS Building Block

Synthesis of CBS-Lys-Lys-Phe-aminocaproicacid-Lys(Dansyl)-NH_2 (71)
(short form: $(CBS\text{-}KKF)_4$-(Dns))

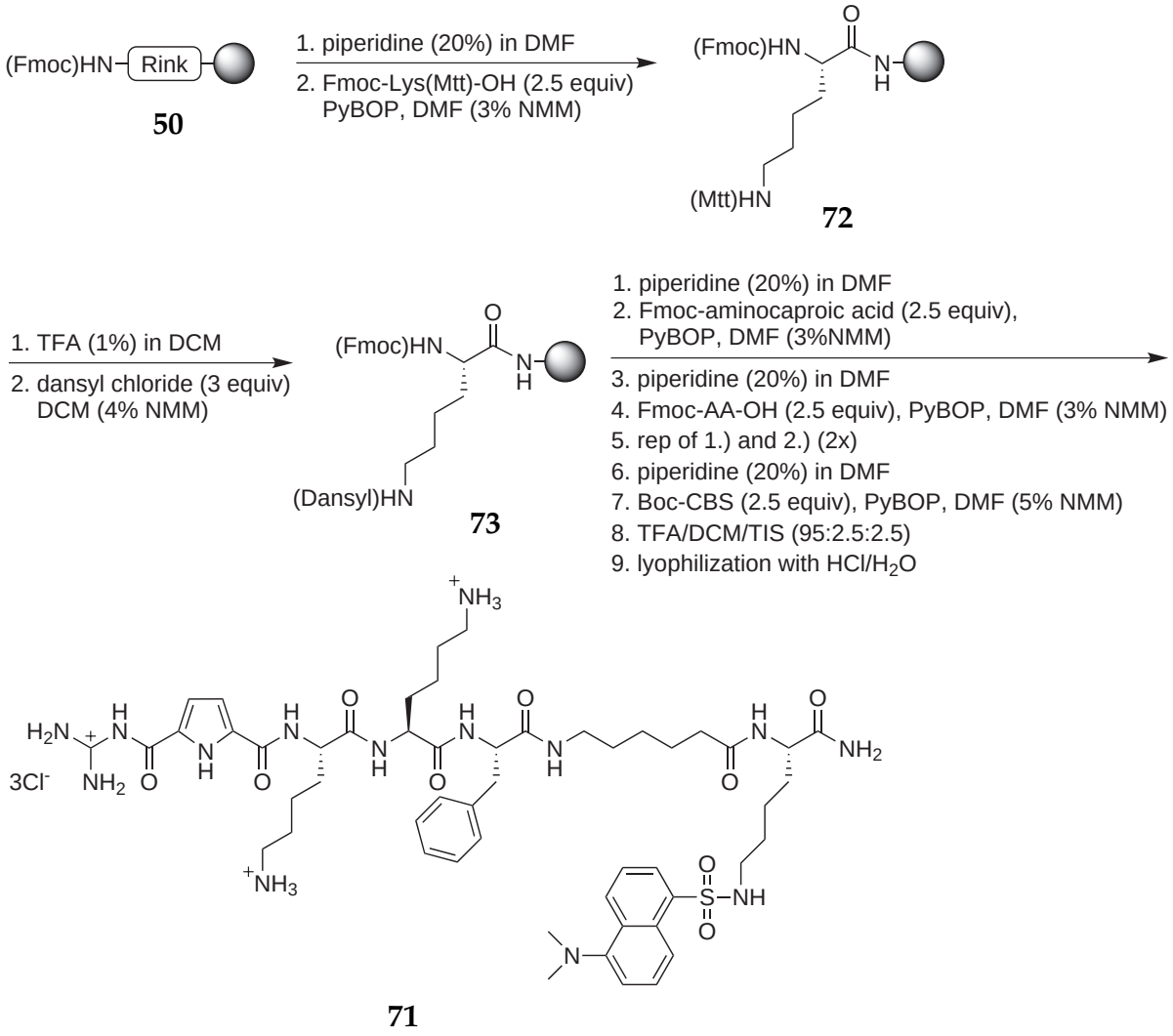

71

Rink amide resin (300 mg, 720 μmol/g, 216 μmol, 1 equiv) was prepared for the attachment of the first amino acid according to the general procedures (see Chapter 7.2.1 on page 165). The resin was treated with Fmoc-Lys(Mtt)-OH (337 mg, 540 μmol, 2.5 equiv) and PyBOP (281 mg, 540 μmol, 2.5 equiv) in DMF containing NMM 3 % (10 ml) for 20 h. To remove the side chain protecting group, the resin was treated (2×15 min, 4×5 min) with TFA (1 %) in DCM (10 mL). The deprotection was complete when the filtrate stopped turning yellow. The resin was washed with DCM (3×10 mL), Methanol (3×10 mL) and again with DCM (3×10 mL, 5–10 minutes each) to remove the last traces

of TFA. The free amine was coupled with dansyl chloride (175 mg, 648 μmol, 3 equiv) in a DCM/DMF mixture (80:20) containing NMM (5 %) for 20 h. The spacer (Fmoc-aminocaproic acid) and the tripeptide were attached under standard conditions for SPPS (see Chapter 7.2.1): Fmoc-protected amino acid (540 μmol, 2.5 equiv), PyBOP (281 mg, 540 μmol, 2.5 equiv) in DMF (10 mL) containing NMM (3 %). The mixture was shaken for 20 h to ensure quantitative coupling. After the final Fmoc deprotection the attachment of the 5-guanidiniocarbonylpyrrole-2-carboxylic acid[122] was performed under related conditions: carboxylic acid (160 mg, 540 μmol, 2.5 equiv), PyBOP (281 mg, 540 μmol, 2.5 equiv) and DMF containing 5 % NMM with a reaction time of 20 h. The last step was repeated to ensure quantitative coupling. The product was cleaved from the solid support according to the general procedure for the Rink amide resin (see Chapter 7.2.3 on page 166).

$C_{52}H_{79}Cl_3N_{14}O_9S$	1182.70 g·mol^{-1}
yield:	230 mg, 194 μmol (90 %)
melting point:	210 °C (decomposition)

^{1}H-NMR (600 MHz, DMSO-d_6): δ [ppm] = 1.09–1.79 (m, 24 H, 12×Lys-CH_2), 2.08 (m, 2 H, CH_2NHCO), 2.66–2.80 (m, 6 H, 3×CH_2), 2.82 (d, 1 H, CH_2Ph), 2.93 (s, 6 H, 2×CH_3), 2.93 (m, 2 H, NHCOCH_2), 3.02 (d, 1 H, CH_2Ph), 4.06 (m, 1 H, C*H*), 4.17 (m, 1 H, C*H*), 4.44 (m, 2 H, 2×C*H*), 6.91 (m, 1 H, py-C*H*), 6.92 (s, 1 H, NH_2), 7.23 (m, 5 H, ar-C*H*), 7.27 (s, 1 H, NH_2), 7.29 (m, 1 H, ar-CH_{dansyl}), 7.61 (m, 1 H, py-C*H*), 7.65 (m, 2 H, ar-CH_{dansyl}), 7.80 (d, 1 H, N*H*), 7.88 (m, 1 H, N*H*), 7.94 (m, 3 H, NH_3^+), 7.99 (m, 3 H, NH_3^+), 8.10 (d, 1 H, ar-CH_{dansyl}), 8.25 (d, 1 H, N*H*), 8.39 (d, 1 H, ar-CH_{dansyl}), 8.52 (bs, 2 H, gua-NH_2), 8.57 (d, 1 H, ar-CH_{dansyl}), 8.68 (d, 1 H, N*H*), 8.72 (bs, 2 H, gua-NH_2), 12.16 (s, 1 H, gua-N*H*), 12.54 (s, 1 H, py-N*H*)

^{13}C-NMR (150 MHz, DMSO-d_6): δ [ppm] = 22.1, 22.5, 24.9, 26.0, 26.4, 26.5, 29.0, 31.4, 34.1, 35.1, 40.8, 42.3 (18×CH_2), 45.4 (2×CH_3), 52.2, 52.5, 52.8, 53.9 (C*H*), 113.7, 115.9 (py-C*H*), 124.2, 125.6, 126.3, 127.7, 128.0, 128.3, 128.9, 129.0 (11×ar-C*H*), 129.2 (2×py-C_q), 129.2, 132.3, 136.3, 137.6 (5×ar-C_q), 155.6 (gua-C_q), 159.0, 159.8 (py-CO-C_q), 170.5, 171.1, 171.6, 172.1, 173.9 (*C*O-C_q)

MS (pos. ESI, MeOH): m/z = 1074.18, calculated for $C_{52}H_{77}N_{14}O_9S^+$ $[M+H]^+$: 1074.32

FT-IR (KBr): $\tilde{\nu}$ [cm^{-1}] = 3396 (s), 3075 (m), 2938 (s), 2855 (m), 1696 (s), 1654 (m), 1542 (s), 1473 (w), 1279 (m), 1143 (w)

7.3.3 Tetrapeptides

Synthesis of Lys-Lys-Phe-Gly-NH_2 (117)

(short form: KKFG)

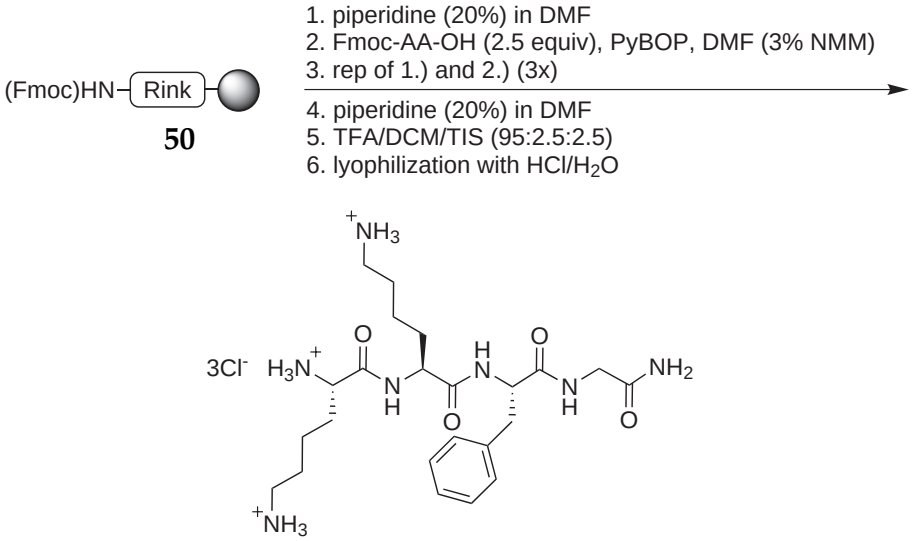

117

Rink amide resin (200 mg, 940 μmol/g, 188 μmol, 1 equiv) was prepared for the attachment of the first amino acid according to the general procedures (see Chapter 7.2.1 on page 165). The following four amino acids were attached under standard conditions for SPPS: Fmoc-protected amino acid (470 μmol, 2.5 equiv), PyBOP (245 mg, 470 μmol, 2.5 equiv) in DMF (10 mL) containing NMM (3 %). The mixture was shaken for 20 h to ensure quantitative coupling. After the final Fmoc deprotection the product was cleaved from the solid support according to the general procedure for the Rink amide resin (see Chapter 7.2.3 on page 166).

$C_{23}H_{42}Cl_3N_7O_4$	586.98 g·mol^{-1}
yield:	95.5 mg, 163 μmol (87 %)
melting point:	189 °C (decomposition)

^{1}H-NMR (400 MHz, DMSO-d_6): δ [ppm] = 1.19–1.80 (m, 12 H, 6×Lys-CH_2), 2.60–2.80 (m, 4 H, 2×CH_2), 2.87 (m, 1 H, CH_2Ph), 3.03 (m, 1 H, CH_2Ph), 3.63 (m, 2 H, Gly-CH_2), 3.84 (m, 1 H, CH), 4.25 (m, 1 H, CH), 4.52 (m, 1 H, CH), 7.09 (2 H, NH_2), 7.26 (m, 5 H, ar-CH), 7.96–8.11 (br, 6 H, NH_3^+), 8.25 (d, $^3J_{HH}$ = 8.0 Hz, 2 H, 2×NH), 8.34 (m, 3 H, NH_3^+), 8.80 (d, $^3J_{HH}$ = 8.0 Hz, 1 H, NH)

^{13}C-NMR (100 MHz, DMSO-d_6): δ [ppm] = 20.9, 22.1, 26.2, 26.4, 30.3, 31.2, 37.2, 39.5, 39.6, 41.9 (10×CH_2), 51.7, 52.8, 54.1 (*C*H), 126.2, 128.0, 129.2 (5×ar-*C*H), 137.7 (Phe-C_q), 168.4, 170.7, 171.1 (*C*O-C_q)

MS (pos. ESI, ACN): m/z = 478.3136, calculated for $C_{23}H_{40}N_7O_4^+$ $[M+H]^+$: 478.6077

FT-IR (pure): $\tilde{\nu}$ [cm^{-1}] = 3196 (br), 3043 (br), 2916 (br), 1650 (s), 1516 (s), 1398 (w), 1242 (m), 1144 (w), 1012 (w)

Synthesis of Arg-Trp-Lys-Gly-NH_2 (118)
(short form: RWKG)

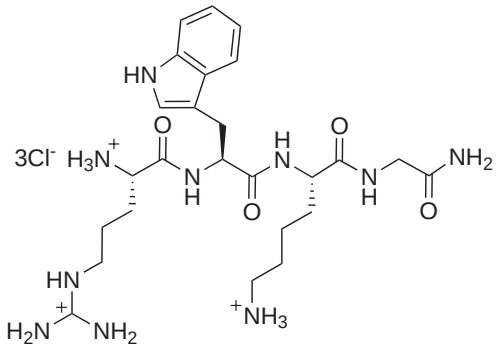

118

The synthesis of Arg-Trp-Lys-Gly-NH_2 (**118**) was performed under analogous conditions as previously described for Lys-Lys-Phe-Gly-NH_2 (**117**). Reaction batch: Rink amide resin (200 mg, 940 μmol/g, 188 μmol, 1 equiv)

$C_{25}H_{43}Cl_3N_{10}O_4$	654.03 g·mol^{-1}
yield:	110.4 mg, 0.1688 mmol (90 %)
melting point:	194 °C (decomposition)

^{1}H-NMR (400 MHz, DMSO-d_6): δ [ppm] = 1.15–1.94 (m, 10 H, 5×CH_2), 2.73 (m, 2 H, CH_2NHCO), 2.94–3.25 (m, 4 H, 2×CH_2), 3.63 (m, 2 H, Gly-CH_2), 3.81 (m, 1 H, C*H*), 4.22 (m, 1 H, C*H*), 4.61 (m, 1 H, C*H*), 6.92–7.40 (m, 9 H, 2×NH_2, 5×Trp-C*H*), 7.68 (d, $^3J_{HH}$ = 8.0 Hz, 1 H, N*H*), 7.82 (m, 1 H, N*H*), 7.98 (m, 3 H, NH_3^+), 8.04 (m, 1 H, N*H*), 8.26 (m, 3 H, NH_3^+), 8.33 (d, $^3J_{HH}$ = 7.6 Hz, 1 H, N*H*), 8.85 (d, $^3J_{HH}$ = 7.2 Hz, 1 H, N*H*), 10.90 (s, 1 H, gua-N*H*)

^{13}C-NMR (100 MHz, DMSO-d_6): δ [ppm] = 21.8, 23.6, 26.2, 27.2, 28.0, 30.6, 38.2, 39.9, 41.6 (9×CH_2), 51.2, 52.5, 53.7 (*C*H), 109.6, 127.2, 136.1, (2×Trp-C_q), 111.0, 117.9, 118.3, 120.6, 123.8 (5×Trp-CH), 156.9 (Arg-C_q), 168.6, 170.8, 171.3, 171.5 (*C*O-C_q)

MS (MALDI, DCTB): m/z = 545.337 calculated for $C_{25}H_{41}N_{10}O_4^+$ $[M+H]^+$: 545.657

FT-IR (pure): $\tilde{\nu}$ [cm^{-1}] = 3185 (br), 2935 (br), 2511 (br), 2153 (w), 2009 (w), 1651 (s), 1516 (s), 1180 (s), 1045 (s), 860 (m)

7.4 Synthesis of Multivalent Peptide Systems

7.4.1 Fluorescence Labelled Multivalent Peptides Containing the CBS Building Block

Synthesis of (CBS-Lys-Lys-Phe)$_4$(Lys)$_2$Lys-Lys(Dansyl)-NH$_2$ (75)

(short form: (CBS-KKF)$_4$-(Dns))

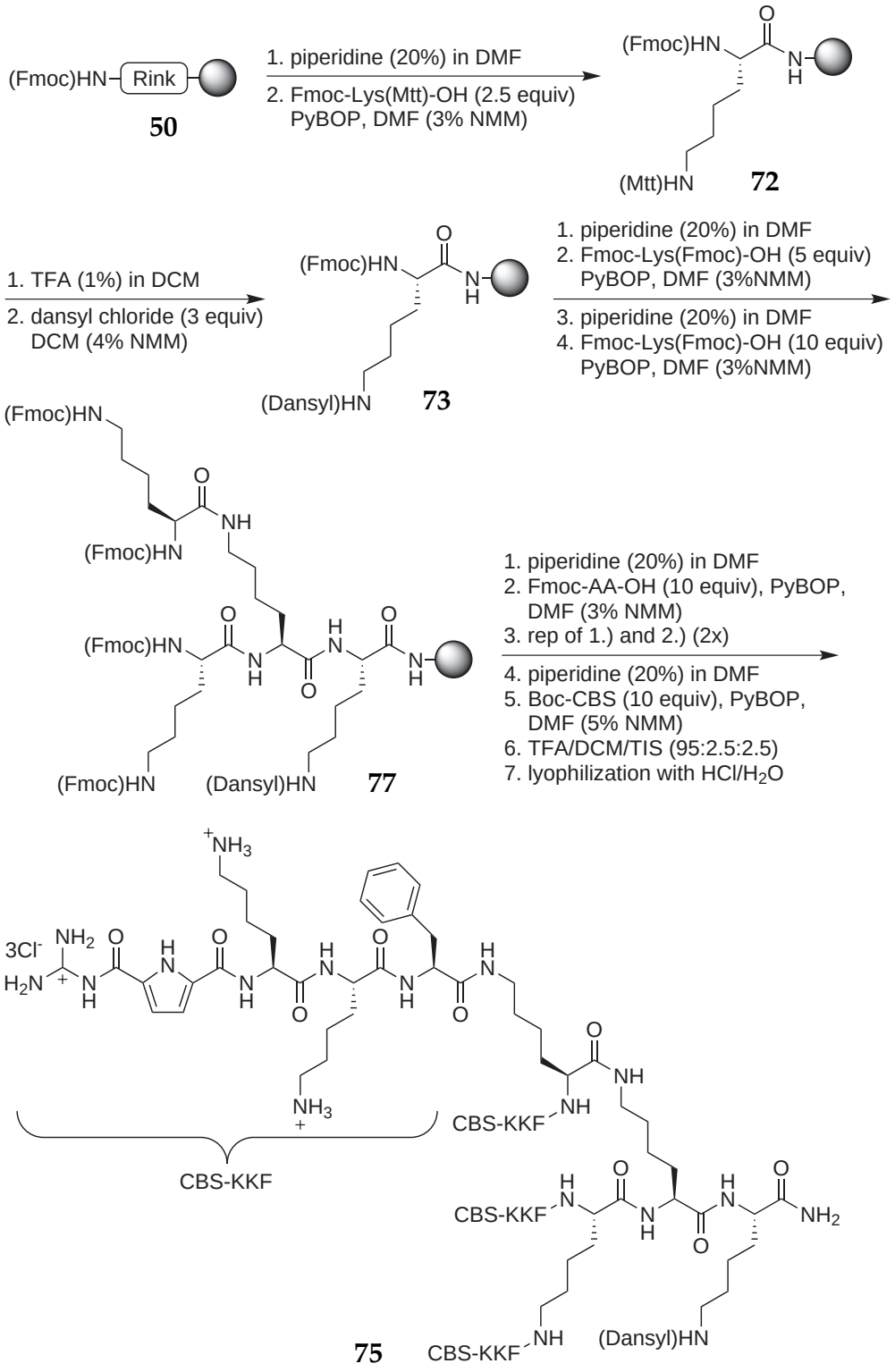

Rink amide resin (100 mg, 720 μmol/g, 72.0 μmol, 1 equiv) was prepared for the attachment of the first amino acid according to the general procedures (see Chapter 7.2.1 on page 165). Then the resin was treated with Fmoc-Lys(Mtt)-OH (112 mg, 180 μmol, 2.5 equiv) and PyBOP (94 mg, 180 μmol, 2.5 equiv) in DMF containing NMM 3 % (10 mL) for 20 h. To remove the side chain protecting group, the resin was treated (2×15 min, 4×5 min) with TFA (1 %) in DCM (10 mL). The deprotection was complete when the filtrate stopped turning yellow. The resin was washed with DCM (3×10 mL), Methanol (3×10 mL) and again with DCM (3×10 mL, 5–10 minutes each) to remove the last traces of TFA. The free amine was coupled with dansyl chloride (58.3 mg, 216 μmol, 3 equiv) in a DCM/DMF mixture (80:20) containing NMM (5 %) for 20 h. After the removal of the Fmoc protection group the resin was allowed to react with Fmoc-Lys(Fmoc)-OH (106 mg, 180 μmol, 2.5 equiv) and PyBOP (93.7 mg, 180 μmol, 2.5 equiv) in DMF containing NMM 3 % (10 mL) for 20 h to introduce the first branching. Then, all Fmoc groups were again removed under standard deprotection conditions and the resin was treated once more with Fmoc-Lys(Fmoc)-OH (213 mg, 360 μmol, 5 equiv) and PyBOP (187 mg, 360 μmol, 5 equiv) in DMF containing NMM 3 % (10 mL) for 20 h. From this step on the Kaiser test showed no consistent results. Resin beads with protected or deprotected amines turned almost into the same blue color. Regardless of these results the synthesis was continued. The following tripeptide sequence was attached under standard conditions for SPPS (see Chapter 7.2.1), each time with 10 equivalents of amino acid to ensure a complete coupling in all four positions: Fmoc-protected amino acid (720 μmol, 10 equiv), PyBOP (375 mg, 720 μmol, 10 equiv) in DMF (10 mL) containing NMM (3 %). The mixture was shaken for 20 h to ensure quantitative coupling. After the final Fmoc deprotection the attachment of the 5-guanidiniocarbonylpyrrole-2-carboxylic acid[122] was performed under related conditions: carboxylic acid (286 mg, 720 μmol, 10 equiv), PyBOP (375 mg, 720 μmol, 10 equiv) and DMF containing 5 % NMM with a reaction time of 20 h. The last step was repeated to ensure quantitative coupling. The product was cleaved from the solid support according to the general procedure for the Rink amide resin (see Chapter 7.2.3 on page 166).

$\mathbf{C_{148}H_{230}Cl_{12}N_{46}O_{26}S}$	3527.20 g·mol^{-1}
yield:	130 mg, 36.8 μmol (51 %)
melting point:	210 °C (decomposition)

^{1}H-NMR (600 MHz, DMSO-d_6): δ [ppm] = 0.99–1.80 (m, 76 H, 35×Lys-CH_2, 2×CH_3), 2.63–3.15 (m, 34 H, 17×Lys-CH_2), 3.98–4.65 (m, 16 H, C*H*), 6.77–8.87 (96 H, 34×ar-C*H* (6.92, 7.21), 20×N*H* (7.50, 8.06, 8.20, 8.23), 9×NH_2 (8.64), 8×NH_3^+ (7.90)), 12.01 (s, 4 H, gua-N*H*), 12.51 (s, 4 H, py-N*H*)

^{13}C-NMR (150 MHz, DMSO-d_6): δ [ppm] = 22.1, 22.6, 22.9, 26.5, 26.6, 28.7, 28.9, 31.1, 31.3, 31.9, 34.3, 37.4, 37.9, 38.6 (bs, 52 C, 52×*C*H$_2$), 45.1 (s, 2 C, 2×*C*H$_3$), 52.5, 52.8, 53.6, 53.9 (m, 16 C, *C*H), 113.6, 115.7 (bs, 8 C, 8×py-CH), 119.7, 128.0, 129.2 (bs, 26 C, 20×Phe-*C*H, 6×dansyl-CH), 117.7, 125.7 (s, 8 C, 8×py-C_q), 132.2 (s, 4 C, 4×Phe-C_q), 132.3, 137.5 (s, 4 C, 4×dansyl-C_q), 155.5 (s, 4 C, 4×gua-C_q), 158.5, 158.7, 159.1, 159.8, 171.2 171.6 (m, 24 C, 24×*C*O-C_q)

MS (pos. ESI, MeOH): m/z = 1545.855, calculated for $C_{148}H_{220}N_{46}O_{26}S^{2+}$ $[M+2H]^{2+}$: 1545.8435

FT-IR (pure): $\tilde{\nu}$ [cm^{-1}] = 3410 (br), 3096 (w), 2940 (w), 2087 (w), 1650 (s), 1542 (s), 1280 (m), 1200 (m), 1145 (m)

Synthesis of (CBS-Lys-Lys-Phe)$_4$(Lys)$_2$-(TEG)$_2$Lys-TEG-Lys(Dansyl)-NH$_2$ (78)
(short form: (CBS-KKF)$_4$-TEG-(Dns))

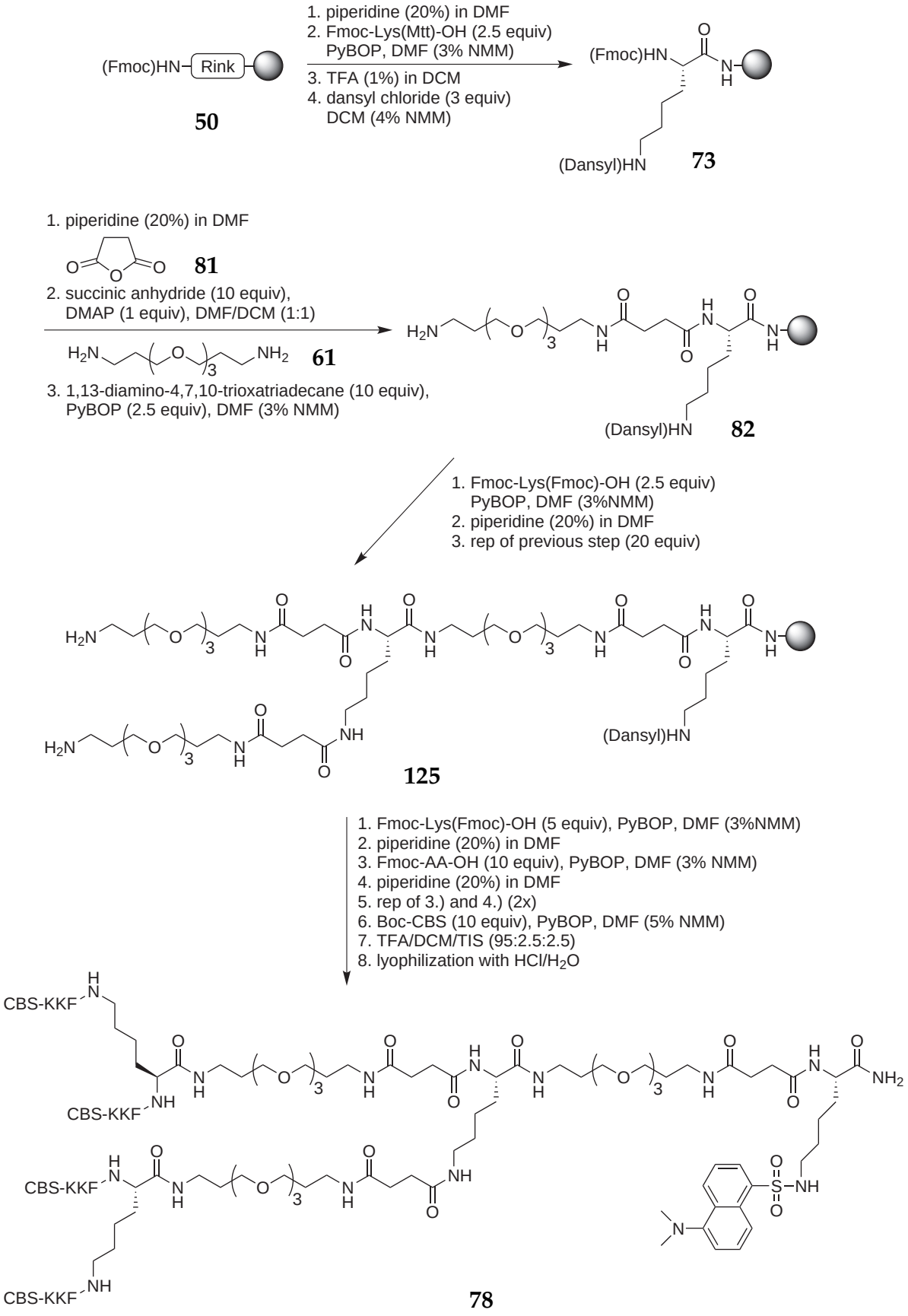

Rink amide resin (100 mg, 720 μmol/g, 72.0 μmol, 1 equiv) was prepared for the attachment of the first amino acid according to the general procedures (see Chapter 7.2.1 on page 165). Then the resin was treated with Fmoc-Lys(Mtt)-OH (109 mg, 180 μmol, 2.5 equiv) and PyBOP (93.7 mg, 180 μmol, 2.5 equiv) in DMF containing NMM 3 % (10 mL) for 20 h. To remove the side chain protecting group, the resin was treated (2×15 min, 4×5 min) with TFA (1 %) in DCM (10 mL). The deprotection was complete when the filtrate stopped turning yellow. The resin was washed with DCM (3×10 mL), Methanol (3×10 mL) and again with DCM (3×10 mL, 5–10 minutes each) to remove the last traces of TFA. The free amine was coupled with dansyl chloride (58.3 mg, 216 μmol, 3 equiv) in a DCM/DMF mixture (80:20) containing NMM (5 %) for 20 h. In the next step the Fmoc protection group was removed by agitation with piperidine in DMF (20 %) twice for 20 min (10 mL each). After the washing succinic anhydride (72.1 mg, 720 μmol, 10 equiv) and DMAP (8.80 mg, 72.0 μmol, 1 equiv) were added in a DMF/DCM (1:1) mixture (10 mL) for 20 h. A malachite green test indicated the successful conversion to the free acid. In the next step 1,13-diamino-4,7,10-trioxatriadecane (159 mg, 0.15 mL, 720 μmol, 10 equiv) and PyBOP (93.7 mg, 180 μmol, 2.5 equiv) in DMF (10 mL) containing NMM (3 %) were added and shaken for 20 h. A negative malachite green and a positive Kaiser test confirmed the complete reaction. In the next step the resin was allowed to react with Fmoc-Lys(Fmoc)-OH (109 mg, 180 μmol, 2.5 equiv) and PyBOP (93.7 mg, 180 μmol, 2.5 equiv) in DMF containing NMM 3 % (10 mL) for 20 h to introduce the first branching. Then, all Fmoc groups were again removed under standard deprotection conditions and the resin was treated once more with succinic anhydride, 1,13-diamino-4,7,10-trioxatriadecane and then again with Fmoc-Lys(Fmoc)-OH, but this time always with twice the equivalents as before. The attachment of the following three amino acids and the 5-guanidiniocarbonylpyrrole-2-carboxylic acid in each of the side chains was performed under analogous conditions as previously described for $(CBS\text{-}KKF)_4$-(Dns) (**75**) (on page 184). The product was cleaved from the solid support according to the general procedure for the Rink amide resin (see Chapter 7.2.3 on page 166).

$\mathbf{C_{190}H_{308}Cl_{12}N_{52}O_{41}S}$	4434.30 g·mol^{-1}
yield:	73.3 mg, 16.5 μmol (24 %)
melting point:	>250 °C (decomposition)

^{1}H-NMR (600 MHz, DMSO-d_6): δ [ppm] = 1.09–1.89 (68 H), 2.20–2.41 (20 H), 2.64–2.86 (14 H), 2.88–3.17 (34 H), 3.26–3.56 (46 H) (m, 182 H, 4×Phe-CH_2, 6×Suc-CH_2, 30×TEG-CH_2, 48×Lys-CH_2, 2×CH_3), 3.98–4.65 (m, 16 H, C*H*), 3.95–4.62 (m, 16 H, C*H*), 6.86–8.83 (102 H, 8×py-C*H* (6.92, 7.24), 1×NH_2 (7.18), 20×Phe-C*H* (7.22), 26×N*H* (7.45, 7.61, 7.65, 7.83, 7.87, 8.11, 8.26, 8.40), 6×dansyl-C*H* (7.85), 8×NH_3^+ (7.98), 8×NH_2 (8.56, 8.72)), 12.17 (s, 4 H, gua-N*H*), 12.54 (s, 4 H, py-N*H*)

^{13}C-NMR (150 MHz, DMSO-d_6): δ [ppm] = 15.2, 20.5, 22.1, 22.6, 22.9, 26.4, 26.5, 28.9, 29.3, 30.7, 30.9, 31.1, 35.8, 38.5, 42.3, 68.0, 69.5, 69.7 (bs, 88 C, 88×*C*H_2), 45.4 (s, 2 C, 2×*C*H_3), 52.3, 52.4, 52.7, 52.8, 53.7, 53.9 (m, 16 C, *C*H), 113.7, 115.8, 116.2, 124.2, 126.3, 127.7, 128.0, 128.4, 128.8, 129.2 (s, 34 C, 20×Phe-*C*H, 6×dansyl-*C*H, 8×py-*C*H), 125.7, 129.0, 132.3, 136.3, 137.6 (s, 16 C, 4×Phe-C_q, 4×dansyl-C_q, 8×py-C_q), 155.6, 158.2, 158.4, 149.0, 159.1, 159.8, 170.6, 170.7, 171.2, 171.3, 171.4, 171.5, 171.7, 173.9 (m, 34 C, 30×*C*O-C_q, 4×gua-C_q)

MS (MALDI, DHB/MeOH 1:5): m/z = 3999.857, calculated for $C_{190}H_{297}N_{52}O_{41}S^+$ $[M+H]^+$: 3997.779

HPLC anal. (*Supelcosil* LC-8, 25 cm × 4.6 mm, 5 μm): 5 min ACN/H_2O 10:90 + 0.1 % TFA, then in 35 min to ACN + 0.1 % TFA, 1.5 mL/min, τ_R = 18.8 min (290 nm)

FT-IR (pure): $\tilde{\nu}$ [cm^{-1}] = 3414 (br,s), 2939 (w), 1649 (s), 1542 (m), 1438 (w), 1278 (w), 1138 (w), 1090 (w)

Synthesis of (CBS-Lys-Lys-Phe)$_4$(Lys)$_2$-(pyArg)$_2$Lys-pyArg-Lys(Dansyl)-NH$_2$ (79)
(short form: (CBS-KKF)$_4$-pyArg-(Dns))

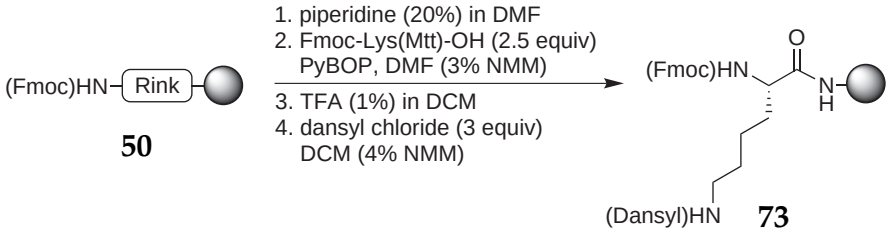

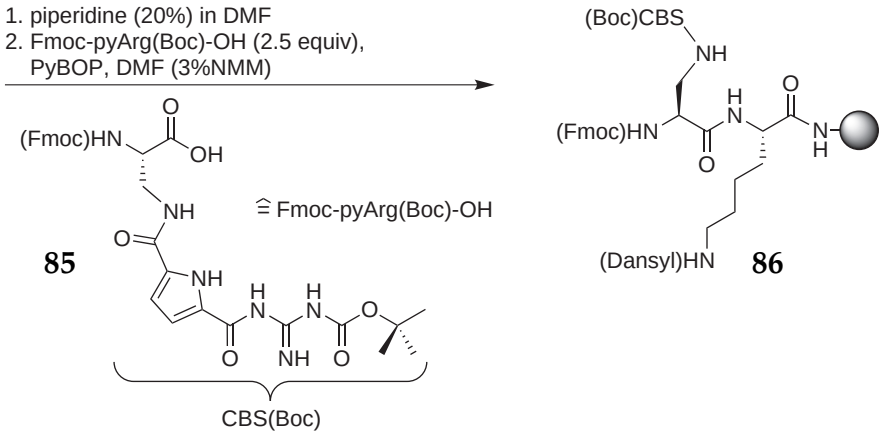

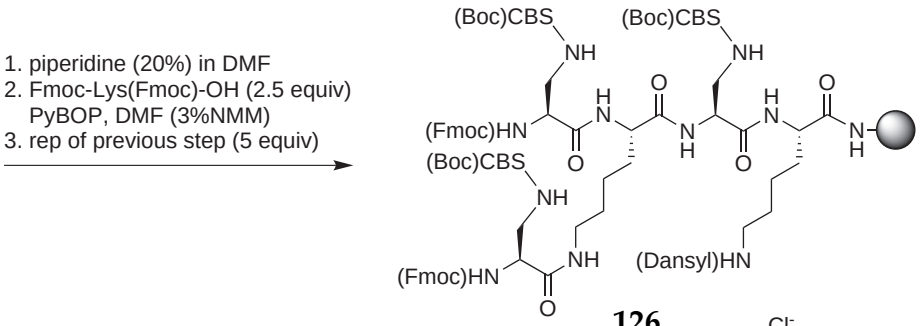

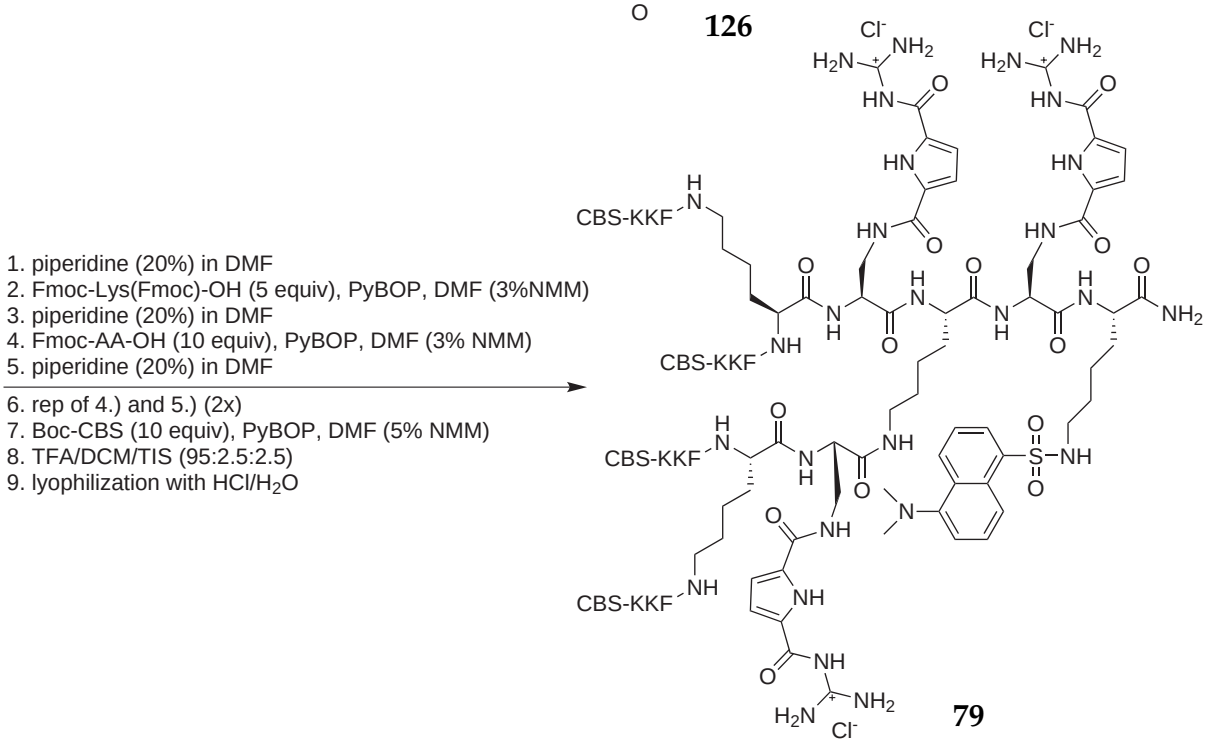

The synthesis of peptide **79** was performed in a similar way as previously described for compound **78** (on page 187). The only difference is, that instead of succinic anhydride and 1,13-diamino-4,7,10-trioxatriadecane this time the Boc-protected arginine analog (**85**) (109 mg, 180 μmol, 2.5 equiv) was incorporated into the lysin branched scaffold. The first time right after the first dansylated lysine and the second time after the first lysine branching with twice the equivalents (218 mg, 360 μmol, 5 equiv). Reaction batch: Rink amide resin (100 mg, 720 μmol/g, 72.0 μmol, 1 equiv)

$\mathbf{C_{178}H_{269}Cl_{15}N_{64}O_{35}S}$	4429.31 g·mol^{-1}
yield:	61.1 mg, 13.8 μmol (20 %)
melting point:	>250 °C (decomposition)

^{1}H-NMR (600 MHz, DMSO-d_6): δ [ppm] = 0.98–1.92 (m, 76 H, 35×Lys-CH_2, 2×CH_3), 2.60–3.14 (m, 40 H, 17×Lys-CH_2, 3×pyArg-CH_2), 3.99–4.70 (m, 19 H, C*H*), 6.64–8.91 (104 H, 14×py-C*H* (6.77, 7.15), 1×NH_2 (7.18), 20×Phe-C*H* (7.22), 26×N*H* (6.92, 7.58, 8.22, 8.28, 8.42), 6×dansyl-C*H* (8.04), 8×NH_3^+ (7.92), 14×NH_2 (8.54, 8.70)), 12.12 (s, 7 H, gua-N*H*), 12.53 (s, 7 H, py-N*H*)

^{13}C-NMR (150 MHz, DMSO-d_6): δ [ppm] = 22.1, 22.5, 22.6, 26.3, 26.5, 28.6, 29.0, 31.1, 31.2, 34.2, 37.4, 37.5 39.6, 39.7 (bs, 55 C, 55×CH_2), 45.1 (s, 2 C, 2×CH_3), 52.4, 52.8, 53.6, 53.9 (m, 16 C, *C*H), 113.6, 115.1, 115.8, 119.2, 123.6, 126.3, 127.9, 129.2 (s, 40 C, 20×Phe-*C*H, 6×dansyl-CH, 14×py-*C*H), 117.7, 119.7, 124.2, 125.6, 129.1, 132.3, 136.1, 137.5 (s, 22 C, 4×Phe-C_q, 4×dansyl-C_q, 14×py-C_q), 151.2, 155.5, 158.0, 158.1, 158.3, 158.4, 159.0, 159.6, 159.8, 170.6, 171.2, 171.6, 176.3 (m, 40 C, 33×*C*O-C_q, 7×gua-C_q)

HPLC anal. (*Supelcosil* LC-8, 25 cm × 4.6 mm, 5 μm): 5 min ACN/H_2O 10:90 + 0.1 % TFA, then in 35 min to ACN + 0.1 % TFA, 1.2 mL/min, τ_R = 14.8 min (295 nm)

FT-IR (pure): $\tilde{\nu}$ [cm^{-1}] = 3400 (br,s), 1654 (s), 1541 (m), 1282 (w), 1200 (w), 1138 (w)

7.4.2 Fluorescence Labelled Multivalent Peptides with Tetrapeptidic Side Chains

Synthesis of (Arg-Lys-Lys-Phe)$_4$(Lys)$_2$Lys-Lys(Dansyl)-NH$_2$ (80)
(short form: (RKKF)$_4$-(Dns))

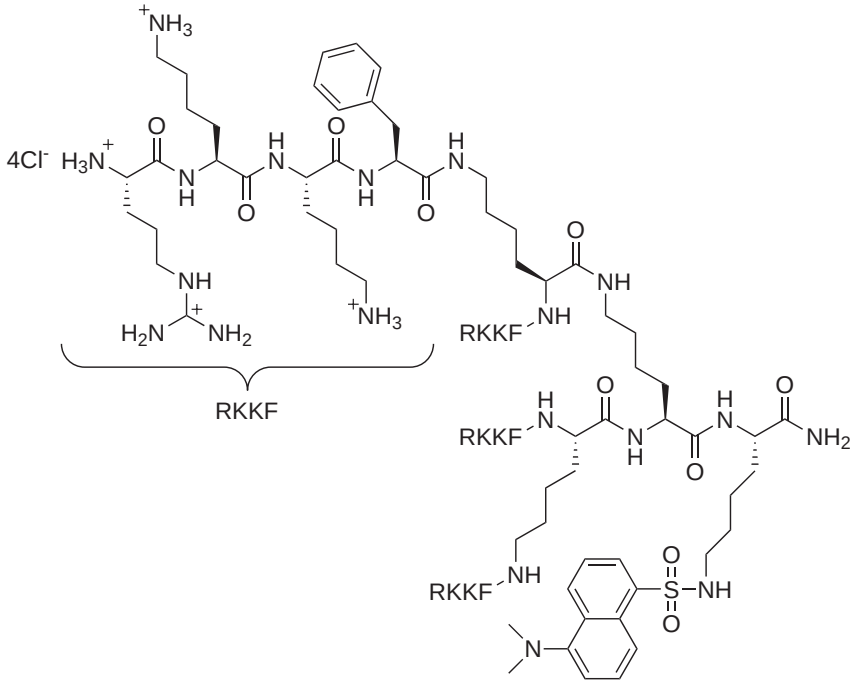

80

The synthesis of peptide **80** was performed under analogous conditions as previously described for (CBS-KKF)$_4$-(Dns) (**75**, on page 184). The only difference is the exchange of the CBS group with an arginine in the final reaction step. Reaction batch: Rink amide resin (100 mg, 720 μmol/g, 72.0 μmol, 1 equiv)

$C_{144}H_{258}Cl_{16}N_{46}O_{22}S$	3585.20 g·mol^{-1}
yield:	144 mg, 40.2 μmol (60 %)
melting point:	>250 °C (decomposition)

^{1}H-NMR (600 MHz, DMSO-d_6): δ [ppm] = 0.94–1.87 (m, 86 H, 40×Lys-CH_2, 2×CH_3), 2.62–3.17 (m, 48 H, 20×Lys-CH_2, 4×Phe-CH_2), 3.76–4.66 (m, 20 H, CH), 6.67–8.87 (104 H, 26×ar-CH (7.11–7.29), 24×NH, 9×NH_2, 12×NH_3^+ (7.90))

^{13}C-NMR (150 MHz, DMSO-d_6): δ [ppm] = 21.0, 21.1, 22.2, 22.3, 25.1, 26.5, 28.7, 29.0, 30.4, 31.3, 31.4, 37.5, 38.0, 38.4, 38.6, 40.4, 42.3 (bs, 64 C, 64×CH_2), 45.1, 46.7 (s, 2 C, 2×CH_3), 51.8, 52.3, 52.6, 52.8, 53.7, 53.9, 54.2 (m, 20 C, 20×CH), 113.9, 115.9, 117.9, 119.9, 129.1, 129.1, 126.1, 137.5, 140.8, 143.7, 143.9 (s, 26 C, 20×Phe-CH, 6×dansyl-CH), 120.2, 123.6, 125.3, 126.3, 127.1, 127.7, 128.1, 129.3 (s, 8 C, 4×Phe-C_q, 4×dansyl-C_q), 151.3, 156.0, 156.9, 158.1, 158.3, 158.5, 158.7, 168.4, 170.6, 170.8, 170.9, 171.3, 171.6, 171.8, 173.6 (m, 24 C, 20×CO-C_q, 4×gua-C_q)

MS (MALDI, HCCA/TA50 1:1): m/z = 3002.897, calculated for $C_{144}H_{243}N_{46}O_{22}S^+$ $[M+H]^+$: 3002.8297

HPLC anal. (*Supelcosil* LC-8, 25 cm × 4.6 mm, 5 μm): 5 min ACN/H_2O 10:90 + 0.1 % TFA, then in 35 min to ACN + 0.1 % TFA, 1.5 mL/min, τ_R = 27.5 min (254 nm)

FT-IR (pure): $\tilde{\nu}$ [cm^{-1}] = 3423 (br,s), 3068 (w), 2945 (w),1655 (s), 1542 (m), 1203 (m), 1135 (m)

7.4.3 Multivalent Peptides Containing the CBS Building Block

Synthesis of (CBS-Lys-Lys-Phe)$_3$TREN (65)
(short form: (CBS-KKF)$_3$)

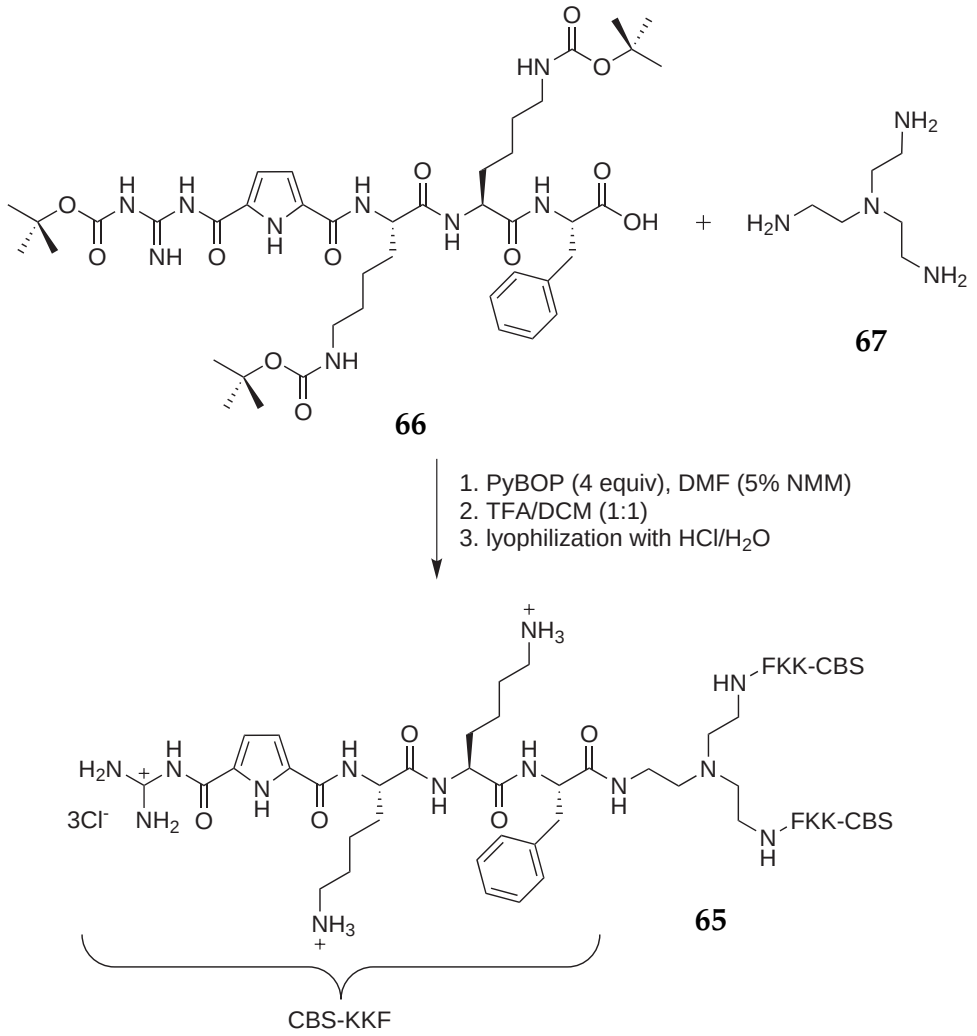

To a solution of peptide compound **66** (53.3 mg, 53.2 μmol, 4 equiv) in DMF (10 ml) containing NMM (3 %), PyBOP (27.7 mg, 53.2 μmol, 4 equiv) and tris-(2-aminoethyl)-amine (TREN) (1.95 mg, 13.3 μmol, 1 equiv) were added. The reaction mixture was stirred for 20 h at room temperature before water (20 mL) was added. The colorless precipitate was filtered and directly used for the following step. The Boc-deprotection was performed in a 1:1 mixture (10 mL) of DCM and TFA. The solution was stirred for 1 h and then concentrated in vacuo. To obtain the colorless hydrochloride salt (**65**), the solid was dissolved in water (40 mL), acidified with hydrochloric acid (0.1 N, 4 mL) and lyophilized.

$C_{90}H_{144}Cl_9N_{31}O_{15}$	2219.38 g·mol^{-1}
yield:	8.10 mg, 3.65 μmol (28 %)
melting point:	220 °C (decomposition)

^{1}H-NMR (600 MHz, DMSO-d_6): δ [ppm] = 1.07–1.82 (m, 48 H, 18×Lys-CH_2, 6×TREN-CH_2), 2.65–2.86 (m, 18 H, 6×Lys-CH_2, 3×CH_2Ph), 4.12–4.31 (m, 3 H, 3×CH), 4.36–4.64 (m, 6 H, 6×CH), 6.79 (bs, 3 H, 3×py-CH), 7.19 (s, 3 H, 3×py-CH), 7.12–7.40 (m, 15 H, 15×Phe-CH), 7.57 (3 H, 3×NH), 7.73–8.12 (br, 24 H, 8×NH_3^+), 7.80 (3 H, 3×NH), 8.26 (3 H, 3×NH), 8.46 (bs, 6 H, 3×gua-NH_2), 8.67 (bs, 6 H, 3×gua-NH_2), 12.01 (bs, 3 H, 3×gua-NH), 12.53 (s, 3 H, 3×py-NH)

^{13}C-NMR (150 MHz, DMSO-d_6): δ [ppm] = 22.1, 22.5, 26.4, 26.6, 28.6, 29.0, 31.1, 31.3, 38.5 (24×Lys-CH_2, 3×Phe-CH_2, 6×TREN-CH_2), 51.4, 52.5, 52.8, 54.1 (9×CH), 113.6, 115.8 (6×py-CH), 126.3, 128.0, 129.3 (15×Phe-CH), 132.3 (3×Phe-C_q), 155.5, 159.0 (6×py-C_q), 159.0, 160.5 (6×py-CO-C_q), 171.2, 171.4, 171.6 (9×CO-C_q)

HPLC prep. (*Varian* Microsorb C18, 25 cm × 4.6 mm, 5 μm): for 2 min MeOH/H_2O 10:90 + 0.1 % TFA, then over 38 min to MeOH/H_2O 90:10 + 0.1 % TFA, 1.2 mL/min, τ_R = 13.8 min, rel. area 97 % (300 nm)

MS (pos. ESI, MeOH): m/z = 1892.542, calculated for $C_{90}H_{136}N_{31}O_{15}^+$ $[M+H]^+$: 1892.241

FT-IR (pure): $\tilde{\nu}$ [cm^{-1}] = 3149 (w), 2982 (w), 2879 (w) 1702 (s), 1654 (s) 1541 (m), 1472 (w), 1276 (w), 1198 (w), 815 (w), 754 (w)

Synthesis of (CBS-Lys-Lys-Phe)$_4$(Lys)$_2$Lys-NH$_2$ (90)

(short form: (CBS-KKF)$_4$)

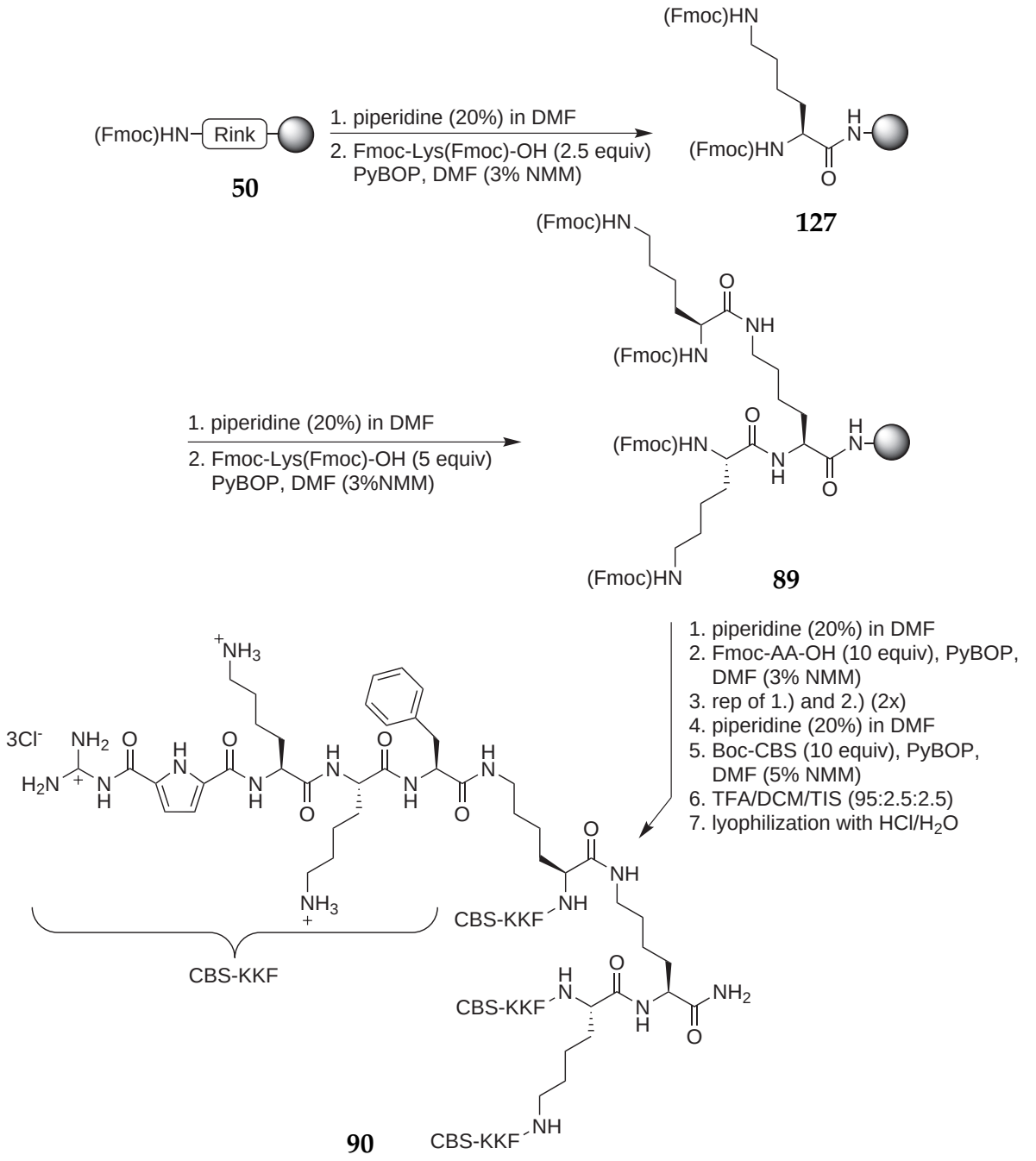

Rink amide resin (100 mg, 940 μmol/g, 94.0 μmol, 1 equiv) was prepared for the attachment of the first amino acid according to the general procedures (see Chapter 7.2.1 on page 165). Then the resin was allowed to react with Fmoc-Lys(Fmoc)-OH (139 mg, 235 μmol, 2.5 equiv) and PyBOP (122 mg, 235 μmol, 2.5 equiv) in DMF containing NMM 3 % (10 mL) for 20 h to introduce the first branching. Again, all Fmoc groups were removed under standard deprotection conditions and the resin was treated once more

with Fmoc-Lys(Fmoc)-OH (278 mg, 470 μmol, 5 equiv) and PyBOP (245 mg, 470 μmol, 5 equiv) in DMF containing NMM 3 % (10 mL) for 20 h. From this step on the Kaiser test showed no consistent results. Resin beads with protected or deprotected amines turned almost into the same blue color. Regardless of these results the synthesis was continued. The following tripeptide sequence was attached under standard conditions for SPPS (see Chapter 7.2.1), each time with 10 equivalents of amino acid to ensure a complete coupling in all four positions: Fmoc-protected amino acid (940 μmol, 10 equiv), PyBOP (489 mg, 940 μmol, 10 equiv) in DMF (10 mL) containing NMM (3 %). The mixture was shaken for 20 h to ensure quantitative coupling. After the final Fmoc deprotection the attachment of the 5-guanidiniocarbonylpyrrole-2-carboxylic acid[122] was performed under related conditions: carboxylic acid (374 mg, 940 μmol, 10 equiv), PyBOP (489 mg, 940 μmol, 10 equiv) and DMF containing 5 % NMM with a reaction time of 20 h. The last step was repeated to ensure quantitative coupling. The product was cleaved from the solid support according to the general procedure for the Rink amide resin (see Chapter 7.2.3 on page 166) and further purified by RP-HPLC (MeOH/H_2O + 0.1 % TFA; 40/60).

$\mathbf{C_{130}H_{207}Cl_{12}N_{43}O_{23}}$	3165.75 g·mol^{-1}
yield:	94.5 mg, 29.5 μmol(32 %)
melting point:	192 °C (decomposition)

^{1}H-NMR (600 MHz, DMSO-d_6): δ [ppm] = 0.94–1.93 (m, 64 H, 32×Lys-CH_2), 2.63–3.15 (m, 32 H, 12×Lys-CH_2, 4×Phe-CH_2), 3.93–4.71 (m, 15 H, C*H*), 6.74–8.95 (m, 88 H, 28×ar-C*H*, 18×N*H*, 9×NH_2, 8×NH_3^+), 12.17 (s, 4 H, gua-N*H*), 12.53 (s, 4 H, py-N*H*)

^{13}C-NMR (150 MHz, DMSO-d_6): δ [ppm] = 22.1, 22.6, 22.7, 26.2, 26.4, 26.6, 28.3, 28.7, 28.8, 30.3, 31.1, 31.7, 31.9, 36.9, 37.1, 38.3, 38.6, 44.6 (bs, 48 C, 48×CH_2), 51.7, 51.8, 52.4, 52.5, 52.6, 52.8, 52.9, 53.4, 53.5, 53.6, 53.9, 54.3, 54.4, 54.7 (m, 15 C, C*H*), 113.6, 115.8 (bs, 8 C, 8×py-C*H*), 126.3, 126.4, 127.1, 128.0, 128.2, 128.5, 129.3, 129.6 (bs, 20 C, 20×Phe-C*H*), 125.6, 132.3, 135.0, 137.6, 155.5, 159.0, 159.8, 167.6, 168.4, 170.6, 171.1, 171.6, 173.7 (bs, 39 C, 23×*C*O-C_q, 16×ar-C_q)

MS (MALDI, DHB/HCCA 1:1, MeOH,H_2O): m/z = 2876.552
calculated for $C_{130}H_{200}Cl_4N_{43}O_{23}^+$ [M+4HCl+H]$^+$: 2875.0648

FT-IR (pure): $\tilde{\nu}$ [cm^{-1}] = 3243 (br), 3046 (br), 2918 (br), 2087 (w), 1644 (s), 1526 (s), 1450 (m)

Synthesis of (CBS-Trp-His-Arg)$_4$(Lys)$_2$Lys-NH$_2$ (92)
(short form: (CBS-WHR)$_4$)

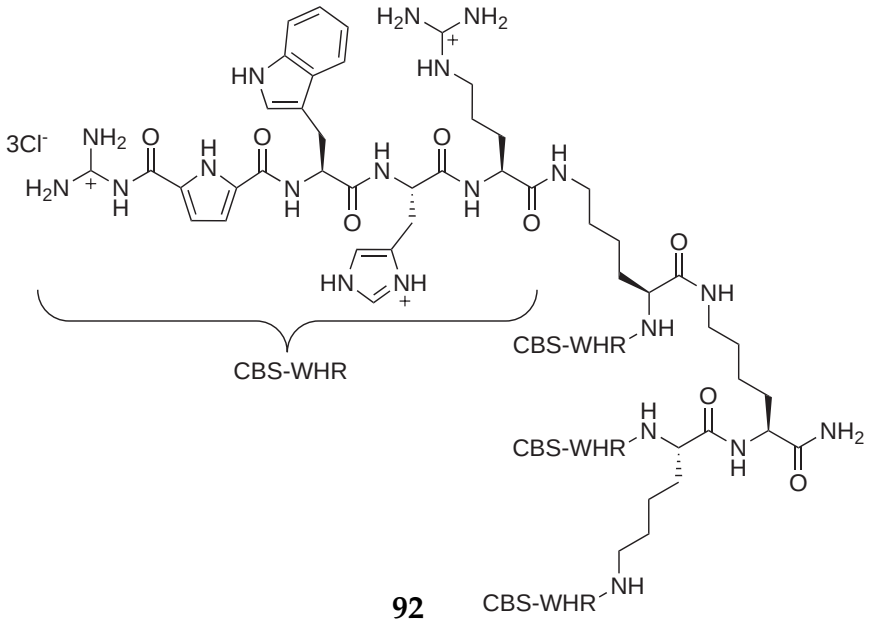

92

The synthesis of (CBS-WHR)$_4$ (**92**) was performed under analogous conditions as previously described for (CBS-KKF)$_4$ (**90**). Reaction batch: Rink amide resin (100 mg, 940 μmol/g, 94.0 μmol, 1 equiv)

$C_{138}H_{191}Cl_{12}N_{59}O_{23}$	3469.81 g·mol^{-1}
yield:	57.1 mg, 16.5 μmol (17 %)
melting point:	199 °C (decomposition)

^{1}H-NMR (600 MHz, DMSO-d_6): δ [ppm] = 1.05–1.96, 2.67–3.24 (m, 64 H, 12×Lys-CH_2, 4×Trp-CH_2, 4×His-CH_2, 12×Arg-CH_2), 3.97–4.49 (m, 15 H, C*H*), 6.70–9.25 (m, 96 H, 36×ar-C*H*, 26×N*H*, 17×NH_2), 12.16 (s, 4 H, gua-N*H*), 12.55 (s, 4 H, py-N*H*), 14.46 (bs, 8 H, His-N*H*)

^{13}C-NMR (150 MHz, DMSO-d_6): δ [ppm] = 20.4, 20.9, 21.2, 21.7, 22.1, 22.7, 23.7, 24.2, 25.0, 26.3, 26.4, 28.2, 28.3, 28.7, 29.9, 30.4, 30.6, 31.5, 32.5, 38.3, 38.4, 41.4, 43.6, 44.6 (bs, 32 C, 32×CH_2), 113.7, 115.9, 116.9, 117.7, 118.1, 118.2, 133.6, 133.9, 134.0, 134.1, 134.2 (bs, 36 C, 8×ar-CH, 8×His-CH, 20×Trp-CH), 124.2, 125.8, 126.6, 126.9, 155.6, 156.9, 157.0, 159.0, 165.5, 165.8, 166.8, 166.9, 167.2, 167.4, 168.2, 168.3, 171.3, 171.4, 173.0, 173.3, 173.9 (bs, 55 C, 23×*C*O-C_q, 32×C_q)

MS (MALDI, DHB/HCCA 1:1, MeOH,H_2O): m/z = 3033.564
calculated for $C_{138}H_{180}N_{59}O_{23}^{+}$ $[M+H]^{+}$: 3033.287

FT-IR (pure): $\tilde{\nu}$ [cm^{-1}] = 3230 (br), 3140 (br), 1659 (s), 1540 (s), 1453 (m), 1275 (w), 1070 (m), 820 (w)

7.4.4 Multivalent Peptides with Tetrapeptidic Side Chains

Synthesis of (Lys-Lys-Phe-Gly)$_4$(Lys)$_2$Lys-NH$_2$ (106)
(short form: (KKFG)$_4$)

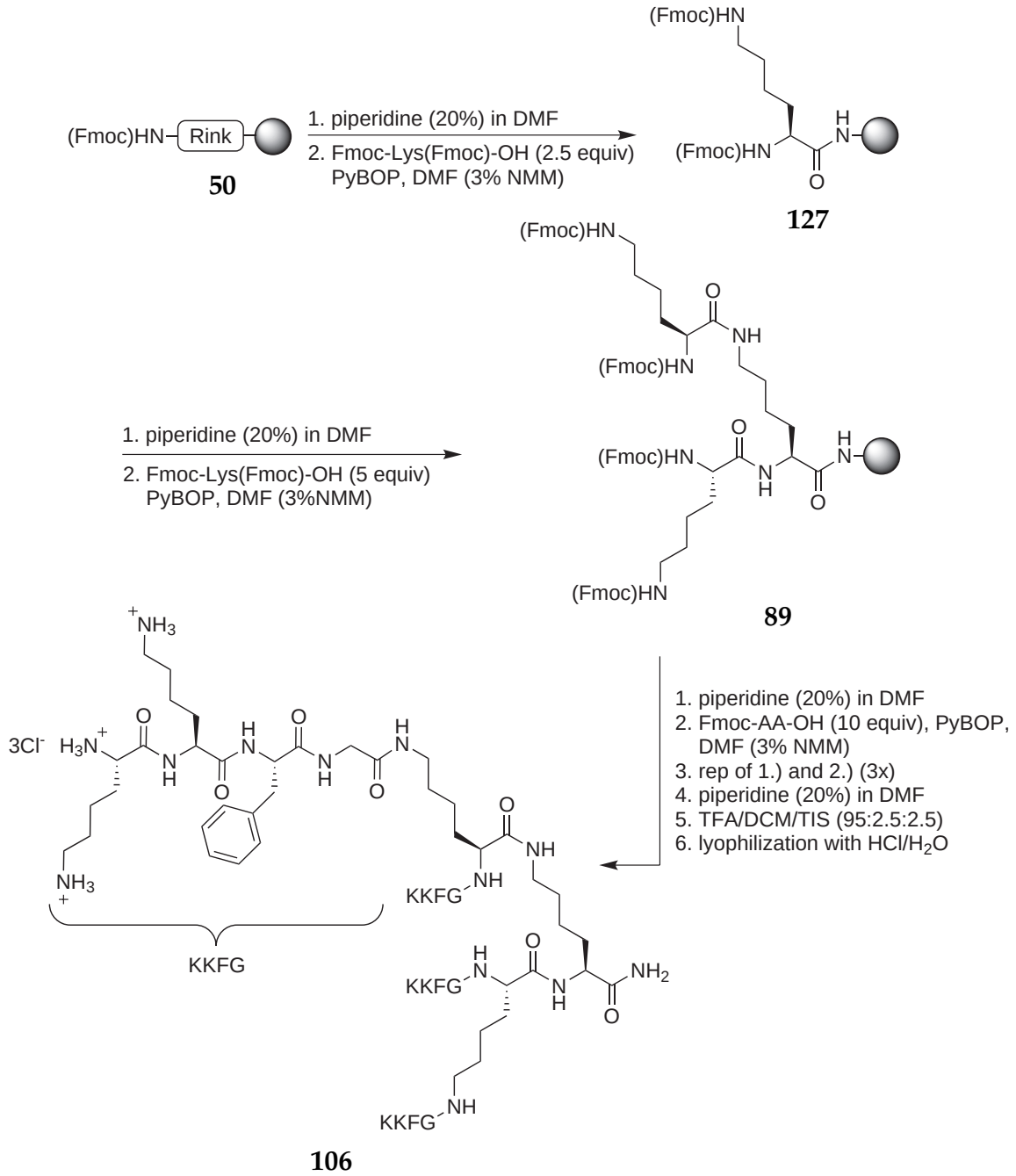

Rink amide resin (100 mg, 940 μmol/g, 94.0 μmol, 1 equiv) was prepared for the attachment of the first amino acid according to the general procedures (see Chapter 7.2.1 on page 165). Then the resin was allowed to react with Fmoc-Lys(Fmoc)-OH (278 mg,

470 μmol, 5 equiv) and PyBOP (245 mg, 470 μmol, 5 equiv) in DMF containing NMM 3 % (10 mL) for 20 h to introduce the first branching. Again, all Fmoc groups were removed under standard deprotection conditions and the resin was treated once more with Fmoc-Lys(Fmoc)-OH (555 mg, 940 μmol, 10 equiv) and PyBOP (489 mg, 940 μmol, 10 equiv) in DMF containing NMM 3 % (10 mL) for 20 h. From this step on the Kaiser test showed no consistent results. Resin beads with protected or deprotected amines turned almost into the same blue color. Regardless of these results the synthesis was continued. The following tetrapeptide sequence was attached under standard conditions for SPPS (see Chapter 7.2.1), each time with 10 equivalents of amino acid to ensure a complete coupling in all four positions: Fmoc-protected amino acid (940 μmol, 10 equiv), PyBOP (489 mg, 940 μmol, 10 equiv) in DMF (10 mL) containing NMM (3 %). The mixture was shaken for 20 h to ensure quantitative coupling. After the final Fmoc deprotection the product was cleaved from the solid support according to the general procedure for the Rink amide resin (see Chapter 7.2.3 on page 166).

$C_{110}H_{195}Cl_{12}N_{31}O_{19}$ 2681.36 g·mol^{-1}
yield: 105 mg, 393 μmol (41 %)
melting point: 185 °C (decomposition)

^{1}H-NMR (600 MHz, DMSO-d_6): δ [ppm] = 1.05–1.95 (m, 64 H, 32×Lys-CH_2), 2.63–3.15 (m, 32 H, 12×Lys-CH_2, 4×Phe-CH_2) 3.56–3.96 (m, 8 H, 4×Gly-CH_2), 4.05–4.63 (m, 15 H, CH), 6.88–7.50 (m, 28 H, 4×Phe-CH, 6×NH, 1×NH_2), 7.63–9.08 (m, 48 H, 12×NH, 12×NH_3^+)

^{13}C-NMR (150 MHz, DMSO-d_6): δ [ppm] = 21.0, 22.1, 22.8, 26.2, 26.4, 28.7, 30.3, 31.3, 31.8, 36.8, 37.5, 38.3, 40.0, 42.0 (bs, 52 C, 52×CH_2), 51.7, 52.7, 53.5, 54.0, 54.5 (m, 15 C, 15×CH), 126.3, 127.1, 128.1, 128.5, 129.2, 129.5 (bs, 20 C, 20×Phe-CH), 137.6 (s, 4 C, 4×Phe-C_q, 168.3, 168.7, 171.0, 171.2, 171.4, 173.8 (bs, 19 C, 19×CO-C_q)

MS (MALDI, DHB/HCCA 1:1, MeOH, TA50): m/z = 2244.450
calculated for $C_{110}H_{184}N_{31}O_{19}^+$ [M+H]$^+$: 2244.833

FT-IR (pure): $\tilde{\nu}$ [cm^{-1}] = 3236 (br), 3040 (br), 2920 (br), 2103 (w), 1651 (s), 1524 (s), 1443 (w), 1236 (m)

Synthesis of (Arg-Trp-Lys-Gly)$_4$(Lys)$_2$Lys-NH$_2$ (107)
(short form: (RWKG)$_4$)

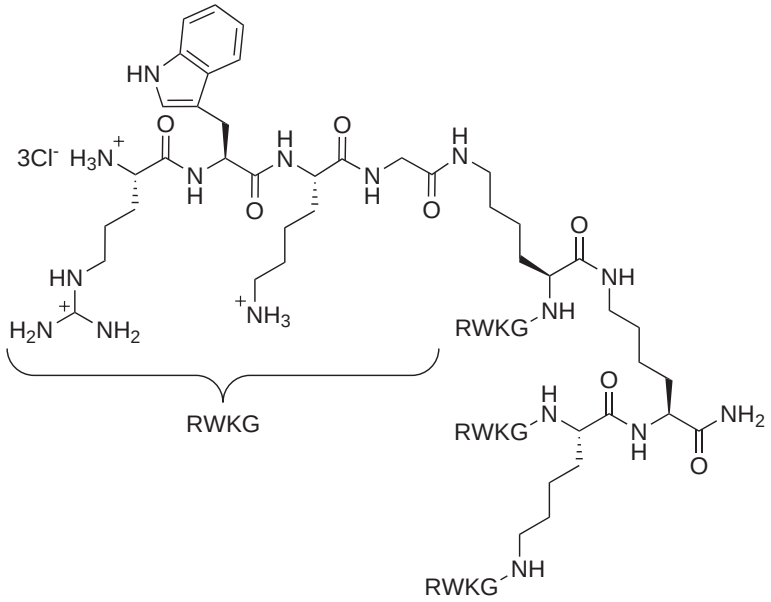

107

The synthesis of (Arg-Trp-Lys-Gly)$_4$(Lys)$_2$Lys-NH$_2$ (**107**) was performed under analogous conditions as (Lys-Lys-Phe-Gly)$_4$(Lys)$_2$Lys-NH$_2$ (**106**). Reaction batch: Rink amide resin (100 mg, 940 μmol/g, 94.0 μmol, 1 equiv)

$C_{118}H_{199}Cl_{12}N_{43}O_{19}$	2949.56 g·mol^{-1}
yield:	87.4 mg, 29.6 μmol (31 %)
melting point:	195 °C (decomposition)

^{1}H-NMR (600 MHz, DMSO-d_6): δ [ppm] = 1.02–1.91, 2.86–3.20 (m, 80 H, 15×Arg-CH_2, 25×Lys-CH_2), 2.66–2.84 (m, 8 H, 4×Trp-CH_2), 3.44–4.52 (m, 23 H, 8×Gly-CH_2, 15×Trp-CH), 6.80–7.49 (m, 20 H, 20×Trp-CH), 7.77–8.51 (m, 58 H, 16×NH, 9×NH_2, 8×NH_3^+), 8.76–9.12 (m, 6 H, 6×NH), 11.05 (s, 4 H, 4×gua-NH)

^{13}C-NMR (150 MHz, DMSO-d_6): δ [ppm] = 20.9, 22.1, 22.5, 22.7, 23.6, 24.0, 26.3, 27.1, 28.6, 30.1, 20.1, 31.2, 31.6, 38.1, 38.3, 38.4, 41.8, 41.9, 44.4 (bs, 48 C, 48×CH_2), 51.7, 51.8, 52.4, 52.5, 52.6 (bs, 15 C, 15×CH), 106.8, 127.1, 136.3 (2×Trp-C_q), 111.3, 118.3, 120.9, 124.9 (s, 20 C, 20×Trp-CH), 157.0 (s, 4 C, 4×Arg-C_q), 165.6, 167.9, 168.4, 168.5, 168.9, 171.1, 171.3, 171.4, 173.7, 173.8, 177.2 (bs, 19 C, 19×CO-C_q)

MS (MALDI, DHB, MeOH/TA50): m/z = 2513.102, calculated for $C_{118}H_{188}N_{43}O_{19}^{+}$ $[M+H]^{+}$: 2513.031

FT-IR (pure): $\tilde{\nu}$ [cm^{-1}] = 3227 (br), 3038 (br), 2930 (br), 2356 (m), 2334 (w), 2163 (w), 1647 (s), 1539 (s), 1459 (w), 1240 (m), 995 (m)

7.4.5 Synthesis of a Combinatorial Inhibitor Library for Tryptase

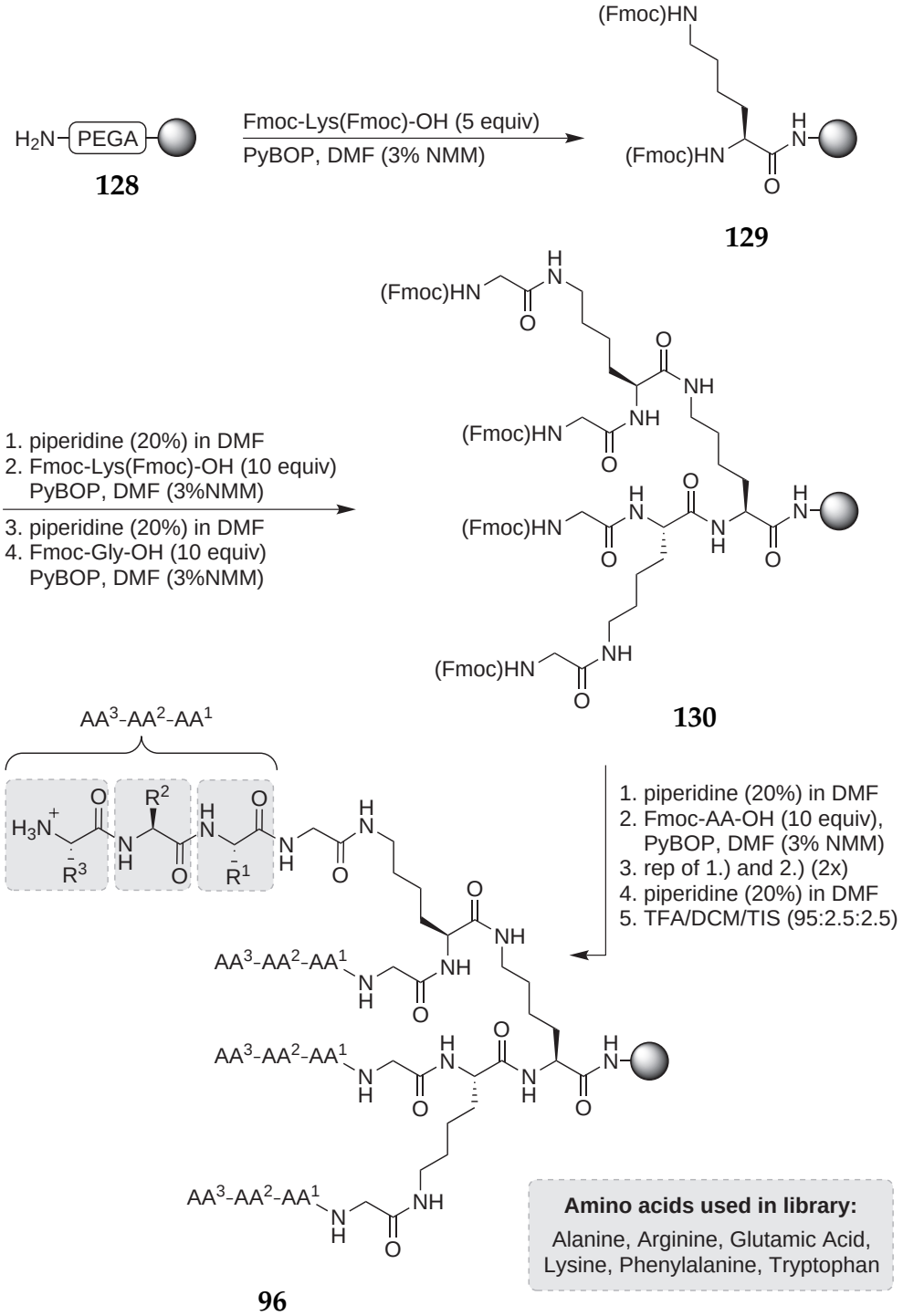

The amino-PEGA resin (*Novabiochem*) is very hygroscopic and had to be dried prior the distribution to the 216 *IRORI MicroKans* of the combinatorial library. Therefore the resin (7.13 g, 400 μmol/g, 2.85 mmol, 1 equiv; correlating to 30 mg per *MicroKan* +10 % extra)

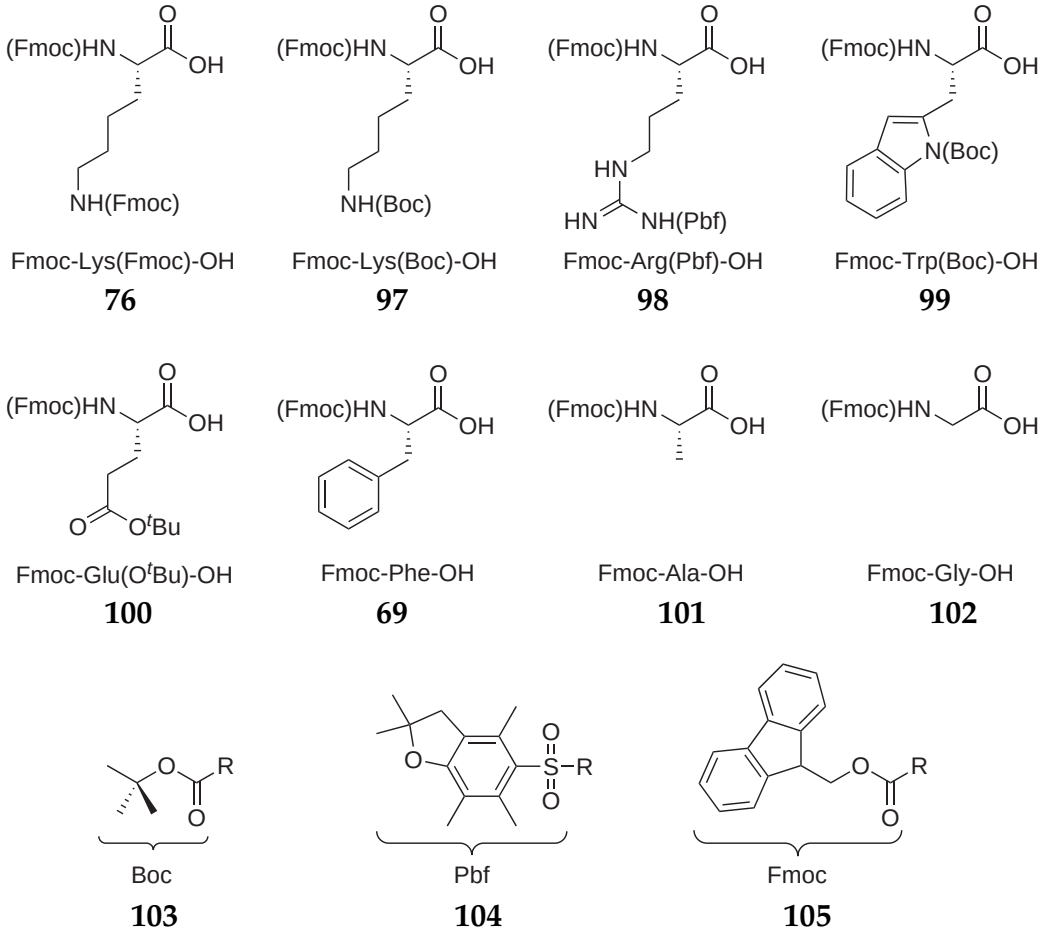

Figure 7.1: *Amino acids and protecting groups used in the synthesis of the combinatorial inhibitor library (**96**).*

was washed with MeOH and DCM and dried in high vacuum (3–4 h). To distribute the resin equally to the *MicroKans*, a mixture of DCM and Hexan (9:1, 216 mL) was prepared and the resin suspended. Due to the fact that the resin had the same density of the mixture (isopycnic principle) it was possible to handle the resin as a "solution" and therefore to portion it out in 1 mL fractions with an micropipette. Hence, the average *MicroKan* was loaded with approx. 30–33 mg of resin to give a theoretical yield of ca. 13.2 μmol/Kan. All micro-reactors were equipped with an *IRORI AccuTag* radio frequency chip and scanned with the computer according to the *IRORI* synthesis software.

STEP 1: Prior to the first reaction all *MicroKans* were washed with fresh DMF and allowed to swell for 3 h. The 216 *MicroKans* were portioned into three glass shaking reactors á 72 Kans in order to attach the first amino acid. For the first coupling the resin was allowed to react with Fmoc-Lys(Fmoc)-OH (total for 216 Kans: 8.42 g, 14.3 mmol, 5 equiv) and PyBOP (total for 216 Kans: 7.42 g, 14.3 mmol, 5 equiv) in DMF (80 mL per

glass reactor) containing 3 % NMM for 20 h to introduce the first branching. The next day, the resin was washed with DMF (2×50 mL per glass reactor) and the last reaction step was repeated with 3 equivalents of reagents. The resin was washed with DMF (3× 50 mL) and a Kaiser test was performed to determine if the coupling step was complete. For the Fmoc deprotection the *MicroKans* were agitated in DMF containing 20 % piperidine (2×70 mL per glass reactor, 2×60 min) followed by thorough washing steps to remove all traces of piperidine (3×DMF, 3×DCM and again 4×DMF, 5–10 minutes each)

STEP 2: In the second coupling step all the library members were treated once more with Fmoc-Lys(Fmoc)-OH (total for 216 Kans: 16.8 g, 28.5 mmol, 10 equiv) and PyBOP (total for 216 Kans: 14.8 g, 28.5 mmol, 10 equiv) in DMF (80 mL per glass reactor) containing 3 % NMM for 20 h. Again the coupling step was repeated, this time with 6 equivalents of reagents. A negative Kaiser test confirmed the quantitative coupling and permitted the following Fmoc deprotection as described before.

STEP 3: As first amino acid after the lysine scaffold glycine was introduced in all library members. Therefore the resin was allowed to react with Fmoc-Gly-OH (total for 216 Kans: 8.48 g, 28.5 mmol, 10 equiv) and PyBOP (total for 216 Kans: 14.8 g, 28.5 mmol, 10 equiv) in DMF (80 mL per glass reactor) containing 3 % NMM for 20 h. This coupling step was repeated overnight with the same amounts of reagents, followed by a short washing step, Kaiser test and the Fmoc deprotection.

STEP 4: Prior to the next coupling step the 216 *MicroKans* were split according to the *IRORI* software in six separate portions (á 36 Kans) for the introduction of the following amino acids: lysine, arginine, tryptophan, glutamic acid, phenylalanine and alanine. All amino acids were coupled under standard conditions, each time with 10 equivalents to ensure a complete coupling: Fmoc-protected amino acid (each vessel á 36 Kans: 4.75 mmol, 10 equiv), PyBOP (each vessel á 36 Kans: 2.47 g, 4.75 mmol, 10 equiv) in DMF (50 mL per glass reactor) containing 3 % NMM. This coupling step was repeated overnight with the same amounts of reagents.

STEP 5+6: The second (AA^2) and third (AA^3) combinatorial varied position in the library was introduced by repeating of step no. 4 according to the previous protocol. As during the synthesis of the multivalent peptides in solution, the Kaiser tests showed no consistent results in step no. 4–5, but due to the good results of the previous model systems in solution the synthesis was continued.

STEP 7: After the final Fmoc deprotection the library was prepared for the concluding deprotection of all amino acid side chain protecting groups. In addition to the normal washing steps to remove piperidine three extra washing steps with DCM were added, followed by the complete drying of the resin in high vacuum at RT. Due to the high stability of PEGA resin towards acids, all library members were agitated in a mixture of TFA/triisopropylsilane/H_2O (95:2.5:2.5, 2×2 h) to remove all protecting groups without any detachment of product from the resin. To remove all traces of trifluoroacetic acid, the library was washed several times with diluted hydrochloric acid (0.1 N) and water until a neutral pH value of the filtrate. Unfortunately it cannot be avoided to loose a significant amount of resin during this step due to the intensive washing cycles.

7.5 Inhibitor Assays

The following chapter describes the details of the enzyme assays with inhibitors in solution and the screening of the combinatorial inhibitor library.

7.5.1 General Experimental Remarks

All concentrations mentioned in the protocols are final concentrations (of all reagents during the screening). Used abbreviations: E = enzyme, S = substrate, B = buffer, I = inhibitor.

The following equipment, enzymes, substrates and reagents were used in the inhibitor assays:

Fluorescence well plate readout

Equipment: *Varian* Cary Eclipse Fluorescence spectrophotometer with microplate reader unit
Nunc FluoroNunc white 96 well plates (Cat. No. 136101)

Substrates

Tos-Gly-Pro-Arg-AMC:	*Bachem*, catalog no. I-1365 (for tryptase assay)
Z-Phe-Arg-AMC:	*Bachem*, catalog no. I-1160 (for trypsin assay)
Suc-Leu-Tyr-AMC:	*Bachem*, catalog no. I-1355 (for chymotrypsin assay)

Reagents

p-Aminobenzamidine:	*Bachem*, catalog no. Q-1960
Glycerol:	*Fluka*, BioUltra anhydrous, catalog no. 49767
Heparin:	*Sigma-Adrich*, catalog no. H3149 sodium salt from porcine intestinal
Trizma hydrochloride:	*Sigma-Adrich*, reagent grade, catalog no. T3253
Triton X-100:	*Sigma-Adrich*

Enzymes

rhSkin β-tryptase (human):	*Promega*, catalog no. G7061, conc.: 200 μg/mL
rhLung β-tryptase (human):	*Promega*, catalog no. G5631, conc.: 2 mg/mL
Trypsin (bovine pancreas):	*Merck*
α-Chymotrypsin (bovine pancreas):	*Merck*

Both forms of tryptase were commercial available and delivered in single vials (each 100 μg). They had to be aliquoted for a comfortable use during the enzyme assays. Each enzyme was diluted to a concentration of 0.1 mg/ml resulting in 50 vials, each containing 2 μg of protein (50$\times$20μL). To obtain the required dilution 0.5 mL of formulation mixture (for rhSkin-tryptase) and 0.95 mL of formulation mixture (for rhLung-tryptase) were needed:

rhSkin β-Tryptase

reagent	**amount**
MES	10.0 mM, 19.5 mg
NaCl	200 mM, 117 mg
Heparin	500 μg/mL, 5.00 mg
Glycerol	10 %, 1.00 mL
dest. H_2O	9.00 mL

rhLung β-Tryptase

reagent	**amount**
MES	10.0 mM, 19.5 mg
NaCl	2.00 M, 1.17 g
dest. H_2O	10.0 mL

Buffer solutions

Depending on the enzyme different buffer systems had to be used. The following tables list the compositions (for 500 mL) and the adjusted pH value:

rhSkin β-Tryptase (pH = 7.4)

reagent	**amount**
Tris	50.0 mM, 3.03 g
NaCl	100 mM, 2.92 g
Heparin	50.0 μg/ml, 250 μg
Triton-X	0.02 %, 100 μL
dest. H_2O	500 mL

rhLung β-Tryptase (pH = 7.4)

reagent	**amount**
Tris	50.0 mM, 3.03 g
NaCl	100 mM, 2.92 g
Triton-X	0.02 %, 100 μL
dest. H_2O	500 mL

Trypsin (pH = 8.0)

reagent	**amount**
Tris	50.0 mM, 3.03 g
NaCl	100 mM, 2.92 g
EDTA	5.00 mM, 731 μg
dest. H_2O	500 mL

α-Chymotrypsin (pH = 8.0)

reagent	**amount**
Tris	50.0 mM, 3.03 g
NaCl	100 mM, 2.92 g
EDTA	5.00 mM, 731 μg
dest. H_2O	500 mL

7.5.2 Screening in Solution

Determination of IC_{50} and K_i

To reveal the potential as inhibitor all synthesized peptides were tested at a concentration of 100 μM at first. If the inhibition was higher than 80 % also the half maximal inhibitory concentration (IC_{50}) and the absolute inhibition constant (K_i) was determined at varying inhibitor concentrations.

The following settings at the fluorescence spectrophotometer were used for all inhibitor assays:

Spectrophotometer Settings

ex. wavelength	380 nm
em. wavelength	460 nm
ex. slit	10 nm
em. slit	20 nm
detector	manual (250V)
temperatur	25 °C
sampling interval	one measurement per minute

Each position on the white well plates was filled with a total volume of 200 μL of analyte solution, containing the assay buffer, an enzyme solution in buffer, the inhibitor in DMSO and the substrate in DMSO in the following order:

Order of Addition during Enzyme Assay

buffer	165 μL
enzyme	10 μL
DMSO or inhibitor	20 μL, c(final) = 100 μM
substrate	10 μL, c(final) = 50 μM
total volume	**200 μL**

The final concentration of the enzyme used in the assay had to be determined prior to the tests. Therefore the enzyme was measured at different dilutions without inhibitor until the slope of the linear graph representing the product conversion over time was

between 15 and 30. From the substrate a stock solution of 2 mM concentration in DMSO was prepared (c(final) = 50 μM). The peptide inhibitor was prepared as 1 mM stock solution in DMSO (c(final) = 100 μM). All individual solutions were added to the vials accordingly to the above mentioned order, thoroughly mixed and finally the increase of fluorescence activity was measured over time.

From the resulting data it is possible to determine the absolute inhibition (in %) at an inhibitor concentration of 100 μM. To determine in addition the half maximal inhibitory concentration (IC_{50}) and the absolute inhibition constant (K_i) it was necessary to make a dilution series of the inhibitor stock solution in DMSO resulting in the following final concentrations: 80 μM, 60 μM, 50 μM, 40 μM, 20 μM, 10 μM, 8 μM, 6 μM, 5 μM, 4 μM, 2 μM, 1 μM and 0.1 μM (depending on the inhibition strength, also bigger and smaller concentration had to be prepared 1000–0.01 μM). The resulting data was processed with Exel® and Grafit® (for background information see Chapter 3.4.1.2 on page 54; for experimental data see Chapter D.3 on page 252).

Determination of K_m (rhSkin β-Tryptase + Tos-Gly-Pro-Arg-AMC)

The Michaelis constant K_m for this enzyme/substrate combination had to be determined experimentally. Therefore the rate of the enzyme reaction was measured at different substrate concentrations (0–1000 μM), always with a fixed enzyme concentration and without inhibitor. The obtained K_m-value was 368 μM.

Test on reversibility of inhibition (dialysis)

The reversibility of the tryptase inhibition was tested in a dialysis experiment using a custom-built dialysis device. A dialysis separation tube (12–14 kDa) was clamped into the device separating a continuous stream of buffer solution (300 mL per hour) from small cavities on top of the instrument. In these chambers the following mixtures were added:

Mixture for Dialysis Experiment

buffer	375 μL
enzyme	25 μL
DMSO or inhibitor	100 μL, c(final) = 200 μM
total volume	**500 μL**

Every two hours over a period of 8 hours a 100 μL sample ($c(E_{final})$ = 500 μM, $c(I_{final})$ = 200 μM) was taken from the cavities and submitted to a fluorescence inhibitor assay to determine the activity of the enzyme. The following volumes were used for the assay:

Enzyme Assay for Dialysis Experiment

from dialysis chamber	100 μL, $c(E_{final})$ = 500 μM, $c(I_{final})$ = 200 μM
buffer	95 μL
substrate	10 μL, $c(S_{final})$ = 50 μM
total volume	**200 μL**

Test on reversibility of inhibition (heparin addition)

In the second experiment to test the reversibility of the inhibition, the enzyme was incubated with the inhibitor for 5 minutes. Then, in a parallel experiment either a mixture of buffer and heparin or buffer alone was added to the vials. Both vials were mixed and again incubated for 5 minutes before the final addition of the substrate. If the enzyme activity is higher in the vial with heparin, then this is an indication for a reversible binding of the inhibitor because is favors heparin over the enzyme. The following procedure was applied in the reversibility test:

Enzyme Assay for Reversibility Experiment using Heparin

buffer	160 μL
enzyme	10 μL
inhibitor	20 μL, c(final) = 100 μM
incubation break	**5 min** $\downarrow$
buffer (+ heparin)	5 μL, c(heparin) = 10 μg/mL
incubation break	**5 min** $\downarrow$
substrate	10 μL, c(final) = 50 μM
total volume	**200 μL**

Classification of enzyme inhibition

To elucidate the mode of enzyme inhibition (competitive, uncompetitive, non-competitive) a similar experiment like the K_m determination was performed. Again the rate

of the enzyme reaction was measured at different substrate concentrations (0–1000 μM) and a fixed enzyme concentration, but this time also inhibitor (1, 10 and 100 μM) was added instead of DMSO during the tests. The type of inhibition was then determined with the interpretation of the resulting Lineweaver-Burk and Hanes-Woolf plots as well as the non-linear regression fits (for experimental data see Chapter D.2 on page 247).

7.5.3 Screening of the Combinatorial Inhibitor Library

The screening of the immobilized inhibitor library was performed under similar conditions as the screening in solution. Both enzyme and buffer solution, as well as the substrate solution were composed of the standard reagents used for the rhSkin β-tryptase (see 7.5.1). Also the same settings of the fluorescence spectrophotometer could be used. Each of the 216 library members was measured twice (432 samples). In addition 62 "blank" PEGA samples for comparison were measured, resulting in 494 samples in total distributed over six 96-well plates. According to this number of samples approx. 5 mL of enzyme in buffer (494 $\times$ 10 μL), approx. 2.5 mL of substrate in DMSO (494 $\times$ 5 μL) and approx. 100 mL of buffer (494 $\times$ 165 μL) were needed.

Prior to the screening of the immobilized library samples of all members (5–10 mg) had to be weighted into small vessels and were mixed with a defined amount of DMSO (20 mg of resin per 1 mL of DMSO). In addition 60 mg of "blank" PEGA resin as reference material were mixed with 3 mL DMSO. All samples were allowed to swell for at least 1 h. This method, to use an isopycnic solution, allowed the distribution of an equal amount of resin into the corresponding positions of the white well plates. The preparation procedure for the incubation of the inhibitors with the enzyme is following the same order of addition as during the screening in solution (see above). Starting with buffer, then the isopycnic solution of inhibitor and the enzyme, each well has to be mixed with a multichannel pipette. The necessary six well plates were prepared over a period of approx. 6 hours and then incubated for 20 hours at room temperature. During the screening on the next day, it was important to ensure the same incubation time for all samples. One has to take into account that each screening cycle (4 rows) takes approx. 20 minutes, including the addition of the substrate (5 μL), mixing and measurement of the fluorescence activity (10 min). With this method it was possible to determine the absolute inhibition of all library members.

Appendix A

Bibliography

[1] C. Soto, *Nat. Rev. Neurosci.* **2003**, *4*, 49–60.

[2] H.-J. Schneider, *Angew. Chem. Int. Ed.* **1993**, *32*, 848–850.

[3] M. W. Peczuh, A. D. Hamilton, *Chem. Rev.* **2000**, *100*, 2479–2494.

[4] G. Sun, M. A. Fazal, B. C. Roy, S. Mallik, *Org. Lett.* **2000**, *2*, 911–914.

[5] C. Schmuck, M. Heil, *ChemBioChem* **2003**, *4*, 1232–1238.

[6] R. Xu, G. Greiveldinger, L. E. Marenus, A. Cooper, J. A. Ellman, *J. Am. Chem. Soc.* **1999**, *121*, 4898–4899.

[7] R. Breslow, Z. W. Yang, R. Ching, G. Trojandt, F. Odobel, *J. Am. Chem. Soc.* **1998**, *120*, 3536–3537.

[8] C. Schmuck, M. Heil, *Chem. Eur. J.* **2006**, *12*, 1339–1348.

[9] C. Schmuck, P. Wich, *Angew. Chem. Int. Ed.* **2006**, *45*, 4277–4281.

[10] M. Mammen, S. K. Choi, G. M. Whitesides, *Angew. Chem. Int. Ed.* **1998**, *37*, 2755–2794.

[11] L. L. Kiessling, J. E. Gestwicki, L. E. Strong, *Curr. Opin. Chem. Biol.* **2000**, *4*, 696–703.

[12] W. E. Stites, *Chem. Rev.* **1997**, *97*, 1233–1250.

[13] P. I. Kitov, J. M. Sadowska, G. Mulvey, G. D. Armstrong, H. Ling, N. S. Pannu, R. J. Read, D. R. Bundle, *Nature* **2000**, *403*, 669–672.

[14] J. E. Gestwicki, C. W. Cairo, L. E. Strong, K. A. Oetjen, L. L. Kiessling, *J. Am. Chem. Soc.* **2002**, *124*, 14922–14933.

[15] J. D. Badjic, A. Nelson, S. J. Cantrill, W. B. Turnbull, J. F. Stoddart, *Acc. Chem. Res.* **2005**, *38*, 723–732.

[16] A. Mulder, J. Huskens, D. Reinhoudt, *Org. Biomol. Chem.* **2004**, *2*, 3409–3424.

[17] U. Boas, P. M. H. Heegaard, *Chem. Soc. Rev.* **2004**, *33*, 43–63.

[18] J.-M. Lehn, *Supramolecular Chemistry: Concepts and Perspectives*, VCH, Weinheim, **1995**.

[19] N. J. V. Lindgren, L. Geiger, J. Razkin, C. Schmuck, L. Baltzer, *Angew. Chem. Int. Ed.* **2009**, in press.

[20] H. G. Boman, *J. Intern. Med.* **2003**, *254*, 197–215.

[21] M. Zasloff, *Nature* **2002**, *415*, 389–395.

[22] M. Q. Zhang, H. Timmerman, *Mediators Inflamm.* **1997**, *6*, 311–317.

[23] J. Hallgren, G. Pejler, *FEBS J.* **2006**, *273*, 1871–1895.

[24] C. A. Schalley, *Int. J. Mass Spectrom.* **2000**, *194*, 11–39.

[25] K. A. Schug, W. Lindner, *J. Sep. Sci.* **2005**, *28*, 1932–1955.

[26] M. F. Jarrold, *Annu. Rev. Phys. Chem.* **2000**, *51*, 179–207.

[27] W. Wang, E. N. Kitova, J. S. Klassen, *J. Am. Chem. Soc.* **2003**, *125*, 13630–13631.

[28] C. A. Schalley, *Analytical Methods in Supramolecular Chemistry*, Wiley-VCH, **2007**.

[29] M. Haj-Zaroubi, N. W. Mitzel, F. P. Schmidtchen, *Angew. Chem. Int. Ed.* **2002**, *41*, 104–107.

[30] T. Auletta, M. R. de Jong, A. Mulder, F. C. J. M. van Veggel, J. Huskens, S. Zou, D. Reinhoudt, S. Zapotoczny, H. Schonherr, G. J. Vancso, L. Kuipers, *J. Am. Chem. Soc.* **2004**, *126*, 1577–1584.

[31] R. Eckel, R. Ros, B. Decker, J. Mattay, D. Anselmetti, *Angew. Chem. Int. Ed.* **2005**, *44*, 484–488.

[32] C. B. Aakeröy, K. R. Seddon, *Chem. Soc. Rev.* **1993**, *22*, 397–407.

[33] A. Geerlof, J. Brown, B. Coutard, M.-P. Egloff, F. J. Enguita, M. J. Fogg, R. J. C. Gilbert, M. R. Groves, A. Haouz, J. E. Nettleship, P. Nordlund, R. J. Owens, M. Ruff, S. Sainsbury, D. I. Svergun, M. Wilmanns, *Acta Crystallogr. D Biol. Crystallogr.* **2006**, *62*, 1125–1136.

[34] S. Scheiner, *Hydrogen Bonding. A Theoretical Perspective*, Oxford University Press, **1997**.

[35] A. Bax, *Annu. Rev. Biochem.* **1989**, *58*, 223–256.

[36] A. Kumar, R. R. Ernst, K. Wüthrich, *Biochem. Biophys. Res. Commun.* **1980**, *95*, 1–6.

[37] G. Wagner, W. Braun, T. F. Havel, T. Schaumann, N. Go, K. Wüthrich, *J. Mol. Biol.* **1987**, *196*, 611–639.

[38] D. Neuhaus, M. P. Williamson, *The Nuclear Overhauser Effect in Structural and Conformational Analysis*, Wiley-VCH, **2000**.

[39] M. Rance, O. W. Sørensen, G. Bodenhausen, G. Wagner, R. R. Ernst, K. Wüthrich, *Biochem. Biophys. Res. Commun.* **1983**, *117*, 479–485.

[40] H. Friebolin, *Basic One- and Two-Dimensional NMR Spectroscopy*, Wiley-VCH, **2005**.

[41] L. Braunschweiler, R. R. Ernst, *J. Magn. Reson.* **1983**, *53*, 521–528.

[42] S. Macura, R. R. Ernst, *Mol. Phys.* **2002**, *100*, 135–147.

[43] J. Jeener, B. H. Meier, P. Bachmann, R. R. Ernst, *J. Chem. Phys.* **1979**, *71*, 4546–4553.

[44] A. Bax, D. G. Davis, *J. Magn. Reson.* **1985**, *63*, 207–213.

[45] A. A. Bothner-By, R. L. Stephens, C. D. Warren, R. W. Jeanloz, *J. Am. Chem. Soc.* **1984**, *106*, 811–813.

[46] K. Inomata, A. Ohno, H. Tochio, S. Isogai, T. Tenno, I. Nakase, T. Takeuchi, S. Futaki, Y. Ito, H. Hiroaki, M. Shirakawa, *Nature* **2009**, *458*, 106–110.

[47] H.-J. Schneider, H. Dürr, *Frontiers in Supramolecular Organic Chemistry and Photochemistry*, Wiley-VCH, **1991**, pp. 123–144.

[48] K. A. Connors, *Binding Constants: The Measurement of Molecular Complex Stability*, Wiley, New York, **1987**.

[49] L. Fielding, *Tetrahedron* **2000**, *56*, 6151–6170.

[50] R. Petry, M. Schmitt, J. Popp, *ChemPhysChem* **2003**, *4*, 14–30.

[51] T. G. Spiro, *Biological Applications of Raman Spectroscopy*, Wiley, New York, **1988**.

[52] S. Schluecker, R. K. Singh, B. P. Asthana, J. Popp, W. Kiefer, *J. Phys. Chem. A* **2001**, *105*, 9983–9989.

[53] S. Schluecker, J. Koster, R. K. Singh, B. P. Asthana, *J. Phys. Chem. A* **2007**, *111*, 5185–5191.

[54] C. V. Raman, K. S. Krishnan, *Nature* **1928**, *122*, 169–169.

[55] S. A. Asher, *Anal. Chem.* **1993**, *65*, 59A–66A.

[56] S. A. Asher, *Anal. Chem.* **1993**, *65*, 201A–210A.

[57] A. B. Myers, T. R. Rizzo, *Laser Techniques in Chemistry*, John Wiley & Sons, New York, **1995**, pp. 325–384.

[58] M. Schmitt, M. Heid, S. Schlücker, W. Kiefer, *Biopolymers* **2002**, *67*, 226–232.

[59] M. Moskovits, *Rev. Mod. Phys.* **1985**, *57*, 783–826.

[60] K. Kneipp, H. Kneipp, I. Itzkan, R. R. Dasari, M. S. Feld, *Chem. Rev.* **1999**, *99*, 2957–2976.

[61] Z. Q. Tian, *J. Raman Spectrosc.* **2005**, *36*, 466–470.

[62] R. Aroca, *Surface Enhanced Vibrational Spectroscopy*, Wiley, New York, **2006**.

[63] M. Fleischmann, P. J. Hendra, A. J. McQuillan, *Chem. Phys. Lett.* **1974**, *26*, 163–166.

[64] B. Schrader, D. Bougeard, *Infrared and Raman Spectroscopy: Methods and Applications*, VCH, Weinheim, **1995**, pp. 465–517.

[65] I. Connell, W. Agace, P. Klemm, M. Schembri, S. Mărild, C. Svanborg, *Proc. Natl. Acad. Sci. U. S. A.* **1996**, *93*, 9827–9832.

[66] B. Westerlund, T. K. Korhonen, *Mol. Microbiol.* **1993**, *9*, 687–694.

[67] S. K. Dower, J. A. Titus, C. DeLisi, D. M. Segal, *Biochemistry* **1981**, *20*, 6335–6340.

[68] H. Chen, M. L. Privalsky, *Proc. Natl. Acad. Sci. U. S. A.* **1995**, *92*, 422–426.

[69] T. W. Hamelryck, J. G. Moore, M. J. Chrispeels, R. Loris, L. Wyns, *J. Mol. Biol.* **2000**, *299*, 875–883.

[70] T. K. Lindhorst, *Top. Curr. Chem.* **2002**, *218*, 201–235.

[71] J. C. Sacchettini, L. G. Baum, C. F. Brewer, *Biochemistry* **2001**, *40*, 3009–3015.

[72] W. J. Lees, A. Spaltenstein, J. E. Kingery-Wood, G. M. Whitesides, *J. Med. Chem.* **1994**, *37*, 3419–3433.

[73] H.-J. Schneider, *Angew. Chem. Int. Ed. Engl.* **2009**, *48*, 3924–3977.

[74] S.-K. Choi, *Synthetic Multivalent Molecules: Concepts and Biomedical Applications*, Wiley & Sons, **2004**.

[75] J. N. Lowe, D. A. Fulton, S.-H. Chiu, A. M. Elizarov, S. J. Cantrill, S. J. Rowan, J. F. Stoddart, *J. Org. Chem.* **2004**, *69*, 4390–4402.

[76] P. V. Murphy, *Eur. J. Org. Chem.* **2007**, 4177–4187.

[77] R. M. Fairchild, K. T. Holman, *J. Am. Chem. Soc.* **2005**, *127*, 16364–16365.

[78] Y. Liu, Y. Chen, *Acc. Chem. Res.* **2006**, *39*, 681–691.

[79] L. Baldini, A. Casnati, F. Sansone, R. Ungaro, *Chem. Soc. Rev.* **2007**, *36*, 254–266.

[80] R. Roy, *Curr. Opin. Struct. Biol.* **1996**, *6*, 692–702.

[81] M. Kanai, K. H. Mortell, L. L. Kiessling, *J. Am. Chem. Soc.* **1997**, *119*, 9931–9932.

[82] B. S. Kim, D. J. Hong, J. Bae, M. Lee, *J. Am. Chem. Soc.* **2005**, *127*, 16333–16337.

[83] I. A. Banerjee, L. Yu, H. Matsui, *J. Am. Chem. Soc.* **2003**, *125*, 9542–9543.

[84] G. Ercolani, *J. Am. Chem. Soc.* **2003**, *125*, 16097–16103.

[85] W. A. Eaton, E. R. Henry, J. Hofrichter, A. Mozzarelli, *Nat. Struct. Biol.* **1999**, *6*, 351–358.

[86] W. A. Eaton, E. R. Henry, J. Hofrichter, S. Bettati, C. Viappiani, A. Mozzarelli, *IUBMB Life* **2007**, *59*, 586–599.

[87] W. E. Royer, J. E. Knapp, K. Strand, H. A. Heaslet, *Trends Biochem. Sci.* **2001**, *26*, 297–304.

[88] I. M. Klotz, *Biophys. Chem.* **2003**, *100*, 123–129.

[89] L. Kovbasyuk, R. Krämer, *Chem. Rev.* **2004**, *104*, 3161–3187.

[90] H.-J. Schneider, D. Ruf, *Angew. Chem. Int. Ed.* **1990**, *29*, 1159–1160.

[91] J. H. Rao, J. Lahiri, R. M. Weis, G. M. Whitesides, *J. Am. Chem. Soc.* **2000**, *122*, 2698–2710.

[92] P. C. Weber, D. H. Ohlendorf, J. J. Wendoloski, F. R. Salemme, *Science* **1989**, *243*, 85–88.

[93] P. C. Weber, J. J. Wendoloski, M. Pantoliano, F. R. Salemme, *J. Am. Chem. Soc.* **1992**, *114*, 3197–3200.

[94] K. N. Houk, A. G. Leach, S. P. Kim, X. Zhang, *Angew. Chem. Int. Ed.* **2003**, *42*, 4872–4897.

[95] F. Hof, S. L. Craig, C. Nuckolls, J. Rebek, *Angew. Chem. Int. Ed.* **2002**, *41*, 1488–1508.

[96] J. H. Hartley, T. D. James, C. J. Ward, *J. Chem. Soc., Perkin Trans. 1* **2000**, 3155–3184.

[97] A. T. Wright, Z. Zhong, E. V. Anslyn, *Angew. Chem. Int. Ed.* **2005**, *44*, 5679–5682.

[98] K. B. Jensen, T. M. Braxmeier, M. Demarcus, J. G. Frey, J. D. Kilburn, *Chem. Eur. J.* **2002**, *8*, 1300–1309.

[99] A. B. Clippingdale, J. D. Wade, C. J. Barrow, *J. Pept. Sci.* **2001**, *7*, 227–249.

[100] P. T. Lansbury, H. A. Lashuel, *Nature* **2006**, *443*, 774–779.

[101] J. Kang, H. G. Lemaire, A. Unterbeck, J. M. Salbaum, C. L. Masters, K. H. Grzeschik, G. Multhaup, K. Beyreuther, B. Müller-Hill, *Nature* **1987**, *325*, 733–736.

[102] Z. Datki, R. Papp, D. Zádori, K. Soós, L. Fülöp, A. Juhász, G. Laskay, C. Hetényi, E. Mihalik, M. Zarándi, B. Penke, *Neurobiol. Dis.* **2004**, *17*, 507–515.

[103] K. N. Dahlgren, A. M. Manelli, W. B. Stine, L. K. Baker, G. A. Krafft, M. J. LaDu, *J. Biol. Chem.* **2002**, *277*, 32046–32053.

[104] T. Lührs, C. Ritter, M. Adrian, D. Riek-Loher, B. Bohrmann, H. Döbeli, D. Schubert, R. Riek, *Proc. Natl. Acad. Sci. U. S. A.* **2005**, *102*, 17342–17347.

[105] C. Sachse, M. Fändrich, N. Grigorieff, *Proc. Natl. Acad. Sci. U. S. A.* **2008**, *105*, 7462–7466.

[106] C. Soto, E. M. Sigurdsson, L. Morelli, R. A. Kumar, E. M. Castano, B. Frangione, *Nat. Med.* **1998**, *4*, 822–826.

[107] N. G. Milton, *Biochem. J.* **1999**, *344 Pt 2*, 293–296.

[108] J. W. Lustbader, M. Cirilli, C. Lin, H. W. Xu, K. Takuma, N. Wang, C. Caspersen, X. Chen, S. Pollak, M. Chaney, F. Trinchese, S. Liu, F. Gunn-Moore, L.-F. Lue, D. G. Walker, P. Kuppusamy, Z. L. Zewier, O. Arancio, D. Stern, S. S. Yan, H. Wu, *Science* **2004**, *304*, 448–452.

[109] P. Inbar, J. Yang, *Bioorg. Med. Chem. Lett.* **2006**, *16*, 1076–1079.

[110] H. LeVine, *Protein Sci.* **1993**, *2*, 404–410.

[111] M. R. H. Krebs, E. H. C. Bromley, A. M. Donald, *J. Struct. Biol.* **2005**, *149*, 30–37.

[112] P. Inbar, C. Q. Li, S. A. Takayama, M. R. Bautista, J. Yang, *ChemBioChem* **2006**, *7*, 1563–1566.

[113] P. Inbar, M. R. Bautista, S. A. Takayama, J. Yang, *Anal. Chem.* **2008**, *80*, 3502–3506.

[114] Y. Kim, J. H. Lee, J. Ryu, D. J. Kim, *Curr. Pharm. Des.* **2009**, *15*, 637–658.

[115] H. F. Kung, C. W. Lee, Z. P. Zhuang, M. P. Kung, C. Hou, K. Plössl, *J. Am. Chem. Soc.* **2001**, *123*, 12740–12741.

[116] K. Watanabe, K. Nakamura, S. Akikusa, T. Okada, M. Kodaka, T. Konakahara, H. Okuno, *Biochem. Biophys. Res. Commun.* **2002**, *290*, 121–124.

[117] S. M. Chafekar, H. Malda, M. Merkx, E. W. Meijer, D. Viertl, H. A. Lashuel, F. Baas, W. Scheper, *ChemBioChem* **2007**, *8*, 1857–1864.

[118] C. Schmuck, W. Wienand, *J. Am. Chem. Soc.* **2003**, *125*, 452–459.

[119] C. Schmuck, *Chem. Eur. J.* **2000**, *6*, 709–718.

[120] C. Schmuck, *Chem. Commun.* **1999**, 843–844.

[121] C. Schmuck, *Coord. Chem. Rev.* **2006**, *250*, 3053–3067.

[122] C. Schmuck, V. Bickert, M. Merschky, L. Geiger, D. Rupprecht, J. Dudaczek, P. Wich, T. Rehm, U. Machon, *Eur. J. Org. Chem.* **2008**, 324–329.

[123] C. Schmuck, M. Heil, *Org. Biomol. Chem.* **2003**, *1*, 633–636.

[124] C. Schmuck, P. Frey, M. Heil, *ChemBioChem* **2005**, *6*, 628–631.

[125] K. M. Stewart, K. L. Horton, S. O. Kelley, *Org. Biomol. Chem.* **2008**, *6*, 2242–2255.

[126] E. A. Goun, T. H. Pillow, L. R. Jones, J. B. Rothbard, P. A. Wender, *ChemBioChem* **2006**, *7*, 1497–1515.

[127] S. Futaki, *Biopolymers* **2006**, *84*, 241–249.

[128] S. Futaki, S. Goto, Y. Sugiura, *J. Mol. Recognit.* **2003**, *16*, 260–264.

[129] H. H. Chung, G. Harms, C. M. Seong, B. H. Choi, C. H. Min, J. P. Taulane, M. Goodman, *Biopolymers* **2004**, *76*, 83–96.

[130] S. Futaki, I. Nakase, T. Suzuki, Z. Youjun, Y. Sugiura, *Biochemistry* **2002**, *41*, 7925–7930.

[131] E. Vives, P. Brodin, B. Lebleu, *J. Biol. Chem.* **1997**, *272*, 16010–16017.

[132] D. Derossi, A. H. Joliot, G. Chassaing, A. Prochiantz, *J. Biol. Chem.* **1994**, *269*, 10444–10450.

[133] N. Umezawa, M. A. Gelman, M. C. Haigis, R. T. Raines, S. H. Gellman, *J. Am. Chem. Soc.* **2002**, *124*, 368–369.

[134] T. Schroeder, N. Niemeier, S. Afonin, A. S. Ulrich, H. F. Krug, S. Braese, *J. Med. Chem.* **2008**, *51*, 376–379.

[135] N. Sakai, T. Takeuchi, S. Futaki, S. Matile, *ChemBioChem* **2005**, *6*, 114–122.

[136] J. B. Rothbard, T. C. Jessop, R. S. Lewis, B. A. Murray, P. A. Wender, *J. Am. Chem. Soc.* **2004**, *126*, 9506–9507.

[137] J. R. Lakowicz, *Principles of Fluorescence Spectroscopy*, Springer, **2006**.

[138] W. M. Leevy, J. R. Johnson, C. Lakshmi, J. Morris, M. Marquez, B. D. Smith, *Chem. Commun.* **2006**, 1595–1597.

[139] W. M. Leevy, S. T. Gammon, H. Jiang, J. R. Johnson, D. J. Maxwell, E. N. Jackson, M. Marquez, D. Piwnica-Worms, B. D. Smith, *J. Am. Chem. Soc.* **2006**, *128*, 16476–16477.

[140] J. R. Johnson, N. Fu, E. Arunkumar, W. M. Leevy, S. T. Gammon, D. Piwnica-Worms, B. D. Smith, *Angew. Chem. Int. Ed.* **2007**, *46*, 5528–5531.

[141] W. M. Leevy, S. T. Gammon, J. R. Johnson, A. J. Lampkins, H. Jiang, M. Marquez, D. Piwnica-Worms, M. A. Suckow, B. D. Smith, *Bioconjug. Chem.* **2008**, *19*, 686–692.

[142] J. M. Boon, B. D. Smith, *Med. Res. Rev.* **2002**, *22*, 251–281.

[143] S. G. Wilkinson, C. Ratledge, *Microbial Lipids. Vol. 1*, Academic Press, **1988**.

[144] B. Fournier, D. J. Philpott, *Clin. Microbiol. Rev.* **2005**, *18*, 521–540.

[145] T. C. Meredith, P. Aggarwal, U. Mamat, B. Lindner, R. W. Woodard, *ACS Chem. Biol.* **2006**, *1*, 33–42.

[146] K. A. Brogden, *Nat. Rev. Microbiol.* **2005**, *3*, 238–250.

[147] R. E. Hancock, D. S. Chapple, *Antimicrob. Agents Chemother.* **1999**, *43*, 1317–1323.

[148] Z. Liu, H. Deshazer, A. J. Rice, K. Chen, C. H. Zhou, N. R. Kallenbach, *J. Med. Chem.* **2006**, *49*, 3436–3439.

[149] Z. Liu, A. Brady, A. Young, B. Rasimick, K. Chen, C. H. Zhou, N. R. Kallenbach, *Antimicrob. Agents Chemother.* **2006**, *51*, 597–603.

[150] A. Wessolowski, M. Bienert, M. Dathe, *J. Pept. Res.* **2004**, *64*, 159–169.

[151] M. B. Strøm, O. Rekdal, J. S. Svendsen, *J. Pept. Sci.* **2002**, *8*, 431–437.

[152] J. P. Tam, Y. A. Lu, J. L. Yang, *Eur. J. Biochem.* **2002**, *269*, 923–932.

[153] C. Chamorro, R. Liskamp, *Tetrahedron* **2004**, *60*, 11145–11157.

[154] J. Shepherd, T. Gale, K. B. Jensen, J. D. Kilburn, *Chem. Eur. J.* **2006**, *12*, 713–720.

[155] P. Krattiger, H. Wennemers, *Synlett* **2005**, 706–708.

[156] J. Bernard, H. Wennemers, *Org. Lett.* **2007**, *9*, 4283–4286.

[157] C. F. J. Faul, P. Krattiger, B. M. Smarsly, H. Wennemers, *J. Mater. Chem.* **2008**, *18*, 2962–2967.

[158] J. J. Reczek, A. A. Kennedy, B. T. Halbert, A. R. Urbach, *J. Am. Chem. Soc.* **2009**, *131*, 2408–2415.

[159] L. M. Heitmann, A. B. Taylor, P. J. Hart, A. R. Urbach, *J. Am. Chem. Soc.* **2006**, *128*, 12574–12581.

[160] S. M. Liu, C. Ruspic, P. Mukhopadhyay, S. Chakrabarti, P. Y. Zavalij, L. Isaacs, *J. Am. Chem. Soc.* **2005**, *127*, 15959–15967.

[161] M. E. Bush, N. D. Bouley, A. R. Urbach, *J. Am. Chem. Soc.* **2005**, *127*, 14511–14517.

[162] M. V. Rekharsky, H. Yamamura, Y. H. Ko, N. Selvapalam, K. Kim, Y. Inoue, *Chem. Commun.* **2008**, 2236–2238.

[163] S. Stadlbauer, A. Riechers, A. Späth, B. König, *Chem. Eur. J.* **2008**, *14*, 2536–2541.

[164] A. Buryak, K. Severin, *Angew. Chem. Int. Ed. Engl.* **2004**, *43*, 4771–4774.

[165] S. Tashiro, M. Tominaga, Y. Yamaguchi, K. Kato, M. Fujita, *Angew. Chem. Int. Ed. Engl.* **2005**, *45*, 241–244.

[166] S. Tashiro, M. Tominaga, M. Kawano, B. Therrien, T. Ozeki, M. Fujita, *J. Am. Chem. Soc.* **2005**, *127*, 4546–4547.

[167] C. Frisch, A. R. Fersht, G. Schreiber, *J. Mol. Biol.* **2001**, *308*, 69–77.

[168] G. Schreiber, A. M. Buckle, A. R. Fersht, *Structure* **1994**, *2*, 945–951.

[169] G. Schreiber, A. R. Fersht, *J. Mol. Biol.* **1995**, *248*, 478–486.

[170] V. Martos, P. Castreño, J. Valero, J. de Mendoza, *Curr. Opin. Chem. Biol.* **2008**, *12*, 698–706.

[171] S. Fletcher, A. D. Hamilton, *Curr. Opin. Chem. Biol.* **2005**, *9*, 632–638.

[172] T. Schrader, S. Koch, *Mol. BioSyst.* **2007**, *3*, 241–248.

[173] R. Jain, J. T. Ernst, O. Kutzki, H. S. Park, A. D. Hamilton, *Mol. Divers.* **2004**, *8*, 89–100.

[174] M. R. Arkin, J. A. Wells, *Nat. Rev. Drug Discov.* **2004**, *3*, 301–317.

[175] A. G. Cochran, *Curr. Opin. Chem. Biol.* **2001**, *5*, 654–659.

[176] P. L. Toogood, *J. Med. Chem.* **2002**, *45*, 1543–1558.

[177] A. A. Bogan, K. S. Thorn, *J. Mol. Biol.* **1998**, *280*, 1–9.

[178] H. S. Park, Q. Lin, A. D. Hamilton, *J. Am. Chem. Soc.* **1999**, *121*, 8–13.

[179] X. Salvatella, M. Martinell, M. Gairí, M. G. Mateu, M. Feliz, A. D. Hamilton, J. de Mendoza, E. Giralt, *Angew. Chem. Int. Ed.* **2004**, *43*, 196–198.

[180] M. Martinell, X. Salvatella, J. Fernandez-Carneado, S. Gordo, M. Feliz, M. Menendez, E. Giralt, *ChemBioChem* **2006**, *7*, 1105–1113.

[181] S. Gordo, V. Martos, E. Santos, M. Menendez, C. Bo, E. Giralt, J. de Mendoza, *Proc. Natl. Acad. Sci. U. S. A.* **2008**, *105*, 16426–16431.

[182] H. Wulff, B. S. Zhorov, *Chem. Rev.* **2008**, *108*, 1744–1773.

[183] D. A. Doyle, J. M. Cabral, R. A. Pfuetzner, A. Kuo, J. M. Gulbis, S. L. Cohen, B. T. Chait, R. MacKinnon, *Science* **1998**, *280*, 69–77.

[184] S. N. Gradl, J. P. Felix, E. Y. Isacoff, M. L. Garcia, D. Trauner, *J. Am. Chem. Soc.* **2003**, *125*, 12668–12669.

[185] C. Ader, R. Schneider, S. Hornig, P. Velisetty, E. M. Wilson, A. Lange, K. Giller, I. Ohmert, M.-F. Martin-Eauclaire, D. Trauner, S. Becker, O. Pongs, M. Baldus, *Nat. Struct. Mol. Biol.* **2008**, *15*, 605–612.

[186] V. Martos, S. C. Bell, E. Santos, E. Y. Isacoff, D. Trauner, J. de Mendoza, *Proc. Natl. Acad. Sci. U. S. A.* **2009**, *106*, 10482–10486.

[187] T. A. Larsen, A. J. Olson, D. S. Goodsell, *Structure* **1998**, *6*, 421–427.

[188] H. Pelletier, J. Kraut, *Science* **1992**, *258*, 1748–1755.

[189] A. N. Volkov, J. A. R. Worrall, E. Holtzmann, M. Ubbink, *Proc. Natl. Acad. Sci. U. S. A.* **2006**, *103*, 18945–18950.

[190] O. Maneg, F. Malatesta, B. Ludwig, V. Drosou, *Biochim. Biophys. Acta* **2004**, *1655*, 274–281.

[191] P. B. Crowley, P. Ganji, H. Ibrahim, *ChemBioChem* **2008**, *9*, 1029–1033.

[192] Y. Hamuro, M. C. Calama, H. S. Park, A. D. Hamilton, *Angew. Chem. Int. Ed. Engl.* **1997**, *36*, 2680–2683.

[193] A. J. Wilson, J. Hong, S. Fletcher, A. D. Hamilton, *Org. Biomol. Chem.* **2007**, *5*, 276–285.

[194] M. Arendt, W. Sun, J. Thomann, X. Xie, T. Schrader, *Chem. Asian J.* **2006**, *1*, 544–554.

[195] K. Kano, Y. Ishida, *Angew. Chem. Int. Ed. Engl.* **2007**, *46*, 727–730.

[196] K. Groves, A. J. Wilson, A. D. Hamilton, *J. Am. Chem. Soc.* **2004**, *126*, 12833–12842.

[197] H. Zhou, L. Baldini, J. Hong, A. J. Wilson, A. D. Hamilton, *J. Am. Chem. Soc.* **2006**, *128*, 2421–2425.

[198] Q. Lin, H. S. Park, Y. Hamuro, C.-S. Lee, A. D. Hamilton, *Biopolymers* **1998**, *47*, 285–297.

[199] Y. Wei, G. L. Mclendon, M. A. Case, C. B. Purring, T. Yu, A. D. Hamilton, Q. Lin, H. S. Park, C.-S. Lee, *Chem. Commun.* **2001**, 1580–1581.

[200] D. Paul, H. Miyake, S. Shinoda, H. Tsukube, *Chem. Eur. J.* **2006**, *12*, 1328–1338.

[201] P. Niederhafner, J. Sebestík, J. Jezek, *J. Pept. Sci.* **2008**, *14*, 2–43.

[202] O. Hayashida, M. Uchiyama, *Tetrahedron Lett.* **2006**, *47*, 4091–4094.

[203] O. Hayashida, M. Uchiyama, *J. Org. Chem.* **2007**, *72*, 610–616.

[204] O. Hayashida, N. Ogawa, M. Uchiyama, *J. Am. Chem. Soc.* **2007**, *129*, 13698–13705.

[205] O. Hayashida, M. Uchiyama, *Org. Biomol. Chem.* **2008**, *6*, 3166–3170.

[206] M. E. Jones, *Biochem. J.* **1992**, *288*, 533–538.

[207] R. Kitz, I. B. Wilson, *J. Biol. Chem.* **1962**, *237*, 3245–3249.

[208] W. X. Tian, C. L. Tsou, *Biochemistry* **1982**, *21*, 1028–1032.

[209] M. Dixon, *Biochem. J.* **1953**, *55*, 170–171.

[210] K. P. Williams, J. E. Scott, *Methods Mol. Biol.* **2009**, *565*, 107–126.

[211] K. S. Lam, S. E. Salmon, E. M. Hersh, V. J. Hruby, W. M. Kazmierski, R. J. Knapp, *Nature* **1991**, *354*, 82–84.

[212] K. S. Lam, M. Lebl, V. Krchnak, *Chem. Rev.* **1997**, *97*, 411–448.

[213] P. M. St. Hilaire, M. Meldal, *Angew. Chem. Int. Ed. Engl.* **2000**, *39*, 1162–1179.

[214] D.-S. Shin, Y.-G. Kim, E.-M. Kim, M. Kim, H.-Y. Park, J.-H. Kim, B.-S. Lee, B.-G. Kimt, Y.-S. Lee, *J. Comb. Chem.* **2008**, *10*, 20–23.

[215] G. Lowe, R. Quarrell, *Methods* **1994**, *6*, 411–416.

[216] K. D. Greis, *Mass Spectrom. Rev.* **2007**, *26*, 324–339.

[217] B. Spengler, *J. Mass Spectrom.* **1997**, *32*, 1019–1036.

[218] H. S. Hiemstra, W. E. Benckhuijsen, R. Amons, W. Rapp, J. W. Drijfhout, *J. Pept. Sci.* **1998**, *4*, 282–288.

[219] O. H. Aina, R. Liu, J. L. Sutcliffe, J. Marik, C.-X. Pan, K. S. Lam, *Mol. Pharm.* **2007**, *4*, 631–651.

[220] H. J. Olivos, K. Bachhawat-Sikder, T. Kodadek, *ChemBioChem* **2003**, *4*, 1242–1245.

[221] H. Kim, J. K. Cho, W. J. Chung, Y. S. Lee, *Org. Lett.* **2004**, *6*, 3273–3276.

[222] D. H. Kim, H. Y. Lee, H. Kim, Y. S. Lee, S. B. Park, *J. Comb. Chem.* **2006**, *8*, 280–285.

[223] M. Meldal, *Tetrahedron Lett.* **1992**, *33*, 3077–3080.

[224] M. Meldal, I. Svendsen, *J. Chem. Soc., Perkin Trans. 1* **1995**, 1591–1596.

[225] M. Renil, M. Ferreras, J. M. Delaisse, N. T. Foged, M. Meldal, *J. Pept. Sci.* **1998**, *4*, 195–210.

[226] P. M. St. Hilaire, T. L. Lowary, M. Meldal, K. Bock, *J. Am. Chem. Soc.* **1998**, *120*, 13312–13320.

[227] U. Machon, Thesis, Universität Würzburg, **2008**.

[228] K. Nicolaou, X. Xiao, Z. Parandoosh, A. Senyei, M. Nova, *Angew. Chem. Int. Ed.* **1995**, *34*, 2289–2291.

[229] T. Tanaka, B. J. McRae, K. Cho, R. Cook, J. E. Fraki, D. A. Johnson, J. C. Powers, *J. Biol. Chem.* **1983**, *258*, 13552–13557.

[230] I. Schechter, A. Berger, *Biochem. Biophys. Res. Commun.* **1967**, *27*, 157–162.

[231] J. Stürzebecher, D. Prasa, C. P. Sommerhoff, *Bio. Chem. Hoppe-Seyler* **1992**, *373*, 1025–1030.

[232] G. H. Caughey, W. W. Raymond, E. Bacci, R. J. Lombardy, R. R. Tidwell, *J. Pharmacol. Exp. Ther.* **1993**, *264*, 676–682.

[233] P. J. B. Pereira, A. Bergner, S. Macedo-Ribeiro, R. Huber, G. Matschiner, H. Fritz, C. P. Sommerhoff, W. Bode, *Nature* **1998**, *392*, 306–311.

[234] C. P. Sommerhoff, W. Bode, G. Matschiner, A. Bergner, H. Fritz, *Biochim. Biophys. Acta* **2000**, *1477*, 75–89.

[235] N. Schaschke, A. Dominik, G. Matschiner, C. P. Sommerhoff, *Bioorg. Med. Chem. Lett.* **2002**, *12*, 985–988.

[236] C. P. Sommerhoff, W. Bode, P. J. B. Pereira, M. T. Stubbs, J. Stürzebecher, G. P. Piechottka, G. Matschiner, A. Bergner, *Proc. Natl. Acad. Sci. U. S. A.* **1999**, *96*, 10984–10991.

[237] J. S. Miller, G. Moxley, L. B. Schwartz, *J. Clin. Invest.* **1990**, *86*, 864–870.

[238] P. Vanderslice, S. M. Ballinger, E. K. Tam, S. M. Goldstein, C. S. Craik, G. H. Caughey, *Proc. Natl. Acad. Sci. U. S. A.* **1990**, *87*, 3811–3815.

[239] H. Z. Xia, C. L. Kepley, K. Sakai, J. Chelliah, A. M. Irani, L. B. Schwartz, *J. Immunol.* **1995**, *154*, 5472–5480.

[240] L. B. Schwartz, A. M. Irani, K. Roller, M. C. Castells, N. M. Schechter, *J. Immunol.* **1987**, *138*, 2611–2615.

[241] C. D. Wright, A. M. Havill, S. C. Middleton, M. A. Kashem, D. J. Dripps, W. M. Abraham, D. S. Thomson, L. E. Burgess, *Biochem. Pharmacol.* **1999**, *58*, 1989–1996.

[242] J. F. Molinari, M. Scuri, W. R. Moore, J. Clark, R. D. Tanaka, W. M. Abraham, *Am. J. Respir. Crit. Care Med.* **1996**, *154*, 649–653.

[243] W. M. Abraham, *Am. J. Physiol. Lung Cell. Mol. Physiol.* **2002**, *282*, L193–L196.

[244] E. K. Tam, G. H. Caughey, *Am. J. Respir. Cell Mol. Biol.* **1990**, *3*, 27–32.

[245] A. Kozik, R. B. Moore, J. Potempa, T. Imamura, M. Rapala-Kozik, J. Travis, *J. Biol. Chem.* **1998**, *273*, 33224–33229.

[246] D. Proud, E. S. Siekierski, G. S. Bailey, *Biochem. Pharmacol.* **1988**, *37*, 1473–1480.

[247] T. J. Smith, M. W. Hougland, D. A. Johnson, *J. Biol. Chem.* **1984**, *259*, 11046–11051.

[248] T. Selwood, H. Smolensky, D. R. McCaslin, N. M. Schechter, *Biochemistry* **2005**, *44*, 3580–3590.

[249] N. M. Schechter, E.-J. Choi, T. Selwood, D. R. McCaslin, *Biochemistry* **2007**, *46*, 9615–9629.

[250] S. C. Alter, J. A. Kramps, A. Janoff, L. B. Schwartz, *Arch. Biochem. Biophys.* **1990**, *276*, 26–31.

[251] K. C. Elrod, W. R. Moore, W. M. Abraham, R. D. Tanaka, *Am. J. Respir. Crit. Care Med.* **1997**, *156*, 375–381.

[252] L. Cregar, K. C. Elrod, D. Putnam, W. R. Moore, *Arch. Biochem. Biophys.* **1999**, *366*, 125–130.

[253] J. Hallgren, S. Estrada, U. Karlson, K. Alving, G. Pejler, *Biochemistry* **2001**, *40*, 7342–7349.

[254] A. Lundequist, M. A. Juliano, L. Juliano, G. Pejler, *Biochem. Pharmacol.* **2003**, *65*, 1171–1180.

[255] C. P. Sommerhoff, C. Sollner, R. Mentele, G. P. Piechottka, E. A. Auerswald, H. Fritz, *Bio. Chem. Hoppe-Seyler* **1994**, 685–694.

[256] S. D. Marco, J. P. Priestle, *Structure* **1997**, *5*, 1465–1474.

[257] M. T. Krishna, A. Chauhan, L. Little, K. Sampson, R. Hawksworth, T. Mant, R. Djukanovic, T. Lee, S. Holgate, *J. Allergy Clin. Immunol.* **2001**, *107*, 1039–1045.

[258] M. J. Costanzo, S. C. Yabut, H. R. Almond, P. Andrade-Gordon, T. W. Corcoran, L. de Garavilla, J. A. Kauffman, W. M. Abraham, R. Recacha, D. Chattopadhyay, B. E. Maryanoff, *J. Med. Chem.* **2003**, *46*, 3865–3876.

[259] K. D. Rice, V. R. Wang, A. R. Gangloff, E. Y. Kuo, J. M. Dener, W. S. Newcomb, W. B. Young, D. Putnam, L. Cregar, M. Wong, P. J. Simpson, *Bioorg. Med. Chem. Lett.* **2000**, *10*, 2361–2366.

[260] T. Selwood, K. C. Elrod, N. M. Schechter, *Biol. Chem.* **2003**, *384*, 1605–1611.

[261] W. J. Tremaine, A. Brzezinski, J. A. Katz, D. C. Wolf, T. J. Fleming, J. Mordenti, L. C. Strenkoski-Nix, M. C. Kurth, *Aliment. Pharmacol. Ther.* **2002**, *16*, 407–413.

[262] M. del Fresno, D. Fernández-Forner, M. Miralpeix, V. Segarra, H. Ryder, M. Royo, F. Albericio, *Bioorg. Med. Chem. Lett.* **2005**, *15*, 1659–1664.

[263] M. García, X. del Rio, S. Silvestre, M. Rubiralta, E. Lozoya, V. Segarra, D. Fernández, M. Miralpeix, M. Aparici, A. Diez, *Org. Biomol. Chem.* **2004**, *2*, 1633–1642.

[264] N. Schaschke, G. Matschiner, F. Zettl, U. Marquardt, A. Bergner, W. Bode, C. P. Sommerhoff, L. Moroder, *Chem. Biol.* **2001**, *8*, 313–327.

[265] T. Mecca, G. Consoli, C. Geraci, F. Cunsolo, *Bioorg. Med. Chem.* **2004**, *12*, 5057–5062.

[266] D. Scarpi, J. D. McBride, R. J. Leatherbarrow, *Bioorg. Med. Chem.* **2004**, *12*, 6045–6052.

[267] B. Spichalska, A. Lesner, M. Wysocka, M. Sledź, A. Legowska, A. Jaśkiewicz, H. Miecznikowska, K. Rolka, *J. Pept. Sci.* **2008**, *14*, 917–923.

[268] J. L. Harris, A. L. Niles, K. Burdick, M. Maffitt, B. J. Backes, J. A. Ellman, I. Kuntz, M. Haak-Frendscho, C. S. Craik, *J. Biol. Chem.* **2001**, *276*, 34941–34947.

[269] C. Schmuck, M. Heil, J. Scheiber, K. Baumann, *Angew. Chem. Int. Ed.* **2005**, *44*, 7208–7212.

[270] D. Moiani, C. Cavallotti, A. Famulari, C. Schmuck, *Chem. Eur. J.* **2008**, *14*, 5207–5219.

[271] B. Küstner, C. Schmuck, P. Wich, C. Jehn, S. K. Srivastava, S. Schlücker, *Phys. Chem. Chem. Phys.* **2007**, *9*, 4598–4603.

[272] S. K. Srivastava, S. Niebling, B. Küstner, P. R. Wich, C. Schmuck, S. Schlücker, *Phys. Chem. Chem. Phys.* **2008**, *10*, 6770–6775.

[273] C. Schmuck, P. Wich, B. Küstner, W. Kiefer, S. Schlücker, *Angew. Chem. Int. Ed.* **2007**, *46*, 4786–4789.

[274] M. Mergler, R. Tanner, J. Gosteli, P. Grogg, *Tetrahedron Lett.* **1988**, *29*, 4005–4008.

[275] M. Mergler, R. Nyfeler, R. Tanner, J. Gosteli, P. Grogg, *Tetrahedron Lett.* **1988**, *29*, 4009–4012.

[276] C. Schmuck, L. Geiger, *Chem. Commun.* **2005**, 772–774.

[277] R. C. Benyon, J. A. Enciso, A. D. Befus, *J. Immunol.* **1993**, *151*, 2699–2706.

[278] P. Sommer, V. S. Fluxa, T. Darbre, J.-L. Reymond, *ChemBioChem* **2009**, *10*, 1527–1536.

[279] C. Hopkins, K. Neuenschwander, A. Scotese, S. Jackson, T. Nieduzak, H. Pauls, G. Liang, K. Sides, D. Cramer, J. Cairns, S. Maignan, M. Mathieu, *Bioorg. Med. Chem. Lett.* **2004**, *14*, 4819–4823.

[280] S. A. Evans, S. T. Olson, J. D. Shore, *J. Biol. Chem.* **1982**, *257*, 3014–3017.

[281] N. Maillard, A. Clouet, T. Darbre, J.-L. Reymond, *Nat. Protoc.* **2009**, *4*, 132–142.

[282] H. S. Marsden, A. M. Owsianka, S. Graham, G. W. McClean, C. A. Robertson, J. H. Subaksharpe, *J. Immunol. Methods* **1992**, *147*, 65–72.

[283] K. Sadler, J. P. Tam, *J. Biotechnol.* **2002**, *90*, 195–229.

[284] R. A. Houghten, C. Pinilla, S. E. Blondelle, J. R. Appel, C. T. Dooley, J. H. Cuervo, *Nature* **1991**, *354*, 84–86.

[285] C. Schmuck, P. Wich, *New J. Chem.* **2006**, *30*, 1377–1385.

[286] C. Schmuck, P. Wich, *Top. Curr. Chem.* **2007**, *277*, 3–30.

[287] O. Melnyk, J. S. Fruchart, C. Grandjean, H. Gras-Masse, *J. Org. Chem.* **2001**, *66*, 4153–4160.

[288] S. Cha, *Biochem. Pharmacol.* **1975**, *24*, 2177–2185.

[289] J. F. Morrison, *Biochim. Biophys. Acta* **1969**, *185*, 269–286.

[290] W. Huang, B. Nardelli, J. P. Tam, *Mol. Immunol.* **1994**, *31*, 1191–1199.

[291] K. W. Hahn, W. A. Klis, J. M. Stewart, *Science* **1990**, *248*, 1544–1547.

[292] P. Sommer, N. A. Uhlich, J.-L. Reymond, T. Darbre, *ChemBioChem* **2008**, *9*, 689–693.

[293] J. Frackenpohl, P. I. Arvidsson, J. V. Schreiber, D. Seebach, *ChemBioChem* **2001**, *2*, 445–455.

[294] J. D. Sadowsky, J. K. Murray, Y. Tomita, S. H. Gellman, *ChemBioChem* **2007**, *8*, 903–916.

[295] R. Tugyi, K. Uray, D. Iván, E. Fellinger, A. Perkins, F. Hudecz, *Proc. Natl. Acad. Sci. U. S. A.* **2005**, *102*, 413–418.

[296] S. Pujals, J. Fernandez-Carneado, M. D. Ludevid, E. Giralt, *ChemMedChem* **2008**, *3*, 296–301.

[297] R. Kluger, J. Lock-O'Brien, A. Teytelboym, *J. Am. Chem. Soc.* **1999**, *121*, 6780–6785.

[298] F. Wurm, J. Klos, H. J. Räder, H. Frey, *J. Am. Chem. Soc.* **2009**, *131*, 7954–7955.

[299] K. Okuro, K. Kinbara, K. Tsumoto, N. Ishii, T. Aida, *J. Am. Chem. Soc.* **2009**, *131*, 1626–1627.

[300] J. Leonard, B. Lygo, G. Procter, *Praxis der Organischen Chemie*, Wiley-VCH, **1996**.

[301] M. Hesse, H. Meier, B. Zeeh, *Spektroskopische Methoden in der organischen Chemie*, Thieme, **2005**.

[302] E. Kaiser, R. L. Colescott, C. D. Bossinger, P. I. Cook, *Anal. Biochem.* **1970**, *34*, 595–598.

[303] M. E. Attardi, G. Porcu, M. Taddei, *Tetrahedron Lett.* **2000**, *41*, 7391–7394.

Appendix B

Picture References

[304] *Reprinted by permission from Macmillan Publishers Ltd: Nature Chemical Biology, J. C. Paulson, O. Blixt, B. E. Collins, Nat. Chem. Biol. 2006, 2, 238–248, Copyright 2006.*

[305] *J. M. P. Canadillas, H. Tidow, S. M. V. Freund, T. J. Rutherford, H. C. Ang, A. R. Fersht, Proc. Natl. Acad. Sci. U.S.A. 2006, 103, 2109–2114. Copyright 2009 National Academy of Sciences, U.S.A.*

[306] *Reprinted with permission from K. Kneipp, H. Kneipp, J. Kneipp, Acc. Chem. Res. 2006, 39, 443–450. Copyright 2009 American Chemical Society.*

[307] *M. Mammen, S. Choi, G. M. Whitesides: Polyvalent Interactions in Biological Systems: Implications for Design and Use of Multivalent Ligands and Inhibitors, Angew. Chem. Int. Ed. 1998, 37, 2754–2794. Copyright Wiley-VCH Verlag GmbH & Co. KGaA. Reproduced with permission.*

[308] *A. Mulder, J. Huskens, D. N. Reinhoudt, Org. Biomol. Chem. 2004, 2, 3409–3424 – Reproduced by permission of The Royal Society of Chemistry.*

[309] *L. Baldini, A. Casnati, F. Sansone and R. Ungaro, Chem. Soc. Rev. 2007, 36, 254–266 – Reproduced by permission of The Royal Society of Chemistry.*

[310] *H. J. Schneider, D. Ruf: A Synthetic AIlosteric System with High Cooperativity between Polar and Hydrophobic Binding Sites, Angew. Chem. Int. Ed. Engl. 1990, 10, 1159–1160. Copyright Wiley-VCH Verlag GmbH & Co. KGaA. Reproduced with permission.*

[311] *Reprinted with permission from J. D. Badjić, A. Nelson, S. J. Cantrill, W. B. Turnbull, J. F. Stoddart, Acc. Chem. Res. 2005, 38, 723–732. Copyright 2009 American Chemical Society.*

[312] *Reprinted with permission from J. Rao, J. Lahiri, R. M. Weis, G. M. Whitesides, J. Am. Chem. Soc. 2000, 122, 2698–2710. Copyright 2009 American Chemical Society.*

[313] *T. Lührs, C. Ritter, M. Adrian, D. Riek-Loher, B. Bohrmann, H. Döbeli, D. Schubert, R. Riek, Proc. Natl. Acad. Sci. U.S.A. 2005, 48, 7342–17347. Copyright 2009 National Academy of Sciences, U.S.A.*

[314] *Reprinted from Bioorganic & Medicinal Chemistry Letters, Vol. 16 (4), P. Inbar, J. Yang, Inhibiting protein-amyloid interactions with small molecules: a surface chemistry approach, 1076–1079, Copyright 2006, with permission from Elsevier.*

[315] *K. M. Stewart, K. L. Horton, S. O. Kelley, Org. Biomol. Chem. 2008, 6, 2242–2255 – Reproduced by permission of The Royal Society of Chemistry.*

[316] *Reprinted with permission from S. Futaki, I. Nakase, T. Suzuki, Z. Youjun, Y. Sugiura, Biochemistry, 2002, 25, 7925–7930. Copyright 2009 American Chemical Society.*

[317] *Reprinted with permission from W. M. Leevy, S. T. Gammon, J. Johnson, A. J. Lampkins, H. Jiang, M. Marquez, D. Piwnica-Worms, M. A. Suckow, B. Smith, Bioconjugate Chem. 2008, 3, 686–692. Copyright 2009, American Chemical Society.*

[318] *C. F. J. Faul, P. Krattiger, B. M. Smarsly, H. Wennemers, J. Mater. Chem. 2008, 18, 2962–2967 – Reproduced by permission of The Royal Society of Chemistry.*

[319] *Reprinted with permission from L. M. Heitmann, A. B. Taylor, P. J. Hart, A. R. Urbach, J. Am. Chem. Soc. 2006, 38, 12574–12581. Copyright 2009 American Chemical Society.*

[320] *Reprinted with permission from J. J. Reczek, A. A. Kennedy, B. T. Halbert, A. R. Urbach, J. Am. Chem. Soc. 2009, 131, 2408–2415. Copyright 2009 American Chemical Society.*

[321] *Reprinted from Current Opinion in Chemical Biolog, Vol. 12, V. Martos, P. Castreno, J. Valero, J. de Mendoza, Binding to protein surfaces by supramolecular multivalent scaffolds, 698–706, Copyright 2009, with permission from Elsevier.*

[322] *With kind permission from Springer Science+Business Media: Molecular Diversity, Protein recognition using synthetic surface-targeted agents, 8, 2004, 1381–1991, R. Jain, J. T. Ernst, O. Kutzki, H. S. Park, A. D. Hamilton, Figure 1.*

[323] *S. Gordo, V. Martos, E. Santos, M. Menendez, C. Bo, E. Giralt, J. de Mendoza, Proc. Natl. Acad. Sci. U.S.A. 2008, 105, 16426–16431, Copyright 2009 National Academy of Sciences, U.S.A.*

[324] *M. Martinell, X. Salvatella, J. Fernández-Carneado, S. Gordo, M. Feliz, M. Menéndez, E. Giralt: Synthetic Ligands Able to Interact with the P53 Tetramerization Domain. Towards Understanding a Protein Surface Recognition Event, ChemBioChem. 2006, 7, 1105–1113. Copyright Wiley-VCH Verlag GmbH & Co. KGaA. Reproduced with permission.*

[325] *Reprinted with permission from S. Gradl, J. Felix, E. Isacoff, M. Garcia, D. Trauner, J. Am. Chem. Soc., 2003, 42, 12668–12669. Copyright 2009 American Chemical Society.*

[326] *Reprinted by permission from Macmillan Publishers Ltd: Nature Structural & Molecular Biology, C. Ader, R. Schneider, S. Hornig, P. Velisetty, E.M. Wilson, A. Lange, K. Giller, I. Ohmert, M. Martin-Eauclaire, D. Trauner, S. Becker, O. Pongs, M. Baldus, Nat. Struct. Mol. Biol. 15, 605–612, Copyright 2008.*

[327] *K. Kano, Y. Ishida: Supramolecular Complex of Cytochrome c with a Polyanionic beta-Cyclodextrin, Angew. Chem. Int. Ed. 2007, 46, 727–730. Copyright Wiley-VCH Verlag GmbH & Co. KGaA. Reproduced with permission.*

[328] *M. Arendt, W. Sun, J. Thomann, X. Xie, T. Schrader, Dendrimeric Bisphosphonates for Multivalent Protein Surface Binding, Chem. Asian J. 2006, 1, 544–554. Copyright Wiley-VCH Verlag GmbH & Co. KGaA. Reproduced with permission.*

[329] *Reprinted with permission from O. Hayashida, N. Ogawa, M. Uchiyama, J. Am. Chem. Soc. 2007, 44 ,13698–13705. Copyright 2009 American Chemical Society.*

[330] *Reprinted with permission from G. A. Petsko, D. Ringe, Primers in Biology – Protein Structure and Function, Oxford University Press, Oxford, 2008.*

[331] *R. A. Roof, K. Sobczyk-Kojiro, A. J. Turbiak, D. L. Roman, I. D. Pogozheva, L. L. Blazer, R. R. Neubig, H. I. Mosberg, Chem. Biol. Drug. Des. 2008, 72, 111–119.*

[332] *Reprinted by permission from Macmillan Publishers Ltd: Nature, E. Erez, D. Fass, E. Bibi, Nature, 459, 371–378, Copyright 2009.*

[333] *Reprinted from Bioorganic & Medicinal Chemistry Letters, Vol. 12, N. Schaschke, A. Dominik, G. Matschiner, C. P. Sommerhoff, Bivalent inhibition of β-Tryptase: distance scan of neighboring subunits by dibasic inhibitors, 985–988, Copyright 2002, with permission from Elsevier.*

[334] *Reprinted from Biochimica et Biophysica Acta, Vol. 1477, C. P. Sommerhoff, W. Bode, G. Matschiner, A. Bergner, H. Fritz, The human mast cell tryptase tetramer: a fascinating riddle solved by structure, 75–89, Copyright 2000, with permission from Elsevier.*

[335] *Reprinted from Structure, Vol. 5, S. Di Marco, J. P. Priestle, Structure of the complex of leech-derived tryptase inhibitor (LDTI) with trypsin and modeling of the LDTI-tryptase system, 1465–1474, Copyright 1997, with permission from Elsevier.*

[336] *Reprinted from Chemistry & Biology, Vol. 8, N. Schaschke, G. Matschiner, F. Zettl, U. Marquardt, A. Bergner, W. Bode, C. P. Sommerhoff, L. Moroder, Bivalent inhibition of human beta-tryptase, 313–327, Copyright 2001, with permission from Elsevier.*

[337] *Reprinted from Bioorganic & Medicinal Chemistry, Vol. 12, T. Mecca, G. Consoli, C. Geraci, F. Cunsolo, Designed calix[8]arene-based ligands for selective tryptase surface recognition, 5057–5062, Copyright 2004, with permission from Elsevier.*

[338] *B. Küstner, C. Schmuck, P. Wich, C. Jehn, S. K. Srivastava, S. Schlücker, Phys. Chem. Chem. Phys. 2007, 9, 4598–4603 – Reproduced by permission of the PCCP Owner Societies.*

[339] *S. K. Srivastava, S. Niebling, B. Küstner, P. R. Wich, C. Schmuck, S. Schlücker, Phys. Chem. Chem. Phys. 2008, 10, 6770–6775 – Reproduced by permission of the PCCP Owner Societies.*

[340] *C. Schmuck, P. Wich, B. Küstner, W. Kiefer, S. Schlücker: Direct and Label-Free Detection of Solid-Phase-Bound Compounds by Using Surface-Enhanced Raman Scattering Microspectroscopy, Angew. Chem. Int. Ed. 2007, 46, 4786–4789. Copyright Wiley-VCH Verlag GmbH & Co. KGaA. Reproduced with permission.*

Appendix C

List of Abbreviations

δ	chemical shift
λ	wavelength
°C	celsius
Å	Ångstrom
A	alanine
abs	absolute
Ac	acetyl
AcOH	acetic acid
Ala	alanine
AMC	7-amino-4-methyl-cumarin
AMPs	antimicrobial peptides
aq	aqueous
Arg	arginine
Asp	asparaginic acid
Boc	*tert*-butyloxycarbonyl
c	concentration
CBS	carboxylate binding site
Cbz	benzyloxycarbonyl
$CDCl_3$	deuterated chloroform
cm	centimeter
COSY	correlated spectroscopy
d	day(s)
Da	dalton
DCM	dichloromethane
DIC	*N,N'*-diisopropylcarbodiimide
DIPEA	*N,N'*-diisopropylethylamine
DMAP	4-(dimethylamino)-pyridine

DMF	*N,N'*-dimethylformamide
DMSO-d_6	deuterated dimethyl sulfoxide
DNA	deoxyribonucleic acid
E	glutamic acid
equiv	equivalent(s)
Eq	equation
ESI-MS	electrospray ionization mass spectrometry
Et	ethyl
et al.	et alii
F	phenylalanine
FAB-MS	fast atom bombardment mass spectrometry
Fmoc	9-fluorenylmethyloxycarbonyl
FT-IR	Fourier-transform infrared
g	gram
G	glycine
Glu	glutamic acid
Gly	glycine
h	hour(s)
H	histidine
HCTU	1-[bis-(dimethylamino)-methylen]-5-chlor-benztriazolium-3-oxid-hexafluorophosphate
HOBt	1-hydroxy-1,2,3-benzotriazole
HPLC	high performance liquid chromatography
HR-MS	high resolution mass spectrometry
Hz	Hertz
I	intensity
IC_{50}	half maximal inhibitory concentration
IR	infrared
ITC	isothermal titration calorimetry
K	lysine
K	Kelvin
K_{ass}	association constant
K_i	dissociation constant
kJ	kilo Joule
K_M	Michaelis constant
L	liter
Lys	lysine
m	milli
m/z	mass per charge
MALDI-MS	matrix-assisted laser desorption ionization mass spectrometry
MBHA	*p*-methylbenzhydrylamine
Me	Methyl
MHz	megahertz
MIC	minimal inhibitory concentration
min	minute(s)
μM	micromolar

mM	millimolar
MS	mass spectrometry
n.d.	not determined
neg.	negative
nm	nanometer
NMM	*N*-methyl morpholine
NMR	nuclear magnetic resonance
NOESY	nuclear Overhauser effect spectroscopy
OBOC	one-bead one-compound
p	para
Pbf	2,2,4,6,7-pentamethyldihydrobenzofuran-5-sulfonyl
Pd	palladium
Pd/C	palladium on charcoal
PEG	polyethylene glycol
PEGA	polyethylene glycol-polyacrylamide
pH	pondus hydrogenii
Phe	phenylalanine
pos.	positive
ppm	parts per million
PS	polystyrene
PyBOP	benzotriazol-1-yl-*N*-oxy-tris(pyrrolidino)phosphonium hexafluorophosphate
R	arginine
R	rest
R_f	retention factor
RP	reversed phase
RT	room temperature
SPPS	solid-phase peptide synthesis
T	temperature
t	time
TEG	triethylene glycol
TFA	trifluoroacetic acid
TFMSA	trifluoromethanesulfonic acid
THF	tetrahydrofuran
TG	TentaGel
TIS	triisopropylsilane
TLC	thin layer chromatography
TMS	tetramethylsilane
Tos	tosyl
Trt	trityl
Trp	tryptophan
UV	ultraviolet
Val	valine
vol %	volume percentage
W	tryptophan

Appendix D

Experimental Data of Enzyme Assays

D.1 Inhibition Data of On-Bead Screening Assay

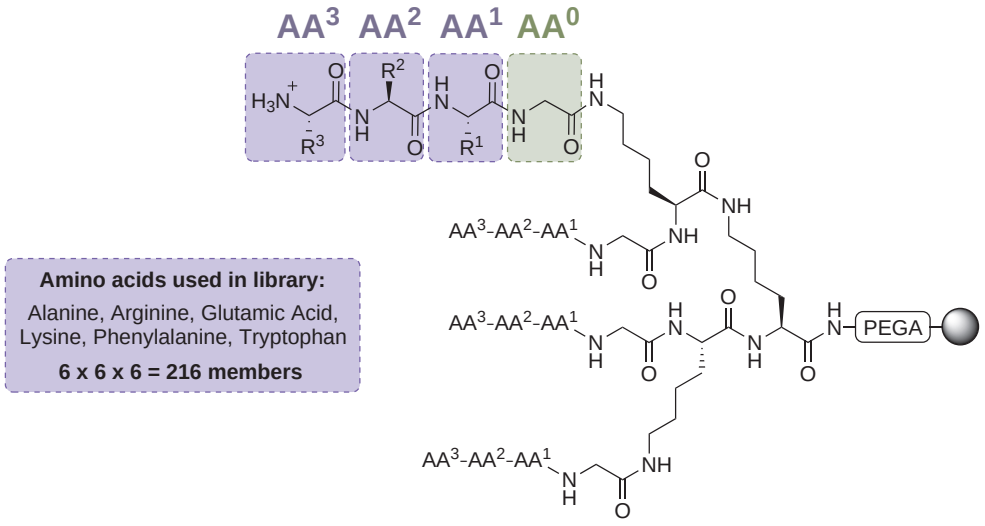

Table D.1: *Screening data of the combinatorial inhibitor library. The inhibitors are listed in descending order of their absolute inhibition (in %) of β-tryptase.*

No.	AA^3	AA^2	AA^1	AA^0	Inhibition (%)	Archive
107	Arg	Trp	Lys	Gly	95	3-G01
108	Lys	Trp	Lys	Gly	94	1-D08
109	Trp	Lys	Phe	Gly	93	3-F01

continued on next page

Table D.1 – continued from previous page

No.	AA^3	AA^2	AA^1	AA^0	Inhibition (%)	Archive
110	Phe	Arg	Lys	Gly	92	2-C07
111	Lys	Arg	Arg	Gly	91	2-G04
112	Phe	Lys	Arg	Gly	91	2-E10
113	Lys	Trp	Arg	Gly	90	1-C11
114	Lys	Phe	Arg	Gly	90	2-H09
115	Lys	Lys	Trp	Gly	90	2-G02
116	Phe	Trp	Lys	Gly	90	2-G11
131	Lys	Ala	Trp	Gly	90	1-G09
132	Trp	Lys	Arg	Gly	90	2-B04
133	Arg	Arg	Lys	Gly	90	3-B02
134	Trp	Lys	Ala	Gly	89	3-E01
135	Ala	Trp	Lys	Gly	89	2-E07
136	Ala	Arg	Arg	Gly	89	2-C02
137	Ala	Lys	Trp	Gly	89	1-D06
138	Lys	Trp	Ala	Gly	88	3-D01
139	Phe	Phe	Lys	Gly	88	1-B07
140	Lys	Phe	Lys	Gly	87	1-G10
141	Phe	Lys	Lys	Gly	87	1-G06
142	Ala	Phe	Lys	Gly	87	1-F01
143	Lys	Ala	Phe	Gly	87	3-H03
144	Lys	Ala	Lys	Gly	87	3-H02
145	Arg	Lys	Lys	Gly	87	1-D01
146	Arg	Phe	Lys	Gly	87	2-F10
147	Phe	Lys	Phe	Gly	87	2-E03
148	Arg	Lys	Arg	Gly	86	1-C07
149	Trp	Lys	Trp	Gly	86	2-F12
150	Trp	Ala	Lys	Gly	86	1-B11
151	Glu	Lys	Lys	Gly	86	1-B02
152	Ala	Lys	Arg	Gly	85	2-B01
153	Trp	Arg	Arg	Gly	84	2-D09
154	Arg	Phe	Arg	Gly	84	1-C04

continued on next page

Table D.1 – continued from previous page

No.	AA^3	AA^2	AA^1	AA^0	Inhibition (%)	Archive
106	Lys	Lys	Phe	Gly	84	1-H06
155	Arg	Lys	Trp	Gly	84	1-A03
156	Lys	Glu	Lys	Gly	83	2-C12
157	Arg	Glu	Arg	Gly	83	1-H07
158	Lys	Lys	Lys	Gly	83	3-C02
159	Glu	Arg	Arg	Gly	82	2-B05
160	Ala	Lys	Lys	Gly	82	2-F08
161	Phe	Ala	Arg	Gly	82	1-C12
162	Trp	Glu	Lys	Gly	82	2-C11
163	Trp	Lys	Lys	Gly	82	2-A05
164	Ala	Phe	Arg	Gly	81	3-F03
165	Lys	Lys	Arg	Gly	81	2-E11
166	Lys	Arg	Trp	Gly	81	2-E01
167	Arg	Trp	Arg	Gly	81	2-D11
168	Lys	Arg	Ala	Gly	81	2-F07
169	Arg	Ala	Lys	Gly	81	2-C10
170	Lys	Arg	Lys	Gly	81	1-H09
171	Arg	Arg	Arg	Gly	81	1-G07
172	Ala	Trp	Arg	Gly	80	2-B10
173	Glu	Phe	Lys	Gly	80	1-F06
174	Lys	Ala	Arg	Gly	80	2-H12
175	Glu	Trp	Arg	Gly	80	2-H02
176	Ala	Arg	Phe	Gly	79	1-D07
177	Trp	Phe	Lys	Gly	79	1-E04
178	Ala	Arg	Lys	Gly	79	2-G08
179	Arg	Arg	Phe	Gly	79	1-D10
180	Lys	Phe	Phe	Gly	79	2-D06
181	Trp	Trp	Lys	Gly	79	1-G12
182	Glu	Arg	Lys	Gly	79	1-C06
183	Glu	Trp	Lys	Gly	78	1-B05
184	Trp	Arg	Lys	Gly	78	2-H06

continued on next page

Table D.1 – continued from previous page

No.	AA^3	AA^2	AA^1	AA^0	Inhibition (%)	Archive
185	Lys	Phe	Ala	Gly	77	1-H05
186	Lys	Glu	Arg	Gly	77	2-D07
187	Ala	Lys	Phe	Gly	77	1-F12
188	Arg	Ala	Arg	Gly	77	2-H03
189	Arg	Glu	Lys	Gly	77	2-A10
190	Phe	Ala	Lys	Gly	76	1-E10
191	Arg	Trp	Ala	Gly	76	2-G01
192	Lys	Arg	Phe	Gly	76	1-B01
193	Ala	Glu	Arg	Gly	75	1-A06
194	Phe	Glu	Arg	Gly	75	2-D01
195	Trp	Ala	Arg	Gly	75	1-A11
196	Arg	Lys	Ala	Gly	75	1-E02
197	Lys	Trp	Trp	Gly	75	2-C09
198	Lys	Trp	Phe	Gly	74	2-H05
199	Lys	Lys	Ala	Gly	74	2-G06
200	Glu	Lys	Arg	Gly	74	2-E05
201	Arg	Ala	Phe	Gly	74	2-C01
202	Ala	Arg	Trp	Gly	74	2-H07
203	Glu	Phe	Arg	Gly	74	2-A02
204	Phe	Glu	Lys	Gly	74	3-A01
205	Phe	Arg	Arg	Gly	73	2-B03
206	Trp	Arg	Ala	Gly	72	2-G03
207	Glu	Lys	Phe	Gly	72	1-B10
208	Phe	Lys	Ala	Gly	72	2-D04
209	Ala	Ala	Lys	Gly	71	1-A02
210	Arg	Arg	Trp	Gly	71	2-D05
211	Arg	Arg	Ala	Gly	70	2-D12
212	Lys	Phe	Trp	Gly	69	1-C08
213	Trp	Glu	Arg	Gly	69	2-F05
214	Phe	Lys	Trp	Gly	69	1-C03
215	Arg	Ala	Trp	Gly	68	2-G09

continued on next page

Table D.1 – continued from previous page

No.	AA^3	AA^2	AA^1	AA^0	Inhibition (%)	Archive
216	Arg	Lys	Phe	Gly	68	2-B08
217	Glu	Ala	Arg	Gly	68	2-C05
218	Glu	Ala	Lys	Gly	67	2-C08
219	Lys	Glu	Trp	Gly	66	1-H01
220	Trp	Arg	Phe	Gly	66	2-F03
221	Phe	Trp	Arg	Gly	66	1-F10
222	Glu	Lys	Trp	Gly	65	2-F02
223	Trp	Trp	Arg	Gly	65	2-G07
224	Arg	Glu	Trp	Gly	65	3-D02
225	Glu	Glu	Lys	Gly	65	3-B01
226	Lys	Arg	Glu	Gly	64	2-B11
227	Ala	Ala	Arg	Gly	63	2-H11
228	Trp	Glu	Trp	Gly	63	2-C06
229	Phe	Phe	Arg	Gly	63	1-B03
230	Ala	Arg	Ala	Gly	63	1-E08
231	Ala	Lys	Ala	Gly	62	2-C03
232	Ala	Glu	Lys	Gly	61	1-A09
233	Lys	Ala	Ala	Gly	60	2-A03
234	Phe	Arg	Ala	Gly	59	1-D12
235	Glu	Arg	Ala	Gly	59	1-E01
236	Ala	Ala	Phe	Gly	58	1-D11
237	Lys	Glu	Phe	Gly	58	2-E02
238	Arg	Arg	Glu	Gly	58	1-A12
239	Trp	Arg	Glu	Gly	58	3-E03
240	Glu	Arg	Trp	Gly	57	1-A07
241	Glu	Glu	Glu	Gly	56	2-F06
242	Phe	Arg	Phe	Gly	56	1-E09
243	Arg	Phe	Ala	Gly	56	2-A11
244	Glu	Glu	Phe	Gly	56	2-A07
245	Trp	Lys	Glu	Gly	55	1-C10
246	Phe	Glu	Glu	Gly	55	3-E02

continued on next page

Table D.1 – continued from previous page

No.	AA^3	AA^2	AA^1	AA^0	Inhibition (%)	Archive
247	Glu	Arg	Phe	Gly	54	1-A05
248	Glu	Phe	Glu	Gly	54	2-G12
249	Arg	Ala	Ala	Gly	54	2-F11
250	Arg	Phe	Phe	Gly	53	2-H01
251	Lys	Trp	Glu	Gly	53	1-F03
252	Ala	Ala	Trp	Gly	53	1-E11
253	Phe	Lys	Glu	Gly	52	2-A01
254	Phe	Arg	Trp	Gly	51	1-E03
255	Phe	Phe	Glu	Gly	51	2-D03
256	Trp	Phe	Arg	Gly	51	1-G03
257	Trp	Glu	Ala	Gly	51	1-H03
258	Glu	Trp	Glu	Gly	51	2-B09
259	Glu	Glu	Trp	Gly	50	2-B06
260	Trp	Phe	Glu	Gly	50	2-B02
261	Arg	Lys	Glu	Gly	50	1-B08
262	Arg	Glu	Phe	Gly	50	2-B12
263	Trp	Glu	Glu	Gly	49	2-F04
264	Glu	Glu	Arg	Gly	49	2-H08
265	Arg	Phe	Glu	Gly	49	2-H10
266	Phe	Trp	Glu	Gly	49	1-A04
267	Lys	Glu	Ala	Gly	49	2-G10
268	Arg	Trp	Glu	Gly	48	1-D04
269	Glu	Trp	Trp	Gly	48	1-G05
270	Lys	Lys	Glu	Gly	48	1-D03
271	Ala	Trp	Glu	Gly	48	1-G01
272	Glu	Ala	Glu	Gly	47	2-A06
273	Trp	Arg	Trp	Gly	47	1-H02
274	Trp	Ala	Glu	Gly	46	2-F01
275	Ala	Glu	Trp	Gly	46	2-E04
276	Phe	Glu	Trp	Gly	45	3-B03
277	Glu	Trp	Ala	Gly	45	1-F09

continued on next page

Table D.1 – continued from previous page

No.	AA^3	AA^2	AA^1	AA^0	Inhibition (%)	Archive
278	Trp	Ala	Ala	Gly	45	2-D10
279	Trp	Glu	Phe	Gly	45	1-A10
280	Ala	Glu	Glu	Gly	44	2-A09
281	Arg	Glu	Glu	Gly	44	1-H10
282	Glu	Lys	Ala	Gly	43	2-E12
283	Ala	Trp	Ala	Gly	43	2-A12
284	Lys	Phe	Glu	Gly	43	1-B12
285	Arg	Trp	Phe	Gly	43	1-D02
286	Phe	Phe	Ala	Gly	43	3-A03
287	Trp	Phe	Trp	Gly	43	1-C05
288	Glu	Ala	Trp	Gly	43	1-H08
289	Phe	Ala	Trp	Gly	43	3-F02
290	Ala	Phe	Phe	Gly	43	2-G05
291	Ala	Trp	Trp	Gly	42	1-D09
292	Phe	Trp	Ala	Gly	41	1-D05
293	Trp	Trp	Trp	Gly	41	2-A08
294	Ala	Glu	Ala	Gly	41	3-H01
295	Phe	Glu	Phe	Gly	41	1-E12
296	Glu	Arg	Glu	Gly	41	1-A08
297	Glu	Phe	Trp	Gly	40	1-F04
298	Lys	Glu	Glu	Gly	40	1-G11
299	Glu	Trp	Phe	Gly	40	1-G02
300	Trp	Phe	Ala	Gly	39	3-C03
301	Ala	Phe	Trp	Gly	39	2-E08
302	Glu	Phe	Phe	Gly	38	3-C01
303	Phe	Arg	Glu	Gly	38	1-E06
304	Phe	Trp	Trp	Gly	38	1-G04
305	Ala	Ala	Ala	Gly	38	3-D03
306	Phe	Trp	Phe	Gly	37	1-B09
307	Glu	Lys	Glu	Gly	37	2-B07
308	Arg	Phe	Trp	Gly	37	1-F02

continued on next page

Table D.1 – continued from previous page

No.	AA^3	AA^2	AA^1	AA^0	Inhibition (%)	Archive
309	Phe	Glu	Ala	Gly	37	1-F08
310	Trp	Trp	Ala	Gly	36	1-H04
311	Glu	Glu	Ala	Gly	36	1-F05
312	Ala	Phe	Ala	Gly	36	1-H12
313	Arg	Trp	Trp	Gly	35	3-G03
314	Phe	Ala	Phe	Gly	35	2-D02
315	Arg	Ala	Glu	Gly	35	1-C02
316	Ala	Lys	Glu	Gly	35	2-E06
317	Phe	Ala	Glu	Gly	34	2-C04
318	Trp	Ala	Trp	Gly	33	2-A04
319	Trp	Ala	Phe	Gly	33	3-G02
320	Glu	Ala	Ala	Gly	33	1-C01
321	Lys	Ala	Glu	Gly	32	1-F11
322	Ala	Ala	Glu	Gly	32	2-E09
323	Arg	Glu	Ala	Gly	32	1-E07
324	Trp	Trp	Phe	Gly	31	1-G08
325	Phe	Phe	Phe	Gly	31	1-C09
326	Ala	Glu	Phe	Gly	29	1-H11
327	Glu	Ala	Phe	Gly	29	1-B04
328	Trp	Phe	Phe	Gly	29	3-A02
329	Phe	Phe	Trp	Gly	28	1-A01
330	Trp	Trp	Glu	Gly	27	2-H04
331	Ala	Arg	Glu	Gly	23	1-F07
332	Ala	Trp	Phe	Gly	23	1-B06
333	Glu	Phe	Ala	Gly	23	1-E05
334	Ala	Phe	Glu	Gly	20	2-F09
335	Phe	Ala	Ala	Gly	10	2-D08

D.2 Classification of Enzyme Inhibition

The following data is based on the enzyme assay for rhSkin β-tryptase, described in Chapter 7.5 on page 208. It lists the residual activity of the enzyme (double measurement; reciprocal value of the absolute inhibition) as obtained at different inhibitor concentrations c(I). The IC_{50}-values were calculated with Grafit® on the basis of non-linear regression fits (average of two measurements; the error range represents the mean deviation from the median). The K_i values were calculated from the IC_{50} values (depending on the substrate concentration).

To elucidate the inhibition type, the IC_{50}-values were determined at different substrate concentrations of 50, 200 and 400 μM (the data at 50 μM can be found in Chapter D.3 on page 252).

Table D.2: *Compound CBS-KKF (**1**); c(S) = 200 μM; synthesis on page 168.*

c(I)[μM]	**Residual Activity No. 1** [%]	**Residual Activity No. 2** [%]	**IC_{50}** [μM]	K_i [μM]
80	35.87	36.37	34.98 $\pm$ 1.17	23.04 $\pm$ 0.77
60	41.61	41.28		
50	40.82	42.42		
40	50.59	53.73		
20	64.39	66.56		
10	73.95	78.04		
1	84.96	86.95		

Table D.3: *Compound CBS-KKF (**1**); c(S) = 400 μM; synthesis on page 168.*

c(I)[μM]	**Residual Activity No. 1** [%]	**Residual Activity No. 2** [%]	**IC_{50}** [μM]	K_i [μM]
80	36.42	38.84	65.83 $\pm$ 22.88	32.33 $\pm$ 11.24
60	47.00	45.01		
50	45.90	49.17		
40	58.03	61.94		
20	69.35	73.21		
10	84.76	83.50		
1	86.56	95.09		

Table D.4: *Compound (CBS-KKF)$_4$ (**90**); c(S) = 200 µM; synthesis on page 196.*

c(I)[μM]	**Residual Activity** [%]	$\mathbf{IC_{50}}$ [μM]	K_i [μM]
8	31.01	0.19 ± 0.18	0.19 ± 0.18
6	34.52		
5	22.84		
4	15.52		
2	39.72		
0.80	46.47		
0.60	46.64		
0.50	57.98		
0.40	58.73		
0.20	69.02		
0.10	90.94		

Table D.5: *Compound (CBS-KKF)$_4$ (**90**); c(S) = 400 µM; synthesis on page 196.*

c(I)[μM]	**Residual Activity** [%]	$\mathbf{IC_{50}}$ [μM]	K_i [μM]
8	25.24	1.15 ± 0.38	0.65 ± 0.22
6	30.16		
5	30.92		
4	36.77		
2	38.49		
1	51.81		
0.8	64.89		
0.6	63.56		
0.5	63.22		
0.4	66.69		
0.2	77.53		
0.1	77.94		
0.01	84.63		

Table D.6: *Compound $(KKFG)_4$ (**106**); c(S) = 200 µM; synthesis on page 200.*

c(I)[μM]	**Residual Activity No. 1** [%]	**Residual Activity No. 2** [%]	$\mathbf{IC_{50}}$ [μM]	K_i [μM]
8	30.71	29.70	0.83 ± 0.028	0.55 ± 0.018
6	33.60	33.26		
5	33.88	35.11		
4	35.12	37.11		
2	42.05	45.17		
1	48.67	50.98		
0.8	62.69	64.35		
0.6	69.89	67.88		
0.5	68.49	67.55		
0.4	76.31	74.76		
0.2	78.72	85.40		
0.1	83.04	87.26		
0.01	86.08	93.07		

Table D.7: *Compound $(KKFG)_4$ (**106**); c(S) = 400 µM; synthesis on page 200.*

c(I)[μM]	**Residual Activity** [%]	$\mathbf{IC_{50}}$ [μM]	K_i [μM]
8	30.71	1.18 ± 0.25	0.67 ± 0.14
6	36.27		
5	38.33		
4	40.57		
2	50.99		
1	63.60		
0.8	68.41		
0.6	70.91		
0.5	72.53		
0.4	74.86		
0.2	82.54		
0.1	85.33		
0.01	88.53		

In a second and more detailed test to elucidate the mode of enzyme inhibition (competitive or non-competitive) the rate of the enzyme reaction was measured at different substrate concentrations (10–1000 μM) and fixed enzyme concentration. The inhibitor **106** ($(KKFG)_4$) was added at different concentrations (c(I) = 0, 1, 10 and 100 μM). The following data was used for the linear and non-linear analysis, described on page 133ff.

Table D.8: *Determination of inhibition mode $(KKFG)_4$ (**106**); c(I) = 0 μM.*

non linear analysis		**Lineweaver-Burk**		**Hanes-Woolf**	
[S]	v	1 / [S]	1 / v	[S]	[S] / v
1000	152.62	0.001	0.006552	1000	6.552066
800	157.37	0.00125	0.006355	800	5.083618
600	175.07	0.001666667	0.005712	600	3.427119
400	136.47	0.0025	0.007328	400	2.931095
200	90.03	0.005	0.011108	200	2.221506
100	42.22	0.01	0.023688	100	2.368812
50	22.47	0.02	0.044497	50	2.224839
10	4.19	0.1	0.238663	10	2.386635

Table D.9: *Determination of inhibition mode $(KKFG)_4$ (**106**); c(I) = 1 μM.*

non linear analysis		**Lineweaver-Burk**		**Hanes-Woolf**	
[S]	v	1 / [S]	1 / v	[S]	[S] / v
800	152.62	0.00125	0.009326	800	7.460564
600	157.37	0.001667	0.008410	600	5.045728
400	175.07	0.0025	0.009850	400	3.940161
300	136.47	0.003333	0.010353	300	3.105892
200	90.03	0.005	0.017314	200	3.462808
100	42.22	0.01	0.044449	100	4.444881
50	22.47	0.02	0.098981	50	4.949035
10	4.19	0.1	0.539263	10	5.392625

Table D.10: *Determination of inhibition mode $(KKFG)_4$ (**106**); c(I) = 10 µM.*

non linear analysis		**Lineweaver-Burk**		**Hanes-Woolf**	
[S]	v	1 / [S]	1 / v	[S]	[S] / v
800	30.49	0.00125	0.032793	800	26.234538
600	28.39	0.001667	0.035229	600	21.137580
400	27.39	0.0025	0.036509	400	14.603651
300	24.33	0.003333	0.041108	300	12.332343
200	22.38	0.005	0.044693	200	8.938508
100	11.03	0.01	0.090690	100	9.068985
50	4.42	0.02	0.226439	50	11.321952
10	0.87	0.1	1.145591	10	11.455905

Table D.11: *Determination of inhibition mode $(KKFG)_4$ (**106**); c(I) = 100 µM.*

non linear analysis		**Lineweaver-Burk**		**Hanes-Woolf**	
[S]	v	1 / [S]	1 / v	[S]	[S] / v
800	10.11	0.00125	0.098950	800	79.160143
600	9.71	0.001667	0.102961	600	61.776534
400	7.99	0.0025	0.125100	400	50.040199
300	4.97	0.003333	0.201203	300	60.360951
200	3.52	0.005	0.283999	200	56.799730
100	1.78	0.01	0.561402	100	56.140153
50	0.93	0.02	1.072910	50	53.645521
10	0.44	0.1	2.286923	10	22.869229

D.3 Determination of Inhibition Constants in Solution

In the case of competitive inhibitors the K_i values were calculated from the IC_{50} values (c(S) = 50 μM, K_m = 368 μM). In the case of non-competitive inhibitors the K_i values were directly calculated with non-linear regression analysis. If not otherwise stated, all enzyme assays were performed with rhSkin β-tryptase (containing heparin).

Table D.12: *Compound CBS-KKF (**1**); competitive; synthesis on page 168.*

c(I) [μM]	**Residual Activity No. 1** [%]	**Residual Activity No. 2** [%]	**IC_{50}** [μM]	**K_i** [μM]
100	26.91	26.91	27.25 $\pm$ 8.90	24.12 $\pm$ 7.88
80	30.03	33.80		
60	34.55	39.22		
50	36.39	40.08		
40	39.33	47.28		
20	53.31	65.39		
10	67.54	76.32		
1	90.49	101.60		

Table D.13: *Compound CBS-KKF (**1**); **rhLung β-tryptase**; competitive; synthesis on page 168.*

c(I) [μM]	**Residual Activity No. 1** [%]	**Residual Activity No. 2** [%]	**IC_{50}** [μM]	**K_i** [μM]
100	26.25	26.25	37.86 $\pm$ 7.63	33.52 $\pm$ 6.76
80	36.27	42.25		
60	48.54	45.23		
50	41.99	53.25		
40	49.25	56.02		
20	66.54	81.01		
10	72.05	108.31		
1	100.86	123.38		

Table D.14: *Compound (CBS-KKF)$_4$ (**90**); non-competitive; synthesis on page 196.*

c(I)[μM]	**Residual Activity No. 1** [%]	**Residual Activity No. 2** [%]	K_i [μM]
100	2.28	2.28	0.28 $\pm$ 0.15
8	25.99	31.80	
6	10.84	31.11	
5	30.48	25.32	
4	27.38	26.89	
2	16.59	26.22	
1	36.14	35.81	
0.8	38.37	35.45	
0.6	43.88	30.19	
0.5	45.65	40.16	
0.4	51.82	48.15	
0.2	65.71	55.37	
0.1	82.11	78.62	
0.01	84.67	88.76	

Table D.15: *Compound (CBS-KKF)$_4$ (**90**); **rhLung β-tryptase**; non-competitive synthesis; on page 196.*

c(I)[μM]	**Residual Activity No. 1** [%]	**Residual Activity No. 2** [%]	K_i [μM]
100	2.27	2.27	0.45 $\pm$ 0.0097
8	5.06	4.03	
6	4.63	5.12	
5	5.63	4.59	
4	4.74	5.13	
2	8.36	7.71	
1	15.70	12.27	
0.8	32.13	33.80	
0.6	44.55	39.69	
0.5	52.05	46.69	
0.4	48.53	51.97	
0.2	84.35	76.57	
0.1	101.33	92.54	
0.01	100.43	93.15	

Table D.16: *Compound CBS-WHR (**91**); competitive; synthesis on page 170.*

c(I)[μM]	**Residual Activity No. 1** [%]	**Residual Activity No. 2** [%]	$\mathbf{IC_{50}}$ [μM]	K_i [μM]
100	52.04	52.04	91.29 $\pm$ 21.47	80.82 $\pm$ 19.01
80	57.72	58.34		
60	65.95	69.26		
50	64.48	74.48		
40	68.31	63.75		
20	79.36	81.85		
10	90.12	90.06		
1	99.92	99.92		

Table D.17: *Compound (CBS-WHR)$_4$ (**92**); non-competitive; synthesis on page 198.*

c(I)[μM]	**Residual Activity No. 1** [%]	**Residual Activity No. 2** [%]	K_i [μM]
100	12.33	12.33	8.95 $\pm$ 0.01
10	38.10	38.10	
8	65.20	65.59	
6	74.08	74.31	
5	77.35	76.26	
4	78.78	81.89	
2	84.01	84.73	
1	87.84	89.40	
0.8	95.27	107.26	
0.6	93.30	97.84	
0.5	92.42	102.23	
0.4	95.45	113.95	
0.2	89.90	98.69	
0.1	93.62	99.83	
0.01	84.55	112.46	

Table D.18: *Compound KKFG (**117**); competitive; synthesis on page 181.*

c(I)[μM]	**Residual Activity No. 1** [%]	**Residual Activity No. 2** [%]	$\mathbf{IC_{50}}$ [μM]	K_i [μM]
1000	56.88	56.88	532.85 $\pm$ 35.32	471.74 $\pm$ 31.27
800	64.60	69.75		
600	73.40	69.86		
500	81.15	72.48		
400	74.39	76.46		
200	77.65	80.32		
100	82.86	84.05		
80	95.10	99.08		
60	99.22	95.27		
50	106.24	99.76		
40	101.12	98.85		
20	103.66	91.30		
10	106.61	94.00		
1	100.30	86.59		

Table D.19: *Compound $(KKFG)_4$ (**106**); non-competitive; synthesis on page 200.*

c(I)[μM]	**Residual Activity No. 1** [%]	**Residual Activity No. 2** [%]	K_i [μM]
100	4.79	4.79	0.63 $\pm$ 0.02
8	32.86	36.18	
6	27.97	35.81	
5	26.29	32.66	
4	27.84	33.54	
2	26.28	36.84	
1	30.61	44.28	
0.80	50.53	53.66	
0.60	55.09	59.25	
0.50	64.30	64.14	
0.40	77.66	69.38	
0.20	79.20	84.80	
0.10	86.87	99.66	
0.01	81.97	101.58	

Table D.20: *Compound RWKG (**118**); competitive; synthesis on page 182.*

c(I)[μM]	**Residual Activity No. 1** [%]	**Residual Activity No. 2** [%]	$\mathbf{IC_{50}}$ [μM]	K_i [μM]
1000	46.04	46.04	345.44 $\pm$ 56.72	305.83 $\pm$ 50.22
800	55.40	55.40		
600	56.74	56.74		
500	63.97	63.97		
400	64.13	64.13		
200	70.54	70.54		
100		72.68		
80	92.73	91.11		
60	99.18	90.68		
50	93.72	92.48		
40	95.30	94.42		
20	89.49	87.58		
10	97.77	96.29		

Table D.21: *Compound $(RWKG)_4$ (**107**); non-competitive; synthesis on page 202.*

c(I)[μM]	**Residual Activity No. 1** [%]	**Residual Activity No. 2** [%]	K_i [μM]
100	2.32	2.32	0.17 $\pm$ 0.02
8	7.41	8.14	
6	8.92	9.77	
5	9.07	9.46	
4	8.45	12.47	
2	11.70	14.37	
1	13.79	21.70	
0.80	23.55	23.21	
0.60	27.29	23.40	
0.50	30.13	33.03	
0.40	38.39	42.73	
0.20	50.86	53.97	
0.10	54.22	66.39	
0.01	90.65	97.05	

Table D.22: *Compound p-Ab (**44**); competitive.*

c(I)[μM]	**Residual Activity No. 1** [%]	**Residual Activity No. 2** [%]	$\mathbf{IC_{50}}$ [μM]	K_i [μM]
100	23.24	23.24	64.35 $\pm$ 9.32	56.97 $\pm$ 8.25
80	24.22	28.37		
60	30.52	35.82		
50	42.38	39.66		
40	37.99	46.17		
20	52.22	59.81		
10	62.53	73.85		
1	75.58	90.51		

Table D.23: *Compound p-Ab (**44**); competitive; **trypsin**; literature value K_i = 7 μM.*[280]

c(I)[μM]	**Residual Activity No. 1** [%]	**Residual Activity No. 2** [%]	$\mathbf{IC_{50}}$ [μM]	K_i [μM]
100	15.91	15.91	19.59 $\pm$ 2.99	5.29 $\pm$ 0.80
80	16.10	19.76		
60	19.16	24.08		
50	23.23	28.47		
40	27.56	32.51		
20	36.36	49.04		
10	52.08	64.11		
1	72.99	89.67		